UNIVERSITÀ DEGLI STUDI DI GENOVA

SCUOLA POLITECNICA – DIME
Dipartimento di Ingegneria Meccanica, Energetica, Gestionale e dei Trasporti

Doctoral Research Thesis
Ingegneria dei Modelli, delle Macchine e dei Sistemi per l'Energia, l'Ambiente e i Trasporti – Curriculum Ingegneria delle Macchine e dei Sistemi per l'Energia, l'Ambiente e la Propulsione (XXXIV ciclo)

Polymer Electrolyte Membrane Fuel Cells for maritime applications: state of art of the technology, experimental assessment of a 240-kW system, and Response Surface Methodology application to data analysis

Advisors:
Prof. Eng. Loredana Magistri
Prof. Eng. Aristide Fausto Massardo
Co-advisor:
Eng. Thomas Lamberti

Ph.D. Candidate:
Eleonora Gadducci

May 2022

The end

Acknowledgments

Benché poco sopra io abbia scritto: "The end", so che la mia relazione con la ricerca, con l'Università, e con il tema dell'idrogeno non è ancora finita. Questo è anche per merito dei miei Relatori e dei miei colleghi, che mi trasmettono interesse ed entusiasmo per quello che facciamo insieme, e che per questo ringrazio fortissimo.

In questi anni sono cambiate tante cose, a partire da me stessa – che sono passata dall'essere un germoglio a un alberello, consentitemi la metafora – fino alle persone che mi circondano, mentre altre sono rimaste com'erano e come spero rimarranno sempre.

In particolare, mi riferisco ai miei genitori e ai miei nonni, che sono le mie origini, le mie radici, che hanno posto le basi di quello che sono dandomi forza e sicurezza sia con il sole sia con la tempesta. Non vi ringrazierò mai abbastanza.

Quindi penso immediatamente ai miei fratelli, Stefano e Sara: il tronco del mio alberello, il mio sostegno quotidiano attraverso il quale mi confronto, mi comprendo, definisco me stessa e il mio contorno rispetto al mondo circostante. Siete sempre nei miei pensieri e il mio punto di riferimento in ogni percorso intrapreso.

Infine, vorrei ringraziare tutte le foglioline della mia chioma: i miei zii, che sono le prime e solide foglioline spuntate; Susi e Rola e la piccola Laura, che sono un bocciolo che si sta aprendo mostrando un fiore bellissimo; i miei amici: Tommi (sei la fogliolina più verde del mio alberello!), Bea, Ali, Franci, Richi, Mela, Acco, Clo, Lucia, Belen: siete ogni giorno la mia fonte di energia attraverso l'affetto, l'entusiasmo e le passioni che mi sapete trasmettere. Tutti voi (e con tutti, intendo proprio tutti!) avete avuto un peso determinante nel conseguimento di questo risultato, punto di arrivo e contemporaneamente di partenza della mia vita. Grazie per aver condiviso con me in questi anni le esperienze più importanti. Vi voglio bene,

Eleonora

Abstract

Hydrogen energy technology allows the production of electricity from hydrogen and backward to store large amounts of energy by converting electricity into hydrogen, using a fuel cell, an electrolyzer, and a hydrogen storage system. The fuel cell market is increasing, offering components with improved converting performances; the expansion of this market and the spread of hydrogen system applications are bringing down the industrial costs of such technology offering new opportunities for commercial applications. This work concerns the Polymer Electrolyte Membrane technology, giving a complete overview of opportunities and problems that may arise from the employment of this type of system for maritime applications. The starting point of the analysis follows a more theoretical approach. Performance and degradation issues have been deeply investigated through thorough literature analysis, to issue the main problematics that can appear in the real operation of the PEM fuel cell system. In this context, a degradation map has been drawn, which can help the prediction of voltage degradation linked to the poisoning of the cell components. Therefore, since the external parameters that can influence the FC performance are highlighted, a statistical approach is investigated to understand how the reactants' flow rates and the thermal control can affect the performance. This has been possible thanks to the employment of the software Design Expert.
In the second part of the Thesis, a more experimental approach to the thematic of PEM fuel cell systems for maritime applications is faced. This has been possible thanks to the test campaign carried out on the HI-SEA system, a 240-kW system located in the IES Laboratory of the University of Genoa (Savona Campus), made up of eight Polymer Membrane Fuel Cell modules supplied by Nuvera. This is one of the few complete and existing real-size laboratories for the assessment of PEMFC technology for maritime applications. The laboratory activities are part of the collaboration between the University and Fincantieri, the main Italian shipbuilder. The system has undergone a commissioning phase, which is accurately described, where previous issues are analyzed, understood, and solved to optimize the control system. Therefore, despite a prolonged inactivity time, the PEM fuel cell stacks have been reactivated thanks to a dedicated and innovative procedure. Finally, the system is fully operative: the results of the whole system operation confirm its suitability for operation in a ship-likely environment.

Index

Index of Figures

Index of Tables

Acronyms and symbols

Acronyms

ABS	American Bureau of Shipping
AD	Alternative Design
AFC	Alkaline Fuel Cell
ANOVA	Analysis of Variance
APU	Auxiliary Power Unit
AST	Accelerated Stress Test
BER	BluEnergy Revolution
BoL	Beginning of Life
BoP	Balance of Plant
CCD	Central Composite Design
CCS	Carbon Capture and Storage
CL	Catalyst Layer
CNR	Italian National Research Centre
CS	Classification Society
CVM	Cell Voltage Monitoring
DE	Design Expert
DMFC	Direct Methanol Fuel Cell
DoE	Design of Experiment
DOE	Department Of Energy
ECA	Emission Control Area
EIS	Electrochemical Impedance Spectroscopy
EMSA	European Maritime Safety Agency
EPA	Environmental Protection Agency
FAT	Factory Acceptance Test
FC	Fuel Cell
FCEV	Fuel Cell Electric Vehicle
FCM0i	Fuel Cell Module-i (i from 1 to 8)
FCS	Fuel Cell System
GDL	Gas Diffusion Layer
GHG	Green House Gases
GWP	Global Warming Potential
HHV	Higher Heating Value
HI-SEA	Hydrogen Initiative for Sustainable Energy Applications
HMI	Human Machine Interface
HO	Hydroxyl radicals
HOO	Hydroperoxyl radicals
HOR	Hydrogen Oxidation Reaction
HT-PEMFC	High-Temperature Polymer Electrolyte Membrane Fuel Cell
ICE	Internal Combustion Engine
IES	Innovative Energy Systems

IMO	International Maritime Organization
JRC	Joint Research Centre
LLT	Long-Lasting Test
LSD	Least Significant Difference
MANOVA	Multivariate Analysis of Variance
MEA	Membrane-Electrode Assembly
MFC	Mass Flow Controller
MH	Metal Hydride
MISE	Ministero per lo Sviluppo Economico
MOS	Manual Override Switch
MS	Mean Squares
OCV	Open Circuit Voltage
ORR	Oxygen Reduction Reaction
PAFC	Phosphoric Acid Fuel Cell
PEMFC	Polymer Electrolyte Membrane Fuel Cell
PLC	Programmable Logic Controller
PMS	Power Management System
PSA	Pressure Swing Adsorption
P&ID	Piping and Information Diagram
RA	Risk Assessment
RE	Reduction Effect
RES	Renewable Energy Sources
RH	Relative Humidity
RMS	Root-mean-square
RSM	Response Surface Methodology
SMR	Steam Methane Reforming
SoA	State of Art
SOFC	Solid Oxide Fuel Cell
SoH	State of Health
SS	Sum of Squares
SU-SD	Start Up-Shut Down
TA	Type Approval
TAC	Type Approval Certificate
TPB	Triple-Phase Boundary
TPG	Thermochemical Power Group
TRL	Technology Readiness Level
UPS	Uninterruptible Power Supply
VDR	Voltage Degradation Rate
ZEUS	Zero Emission Ultimate Ship

Symbols

α_a	Anodic apparent transfer coefficient
α_c	Cathodic apparent transfer coefficient

η_{el}	Electrical efficiency of the system
η_{th}	Thermal efficiency of the system
μ	Treatment
b	Tafel-slope coefficient
c_{HR}	Cooling fluid specific heat
C_{conc}	Contaminant concentration
C_D	Coulomb density
e^-	Electron
E	Reversible potential
$E^0{}_T$	Standard potential for the cell reaction at T temperature
F	Faraday's constant
$g^0{}_f$	Gibbs free energy
H_0	Null hypothesis
i	Observed current density
i_0	Exchange current density of the anodic reaction
I_D	Current density
$\dot{m}_{HR}$	Cooling fluid mass flow
n	Amount of exchanged electrons
p	Partial pressure
P	Pressure
P_{HR}	Recoverable thermal power output
P_{in}	Total power input to the system
P_n	Net electrical power generated by the system
ppm	Part per million (per volume unit)
QM	Air mass flow rate
R	Universal gas constant
$R^{protonic}$	Protonic resistance
T	Temperature
T_{st}	Stack temperature
TT	Cooling temperature
V	Voltage
$V_{Activation}$ or η_{act}	Activation losses
V_{after_test}	Cell voltage after a stress test
V_{avg}	Average Cell Voltage
$V_{baseline}$	Initial cell voltage
V_{cell}	Cell voltage
$V_{Concentration}$	Concentration losses
V_{max}	Maximum Cell Voltage
V_{min}	Minimum Cell Voltage
V_{cell}^{N}	Cell voltage after N cycles
V_{cell}^{N-0}	Cell voltage at N cycles = 0
V_D	Percentage voltage decay
V_{DR_avg}	Average Voltage Decay

V_{Nernst}	Nernst potential
V_{Ohmic} *or* η_{ohmic}	Ohmic losses

Polymer Electrolyte Membrane Fuel Cells for maritime applications: state of art of the technology, experimental assessment of a 240-kW system, and Response Surface Methodology application to data analysis

1. Introduction

1.1. Background and Motivation

The current trends in energy supply are not sustainable, from the economic, environmental, and social points of view. Green House Gases (GHG) emissions have been continuously growing since the first industrial revolution, and even more stiffly since World War II. Without taking decisive action, GHG emissions are even foreseen to continue the current increasing trend and be more than double 2019 values by 2050 [1]. Carbon dioxide is the most known gas found in the exhaust flow from the use of fossil fuels for different purposes; its greenhouse potential effect is lower than the one of other gases (such as methane), but it is usually taken as a reference to measure the emission trends of the countries and the source fields. In fact, CO_2 is taken as a reference in the assessment of the impact of other polluting gases on the greenhouse effect through the Global Warming Potential (GWP), an important indicator of the environmental impact of a given substance. It is the ratio between the impact caused by a gas in a given time, compared to that caused in the same period by the same amount of carbon dioxide (CO_2), which is the reference gas and therefore has a value of 1. The higher the value of the GWP index, the greater the incidence of gas in global warming. As reported in Table 1, methane (CH_4) has a GWP index of 28; this means that the amount of methane released into the atmosphere is 28 times more polluting than the same amount of carbon dioxide (CO_2).

Table 1: GWP index computed on 100 years.

Substance	GWP100
CO_2	1
CH_4	28
N_2O	265
CFC-11	4600
CFC-13	13900

The emission trends shown in Figure 1 describe the annual total CO_2 emissions divided by world region from 1750 to 2019 [https://ourworldindata.org/].

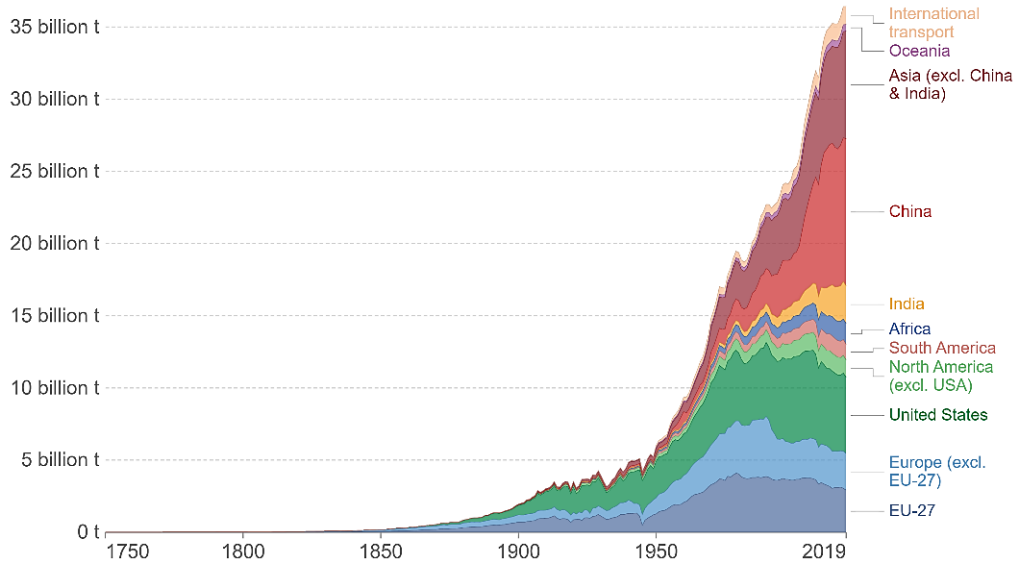

Figure 1: Annual total CO_2 emissions by world region from 1750 to 2019 [https://ourworldindata.org/].

It is possible from Figure 1 to define – from the highest to the lowest – China, the United States of America, and Europe as the biggest emitters when the local CO_2 emissions are considered. Considering however that the production processes can be associated with goods destined for exports, the consumption-based CO_2 emissions can be adjusted for trade, as represented in Figure 2 [https://ourworldindata.org/]. In this case, it can be evidenced that Mongolia, North America, and Saudi Arabia are associated with the largest per capita emissions.

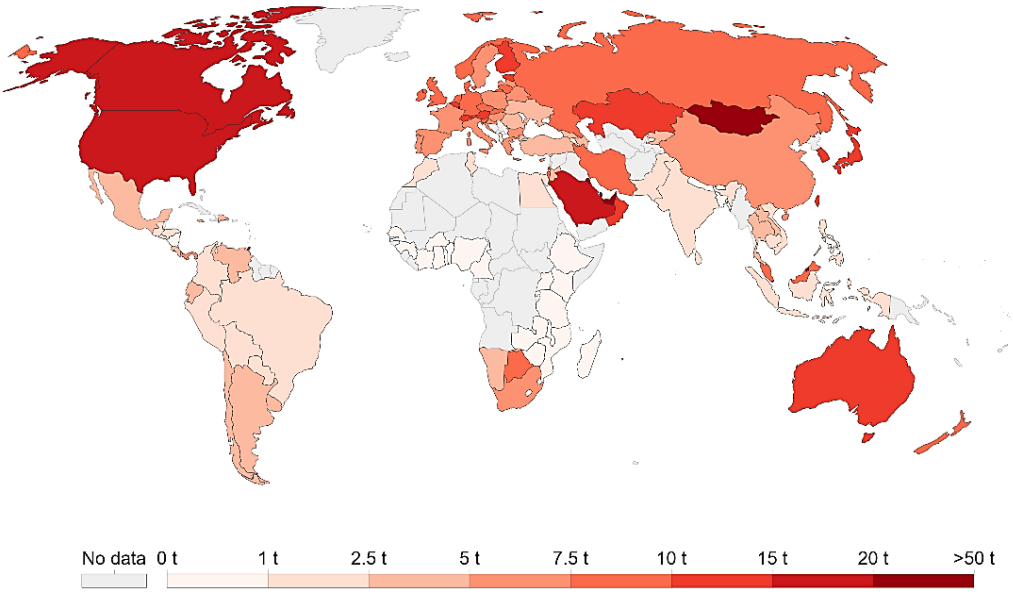

Figure 2: Per capita consumption-based CO_2 emissions in 2019 [https://ourworldindata.org/].

The main concern about the presence of GHG in the atmosphere is linked to their climate-altering effect: anthropogenic emissions are indeed the cause of the temperature anomalies measured across the globe, that have recently been rising in frequency and intensity.

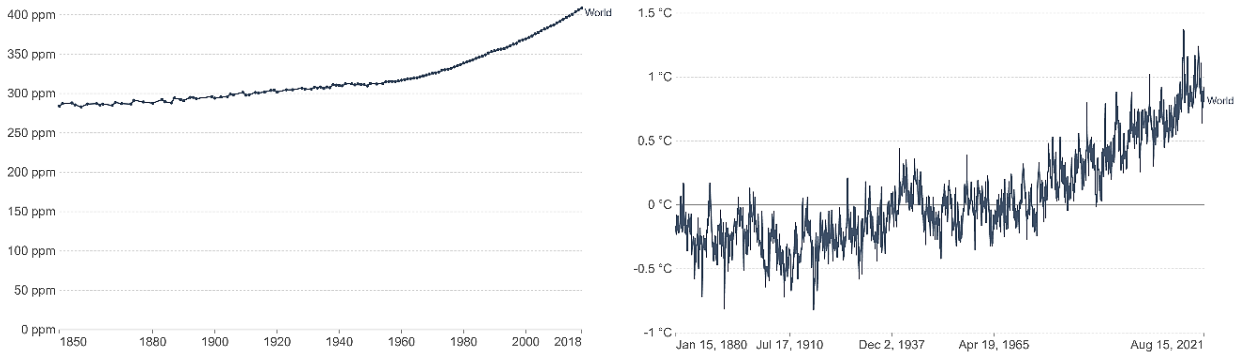

Figure 3: Increasing trend of the atmospheric CO_2 concentration and monthly temperature anomalies registered from 1850 to 2018 [https://ourworldindata.org/].

From the Industrial Revolution to the present day, the world's energy needs have indeed grown exponentially. In the last ten years, primary energy consumption has grown by 1.5% every year, except in 2019 which grew by 2.9%, about twice as much [2]. At the same time, even nowadays, in Italy and the European Union over 80% of primary energy is obtained from fossil sources (coal, oil, and natural gas). Experts believe that the opportunity to reverse the emissions trends relies on the exploitation of Renewable Energy Sources (RES) [3] that nevertheless are not controllable and difficult to be stored. For this reason, huge efforts are made in the development of energy storage systems worldwide [4]. Meanwhile, different players are taking actions to limit the emissions linked to the different fields, which are mainly divided into energy, industry, waste, agriculture, forestry, and land use. Each sector has its impact in terms of GHG emissions; data referred to the year 2019 are reported in Table 2.

Table 2: Global GHG emissions referred to the origin sector in 2019.

Sector	**Global GHG emissions**
Energy (electricity, heat, and transport)	73.2%
Agriculture, Forestry, and Land Use	18.4%
Direct Industrial Processes	5.2%
Waste	3.2%

As the world's energy demand is related to the most emitting sector and it is constantly increasing, it is crucial to find a solution to compensate for the emissions associated with the energy production. In this context, around 24% of global GHG emissions linked to the energy sector are due to transport, considering the different contributions (road, aviation, shipping, and rail) depicted in Figure 4. Road vehicles alone (passenger and freight) account for 74.5% of CO_2 transport emissions.

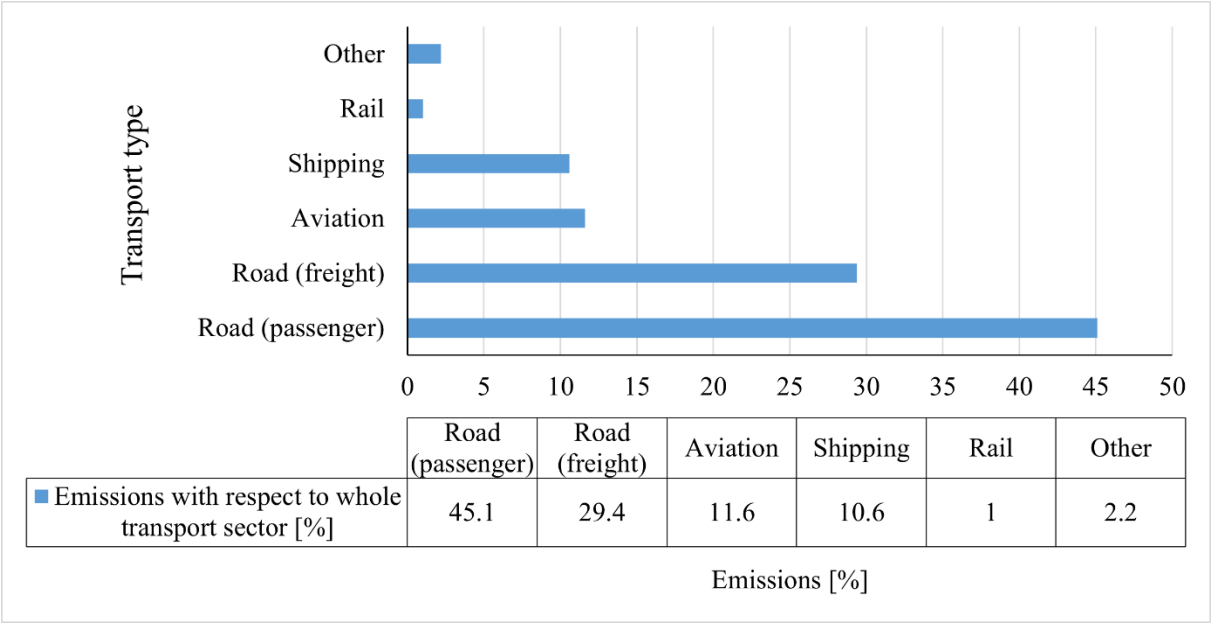

	Road (passenger)	Road (freight)	Aviation	Shipping	Rail	Other
Emissions with respect to whole transport sector [%]	45.1	29.4	11.6	10.6	1	2.2

Figure 4: Global CO_2 emissions from the transport sector in 2018 [https://ourworldindata.org/].

However, many solutions exist nowadays that allow full electric or hybrid propulsion and could substitute the more traditional internal combustion engines in the various transport technologies. The transition to electric propulsion could ensure the reduction of current emissions by the transport sector and contribute to the accomplishment of 2030 and 2070 targets established by the European Community and deal with the objectives of the Paris Agreement [5].

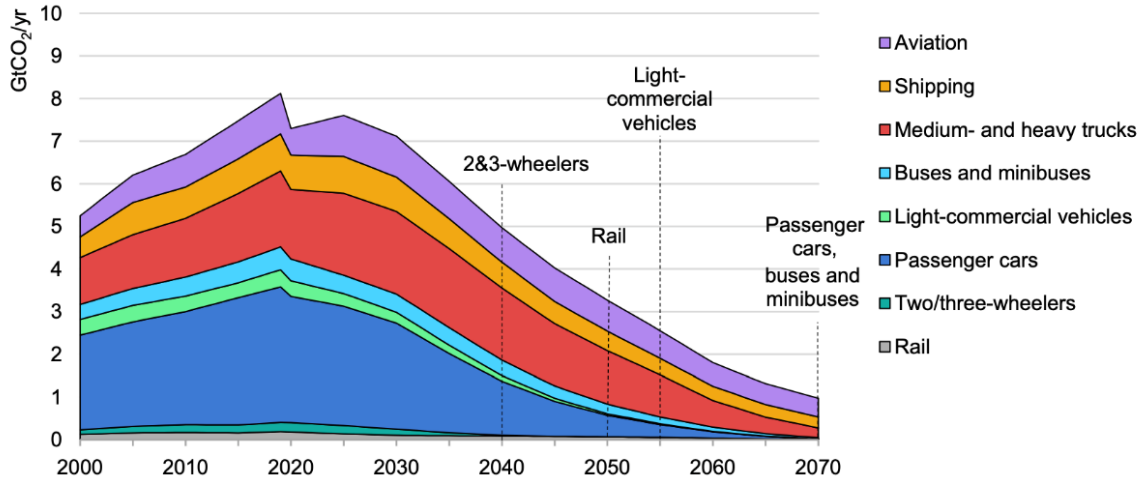

Figure 5: Global CO_2 emissions in transport by mode in the IEA's Sustainable Development Scenario, 2000-2070.

As regards in details the shipping field, the International Maritime Organization (IMO), a specialized agency of the United Nations, composed of 173 Member States, responsible for regulating the safety, security, and environmental performance of international shipping, has established strict objectives for the emissions deriving from the international navigation [6].

The IMO's long-term targets for emissions in the shipping sector, depicted in 2018 in the first initial quantitative GHG reduction strategy for international shipping, include: (i) cut emissions due to transport work by at least 40% and 70% respectively by 2030 and 2050, compared to 2008 levels; (ii) reduce total annual GHG by at least 50% by 2050, compared to 2008 levels [7]. The document underlines the relevance of the topic as well as the significant potential of cost-effective decarbonization for the sector. The emissions are in fact otherwise expected to increase significantly during the next 30 years: the American Bureau of Shipping (ABS) foresees a 250% increase in emissions by 2050 due to international shipping under the current scenario, considering the projections regarding the growth of this sector [8]. Hence, the interest in alternative low-emission power systems is growing, to reach the objectives set by the IMO, to avoid the increase in emissions from shipping foreseen under a business as usual scenario [9], and to comply with the terms of the Paris Agreement [10].

Indeed, a consistent percentage of pollutants such as NO_x, SO_x, CO_x, and CH_4 derives from international shipping, for a total impact of around 3% on global GHG emissions, making maritime transportation among the top 10 emitters [11], according to the IMO. In recent years, shipping emission regulations have changed significantly, mainly regarding what concerns Particulate Matter, SO_x, and NO_x [7,12,13]. Since 2020, SO_x maximum content in terms of weight in the fuel has been set to 0.5% (the previous limit of 3.5%), with a further limitation of 0.1% in Emission Control Areas (ECA). As far as NO_x emissions are concerned, ships built after 2016 must comply with the TIER 3 limit in ECA, which means a reduction from 14 g/kWh to 4 g/kWh in case of navigation at low rated engine speeds (<150 rpm). These limitations are no longer reachable with traditional diesel engines and bunking fuels [14]; this perspective highlights the need to take decisive actions in the maritime field, to investigate the use of alternative fuels and zero-emission electric generators onboard. Therefore, the interest in hydrogen as an energy carrier for zero-emission solutions has been growing significantly.

1.2. Hydrogen potential as an energy carrier

Hydrogen is the most abundant element in the Universe. It constitutes almost 90% of the visible mass of the Universe itself. It is the simplest and lightest element of the periodic table (H_2) as it is made up of a proton and an electron. Although it is the most abundant element, in nature hydrogen occurs in the form of a molecule and is hardly found in the free state; in fact, it is found in large quantities in water (H_2O) and hydrocarbons, therefore bound to carbon atoms. Thus, to obtain it, it is necessary to separate it from the matter in which it is present by providing energy that favors the separation process and therefore supports an economic and environmental

cost. Given that hydrogen is not found alone in nature and that a contribution from another type of energy is required to obtain it, hydrogen is considered an energy vector and not an energy source as are solar and wind power. It is a low density, colorless, odorless, non-toxic, and easily flammable gas. An aspect that should not be underestimated in the flammability of hydrogen is that, when it burns, it is characterized by a very hot and pale flame, so much so that it is almost invisible in sunlight. The flammability range of hydrogen is considerably higher than other fuels; in fact, for hydrogen, the percentage by volume of the flammability limits varies from 4% to 75%, compared to the flammability limits of methane (CH4), which are between 5.3 and 15%, and of petrol, between 1.0 and 7.6%. Reported in Figure 6 are the flammability range differences with the more common fuels (Propane and Methane). Therefore, it is necessary to take into account that the transport and storage of hydrogen, due to the wide flammability range, constitute a high-risk factor.

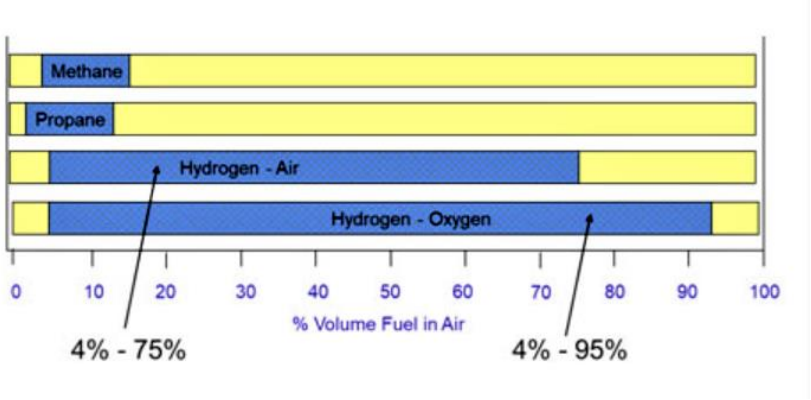

Figure 6: Hydrogen flammability range [https://wha-international.com].

From the energy point of view, hydrogen has a high energy density per unit of mass: one kilogram of hydrogen contains 142 MJ of energy, against the approximately 56 MJ contained in natural gas, approximately 46 MJ in petrol, and diesel, and about 32 MJ in coal. This property certainly makes it more efficient than conventional fuels. On the contrary, however, at room temperature hydrogen has a low energy density per unit of volume. In Section 1.3, the current storage methods necessary to overcome this problem will be explained.

Hydrogen represents one of the most promising energy vectors for the storage of RES [16,17] as well as one of the most promising fuels for marine applications [18,19], while fuel cells have proven to be a potential power generation technology suitable for such application [12]. Thanks to benefits linked to the use of FCs, this market has increased from 24,600 units in 2011 to 78,000 in 2012 [20], up to a global FC market size valued at USD 3.21 billion in 2016, with an expansion projection of 20.9% from 2019 to 2025. The spread of hydrogen systems applications is bringing down their industrial cost [21], opening new market opportunities in the transport

sector. Regarding Polymer Electrolyte Membrane FCs, the US Department of Energy (DOE) targeted a dramatic reduction of the FCs production costs during the last years, which was supposed to approach 40$/kW in 2017 [22–24]. This target was not fully reached but close, as, eventually, the price of a PEMFC system was around 45$/kW in 2017 for automotive systems. The research by Whiston et al. in reference [25] compared – in 2019 – the experts' opinions about the PEMFC system's cost with DOE target and estimations for the next future.

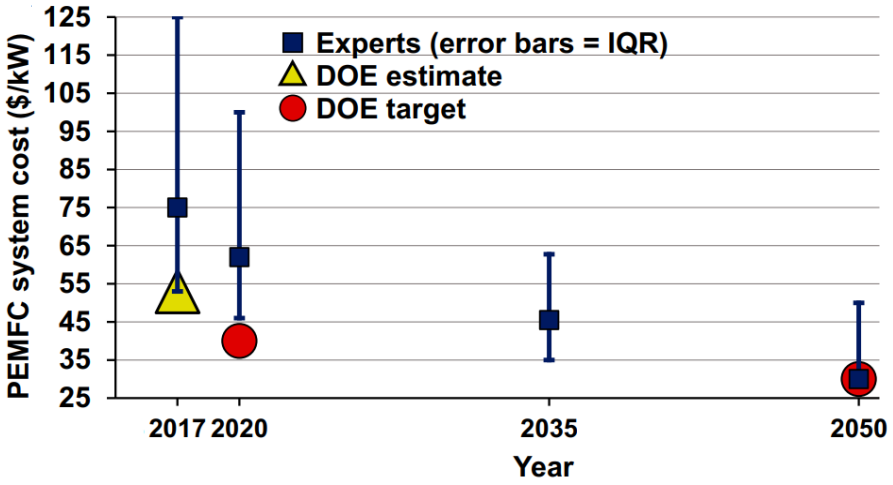

Figure 7: Experts' assessments of PEMFC cost and performance in 2017, 2020, 2035, and 2050 [25].

Even if hydrogen is the most abundant element in the universe, pure hydrogen is a scarce resource on the planet. It, therefore, needs to be extracted from other compounds – with a non-negligible energy consumption – such as water, fossil hydrocarbons like methane and organic compounds, hydrogen sulphide, etc [26]. It is convenient – while it also lowers the global lifecycle emissions – to employ energy for hydrogen extraction from renewable sources like wind power[27], OTEC [28], or even some studies proposed to implement supercritical water gasification of almond shell [29]. In this context, hydrogen is in fact considered an energy carrier. RES energy is stored in the form of this molecule, produced by the water electrolysis process, and therefore employed pure in a FC or mixed with other components (in the form of ammonia, methanol) in Internal Combustion Engines (ICE). The hydrogen produced by a water electrolysis process powered by RES is commonly called "green hydrogen". Although only 5% of world hydrogen production occurs by electrolysis, the following process allows obtaining 99.95% pure molecular hydrogen. The only process that may be necessary to use the hydrogen produced by electrolysis (i.e., in a PEM fuel cell) is dehumidification, to remove the water content that may remain residual in the gas.

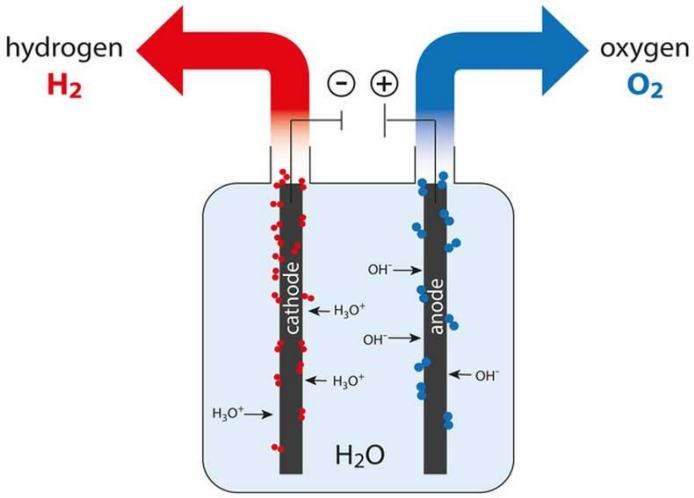

Figure 8: Schematic of the water electrolysis process [https://www.thyssenkrupp.com].

Otherwise, the gas can be produced by Steam Methane Reforming (SMR), combining high-temperature steam with natural gas to extract hydrogen: this is in fact the most common method in the US nowadays [22]. Despite the high production cost of hydrogen, though, several LCA (LifeCycle Assessment) studies proved the advantages in terms of cost and emissions of FC vehicles (FCV) compared to gasoline ones during the entire lifecycle, including the fuel production phase [22,30–35]. Moreover, the research developed by Ahmadi et al. in 2015 [32] found the most favorable economic results for hydrogen production using SMR, for which abundant domestic and currently inexpensive natural gas is used as the energy source. Having advantages such as low cost, high efficiency, and an easily manageable feedstock, steam methane reforming is nowadays known as the most common process for hydrogen production. Nevertheless, the emissions associated with this production method are not negligible and should be handled in a dedicated process stream, while the hydrogen produced should be purified to reach the standards for FC applications. The latter is in particular very strict in the case of PEM fuel cells (99.995% purity is required).

1.3. Hydrogen storage opportunities

A key part of the direct hydrogen use in an energy production system is hydrogen storage: a wide range of storing methods is being considered to find a compromise between energy density, weight, energy efficiency, and cost of the technology. In the case of hydrogen applications in the propulsion sector, for example, the storage volume would be significantly higher than the one occupied by traditional fuels, which entails a greater bulk and greater weight. This aspect, therefore, prevents the storage of hydrogen at room temperature and atmospheric pressure. To overcome the problem, the scientific community is engaged in the

search for light, space-saving, inexpensive, and above all safe tanks for storage onboard mobile applications and rapid refueling at a service station. Mainly, hydrogen can be stored:

- In the compressed gaseous state.
- In the liquid state.
- With metal hydrides.
- With hydrogen carriers.

Table 3 shows the most indicative performance parameters of the various storage systems to determine the best technology available on the market.

Table 3: Performance parameters of the different hydrogen storage technologies.

		Pressure [bar]	**Temperature [°C]**	**Energy/Volume (MJ/m^3) [kWh/m^3]**	**Energy/Weight (kJ/kg) [kWh/kg]**
Compressed H_2		200	14.85	(1158.93) [321.93]	(1559.84) [0.43]
		350	14.85	(2492.15) [692.26]	(8039.20) [2.23]
		700	14.85	(3599.64) [999.90]	(7199.28) [2.00]
Liquid H_2		1	-252.75	(3999.56) [1110.99]	(8999.10) [2.50]
Metal Hydrides	**MgH_2**	1	14.85	(12838.7) [3566.3]	(9599.04) [2.67]
	$LaNi_5H_6$	1	14.85	(13798.6) [3832.9]	(1799.82) [0.50]
	$NaAiH_4$	1	14.85	(11398.8) [33166.3]	(9599.04) [2.67]
Hydrogen carriers	**NH_3**	6	14.85	(17351.35) [4819.8]	(21237.88) [5.90]

The simplest and cheapest way to store hydrogen is to use it in the form of compressed gas at pressures of 200-250 bar and above. Compressed hydrogen cylinders represent the simplest transport system for storing gas but are limited by the fact that hydrogen requires very large tanks, up to ten times larger than those of gasoline [36]. However, traditional steel cylinders represent a technology that cannot be used for storage onboard land propulsion systems, due to their excessive weight and their considerable bulk. Furthermore, steel embrittlement must be considered; at high pressures, the hydrogen molecule could dissociate, allowing the atomic hydrogen to diffuse into the steel. This would lead to a weakening of the metal due to a decrease in the ability to deform plastically making the steel subject to sudden fractures. For these reasons, significant progress has recently been made with the introduction of tanks with a metal or thermoplastic structure reinforced with carbon or glass fibers. The advantage is due to the weight reduction of almost 40% compared to common tanks. The latter can operate in a range of pressures between 350 and 700 bar, allowing for higher and adequate accumulation densities for use onboard vehicles.

To avoid large storage volumes, liquid hydrogen can be used, which occupies a volume smaller even than methane. Although this technology is the best to meet the needs in the propulsion field, it has limitations. The main problem concerns the liquefaction temperature (-253 °C). To reach this temperature, a great deal of energy is required, and special cryogenic tanks are needed to guarantee safety standards and adequate thermal insulation. For this reason, the most modern tanks for liquid hydrogen consist of two or more layers of very resistant steel between which a vacuum is created, ensuring the right strength in the event of an accident. Liquid hydrogen, in addition to the complexity of the system, has a high cost not to be neglected. The energy and economic cost of hydrogen liquefaction correspond indeed to about 30% of the energy content of the fuel, compared to about 8% of compressed hydrogen.

Metal hydrides are special metal alloys capable of absorbing quantities of hydrogen through a reversible reaction. The main metal hydrides belong to two broad categories: binary magnesium alloys and multinary alloys, which include the Alanate family (aluminum Al compounds). Metal hydrides are formed and act through two phases: the absorption and release of hydrogen. The first phase, called hydrogenation, is an exothermic process that requires low temperatures, while the second phase, called dehydrogenation, is an endothermic process that requires heat. During the hydrogenation phase, the hydrogen molecule dissociates on the surface of the alloy, and the hydrogen atoms are deposited in the interatomic space of the metal forming a solid solution (α phase). With the increase in the concentration of hydrogen in the metal in the coexistence region of the two phases, the interaction between the hydrogen atoms allows the growth of the hydride phase (phase $\alpha + \beta$). This process is usually represented in a PCT diagram, that shows the link between Pressure, hydrogen Concentration (given as mass percentage with respect to the metal weight), and Temperature in the hydride. As shown in Figure 9, while the two phases coexist, the isotherms show a flat zone of length proportional to the amount of hydrogen that can be reversibly stored. During the transformation of the metal into hydride (phase β), further additions of hydrogen rapidly increase the pressure thus making it possible to completely absorb the hydrogen in the metal. In the dehydrogenation phase, by providing a certain amount of heat, the chemical bond between the hydrogen and the alloy is broken, thus favoring the release of pure hydrogen. The release is usually never complete, and part of the hydrogen amount stored is not recovered.

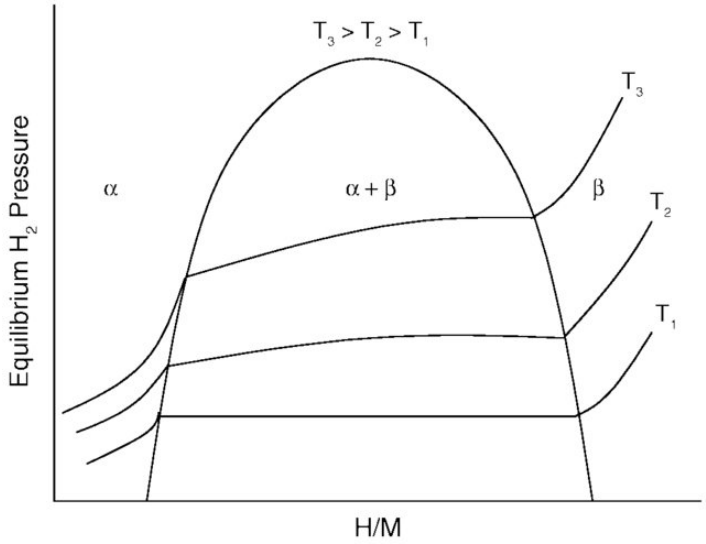

Figure 9: Typical PCT activity diagram for a metal hydride system at various temperatures [37].

Metal hydrides have recently been studied to exploit the waste heat coming from the use of PEM fuel cell systems in different applications. Indeed, the waste heat can be recovered and employed, via the cooling circuit, to enhance the hydrogen release reactions inside the tanks that contain the metal powder. Therefore, the hydrogen released can be employed as the reactant flow to the FCS. In this way, a compact, low temperature, and pressure storage system can be exploited on applications that require a high-safety level – such as onboard ships [38,39].

To overcome the difficulties inherent in the transport and storage of hydrogen, chemical hydrides, or chemicals rich in hydrogen, could also be exploited. These compounds, unlike metal hydrides, are unable to obtain and release hydrogen reversibly. Once dehydrogenated, the chemical hydrides must undergo a process of hydrogenation again; this requires the activation of a closed and complex circuit which foresees the return to the factory of the exhausted product to be recycled. Nevertheless, the use of chemical hydrides maintains several interesting aspects. Being rich in hydrogen, they can be used for local and seasonal storage, if there is a lack of energy at certain times of the year. Furthermore, the use of these chemical systems makes it possible to use existing infrastructures for transport and storage. Among chemical hydrides, ammonia (NH_3) has a strong relevance due to the high hydrogen amount per weight unit that can be stored in it.

1.4. Hydrogen Fuel Cells for the maritime field

During the last years, the shipping field has become interested in hydrogen technologies; nevertheless, at the moment, a specific fuel cell type for maritime applications is not available, and it therefore must be chosen among the existing typologies.

However, the use of such a technology for shipping gains relevance to reach the emission targets set in 2030 and 2050, as described in Section 1.1, and becomes crucial to allow navigation in the Emission Controlled Areas. In fact, besides the established ones, many others are now under consideration, and many shipping critical ports may soon lie in these areas depicted in Figure 10.

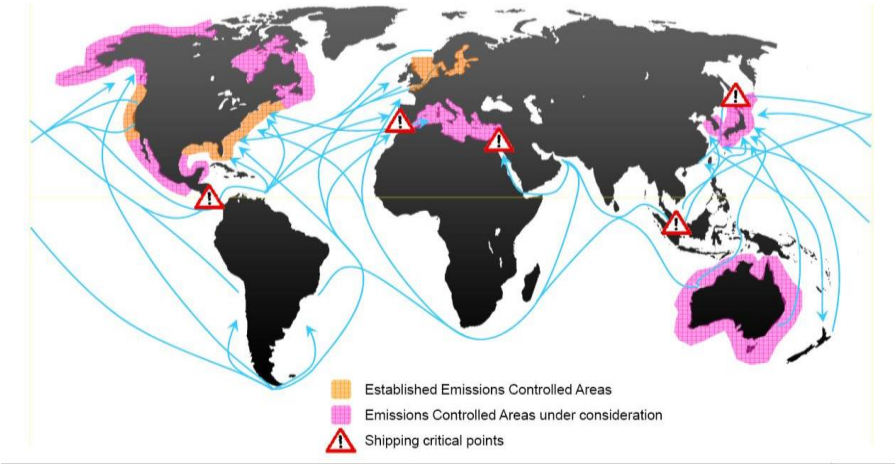

Figure 10: Established and under consideration Emission Control Areas (Source: Lloyd Register).

To generate energy, the unit constituted by the fuel cell must be integrated into a complete system that includes a section of the fuel and air, a system for recovery of the heat developed, and finally a section of regulation and control. For the generation system to be installed onboard there are several alternatives, depending on the choices made concerning the fuel (hydrogen, methanol, or gasoline) and the configuration of the propulsion system. For performing a dedicated risk assessment of fuel cells for maritime application, and therefore to choose among the FC technologies available, a selection of the most promising typologies was created by the European Maritime Safety Agency (EMSA) [40]. A list of the most relevant parameters to be taken into account in this choice was developed:

- Relative cost to other fuel cells.
- Power levels [kW] for the largest available module (which then can be grouped into larger systems).
- Lifetime.
- Tolerance for cycling.
- Flexibility towards the type of fuel.
- Technological maturity.
- Physical size.
- Sensitivity for fuel impurities.

- Emissions.
- Safety aspects.
- Efficiency (Electrical and total including heat recovery if applicable).

Based on these criteria, the fuel cell technologies were evaluated (AFC, PAFC, MCFC, SOFC, PEMFC, HT-PEMFC, and DMF). The above criteria were chosen because they are considered to be vital for evaluating if a fuel cell technology is suitable for maritime use in the near future, and for comparing different technologies. Safety is in fact one of the major issues when it comes to marine use of technology, and safety aspects are fully treated in the work developed by EMSA. The PEMFC technology was the one receiving the highest score in the ranking, despite its sensitivity to impurities in the hydrogen as sulfur and CO, a complex water management system (both gas and liquid), and a moderate lifetime. Therefore, different studies were raised for evaluating its employment in the maritime field.

The most recent publications have underlined the feasibility and the potential of PEMFC technology on maritime applications, also compared to traditional diesel engines and batteries, opening the path to optimization and modeling studies of hybrid systems as well [23,24,41,42]. Nevertheless, the bibliography offers very few examples of real-scale testing of FC systems, especially in test rigs that simulate the operation in a ship-like environment. This underlines the relevance of laboratories such as the HI-SEA one, described in this Thesis, which has proven the feasibility of PEMFC systems for shipping applications, offering as well interesting results that can lead shipbuilders during the choice of the commercially available technologies and the system design phase [43–45].

PEM Fuel Cell Systems appear attractive for the maritime field in terms of both emissions reduction and extended operative ranges with good efficiencies [46–48]. The use of PEMFC for passenger's vessels guarantees very low noise and vibrations, compared to traditional marine engines [49]. Compared to high-temperature FCS (such as Solid Oxide Fuel Cells, SOFC), the use of PEMFC has other advantages, such as zero CO_2 emissions (as they are fuelled by pure H_2), fast dynamics, and higher Technology Readiness Level (TRL), as many commercial products are already available on the market [50–53]. Two examples of PEMFC-powered vessels should be mentioned: the first one is the Zero Emission Ultimate Ship (ZEUS), a research vessel under construction by Fincantieri, the main Italian shipbuilder. The propulsion system integrates a 140-kW PEMFC system, batteries, diesel engines, and a hydrogen storage system based on metal hydrides technology. The heat flux removed by the FCS will be employed for the enhancement of hydrogen release from the metallic powder, making this vessel the first existing example of this system-integration solution. The second one to be

mentioned is the Nemo H2 vessel, already in use in 2010 in Amsterdam. It was the very first example of an FC-powered vessel, with a 70 kW size and compressed hydrogen storage (350 bar), able to carry up to 80 people during 9 hours of navigation.

Feasibility studies on the use of PEMFC for maritime applications have been investigated in recent literature works by many authors [54–57], also considering behavior in dynamic conditions [38,58] and hybrid configurations including batteries [59,60]. Some authors focused on multi-criteria approaches to compare PEMFC systems with diesel engines, highlighting the potential advantages of PEMFC on traditionally employed technologies [61,62]. Thanks to their advantage in terms of noise and vibrations, PEMFC technology is attractive also for submarines and underwater vehicles, as reported in recent studies [63–65]. Depending on the size of the vessel, PEMFC can be used for powering propulsion or as Assistant Power Units (APU) for covering the hotel load. Figure 11 shows the most suitable use of a PEM fuel cell system considering the size and cost of the vessel, in the vision of Fincantieri.

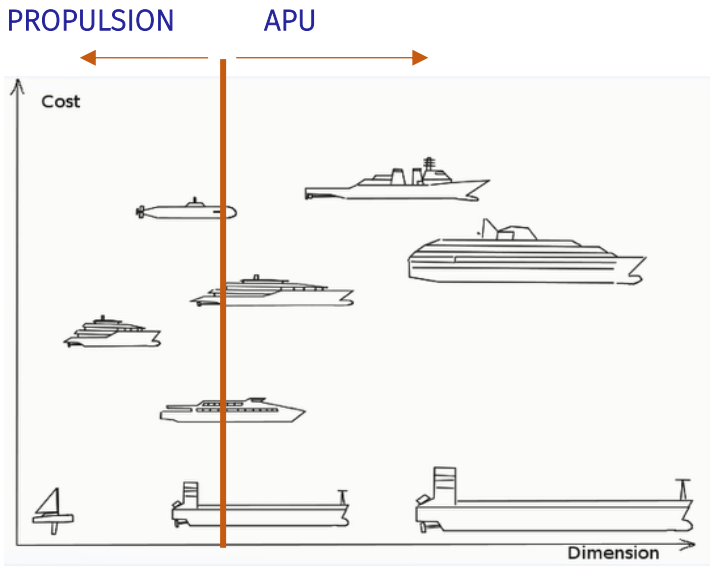

Figure 11: Use of PEMFC systems for propulsion or as APU depending on vessel type.

1.5. General legislation for FCS

The use of alternative fuels onboard ships has become crucial to decrease navigation's strong impact on the environment. In this context, hydrogen is one of the most promising fuels for marine applications [18,19], and PEMFC can be a promising technology to be employed for propulsion [23,24,40,54,57,62,66], also coupled with batteries. Of course, it is crucial to evaluate the best hydrogen storage technology, to increase the practicable navigation distance. Many research projects have deepened the topic of experimental PEMFC systems for maritime applications [43,44], but the absence of shared international legislation specific to fuel cells on marine vessels can create issues in the design phase of real-scale systems. Indeed, the IMO has

not made available any guidelines yet for the installation of FCS on marine vessels, nor guidelines for the Type Approval Test (TA), which is the totality of the tests that an FCS should withstand to obtain a Type Approval Certificate (TAC). For this reason, the dedicated Section 4.1 of the Thesis – which describes part of the work carried out inside the European Project FC-PROMATE (FC TEsting PROtocols for Maritime applications) and of the national research project TecBia (*Technologies at low environmental impact for energy production on ships*), financed by Fincantieri-Isotta Fraschini Motori S.p.A. and Italian Ministry of Economic Development (MISE) as part of "National Operational Programme (PON) 2014/2020 Large R&D Projects" [67] – aims to define a testing routine which can be crucial to carry out a technical comparison between different commercial PEMFC systems and to evaluate their suitability for shipping installations. Starting from the legislations available for fuel cell installations and from the aspects related to naval environment regulations, the main aspects to be checked via the testing protocols have been individuated by the Author. This operation can lay the foundations of a future and specific international standard, defining the experimental steps necessary to assess the suitability of FC stacks for shipping requirements.

Nowadays, as a dedicated regulation does not exist, every integration process of Fuel Cell and hydrogen systems must follow the Alternative Design procedure (AD), a general procedure based on Risk Assessment (RA) that allows the introduction of limited and unregulated variants within the project if they demonstrate, through the RA, a level of security equal or higher than the one required by the regulations for traditional design. To proceed with an objective evaluation of the performance of FCS, it is therefore not possible to refer to any internationally recognized technical document. It is consequently necessary to carry out an analysis of the regulations and available standards published by Classification Societies (CS) and standardization (ISO, IEC) recognized at the European (EU) and national levels. Indeed, while international legislation is expected in the next future, the CS such as the Italian Naval Register (RINA) are equipping themselves with internal rules that define the safety requirements that FC systems must comply with to be installed onboard.

To consider in the broadest but most precise way possible both the aspects related to the naval legislation (as for the environmental conditions) and those related to the rules and standards of FC technology (as regards the operational conditions), the Author has reviewed and accounted the existing regulations of the CS and the standards related to fuel cells, in particular:

- IACS UR-E10: it defines the test specifics for the TA of electrical systems.
- RINA-FC: it is specific for FCS and gives important guidelines for their installation onboard ships, citing the IEC 62282 as a reference for the TA.

- RINA RULES, PART C: these regulations referred to all the machinery, electrical installations, and the automation installed on board; it has also been used as a guideline for the design of the test stations, and it has provided multiple indications and specifications of completion to the IACS UR-E10.
- IEC 62282: it describes the TA for FCS for the installation in stationary, portable, micro, and vehicle applications.

The latter has been considered also for what concerns the environmental conditions – vibrations, temperature, and wind) – which the FCS should withstand, comparing these conditions to the ones applicable to APU on heavy-duty transport installations [68].

1.6. Contents of the Thesis

PEM fuel cells are widely considered among the most promising technology to reach the zero-emission targets for the maritime field while ensuring the current navigation ranges. The recent findings in literature can prove this, as well as the fact that different hydrogen or hybrid vessels are nowadays under development. In this context, the present Thesis aims to understand the potentialities and limits behind the employment of Polymer Electrolyte Membrane Fuel Cell (PEMFC) technology for maritime applications. Chapter 2 will cover the topic of fuel cells, with a dedicated focus on the PEMFC type, regarding components, materials, and performance. In Chapter 3, PEMFC degradation processes and the main monitoring techniques developed in the last years are described. The results of a thorough literature review on the topic of the Platinum catalyst poisoning have led to the definition of equations that can foresee the voltage variation due to catalyst contamination: a piece of useful information that should be enclosed in FC models that aim to predict the performance during the time in the environment where pollutants can be present. Chapter 4 will instead show the results of the experimental activities developed in a real-scale laboratory, which is deeply described in the same Chapter. The results of this part of the Thesis gain importance since, although many research works related to experimental investigation about PEMFC stacks have been carried out in the last years, all the studies are related to small-scale systems (<10 kW), focusing on the behavior of few cells [69,70] or a single stack [71,72]. However, in a near-future perspective, the implementation and the real application of FC systems (FCS) onboard will require more complicated systems, with a multi-stack solution to reach higher installed power (i.e. in the range 200 kW – 1 MW). Furthermore, the study of the Balance of Plant (BoP) and the management of a typical naval energy load profile must be considered as well to perform a complete and realistic analysis for onboard applications. The necessity to deepen and expand the fundamental research on FCS

and installations on real-scale applications gave birth to the Hydrogen Initiative for Sustainable Energy Applications (HI-SEA) Joint Laboratory between the University of Genova and Fincantieri shipbuilding company [44,73]. Eight 30-kW Orion® Nuvera Fuel Cell PEM stacks, for a total power of 240 kW, are installed in the laboratory to assess their onboard integration. For this purpose, the HI-SEA system is complete with BoP components to simulate onboard operating conditions: it represents one of the more complete systems for the simulation of the operations of a large number of PEMFC for maritime applications. The results of the system commissioning, and the experimental campaign carried out on the same, are described in Chapter 4 and have been published in scientific journals [43], offering an interesting view on real PEMFC applications and their performance. Eventually, Chapter 5 will deal with the application of the Response Surface Methodology (RSM), a branch of the Design of Experiment (DoE) investigation, to the data analysis. The data extrapolated from the experimental campaign in the HI-SEA Laboratory are in fact employed to build a statistical model of the system, considered stochastic, where the cooling temperature and the air mass flow rate are considered as input variables, while the FC stack voltage is the objective function depending on the input variables. This part of the work can lay the foundations for the development of a future monitoring tool.

In conclusion, this Thesis will help the reader to gain a global understanding of PEMFC technology both from a more theoretical point of view, considering materials and performance degradation, and from a more practical point of view thanks to the knowledge acquired during the experimental campaign and the consequent data analysis activities.

2. Fuel cells

Fuel cells are interesting electrochemical devices for electricity production, being used to convert chemical into electrical energy, alone or in cogeneration with gas turbines or batteries. They are available in different types; the classification is carried on depending on the electrolyte typology and the operative temperature. The main fuel cell typologies, that will be described in Section 2.1, are:

- Molten Carbonate Fuel Cell (MCFC).
- Solid Oxides Fuel Cell (SOFC).
- Polymer Electrolyte Membrane Fuel Cell (PEMFC).
- Phosphoric Acid Fuel Cell (PAFC).
- Alkaline Fuel Cell (AFC).
- Direct Methanol Fuel Cell (DMFC).

Fuel cells can work with different reactants, such as pure oxygen, air, hydrogen, methane, ammonia, or carbon dioxide. If the devices work with hydrogen and oxygen, as the two components react, they release electrical energy and produce heat and water as a by-product, making the process clean and sustainable. Indeed, in the perspective of moving towards a sustainable energy economy based on hydrogen and electricity as carriers, fuel cells are efficient energy converters. In case the fuel employed is carbon-based, instead, it is possible to adapt the technology to Carbon Capture and Storage (CCS): the exhaust gases from an industrial plant, rich in CO_2, can be used in the fuel cell and, at the bottom of the process, pure CO_2 will be found concentrated at the anode side of the cell, easy to be separated and therefore to be employed in other processes or stored.

2.1. Working principle

The generic FC working principle is based on the fact that the reactants, provided externally by dedicated circuits, reach the two opposite cell sides – anode, the oxidizing side, and cathode, the reducing side, respectively. Therefore, the reactants undergo an oxidation or reduction reaction: at this point the electrolyte – which is layered between the anode and cathode – is able to carry the ionized particle to the other side, while the electrons released are set free to pass through an external circuit, before reaching the other side of the fuel cell. This process allows the development of an electrical current flux, that is employed for energy production. All the discussion on reactants, components, and electrochemical processes depending on the FC type is detailed in the next Sections.

Since the working principle is based on the efficient verification of the electrochemical reaction between the reactants at the two FC sides, the generic performance of a fuel cell is influenced by operational parameters such as cell temperature, pressure, gas composition, as well as by factors like the presence of impurities, which modifies the reversible potential of the cell and the polarizations – Activation, Ohmic, and Concentration (or Diffusive), which will be described in details in Section 2.2.5.

Gibbs free energy *G* is related to the reversible cell voltage *E* by Equation 1:

$$\Delta G = -nFE \qquad \textit{Equation 1}$$

The generic effect of temperature *T* and pressure *P* on the reversible potential *E* of a fuel cell can be analyzed based on changes in Gibbs free energy with the temperature and pressure:

$$\left(\frac{\partial E}{\partial T}\right)_P = \frac{\Delta S}{nF} \qquad \textit{Equation 2}$$

$$\left(\frac{\partial E}{\partial P}\right)_T = -\frac{\Delta v}{nF} \qquad \textit{Equation 3}$$

Where *F is* Faraday's constant and *n* is the amount of exchanged electrons. At constant pressure (Equation 2), the relationship in Equation 1 produces a Maxwell relation that links the change in open-cell voltage with temperature *T* (a measurable quantity) to the change in entropy *S*. At constant temperature, Equation 1 produces an equation that links voltage with pressure, *P*, to the change in volume *v* (Equation 3). In the case of cells that operate with pure hydrogen and oxygen, since the entropy change in the reaction of hydrogen with oxygen is negative, the cell potential decreases with increasing temperature. In the same reaction, the volume change is negative, and therefore the reversible potential increases with increasing pressure. Ultimately, a temperature rise:

- Reduces the Ohmic polarization since it increases the ionic conductivity of the electrolyte.
- Improves the transport phenomena, by reducing the Concentration polarization.
- Improves the kinetics of the reaction, reducing the Activation polarization.
- Improves the tolerance to impurities present in the feed gas.

Furthermore, the higher the operative temperature, the more efficient the recovery of heat energy produced by the cell. The maximum temperature in the different FC types is defined depending on the stability of the materials used. Technical problems may however limit the maximum operative temperature of a cell, since the corrosion phenomena, the problems of

crystallization and sintering of the catalysts, as well as the degradation of the electrolyte, can all be accelerated by an increase in temperature.

An increase in the working pressure of the cell, on the other hand, has a positive effect on the performance: indeed, it produces higher partial pressures of the reactants in the closeness of the electrodes, it improves the transport phenomena – positively influencing the Concentration polarization – and the solubility of gases in the electrolyte. All the previous phenomena can attenuate the losses inside the cell, and also help to reduce the loss of electrolyte (if it is in liquid form) that are particularly evident in the high-temperature cells. Higher pressures, however, may create major problems from the materials' point of view, and therefore they may require more attentive monitoring of differential pressures. The next Section will describe more in detail the existing types of fuel cells, deepening the electrochemical reactions depending on the materials employed and on the operative temperature.

2.1.1. Existing types

Different fuel cell technologies have been developed in the last years. The classification is usually dependent on the operative temperature and the electrolyte material employed. Table 4 resumes the FC classification depending on the above-described characteristics:

Table 4: Fuel Cell types based on operative temperature and electrolyte type.

FC type	**Low Temperature**	**High Temperature**	**Liquid Electrolyte**	**Solid Electrolyte**
Proton Exchange Membrane FC (PEMFC)				
Molten Carbonate FC (MCFC)				
Solid Oxide FC (SOFC)				
Phosphoric Acid FC (PAFC)				
Alkaline FC (AFC)				
Direct Methanol FC (DMFC)				

It is important to underline that, although it is a common definition, PEMFC and DMFC have strictly speaking not solid electrolytes since they are made up of porous and aqueous materials, that require the presence of water for the electrochemical reaction to work. Going more into details on the electrochemical reactions, the operative conditions, and the materials employed,

the main FC types are here below unfolded. Since they are the heart of the present Thesis, Polymer Electrolyte Membrane fuel cells are reported in Table 4 but they are not included in this Section: their operating principles are thoroughly described in the dedicated Section 2.2.

Molten Carbonate Fuel Cells

Molten Carbonate Fuel Cells (MCFC) operate at 650°C. Noble metal catalysts are not required, due to the high operative temperature, decreasing the cost of the technology. This type of FC has been developed for the combined use with natural gas and coal-based power plants for industrial, electrical utility, and military applications. MCFCs have greater flexibility than other typologies thanks to the possibility to use different available fuels keeping a good overall system efficiency. To achieve high performances is however critical to control the distribution of the molten carbonate electrolyte (in liquid form) in the different cell components. The reactions are, respectively, on the anode side:

$$H_2 + CO_3^{=} \rightarrow H_2O + CO_2 + 2e^- \qquad \textit{Equation 4}$$

While at the cathode side:

$$\frac{1}{2}O_2 + CO_2 + 2e^- \rightarrow CO_3^{=} \qquad \textit{Equation 5}$$

Resulting in the overall reaction:

$$H_2 + \frac{1}{2}O_2 + CO_2 \rightarrow H_2O + CO_2 \qquad \textit{Equation 6}$$

In MCFC systems, the CO_2 generated at the anode is usually directed to the cathode by "CO_2 transfer" devices. This is interesting for the application of Molten Carbonate fuel cells in CCS systems. Typical MCFC generally operates in the current density range of 100-200 mA/cm^2 at 750-900 mV/cell.

Solid Oxides Fuel Cells

Solid Oxides Fuel Cells (SOFC) usually operate between 600-1000°C. A solid and non-porous ceramic metal oxide constitutes the electrolyte (made with Y_2O_3-stabilized ZrO_2), while typically the anode is a Ni- ZrO_2 cermet and the cathode is Sr-doped $LaMnO_3$. Some materials-related problems may happen, mainly when temperatures reach high values, such as sensitivity to contaminants, oxidation-reduction intolerance, mechanical and dimensional instability, and poor activity for direct oxidation of hydrocarbons for the anode. On the contrary, for what concerns the cathode the most important issues are linked to poisoning due to chromium vapors coming from the ceramic interconnections, which commonly are doped with lanthanum and

yttrium chromite. Despite this, efficiencies are usually very high. As regards emissions, minimal air pollutants and low greenhouse gases are registered. As well as for MCFC, this technology has wide flexibility in terms of fuels (including various hydrocarbon fuels) and can be employed for internal reforming, cogeneration with high-quality by-product heat, as well as for bottoming cycle. Two types of cell designs are being investigated for SOFC: tubular and planar cells. The interest in tubular cells is unique for SOFC. For this type of cell, if hydrogen and oxygen are employed as reactants, the anode oxidation of hydrogen reaction is:

$$H_2 + O^{2-} \rightarrow H_2O + 2e^- \qquad \textit{Equation 7}$$

Cathode reduction of oxygen is:

$$\frac{1}{2}O_2 + 2e^- \rightarrow O^{2-} \qquad \textit{Equation 8}$$

And finally, the global reaction is:

$$H_2 + \frac{1}{2}O_2 \rightarrow H_2O \qquad \textit{Equation 9}$$

Phosphoric Acid Fuel Cells

Phosphoric Acid Fuel Cell (PAFC): this type of fuel cell employs liquid phosphoric acid for the electrolyte. They were the first fuel cell type to be commercialized. Developed already in the mid-1960s and field-tested since the 1970s, they have improved significantly in stability, performance, and cost. These characteristics have made the PAFC a good candidate for early stationary applications. The electrolyte is highly concentrated or even pure liquid phosphoric acid (H_3PO_4), saturated in a silicon carbide matrix (SiC). The catalyst employed is a platinum-based material. The operating temperature range is about 150 to 210°C and therefore they are classified as high-temperature cells. The electrodes are made of carbon paper coated with a finely dispersed platinum catalyst. As regards the electrochemical reactions, at the anode side the following is verified:

$$2H_2 \rightarrow 4H + + 4e^- \qquad \textit{Equation 10}$$

And at the cathode, instead:

$$O_2 + 4H + + 4e^- \rightarrow 2H_2O \qquad \textit{Equation 11}$$

Having the overall reaction:

$$2H_2 + O_2 \rightarrow 2H_2O \qquad \textit{Equation 12}$$

Hydrogen and oxygen should be provided in gaseous form. As the temperature operating range is 170 to 200°C, the expelled water can be converted to steam for air and water heating (in combined heat and power systems). This potentially allows efficiency increases of up to 70%. PAFCs are CO_2-tolerant and can also tolerate a CO concentration of about 1.5%, which broadens the choice of fuels that they can use. At lower temperatures, phosphoric acid is a poor ionic conductor, and CO poisoning of the platinum electro-catalyst in the anode becomes severe. However, they are much less sensitive to CO than PEFCs. Disadvantages include rather low power density and aggressive electrolytes. If instead gasoline is chosen as the reactant, the sulphur must be previously removed.

Alkaline Fuel Cells

Alkaline Fuel Cells (AFC) are low-temperature devices that operate with a liquid electrolyte that is a Potassium hydroxide solution (KOH). The catalyst is usually a non-noble material (typically nickel-based), allowing a lower cost for this component. Given these characteristics, they are suitable for operation in a more dynamic regime and easily integrable in compact systems. Indeed, this type of FC was successfully exploited in aerospace applications, such as in the NASA Apollo-series missions during the 1960s. The high flexibility and electrical efficiency have however to deal with the need for very pure gases employed as the reactants, which is considered the major constraint for the technology. In particular, CO, S, and CO_2 can become strongly detrimental to the electrolyte. Since the electrolyte is in the liquid form, the cell design is different from the others and it has in principle three chambers, divided by the electrodes. Two of the chambers are dedicated to the reactants while the third one is for the electrolyte itself. The electrochemical reactions verified in this type of FC are:

$$H_2 + 2OH^- \rightarrow 2H_2O + 2e^- \qquad \textit{Equation 13}$$

At the anode; at the cathode, instead:

$$O_2 + 2H_2O + 4e^- \rightarrow 4OH^- \qquad \textit{Equation 14}$$

Having the overall reaction:

$$2H_2 + O_2 \rightarrow 2H_2O \qquad \textit{Equation 15}$$

Direct Methanol Fuel Cells

A Direct Methanol Fuel Cell (DMFC) is an electrochemical energy conversion device that converts the chemical energy of liquid methanol into electrical energy directly. Their operative temperature is low and up to 120°C, while the electrolyte is nowadays a solid polymer

membrane with sulfuric acid chains that transport the hydrogen proton from the anode to the cathode side. The main drawback of direct methanol fuel cells in fact is the very sluggish anode reaction; coupled with the inefficient cathode reaction, it gives rise to low overall performance, particularly at low temperatures. Moreover, if the methanol is supplied to the cell in a water solution, it could pass through the membrane, affecting the performance at the cathode side. The consequent losses are a fundamental limitation to DMFC systems. The methanol can be supplied to the cell both in liquid and vapor form. However, liquid-feed systems are usually preferred as they are mechanically simpler for what concerns cooling and system thermal management [74]. As regards the electrochemical reactions, at the anode side the following is verified:

$$CH_3OH + H_2O \rightarrow CO_2 + 6H^+ + 6e^- \qquad \textit{Equation 16}$$

And at the cathode, instead:

$$\frac{3}{2}O_2 + 6H^+ + 6e^- \rightarrow 3H_2O \qquad \textit{Equation 17}$$

Having the overall reaction:

$$CH_3OH + \frac{3}{2}O_2 \rightarrow 2H_2O + CO_2 \qquad \textit{Equation 18}$$

In conclusion, Table 5 summarizes for each FC typology the electrolyte material employed, the operating temperature, the electrical efficiency, and the reactants employed in the electrochemical processes.

Table 5: Main FC types and their characteristics, based on results reported in [75].

Fuel Cell	**Electrolyte**	**Operating Temperature**	**Electrical Efficiency**	**Fuel "Mixture"**
Alkaline Fuel Cell (AFC)	Potassium hydroxide (KOH) solution	Room temperature to 90°C	60-70%	H_2-O_2
Proton Exchange Membrane Fuel Cell (PEMFC)	Proton exchange membrane	Room temperature to 80°C	40-60%	H_2-O_2 or Air
Direct Methanol Fuel Cell (DMFC)	Proton exchange membrane	Room temperature to 130°C	20-30%	CH_2OH-O_2 or Air
Phosphoric Acid Fuel Cell (PAFC)	Phosphoric acid	160-220°C	55%	Natural Gas, Biogas, H_2-O_2 or Air
Molten Carbonate Fuel Cell (MCFC)	A molten mixture of alkali metal carbonates	620-660°C	65%	Natural Gas, Biogas, Coalgas, H_2-O_2 or Air

Solid Oxide Fuel Cell (SOFC)	Oxide ion-conducting ceramic	800-1000°C	60-65%	Natural Gas, Biogas, Coalgas, H_2-O_2 or Air

2.2. PEM Fuel Cells: components, materials, and maritime applications

A more detailed description of this FC type is hereby presented since this technology is the heart of the research theme for the present Thesis.

Polymer Electrolyte Membrane FC (PEMFC) is a promising technology in terms of performance, costs, safety, and technology maturity, to reduce the environmental impact of transport applications and to improve power flexibility, keeping good performances [12]. The high power density of this technology is combined with the ability to support dynamic working conditions, and the low operating temperature allows fast start-ups and shut-downs. Moreover, the employed fuel is usually pure hydrogen – even though methanol and ammonia are nowadays under investigation – making PEMFCs zero-emission devices. However, it is worth noting that, before their use in PEMFCs, the methanol requires reforming, ammonia requires cracking, and both require purification to 99.995% H_2 to reach standard values that allow using the gas in a PEMFC. These reasons justify the interest in using hydrogen and PEMFC technology for fuelling cars, low and heavy-duty vehicles, trains, and ships [23,24], which has led many researchers to analyze the possibility of installing a PEM fuel cell system also onboard ships of different sizes, whether for propulsion or auxiliaries.

PEMFC can efficiently generate high power density and are therefore attractive for mobile, automobile, transport, and portable applications in general. An aqueous polymer membrane is used as the electrolyte, being also the anode-cathode separator. This kind of cell operates at relatively low temperatures (60 to 80°C) allowing a faster start-up phase than technologies that work at higher temperatures (such as SOFC). Also, easier sealing, assembly, and handling are allowed thanks to these characteristics. PEM fuel cells are usually planar cells and are made up of the anode and cathode (identified with the inlet of hydrogen and air respectively); the proton exchange membrane (made with a thin polymer film); an electrically conductive porous backing layer where also the Catalyst Layer (CL) is spread into small particles; the electrodes at the interface between the backing layer and the membrane; cell interconnects; and flow plates that deliver the reactants to the reactive sites on the membrane through flow channels while electrically connecting the cells (see Figure 12).

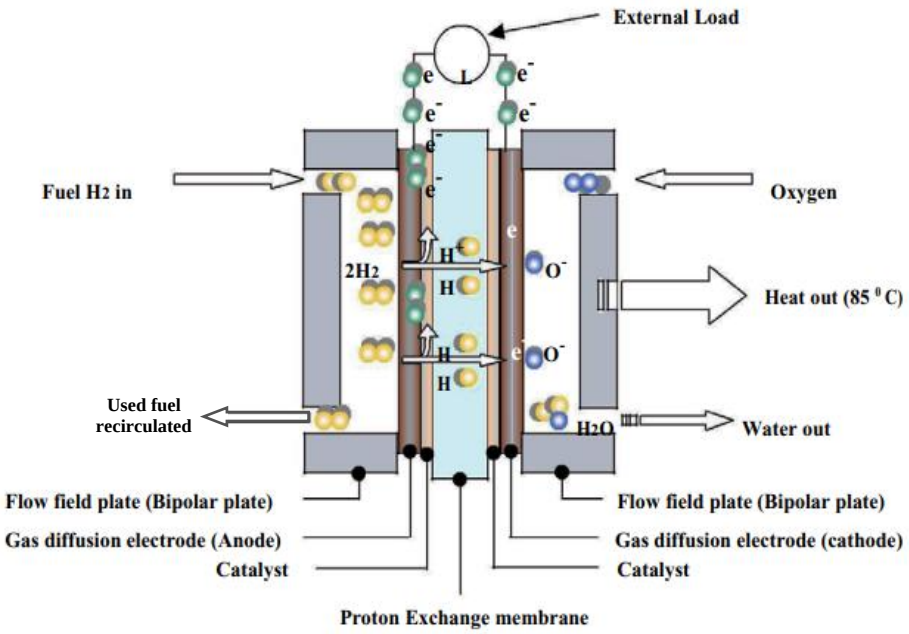

Figure 12: Schematics of the main components of a PEMFC [76].

The electrochemical reactions verified in this type of FC are, at the anode:

$$H_2 \rightarrow 2H^+ + 2e^- \qquad \textit{Equation 19}$$

And at the cathode, instead:

$$\frac{1}{2}O_2 + 2H^+ + 2e^- \rightarrow H_2O \qquad \textit{Equation 20}$$

Resulting in the overall reaction:

$$H_2 + \frac{1}{2}O_2 \rightarrow H_2O \qquad \textit{Equation 21}$$

Since heat is produced by the electrochemical reaction, and the proton-conductive membrane operates at its best in the correct temperature and humidity conditions, thermal control is crucial for this type of FC. Therefore, a cooling circuit is a crucial part of the FC system, to properly remove excess heat and preserve the proper relative humidity inside the cells.

In the next Sections, more details are reported regarding the most relevant cell components.

2.2.1. Proton Exchange Membrane

The proton exchange (or polymer electrolyte) membrane is one of the most important components in PEMFCs. It is the protonic conductive layer between cathode and anode, and it also prevents the direct reaction between oxygen and hydrogen. It is characterized by its active area (usually measured in cm^2) and by its equivalent weight (which is inversely proportional to

the ion exchange capacity). There are many different types of membranes, and they are made using different types of materials. The most employed material for membranes in low-temperature PEMFCs is Nafion, invented and manufactured by DuPont. Some alternatives are Aquivion by Solvay, nanocomposite membranes, and hydrocarbon polymers [77] are under investigation. As a general guideline, since the role of the membrane is to conduct hydrogen protons, the material employed should exhibit high protonic conductivity and simultaneously prevent electron transport and the cross-over of hydrogen and oxygen gases. The operating temperature range is an important factor to be considered when choosing the membrane materials; thus, it should have a wide temperature range (from -30 to 200°C) [78]. The choice of materials for the membrane is dependent on the physical and chemical properties needed to ensure efficient performance [78]. In summarizing, the following identified properties must be met [79]:

- The ionic conductivity must be high.
- It must be chemically stable in the environment with hydroxyl (HO) and hydroperoxyl (HOO) radicals.
- It must be thermally stable throughout the entire operating temperatures
- Good water uptake.
- It must be durable and mechanically robust.
- It must be easy to get or produce and not expensive.

Membranes used in PEMFCs can be classified as:

- Perfluorinated membranes, that are thin, highly conductive, and have a good mechanical resistance (Nafion).
- Partially fluorinated.
- Non-fluorinated.
- Acid-based blends.

New materials are also under investigation, such as:

- Nanocomposite membranes, with some micron of inorganic/organic components – i.e. ZrO2, TiO2, Silica – to reach high water retention and tensile strength.
- Sulfonated hydrocarbons membranes, that have a lower chemical/mechanical stability, but a wide temperature range and a lower cost.

Since the membrane's active area and its ionic conductivity strongly depend on correct hydration [80,81], wrong water and thermal management are the most frequent failure cause for this component [82,83]. This must be considered especially when operating at high current

densities (over 1 A/cm^2) because of mass transport issues, associated with water formation and distribution which may limit the cell output. Water content is determined by the balance of water during operation that depends on: water drag through the cell (linked to transport and membrane); back-diffusion from the cathode (osmotic action along with the proton); and the diffusion of water in the fuel stream through the anode. All parts of the cell must be sufficiently hydrated; at the same time, no excessive flooding must occur. Also, since this component should be as thin as possible to reduce losses across it, mechanical degradation must be carefully considered as it can cause membrane failure [84].

2.2.2. Gas Diffusion Layer (GDL)

The polymer membrane is sandwiched between two sheets of porous backing media, also referred to as Gas Diffusion Layers (GDL) or current collectors, which act as a gas diffuser, provide mechanical support, provide an electrical pathway for electrons, as well as a channel for reaction water to be carried away from the electrodes. The backing layer is typically a carbon-based fiber: the layer incorporates a hydrophobic material, such as polytetrafluoroethylene to prevent water from "pooling" (verified when gases are in free contact with the catalyst sites). Removing the water through the porous plate is necessary to have less water in the reactant streams, to reduce parasitic power needs of the oxidant exhaust condenser, to have higher fuel utilization values, and to better control temperature values, reaching better distributions.

2.2.3. Catalyst layer (CL)

The catalyst layer is in between the membrane and the backing layer, which "fixes" the catalyst particles on the polymer within a layered structure. The catalyst for pure H_2 PEM fuel cells is usually a platinum-based material for both the anode and cathode (pure platinum or graphite supported platinum). This element is preferred as it activates the chemical reactions on the two sides of the cell even at the low operative temperatures typical of PEMFC. The sites on the membrane where the ion-conductive polymer, the Pt particle, and the electrode coexist are called Triple-Phase Boundaries (TPB): here, the fuel is reduced (in the case of oxygen, the reaction is called Oxygen Reduction Reaction – ORR) or oxidized (in the case of hydrogen, the reaction is called Hydrogen Oxidation Reaction – HOR), the proton is conducted through the membrane and the electron flows through the electrode, generating current (see Figure 13). Since the electrodes and the catalyst particles are layered on the polymer membrane forming

together a homogeneous component, these latter are usually referred to as the nomenclature Membrane-Electrode Assembly (MEA).

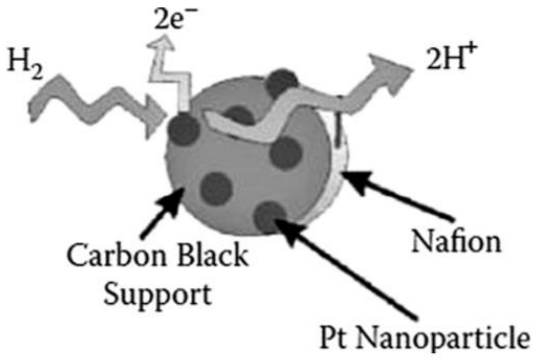

Figure 13: Schematics of the TPB on a Nafion's membrane [85].

Platinum catalyst forms one of the largest cost components in the fuel cells. Fuel cell design with efficient utilization of platinum catalyst could contribute directly to cost reduction of the whole device. Also, finding a platinum-alternative catalyst will cause further cost reduction of the fuel cell [78]. Despite its wide employment, however, since this material is highly reactive, some problems of poisoning can arise from the presence of contaminants. In fact, Pt has a strong affinity to other compounds like carbon, sulphur, nitrogen oxides, ammonia, and hydrocarbons in general. Besides, an excessive amount of water (i.e., in case of membrane flooding) can cause dissolution and aggregation issues of Pt particles, enhancing the degradation.

2.2.4. Cooling circuit

Cooling is accomplished using a circulating fluid, usually water, that is pumped through integrated coolers within the stack. The fuel cell cooling system is responsible for maintaining this temperature at a suitable level. The heat generated by a PEMFC is approximately equal to or sometimes can be even more than the maximum power generated by the fuel cell [86,87] depending on the efficiency curve. Four factors such as entropic heat/reversible heat/Peltier effect of reactions (35% of total heat), irreversibility of electrochemical reactions (55% of total heat), ohmic resistances/ Joule heating (10% of total heat), and water condensation are responsible for the heat generation in a PEMFC [88–92]. A fuel cell stack can dissipate its excessive heat by internal or external mechanisms. Internal heat removal by the cathode fluid stream is more significant than the anode fluid stream, as the exothermic reactions occur at the cathode and the reaction water absorbs the generated heat [93]. Different techniques for heat removal are under investigation, and depending on the fuel cell stacks' sizes, application field, and operating conditions, air and/or water-cooling techniques are commonly employed for thermal management purposes. The main heat removal techniques are hereby listed:

- Liquid water cooling.
- Air cooling.
- Metal foams.
- Nanofluids.

As regards air-cooled PEM fuel cell systems, they can be classified as active type and passive type, depending on the air supply method. In an active-type air-cooled PEM fuel cell system, the reactant air for the ORR and the coolant air are separately supplied through two different flow paths and thus can be properly controlled for optimal fuel cell operation. On the contrary, passive air-cooled PEM fuel cell systems are based on a cooling process implemented via natural convection of the air on the external surface area of the fuel cell stack. Cooling via natural or forced convection of the reactant or product also falls under the category of passive cooling. Therefore, considering the system configuration, a passive-type air-cooled PEM fuel cell system is simpler than an active-type system and is thus better suited to small-scale applications that require a lightweight system [94]. Normally, PEMFC stacks of above 5 kW power mainly require liquid cooling, and those below 2 kW are usually designed to be air-cooled [87] since the lower need for heat removal can be achieved by air cooling, considering the lower heat capacity of air with respect to water. For example, the Ballard Mk1020 ACS fuel cell, an open cathode PEMFC, has been designed to be cooled using air within its wide operating range of 300 W to 4 kW [95]. For an air-cooled PEM fuel cell, the open cathode design – where forced air is supplied to the cathode using fans – plays a major part in improving cell performance [95]. Nevertheless, liquid cooling remains the most employed technique to promote fuel cell output efficiency, especially in automotive applications [95].

Metal foams are under investigation to be combined with air cooling in open cathode stacks, while nanofluids are a new technology that is interesting for the enhancement of the cooling capacity of the cooling system when used as coolants – they are proved successful in reducing the size of fuel cell radiators – while their effects on the liquid conductivity are still not clear. Any increase in electrical conductivity of the coolant is undesirable in PEMFCs: the generated electricity in the PEM fuel cells polarises the coolant by creating the electric field that causes electricity to leak through the coolant; consequently, it affects the electrical performance of the fuel cell negatively. Along with the electricity leakage through coolant, a coolant with high electrical conductivity can shortcut the cells that contributes to stack degradation and performance drop [96].

2.2.5. PEM fuel cell voltage

The cell voltage is one of the most important parameters to be evaluated during the operation of a FCS, since it reflects the presence of criticalities and, in general, the trend of losses associated with the cell polarization, that have been introduced in Section 2.1. Cell voltage is in fact calculated starting from the Nernst equation and subtracting the irreversible losses: Activation, Ohmic, and Concentration. Cell voltage, therefore, is calculated by Equation 22:

$$V_{cell} = V_{Nernst} - V_{Activation} - V_{Ohmic} - V_{Concentration} \quad \textit{Equation 22}$$

To calculate the Nernst Potential V_{Nernst}, it is necessary to start from the electrochemical reactions that are verified inside the cell. The chemical energy released by the FC can be calculated from the difference in Gibbs free energy between the product (liquid water) and the reactants (hydrogen and oxygen). For the H_2/O_2 fuel cells, like the ones employed in this Thesis, the basic chemical reaction – already described in Equation 30 – is:

$$H_2 + \frac{1}{2}O_2 \leftrightarrow H_2O \quad \textit{Equation 23}$$

The change in Gibbs free energy, referring to the standard state (pressure 1 bar, temperature 25 °C), is:

$$\Delta g_f^0 = (g_f^0)_{H_2O} - \left(g_f^0\right)_{H_2} - (g_f^0)_{O_2} \quad \textit{Equation 24}$$

Δgf varies with temperature and pressure according to the Equation 25:

$$\Delta g_f = \Delta g_f^0 - RT_{st} \ln\left(\frac{\left(p_{O_2}\right)^{1/2} * p_{H_2}}{p_{H_2O}}\right) \quad \textit{Equation 25}$$

Where Δg_f^0 is the change in Gibbs free energy at the standard state and it varies with the FC stack's temperature T_{st}. The partial pressure terms are commonly referred to as the values found at the anode and cathode channels. If the system is considered reversible, the electrical work can be considered equal to the change in Gibbs free energy and therefore Nernst Potential is finally defined by the Nernst equation as:

$$V_{nernst} = E_T = {E_T}^0 + \frac{RT_{st}}{2F} \ln\left(\frac{\left(p_{O_2}\right)^{1/2} * p_{H_2}}{p_{H_2O}}\right) [V] \quad \textit{Equation 26}$$

where p_{H_2} is supposed equal to the anode pressure, p_{O_2} is calculated by subtracting the saturation pressure of vapor from the cathode air pressure, considering a 21% of oxygen in the air. Nernst equation correlates ${E_T}^0$, which is the standard potential for the cell reaction at the desired temperature (T_{st} in this case), to the Open Circuit Voltage (OCV) E_T at different partial

pressures of reactants and products and at the desired temperature (in this case, the one of the fuel cell stack T_{st}).

As regards losses, Activation losses are the ones responsible for the difference between the OCV and Nernst Potential at very low currents. These losses are caused by the slowness of the reactions taking place on the surface of the electrodes [97,98]. In a PEMFC, these losses occur mainly at the cathode side since the exchange current density i_0 of the anodic reaction is several orders of magnitude higher than the one of the cathodic reactions. For most values of the overpotential, a logarithmic relationship prevails between the current density and the applied overpotential, which is described by the Tafel equation (Equation 27):

$$\eta_{act} = b \ln \frac{i}{i_0} \qquad \textit{Equation 27}$$

where i is the observed current density and b is the Tafel-slope coefficient, which depends on the electrochemistry of the reaction. An accurate description of the local current density i is given by the Butler-Volmer equation (Equation 28):

$$i = i_0[\exp\left(\frac{\alpha_a F}{RT}\eta_{act}\right) - \exp\left(\frac{\alpha_c F}{RT}\eta_{act}\right)] \qquad \textit{Equation 28}$$

where α_a and α_c are the anodic and cathodic apparent transfer coefficients, respectively, F is Faraday's constant and $\eta_{act}$is the activation overpotential; i_0 is obtained following the curve fitting approach explained by Berning [92].

Ohmic losses result from the resistance to electron transfer in the collector plates and electrodes plus the resistance to proton transfer in the solid polymer membrane. They can mathematically be expressed using the Ohm's Law equation as for resistances in an electrical series:

$$\eta_{ohmic} = \eta_{ohmic}^{electronic} + \eta_{ohmic}^{protonic} = iR^{protonic} \qquad \textit{Equation 29}$$

Resistance to electron flow is approximately constant over the relatively narrow temperature range of PEM fuel cell operation, and it can therefore be considered negligible in comparison with the proton resistance, $R^{protonic}$ [$\Omega \cdot cm^2$], which is considered as the FC internal electrical resistance. The resistance strongly depends on the membrane's specific resistivity, which is difficult to be empirically expressed, as it depends on the type and characteristics of the membrane, the operative temperature, the water content/degree of hydration of the membrane [99], and the current density; its variation can be calculated with the empirical model proposed by Mann's approach [100].

Concentration losses are the result of changes in the concentration of reactants as they are consumed by the electrochemical reaction [101,102]. They are mainly visible at high current

densities (above 1 A/cm^2), since under those conditions the reaction water is produced in large amounts at the cathode whilst some Nitrogen, coming from the airflow entering at the cathode, can accumulate at the anode side. These two components – N_2 and water – can prevent an even distribution of reactants on the active sites of the MEA, causing a sudden and strong increase in losses and therefore a significant voltage loss, up to preventing the whole electrochemical process. Eventually, these phenomena can lead to reactants starvation, a process that brings to irreversible degradation of components such as the Catalyst Layer. This issue will be described more in detail in Chapter 3.

Figure 14 shows the typical polarization curve of a PEMFC. This is usually given by the FC supplier and therefore taken as a reference during operation to detect any anomalies in the voltage value, symptom of an undesired increase in losses. Moreover, in the same figure are shown the regions of the operative ranges where the different losses are more felt by the PEMFC.

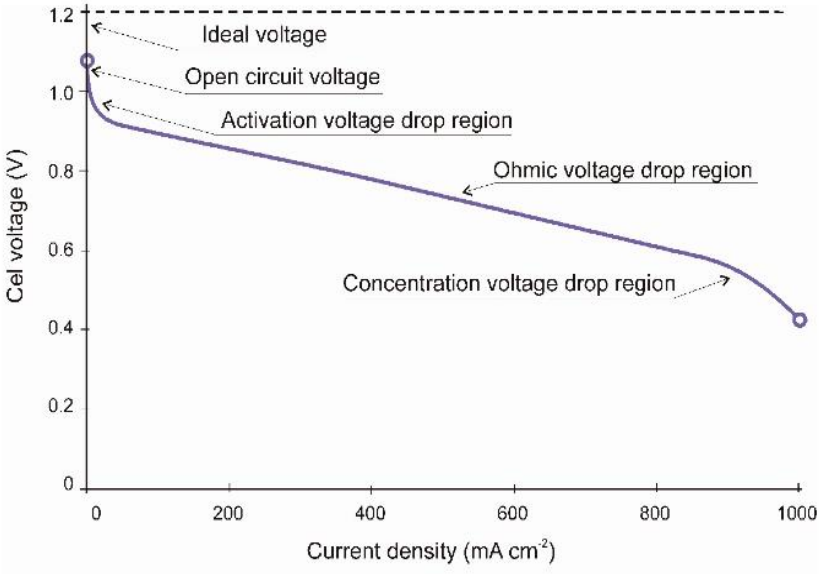

Figure 14: Typical PEMFC polarization curve [103].

3. State of art of monitoring techniques, components, and degradation mechanisms in PEMFC

3.1. PEMFC performance monitoring techniques

The performance of a fuel cell can be influenced by operational parameters such as temperature, pressure, and gas composition, as well as by factors like the presence of impurities, which modifies the reversible potential of the cell and the polarization. The effect of temperature and pressure on the reversible potential of a fuel cell has been deepened in Section 2.1.

The reference for measuring PEMFCs performance is usually found in the Nernst polarization (V-I) curve, depicted at the Beginning of Life (BoL) of the FC, that is showing the trend of cell potential at increasing current densities. The V-I curve is usually supplied by the FC producers, who obtain it experimentally, and has the typical trend which is described in Figure 14 [103].

Starting from Nernst's potential E^0, the OCV is calculated as previously described by Equation 26 depending on operational parameters (cell temperature, partial pressure of reactants, and product water). The theoretical cell potential is obtained via Equation 26 by subtracting losses (Activation, Ohmic, and Concentration respectively) to the OCV, according to Equation 22.

Besides the abovementioned operational parameters, the performance in a PEMFC depends also on the working conditions, such as the operative profile requested, reactants purity, exposure to shock and vibrations, and of course natural aging of components. Since temperature and relative humidity are directly involved in the amount of liquid water content in the polymer membrane, they must be carefully controlled. Indeed, with wrong operating conditions it is easy to incur drying or flooding, the two opposite phenomena where the water content in a cell membrane is respectively too low, or too high. This will directly affect the proton conductivity of the membrane and increase the Ohmic losses related to it: in fact, the membrane's resistance and performance rely on the correct water content. Therefore, wrong thermal-humidity management immediately affects the FC performance, and, in the long term, it irreversibly affects the state of health of the FC components and especially of the MEA. The direct consequence is that, since losses may increase, the cell potential, according to Equation 22, decreases. In fact, losses can be compared to electrical resistance, and when they increase the overall impedance of cells increases. It is hence important to monitor the trend of cell potential during operation, as a deviation from the reference value is a symptom of a wrong working condition or the presence of external disturbance issues.

Different studies have also confirmed that some external components can act as contaminants and have temporary or permanent consequences on PEMFCs, creating damage to the components and causing degradation. Even in the case of contamination, the most sensitive components are the ones belonging to the MEA, i.e., the membrane and the catalyst. For this reason, Section 3.2 will detail the degradation processes linked to them.

Since performance losses and degradation of components can be assimilated to an increase in the Ohmic resistance of the PEMFC, degradation is usually calculated as a cell voltage loss – in terms of mV – depending on the time of exposure (hours) to one of the stress conditions. To this aim, the voltage measurements are taken during tests while keeping the same current density across the cell/stack, in order to avoid any potential variation that can be referred to as a change in the operating conditions.

Monitoring an FC during its operation is critical to different aims:

- Monitoring of the real-time performance and individuating natural aging effect.
- Diagnostic of the stressor that is causing a performance loss.
- Prognostic of the critical situations that can derive from certain parameters that are not optimal during the FC operation.

Indeed, knowing the State of Health (SoH) of an FC device can give useful information about the proper operation of the whole system: the online detection of wrong parameters trends (i.e., temperature, pressure, voltage, current, etc) can indicate issues specifically associated to one of the operating conditions.

Besides, the cell exposure time to the fault is a key factor that determines the capability to recover the cell performance, for most of the faults. Therefore, defining some online, real-time corrective actions is crucial for PEMFC systems, to stop and recover a degradation process that has recently started.

As a general guideline, the best monitoring technique should be non-intrusive, fast individuation of faults, whose consequent resolution can prolong the useful life of the FC in a system. There are two groups of fault diagnosis and fault-tolerant control methods:

- Model-based methods: they are complex and require an in-depth knowledge of the multi-physical mechanisms (thermal, electrical, electrochemical, and fluidic ones) that can occur in FC systems. These models are based on numerous parameters and their values are difficult to estimate. Not suitable to provide an accurate/quantitative description of the FC performances.

- Data-driven methods: they have a good implementation simplicity as well as good performance without profound system structure knowledge. They are supported by efficient signal processing methods. Electrochemical Impedance Spectroscopy (EIS) analyses can for instance supply artificial intelligence algorithms (neural networks) or conventional pattern recognition approaches.

There are a few non-intrusive, free of external/internal disturbance diagnosis tools for monitoring the SoH of PEMFC. The most widely known and employed is Cell Voltage Monitoring (CVM): it is very common and can give information on the SoH of the FC for both automotive and stationary applications. Yet, no information is provided about what parameter in the system is affecting the cell performance while just general feedback is obtained. In reference [104], the voltage singularities are analyzed with Voltage Singularity Spectrum (VSS) obtained in a non-intrusive manner: a setting of the main parameters – i.e. cathode/anode stoichiometry rate, anode/cathode gas pressure, cooling circuit temperature, and anode/cathode relative humidity – is prepared, containing their reference values in a range. If they exit the provided range, a fault is diagnosed thanks to the voltage measurement and the VSS analysis. These methods are well known and established and can operate online, but it is not always immediate the correlation between a voltage loss and a wrong parameter. Moreover, the reference value to be compared to online cell potential should consider cell aging and degradation due to operation.

EIS is instead a diagnostic technique that allows measuring the impedance of the investigated PEMFC (or even of a stack) over a large frequency bandwidth. The impedance analysis responses show the overlapping contributions from various physicochemical processes over a wide frequency range, including Ohmic polarization losses, Activation polarization losses, and Concentration polarization losses throughout the whole cell. The real and imaginary parts of the system's impedance are calculated by letting the FC undergo an alternating current and voltage signal, provided by an external component; usually, the obtained data is presented in a Nyquist plot, like the one shown in Figure 15. Current and voltage perturbation signals are tested at different frequencies; each frequency gives information about one of the sections of the PEMFC – membrane, anode, catalyst, and cathode. EIS measurements not only can encompass in one representation various information about the state of health of the system but, also, can be used efficiently to highlight the influence of changes in operating conditions. Therefore, EIS is successfully used for fault diagnosis in pattern-recognition approaches, as it gives useful information on the presence of the fault while indicating its source. EIS is

commonly implemented off-line, through large-size equipment, in static conditions. Usually, the diagnosis tool consists of different steps:

- Measurable features are extracted.
- To improve fault classification, a feature selection based on different correlations is used to keep only the relevant ones.
- Classification is achieved, to assign each observation to one of the predefined defect classes. The performances are evaluated on an experimental dataset.

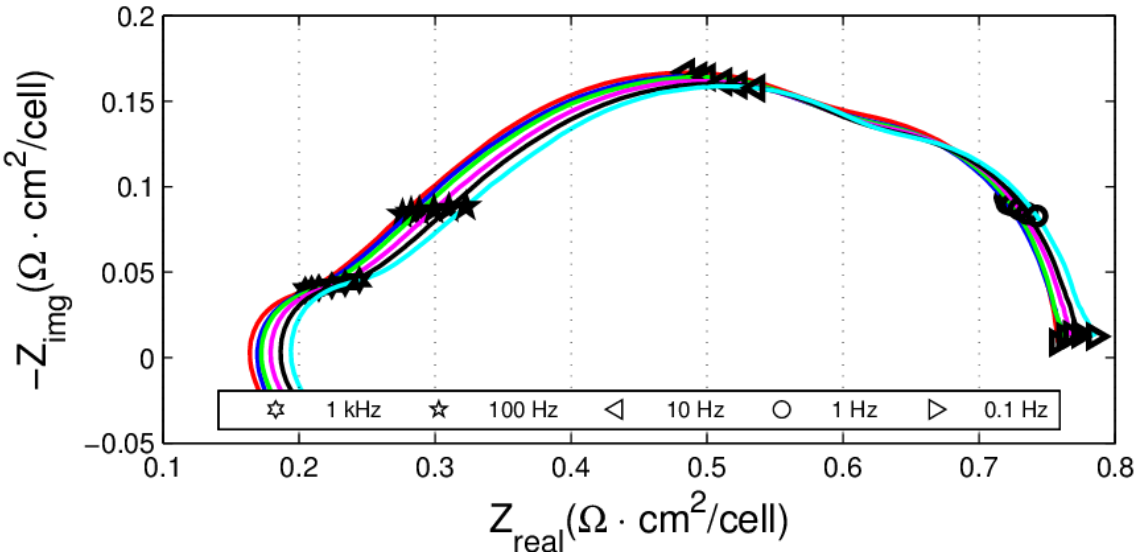

Figure 15: Generic Nyquist plot from the EIS analysis of a PEMFC [105].

Figure 15 shows a Nyquist plot obtained by the EIS analysis developed in [105]. It is possible to distinguish three different arches in the figure: in the first part, where the real and imaginary parts of the impedance value are close to zero, it is usually possible to detect the variation of impedance linked to the anode or membrane's properties. In the central arch, is enclosed information about charge transfer processes linked to the cathode catalyst. Finally, the last arch allows reaching information about mass transport processes linked to cathode diffusion.

New possibilities for EIS are rising: for example, the work by Wang et al. [106] presents the possibility to implement an online diagnosis by EIS. The EIS in this case is obtained exploiting the step-up converter that is usually installed in PEMFC systems, such as FC electric vehicles. In fact, for these applications, the low-voltage and high-current characteristics of PEMFC make a DC/ DC converter essential to increase the output voltage of the fuel cell stack and satisfy the DC bus voltage requirements. Furthermore, the proposed 6-phase Interleaved Boost Converter (IBC) in [106], based on Silicon Carbide (SiC) semiconductors and inverse coupled inductors, has achieved low input current ripple, high efficiency, high voltage gain ratio, high compactness, and high redundancy. Benefiting from these advantages, the drying, flooding, and

air starvation conditions can be rapidly diagnosed right during operation, and the lifespan of the fuel cell stack can be extended.

Figure 16, Figure 17, and Figure 18 show the results of the implementation of the online EIS analysis reported in [106]. Figure 16 shows the Nyquist plot for a PEMFC total impedance under normal operating conditions. Figure 17, instead, shows the new plot (purple line) in case of membrane drying conditions: the real part of the impedance is enhanced, and the plot moves on the Real axis. Figure 18, finally, shows the Nyquist plot in case of cell flooding conditions (green line). Both the real and imaginary parts of the impedance are increased, and the plot is displaced on the two axes.

In conclusion, to monitor the PEMFC performance different techniques are nowadays available. All of them rely on the link between the SoH of fuel cells and the internal resistances; therefore, they can follow two paths: i). monitoring techniques may directly measure the impedance variation of the cell components; ii). or they can deduce it by detecting cell voltage variation during the time. In this case, it is more difficult to predict which component is mostly affecting the global system performance.

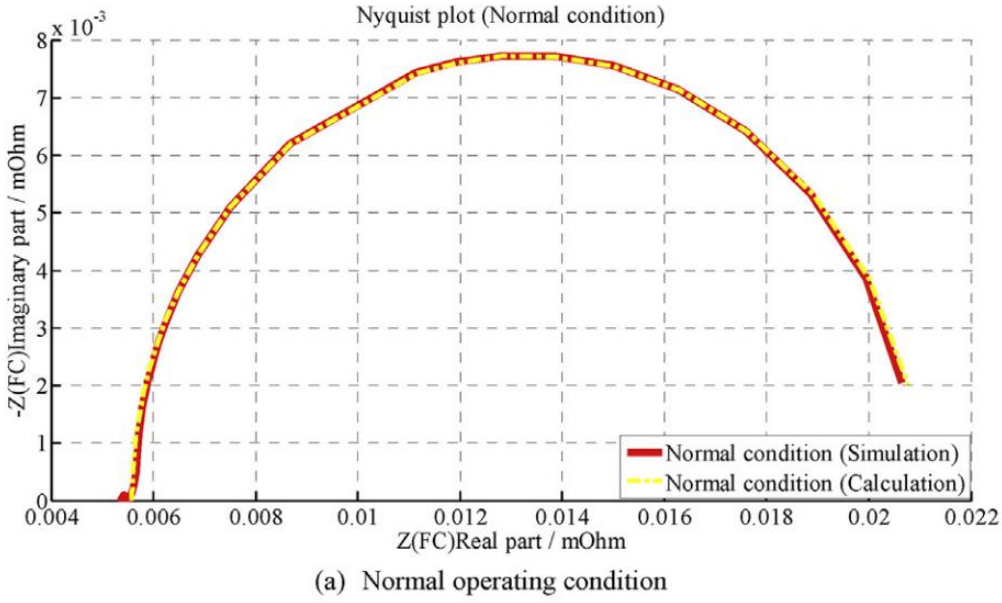

Figure 16: Nyquist plot of the impedance of a PEMFC during normal operating conditions according to reference [106].

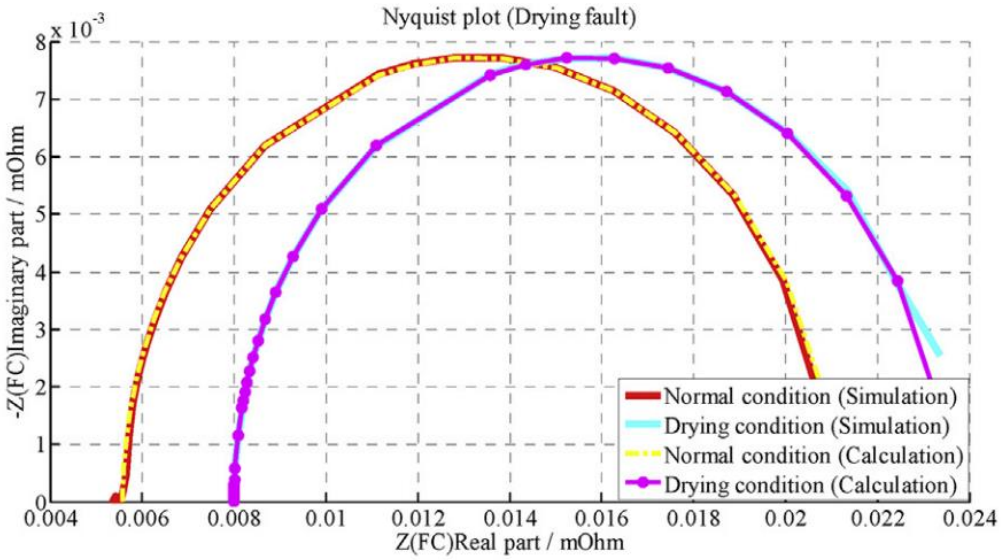

Figure 17: Nyquist plot of the impedance of a PEMFC during membrane drying conditions according to reference [106].

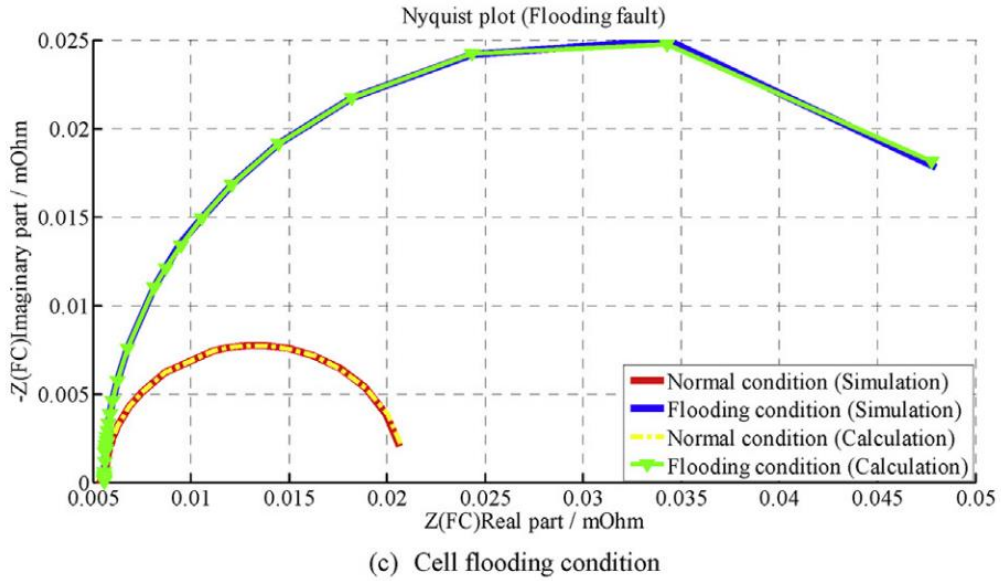

Figure 18: Nyquist plot of the impedance of a PEMFC during cell flooding conditions according to reference [106].

3.2. Literature review on the degradation mechanisms of the PEMFC

Fuel cell degradation and performance decay are amongst the most critical challenges nowadays for the commercialization of FC applications. Researchers have focused on this issue to properly understand why, how, and at which components degradation verifies and at which rate, not neglecting the effect of operating conditions [107–115]. The main aim is to individuate the most durable and least expensive materials for each component, to move ahead and predict the end of life of an FC stack, and to establish the most convenient power management strategy in an FC application to minimize degradation and total costs of operation. Improvements in these fields will help in reducing the global cost of technology, as they should guarantee a tradeoff

between three key factors: performance, cost, and endurance. PEM Fuel Cells can be an alternative for energy supply and substitute for several technologies, for example, internal combustion engines on vehicles, but there still is a need for improvements: according to the 2020 roadmap of the USA DOE, the lifetime of the PEMFCs should be up to at least 5000 hours to be fully commercialized in the automotive industries [116,117], while this target is still not reached: in fact the typical operative profile that would be requested to a PEMFC on a vehicle would be very unsteady and include frequent start and stops. This condition is very often linked to sudden humidity variations in the MEA, and thus to a deviation from the optimal working conditions. Therefore, the lifetime of PEMFC can be reduced, preventing the reach of the lifetime target set by the DOE.

As regards the degradation phenomenon, PEMFCs can be considered as an open reactor [118]: as introduced in Section 3.1, their performance is affected by different external and internal operating conditions such as non-optimal stack temperature, wrong humidity management, materials aging (mostly membrane, electrodes or catalytic degradation) and mechanical stresses that can be caused by shocks/vibrations as well as poor control strategies of the air compressor. Nevertheless, natural degradation/aging is not negligible either: Yuedong Zhan et al. [119] carried out a study on PEMFC natural degradation in 2014. They observed the performance of a 63-cell Horizon® H-300 PEMFC stack (300 W), made by Horizon Fuel Cell Technologies, Singapore. The MEA of cells was comprising a series connection of 63 catalyst coated membranes sandwiched between the anode and cathode GDLs, and the active area of the PEMFC was about 18 cm^2 [120]. The stack was bought in 2008, tested for 18 days, and then left inactive for 39840 hours (more than 4 years). During inactivity, the stack was maintained at a controlled temperature (24±1 C) and relative humidity (65±2%), without contamination sources. Then it was employed again in another experimental campaign, where a recovery procedure was conducted using high-frequency pulse technology and intelligent control methods on the stack. Its effectiveness was tested by measures of the polarization curve during the application of the procedure. The average natural degradation rate on currents from 1 to 8 A (0,44 A/cm^2) was found to be 309 mV/1000 h, which was partially recovered and brought to 170 mV/1000 h through a recovery procedure.

In summarizing, according to Schmittinger et al [80] the main issues linked to PEMFC employment and operation that may affect the useful lifetime and long term performance are:

- Contamination of the electrodes/electrocatalyst and/or of the membrane.
- Water management: Flooding – Cathode flooding and Anode flooding – or Dehydration of the membrane.

- Degradation of the components by: i). corrosion of the electrodes/electrocatalyst at the anode and/or cathode, of the GDL, of the bipolar plates and gaskets; ii). chemical degradation of the membrane; iii). Mechanical degradation of the membrane and/or of the bipolar plates and gaskets.
- Reactant gas starvation.
- Thermal management.

The results of a dedicated literature review are shown in the next Subsections, which have investigated mechanisms of chemical degradation – individuating what are the poisonings to the catalyst, to the polymer membrane, and the other components of PEMFCs –, mechanical degradation and degradation due to real operative cycling of PEM fuel cells. The investigation of the degradation phenomena associated with chemical and mechanical stresses is costly and time-consuming. For this reason, Accelerated Stress Tests (AST) are usually reported in the literature: the concentrations of contaminants, in this case, are strongly higher than the limit values imposed by ISO 14687-2, but, in this way, researchers aim to reach the same results in a shorter time. In the same way, also mechanical stresses, such as vibration and load variations, are exacerbated in AST. References in the literature about long-lasting stress tests are few and usually refer to real cases of PEMFC applications conducted by PEMFC suppliers. Full comprehension of these mechanisms may give interesting suggestions to design control strategies and develop recovery procedures once the degradation has started.

3.2.1. Chemical degradation

Chemical degradation can be defined as the act or process of simplifying or breaking down a molecule into smaller parts. In PEMFCs, this process can take place in the two main components: the polymer membrane and the catalyst layer. Different compounds can enter the FC device during its operation and cause severe consequences on the components depending on the constituting materials. Corrosion of balance of plant materials, dissolution of the transition metals alloyed with Pt in the electrocatalysts, decomposition of roadside air pollution, wrong cleansers, and the presence of salt particles in the inlet air can release ion contaminants. Literature reveals that ionic impurities can severely degrade the lifetime of PEM fuel cells and deteriorate their performance. Only a few research investigations have been conducted on the techniques of studying the effect of liquid-phase organic and inorganic contaminants originating from the BoP components' materials. It was reported that some commonly used materials can produce contaminants in long-term operations and thus contribute to the deterioration of the PEM fuel cells' performance. Cleansers have also been proven to have

negative impacts on PEM fuel cell durability [121]. On the other side, one of the most critical ions that can affect PEMFCs' performance is chlorine. This is in fact found in the cathode inlet air when FCs operate in shipping applications. Different studies tried to evaluate the effect of chlorine compounds, and it resulted that sodium chlorine has not a detrimental effect on the components of the cell, like the membrane or the catalyst. Nevertheless, if salt agglomerates it may obstruct pipes and ducts, therefore air filtration in the marine environment is to be considered. Some results of the studies focusing on the effects of ions on PEMFCs [122,123] can be summarized as follows:

- NaCl, and $CaCl_2$: they do not influence during short operation times.
- A performance reduction is verified if $CaCl_2$ is present at high current densities.
- $CaCl_2$ is more detrimental than NaCl, in case of long operation times.
- Some experimental results run with salt concentrations close to the levels commonly found in the marine atmosphere reported that calcium chloride poisoning has a stronger effect on cell voltage degradation rates [122]:
    - For NaCl, at 10043 ppm, 108 hours of test at 1 A/ cm^2 brought a voltage decay equal to 1.082 mV/h.
    - For $CaCl_2$, at a concentration of 9391 ppm, 108 hours of testing at 1 A/ cm^2 brought a voltage decay equal to 3.446 mV/h.

In general, a poisoning compound that enters the reactants' stream may in fact interact with the materials of the components and modify their operation, either temporarily or permanently. This is due to the intrinsic properties of the materials: from one side, Platinum – mostly employed as a catalyst for PEMFCs due to its high reactivity that compensates for the relatively low operating temperatures – can show a preferentiality towards other than ORR at the cathode or HOR at the anode. In this case, contaminants create bonds with the catalyst particles and inhibit their role as an enhancer of the electrochemical process inside PEMFCs. On the other hand, due to the chemical structure of the membrane – that should conduct hydrogen protons – electrically charged compounds, and in particular ions and free radicals, can act on the carboxylic acid end group sites of the primary chain and sulfonic acid groups from the side chain. Here below is described in detail how the chemical degradation can affect the CL, the membrane, and other components.

Catalyst Layer

Platinum is the most widely employed material for catalyst in PEMFCs; as seen in Section 2.2, it is embedded in a porous conductive material – the electrode – that acts as a catalyst support

layer, and then it is disposed on the membrane in the form of small size particles, to reach the highest possible electrochemically active area. Usually, the amount of Pt on a single cell is around 40 mg/ cm^2. Platinum is very effective with clean reactants, but it is highly expensive, being one of the largest cost components in PEMFCs, which enhances the concerns about a fast degradation of this material. Even though it has been possible to significantly reduce the amount of Pt in PEMFCs, it is important to limit its chemical degradation in order to move as much as possible away from the end of life of the whole electrochemical device. The tolerance limits are in fact generally very low in PEMFCs, as is confirmed by the strict international standards on hydrogen quality for PEMFCs (Limitations given by ISO 14687-2 are reported in Table 6). This is mainly due to the low operative temperature, and the consequent need for a noble material for the CL.

Table 6: ISO 14687-2 limitations on contaminants in hydrogen gas for use in PEM fuel cells.

Component	**Chemical Formula**	**Limit**	**Unit**
Hydrogen, min	H_2	99.97%	%
Total Non-Hydrogen		300	ppm
Argon	Ar	100	ppm
Carbon Dioxide	CO_2	2	ppm
Carbon Monoxide	CO	0.2	ppm
Helium	He	300	ppm
Formic Acid	HCOOH	0.2	ppm
Formaldehyde	HCHO	0.01	ppm
Ammonia	NH_3	0.1	ppm
Nitrogen	N_2	100	ppm
Oxygen	O_2	5	ppm
Water	H_2O	5	ppm
Particulates		1	$mg.kg^{-1}$
Total Sulphur	H_2S, COS, CS_2, etc	0.004	ppm
Total Halogenated Compounds		0.05	ppm
Total Hydrocarbon content ex. Methane		2	ppm
Total Methane Nitrogen & Argon	CH_4, N_2, Ar	100	ppm

Although processes such as Pressure Swing Adsorption (PSA) can increase the hydrogen purity ranging from 99% to 99.999% by adsorbent technology, literature reported that even ppb

amounts of impurities can affect fuel cell performance over time; of course, standards for the quality of hydrogen have been established (Table 6). However, if the hydrogen gas comes mainly from hydrocarbons and the cathodic airflow is taken from contaminated areas (see traffic urban areas), it is crucial to study how degradation rates in PEMFCs can change when the reactants employed contain impurities, even if trace amounts.

The most critical contaminants for the catalyst layer, at the anode and the cathode, derive from particles contained in the hydrogen stream or from the air with low quality, as found in traffic urban areas. They are, as confirmed through the present literature review – in increasing impact on Platinum degradation:

- CO_2, NO_x.
- CO.
- NH_3.
- H_2S.

This list becomes particularly relevant considering that in case the hydrogen gas is produced by SMR – the most employed technique nowadays since it represents a good balance between low fuel cost, low GHG emissions (Carbon Capture and Storage – CCS – is possible), and low Criteria Air Contaminants emissions – its initial composition before purification is, as reported in Table 7 [124]:

Table 7: Hydrogen gas composition after production by SMR process.

Component	**H_2**	**CO**	**CO_2**	**N_2**	**CH_4**
Percent [%]	94.3	0.1	2.5	0.2	2.9

All the named contaminants can create a strong chemical bond with the catalyst and, therefore, occupy the electrochemically active sites of the cell, decreasing the efficiency of the ORR and HOR processes. These two reactions are defined as multi-electron multi-step. There are two models, associative and dissociative, proposed in the literature to determine electro-reduction of oxygen with Pt sites. In the dissociative model, the first step involves dissociative chemisorption of oxygen occurring with charge transfer at the same time:

$$Pt + \frac{1}{2}O_2 + e^- \rightarrow M - O^- \qquad \textit{Equation 30}$$

Contaminants instead affect the reaction depicted in Equation 44, occupying the catalyst layer and poisoning the cathode side of the PEM fuel cell. Moreover, contaminants can permeate through the membrane and therefore affect the catalyst also on the anode side. The problem with catalyst poisoning and chemical degradation is linked to the fact that contaminants in

cathode air get chemisorbed on the Pt layer, occupying the catalyst sites, and decreasing the surface available for ORR. Consequences can be seen on:

- Average current density.
- Maximum power output.
- Diffusive polarization.

The effects and irreversibility of Pt degradation strongly depend on many factors; in particular, the most influent ones are the following:

- Contaminant concentration (usually measured in ppm or ppb).
- Exposure time.
- Temperature.
- Current density.
- Stack dimension.

Once the chemical degradation process on the catalyst layer is started, it results in a decrease in the chemically active area. This is due to two reasons: first, the fact that active sites are occupied by contaminants; secondly, the Pt particles found in wrong conditions may migrate, sinterize, and aggregate (Figure 19). Bigger particles are thus created, with a smaller active area. Eventually, HOR and ORR have the least chances to be verified.

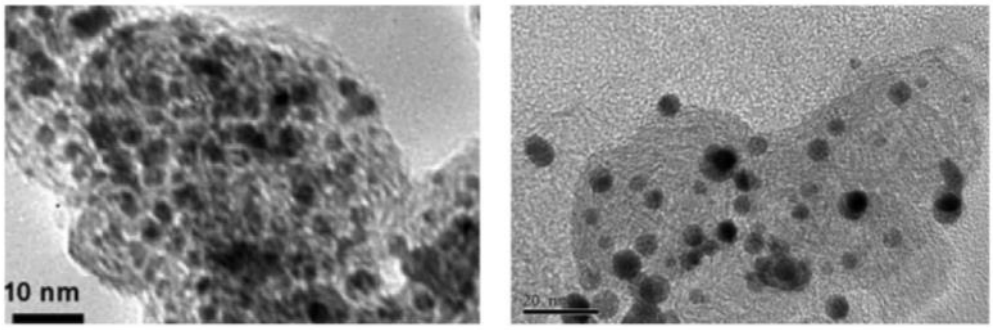

Figure 19:Effect of chemical degradation on Pt particles: sintering and aggregation [125].

Polymer membrane

The polymer membrane is one of the most important components in PEMFCs.

Chemical failure, which takes the form of damage to the ionomer and diminished membrane integrity and conductivity, has been extensively studied by a significant number of researchers. It is usually caused by ions in general and by the free radical attack, that is generated in the course of hydrogen peroxide decomposition on the cathode side, by cationic contaminants, or by the reaction of hydrogen and oxygen at the Pt catalyst [126,127]. In the literature, there are

no results about the effect of external contaminants on the membrane. Indeed, poisoning compounds that affect the catalyst layer are likely to cross the membrane, if they do not first bond with the Platinum particles themselves, due to the electronic charge of the molecules. Therefore, those compounds do not affect the membrane. What act on the polymer membrane are the substances such as ions and free radicals. Many factors contribute to the chemical degradation of polymer electrolyte membrane including changes in the potential and operative temperature, transition metal ions contamination, and reactant gas crossover. These factors can indeed directly or indirectly increase the risk of radical formation and attack on the MEA [128]. Hydroxyl -OH and hydroperoxyl -OOH oxidative radicals form either at anode or cathode by decomposition of hydrogen peroxide (produced from a two-electron oxygen reduction – electrochemical generation) via transition metal cations, or by a thermal process. They are also formed by the direct reaction of H_2 and O_2 on the surface of Pt catalyst as a result of gas crossover through the membrane [129]. The reaction of oxidative radicals such as -OH and -OOH with the polymer electrolyte is known to be the main cause of chemical degradation. Radical attack acts on the carboxylic acid end group sites of the primary chain and sulfonic acid groups from the side chain [128–130]. This process can in fact induce a change in the ionomer's morphology and eventually decrease its ion exchange capacity. Such a fact diminishes its proton conductivity in the earlier stages and leads to a less durable material in advanced stages. Ions' contamination will act similarly, as the ions will occupy the carboxylic acid end group sites and the sulfonic acid groups, leading to a degradation of the membrane, a decrease in conductivity, and the formation of small pinholes, where the direct reaction between oxygen and hydrogen may take place. This process will further degrade the membrane, due to the high temperatures generated and the consequent increase in pinholes size and number. It is important to underline that radical formation is not evitable, and it is part of the natural aging of the membrane's polymer. Nevertheless, free radicals' formation is enhanced by temperature and potential changes: for this reason, it is so important to have a precise control system and an adequate operation strategy with PEMFCs. The operation should be kept as stable as possible and the water management must be able to minimize hydration/dehydration swings, control radical's formation and keep as low as possible the membrane swelling/shrinking process due to the change in its water content. Adequate water management combined with the use of a membrane reinforcing material can minimize the chemical degradation of this component. Eventually, pinholes formation and chemical attacks will cause membrane thinning and failure.

The most frequently reported evidence for radical attack and chemical degradation is fluoride release and membrane thinning. Another important consequence of chemical degradation is

dehydration of the membrane, resulting in a decrease in proton conductivity and the corresponding increase in ohmic loss. The thinning and divot generated in the PEMs are the main results of chemical failure.

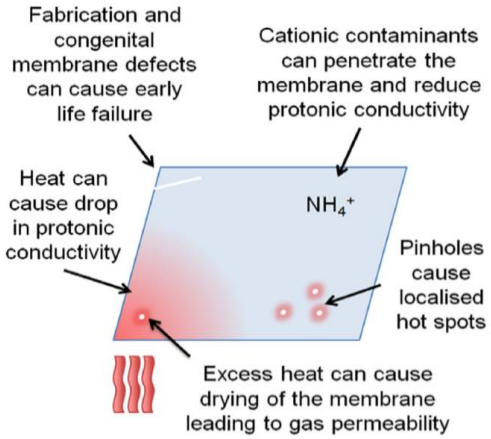

Figure 20: Different contributions to membrane's chemical degradation [131].

Other components

Other components of PEM fuel cells are not subjected to chemical degradation as they are usually made of metallic components that are not exposed to detrimental conditions. However, the cooling circuit, very crucial to thermal-humidity management, reaction kinetics, and membrane stability [132], can operate in harsh conditions depending on its design and the coolant employed.

The main problems with the cooling circuit don't depend on contamination by external contaminants. Indeed, there are no issues linked to external-to-cooling contamination found in the literature: the fluid employed for cooling doesn't contact the most sensitive components of PEMFCs. Nevertheless, issues from cooling can be verified on the FC stack, and these will have an indirect consequence on the thermal and humidity control. Some problems can be arising from leakages and the electrical conductivity of the fluid. While there are no leakages problems in the case of air cooling, liquid cooling (usually obtained with a water and glycol mixture) can see the effect of increasing the electrical conductivity of coolant, which is undesirable in an electrochemical reaction-based device. This is since the generated electricity polarizes the coolant due to the electric field created, eventually causing an electricity leakage through the coolant; the highly electrically conductive coolant can shortcut the cells, causing PEMFC stack degradation and performance loss: coolant conductivity can create electrical bridges where it is possible to verify short circuits among the cells. In this case, the current could not take its normal pattern across the bipolar plates, but it would pass from the cooling flow channels that electrically connect the single cells. This event causes a decrease in the total

output voltage from an FC stack and parasite currents that are dangerous for the stack. Therefore, if liquid cooling is chosen to remove the excess heat from the PEMFC, criticalities arising from water conductivity must be considered and avoided. Water and glycol should be deionized, and their conductivity should be constantly monitored during operation to avoid incurring irreversible damages eventually.

As a rule, to avoid damages deriving directly from the cooling circuit it is advised to [43]:

- Employ deionized water as coolant.
- Install deionizing cartridges.
- Adopt constant monitoring of the coolant conductivity during operation.

3.2.2. Mechanical degradation

Performance reliability and mechanical integrity are some of the main bottlenecks in the mass commercialization of PEMFCs for applications in harsh environments such as the automotive and aerospace ones: the mechanical degradation of PEMFC's components and exposure to vibrations are deepened in this Section. Mechanical degradation is usually due to:

- The inclination of a PEMFC stack during operation.
- To dynamic operating conditions.
- To the exposure to vibration.

In these conditions, the degradation is mainly verified on the catalyst layer, the polymer membrane, and assembly components and their materials.

Stack inclination

The effects of inclination of the operating PEMFC stack are yet to be faced in dedicated experimental studies. The lack of regulation on how to install the device on the different applications has delayed the experimentations on the topic, and nowadays there is no standard protocol yet that concerns the inclination allowed by a stack to keep a good performance during operation. Only recently, some studies have been born to define the inclination that an FC system must tolerate if, for instance, it is installed on board a ship [133]. However, the research on inclination effects has just started and there is no precise advice nowadays. Some PEMFC stack suppliers install their technology inclined or even in the vertical asset on purpose, to drain excess water.

As a general consideration, some operative problems can be verified if the stack inclination is not suitable for the stack design – specific for every FC supplier depending on the stack assembly. In fact, the water produced at the cathode can accumulate and become difficult to be

removed if the exhaust channels are not properly designed, causing the flooding phenomenon. Long exposures to flooding conditions result in damages both:

- To the membrane, due to the reduction of the active area for proton conductivity, which decreases its efficiency and creates a local increase in temperature. This process of hot-spots creation leads to pinholes formation, through which direct O_2-H_2 reaction is verified, bringing to an eventual membrane mechanical failure [134]
- To the catalyst, as the excessive water presence contributes to its mechanical degradation in the forms of dissolution, migration, and aggregation, as already described in 2.2.2. Eventually, the increased-size Pt particles have a lower active area that results in a performance decrease, especially for the oxygen reduction reaction. These processes are enhanced by high operating temperatures and high potentials and explain why PEMFC suppliers usually advise against working in similar conditions, unless for a very short time.

Dynamic operating conditions

Unsteady operating conditions will directly influence the temperature variability and the water management. Repeated high/low relative humidity variations cause a continuous alternating of swelling and shrinking of the polymer membrane, due to changes in water uptake. Again, this leads to the membrane's mechanical failure by pinholes and cracks formation on the polymer itself. Therefore, strongly exothermal O_2/H_2 direct reactions can be verified, bringing to definitive failure of this component: for this reason membrane's material must have a good thermal and chemical stability to limit the effects of this kind of mechanical stress. Membrane aging cannot be completely avoided, but it can be minimized using reinforcing materials – such as a porous conductive catalyst support layer – and having adequate water management. This topic will be faced in Section 3.2.3, to deal with all the implications of dynamic operation for a PEMFC and not only from the mechanical degradation point of view.

Vibration

Among the main reasons for mechanical damage in PEMFCs, for transportation applications, are road-induced vibrations and impact loads; the most vulnerable site of the cells, instead, is the interface between the membrane and the catalyst layer [135]. For safety reasons, as well as for the FC performance, the electrical insulation of FC stacks must be guaranteed, and the hydrogen leakage rate should be minimal.

Many researchers have studied the effect of harmonic vibration on the mechanical stability of non-operating stacks and their components [84,136–141], but yet investigation is needed on the effects of vibration on operating devices [142], with random vibration, and in the case of shock. The fuel cells integrated into vehicles are continuously subjected to mechanical vibrations ranging from 0.9 to 40 Hz, always below 100 Hz [142], with a maximum amplitude of 0.95g – where g is the acceleration of gravity. The verification of shocks and vibration to the fuel cell in transportation applications could bring different issues, among which the most impacting include clamping torque loosening, hydrogen gas leakage, increased electrical resistance – in particular, the Ohmic one – and eventually structural damage and breakage.

The effects of vibration on liquid water transport of PEMFCs during operating conditions were studied by Breziner et al in [143]. They exposed an operating PEMFC to a harmonic vibration with frequencies of 10, 20, and 50 Hz, and acceleration levels of 2 g, 3 g, and 5 g. The study reported an overall decay of the FC performance up to 6%. Nevertheless, the real-world excitations are often better modeled by random vibrations instead [141]. This is particularly true when it comes to automotive and aerospace applications. Banan et al. [136] investigated the combination of hygrothermal cycles and external vibration on a 9 kW stack (90 cells) for 250h. Compared with the performance before the vibration test, the rated voltage of the stack decreased by 3.58% and the voltage decay rate was quantified at 0.77mV/h. Moreover, the OCV decreased and the Ohmic resistance increased by 5.36% as well as the mass transfer losses, which showed an increasing trend. They concluded that strengthened road vibration has a significant influence on degradation.

One of the most rigorous experimental studies found in literature in the context of vibration effects on PEMFCs is the one described by Imen and Shakeri [144], who studied the effects of short-term and long-term exposures of PEMFCs to random vibrations. In the study, they subjected a 36-cell stack with a rated power of 500 W to random vibration for 2 hours in operating mode, and for 44 hours in non-operating mode. The random vibration was based on military standard (MIL-STD-810) with a frequency range of 10-1000 Hz and with a 1.5 g root-mean-square (rms) acceleration level. During both short and long exposures, the performance of the FC stack was assessed at different time intervals, compared to its polarization curve, while hydrogen leakage and clamping torque were observed. The results showed that, in the short run, the mechanical loads do not affect the system performance and reliability; nevertheless, exposure to random vibration, in the long run, degrades the system performance. The 44 hours of exposure to random vibration in fact reduced the FC power by 6.6% and also increased the hydrogen leakage by 1% at the constant current of 10 A. They deduced that

loosened clamping bolts caused increased hydrogen leakage and ohmic losses, and thus resulted in performance degradation.

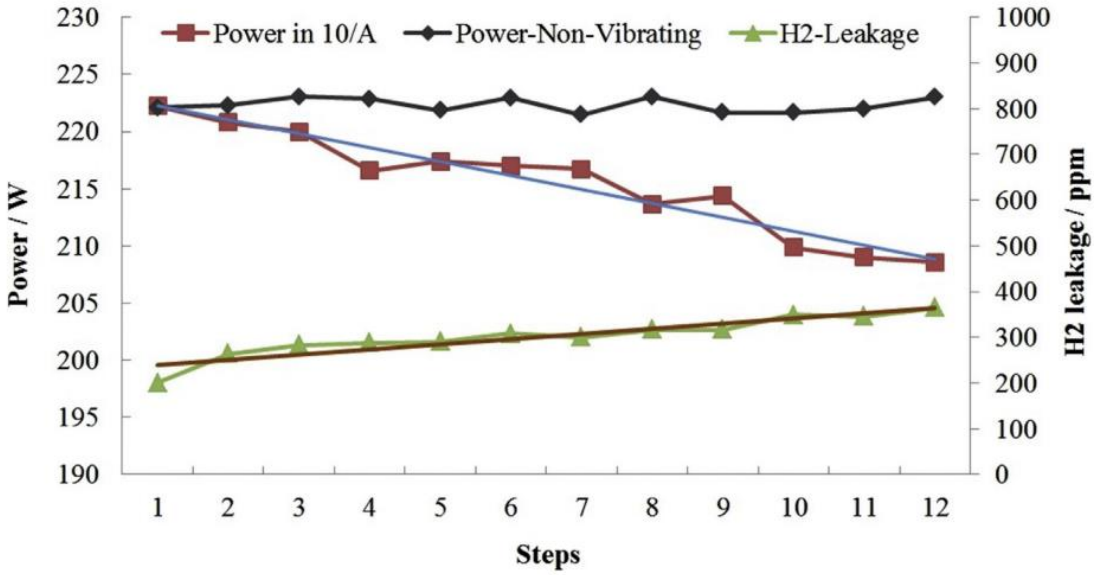

Figure 21: Results of the vibration long-term vibration test on a PEMFC stack as reported in [141].

A more systematic set of experiments was implemented by Hou et al and is described in references [139,140,145–147]. In all the papers, real-world excitations were employed in the experimental campaign. They first excited an actual vehicle with standard road conditions in the laboratory thanks to a six-degree-of-freedom shaker, and then they measured the transmitted acceleration signals to the PEMFC installed on the vehicle. Next, they excited the PEMFC on a shaker with the measured acceleration signals. The goal of all the studies was to investigate the effects of long-term vibration on the performance of PEMFCs used in passenger cars. In all their experiments, PEMFCs were not in operation during the vibration tests. In every test, they obtained drops in the open-circuit voltage and increases in the Ohmic polarization, with consequent performance degradation.

As regards assembly components and their constitutive materials, vibration tests in the literature do not underline significant issues, except for a minor torque release at the bolts. Therefore spring suspensions were suggested in some studies [138]. Ahn et al.[142] found that the loss factor of the torsional stiffness depends on the stack configuration and that it influences the resonant vibration amplitudes. Nevertheless, by selecting the correct material damping of the bipolar plate and membrane, the amplitude of the torsional mode of the PEMFC could be controlled.

However, the results of vibration tests found in the literature are globally inconclusive: some studies have claimed considerable negative effects on the PEMFC performance: exposure to

vibration exacerbates the mechanical stress and enhances the flooding phenomenon (by droplets merging and interference with the mass transfer process). On the other hand, studies by different authors claimed negligible effects; a few studies even suggested the possibility of using vibration for improving the FC performance [148]. This suggests that most of the studies are case-dependent and not generic, so the results and conclusions can vary from one case to another. Besides, tests on cells under different conditions (exposure time, temperature, current, etc) are difficult to be compared, and a test protocol is missing even in this case.

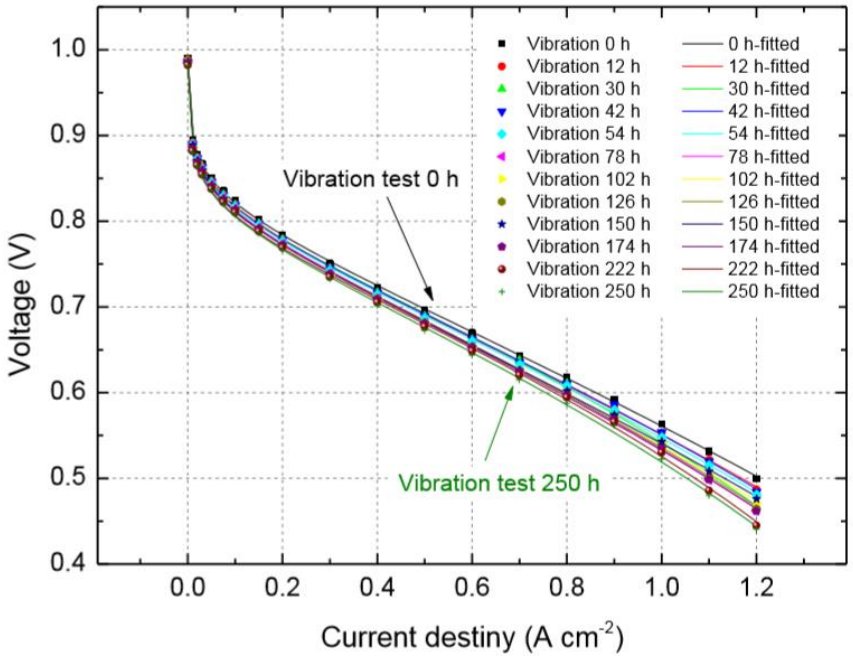

Figure 22: Gradual results of a prolonged vibration test (total duration of 250 hours) on a PEMFC, considering the effects observable on the polarization curve, as described in reference [147].

Focus on the Polymer membrane's mechanical degradation

The mechanical degradation of the membrane may result from the local stress concentration, such as unbalanced pressure at the anode and at the cathode, which affects the mechanical integrity of the polymer. The latter is in fact a thin sensitive film, and it can be weakened if the pressure at the two sides is significantly different – both under stationary and dynamic load conditions. Besides, mechanical stress variation on the constrained membrane is detrimental, under the alternating swelling and shrinking in response to the changes in water content and temperature, which are typical of a non-stationary operating profile. In this case, the dynamic energy demand implies repeated high-low relative humidity cycles, which are reflected on the temperature profile and on the water content that can increase free radicals' formation and lead to severe chemical degradation, as explained in Section 3.2.1. Exposure to vibration can instead exacerbate the membrane degradation process, particularly in conditions of unbalanced water presence and if the exposure time is prolonged. As a result, material fatigue, creep and the

generation of wrinkles, delamination, pinholes, tears, or cracks are initiated and propagated on the surface or across the bulk of the membrane, which would be exacerbated by inherent defects in the membrane that may be occurring during the fabrication process or the improper assembly of fuel cell stacks [149]. Liu and Case's [150] results show that in the system under observation, hydrogen crossover is the primary source of degradation after 500h of operation. Although PEMFC mechanical failure is considered to have the highest occurrence potential and is regarded as the main cause of fuel cell failure in the early period of the cell's lifetime [151,152], a comprehensive understanding of this type of failure is lacking. The mechanical failure of the membrane, such as that resulting from a pinhole or crack, provides a passage by which the hydrogen and oxygen mix and which can trigger a combustion reaction and thus a high heat spot, leading to instantaneous performance decay and the failure of the fuel cell. In particular, recent stacks have been designed to use especially thin membranes to minimize Ohmic losses and enhance proton conductivity [149]. Therefore, the membrane's mechanical integrity and durability have emerged as an even more critical challenge.

3.2.3. Degradation due to operative cycling

Besides degradation due to materials corrosion and contamination, the operative profile followed by the FC system is crucial to determine the degradation processes and the effective useful life that the FC will benefit from. Actual working conditions in PEMFCs can influence:

- Temperature.
- Water generation.
- Free radicals' formation.

Four working conditions strongly affect the catalyst, influencing the lifetime of PEMFCs, and they are typical in the automotive field; Moein-Jahromi et al. [153] have described these conditions as:

- Idling operation: it is verified when a little and constant load is drawn for a prolonged time from the PEMFC – i.e. an auxiliary load. Nevertheless, idling operation at constant voltage ensures a longer lifetime than idling at fluctuating voltage. Wilson et al [154] demonstrated that idling operation at lower voltages has a slighter decline effect on the electrochemical surface area at the anode and cathode sides, acting on the stability of the catalyst.
- OCV operation: in this case, the current density in the FC stack is zero while the potential at the two cell sides is very high. This condition is usually verified immediately before the shutdown procedure or exactly after the startup of the PEMFC; therefore,

during the whole lifetime of an FCEV – considering the 5000 operating hour target for FVEV by DOE – this phenomenon can be verified for up to 100 hours [155]. Idling and OCV operations (that usually correspond to a cell potential around 0.75 and 0.95 V, respectively) were tested by Ferreira et al [156] for 2000 hours each, resulting in a decrease of the electrochemical surface area from 75 m^2/gPt to 40 m^2/gPt for idle and from 75 m^2/gPt to 15 m^2/gPt for OCV operation.

- Cyclic load: this is the most frequent and probable transient operation for an FC Electric Vehicle (FCEV) and has been studied through many AST, with increased attention to the catalyst degradation [156–165]. The transient operation of the PEMFCs has considerable effects on Platinum particles agglomeration, dissolution, and consequently, on the electrochemical surface area decline [155]. It was also found a close correlation between enhanced catalyst degradation and the increased temperature and relative humidity of reactants, during cyclic operation [166–169]. Moreover, it was proven that higher amplitudes of the cyclic load produce a stronger catalyst decline.
- Cyclic start-stop: the instantaneous condition induced by starts and stops leads to filling the anode with hydrogen and air at the same time, increasing the local interfacial voltage to up to 1.5 V – a very dangerous condition for the catalyst, considering that, according to Garche et al [155], a PEMFC in an FCEV could be exposed to these cycles around 38500 times in its lifetime. A proper procedure should be implemented in the control system to limit the detrimental effect of this operating condition.

Several studies and models have been developed in the last years to understand and quantify the effects of these four working conditions on voltage decay. Both long-term experiments and AST have been implemented on PEMFC stacks, achieving interesting results. ASTs in fact reproduce subsequent operating conditions that strongly affect the state of health of the FCs; therefore, they can differ from the real running conditions that a PEMFC should manage. Nevertheless, ASTs have the advantage of increasing the sample range and thus they reduce the experimental time required. Therefore, several fuel cell developers and companies – like Ballard Power Systems, DuPont, Gore, and General Motors – proposed and implemented different ASTs to determine the durability and the performance of PEMFC components, depending on the operating conditions. Indeed, even though the prolonged operation is more similar to the real running conditions and thus reliable, it will increase both time and costs of testing and therefore may not be feasible.

As regards thermal cycling degradation, Dubau et al. [170] performed in 2015 tests for 12860 hours in a “quasi-stationary” mode, on industrial PEMFC stacks (55 cells in series) by AXANE

using proprietary state-of-the-art membrane-electrode assembly from commercial providers. The industrial stacks were operated without an impacting load-cycling, but with 250 starts and stops. Dry hydrogen in dead-end mode and humidified air (around 65 %relative humidity) fed the stack at a stoichiometry of around 2-2.5 (depending on the test), and the stack temperature was around 65 ± 5°C. They observed that there was a different degradation rate on cells belonging to the same stack, and it was mainly due to the hardware and fluidics/thermal conditions of AXANE's PEMFC systems, demonstrating the link between the global Membrane-Electrode Assembly performance and the existence of local degradations. The average voltage decrease after 12860 hours at 0.25 A/cm^2 was quantified in 15 mV/h and as 31 mV/h at 0.5 A/cm^2.

Chen et al. [171] took the real data from an FC bus employed for one year during Beijing Olympic Games, in 2008; the bus was equipped with a 100-cell stack supplied by Shangai Shen-Ii High Tech Co., Ltd, with a 274 cm^2 effective area per cell (the rated power was 10 kW, while the rated current was 100 A, operating at a temperature of 60 °C and atmospheric pressure). The stack operated with a stoichiometric ratio of hydrogen equal to 1,1 and a stoichiometric ratio of air equal to 2,5. Then, they took another PEMFC stack with the same characteristics and simulated a one-hour driving cycle on it, based on the real running data previously obtained – the data acquired during the FC bus running in 2008 – about the average start-stop cycles during one hour (*n1*), the average idling time per hour (*t1*), the average load change per hour (*n2*) and finally the average high power load operation time per hour (*t2*). Chen et al. called these parameters (*n1*, *t1*, *n2*, *t2*) the "load spectrum" of the driving cycle, which results to be for the FC bus in one hour:

- *n1*=1.
- *t1*=13 minutes.
- *n2*=56.
- *t2*=14 minutes.

Following a simulated simplified operative profile, they predicted a degradation rate that resulted equal to 0.0266 mV/h. Four tests lasting 50 hours each were performed, testing the degradation rate, and then during the fifth test, the voltage degradation was calculated. The degradation predicted by the model fitted the real degradation obtained during the tests, demonstrating that 200 hours are enough to finish a test and deduce voltage degradation rate under any driving cycle, assuming that the voltage decays linearly with time. Besides the

average degradation per driving cycle, Chen et al. reported the values of voltage degradation per operating conditions, shown in Table 8:

Table 8: Values of voltage degradation per operating conditions as estimated in [171].

Operating conditions	**Voltage degradation rate**
Start-stop	0.138 mV/cycle
High power load	0.1 mV/h
Idling	0.086 mV/h
Load change	0.0042 mV/cycle
Total driving cycle	0.42 mV/h

This study verified that start and stops are critical states for a PEMFC, causing the highest degradation rate. Frequent start-stop cycling causes an instantaneous condition which leads to filling the anode with hydrogen and air at once, increasing the local interfacial voltage that can reach values as high as 1.5 V, a very dangerous for the catalyst layer lifetime. Moreover, this study is a good start to modeling the degradation of the catalyst layer. Similar values of voltage degradation were adopted in the work by Pouria Ahmadi et al. [22]: considering a voltage degradation rate of 0.0265 mV/h and hydrogen production by SMR, the authors demonstrated the lifecycle convenience of FCEV with respect to gasoline ones, in four different driving modes, both in terms of emissions and of fuel economy. The analysis also considers an option for regenerative braking.

M. Moein-Jahromi et al. in reference [153] created two models that, if coupled, calculate the catalyst's performance during the time and at different operating conditions, number of cycles, and types of cyclic load. These models are based on inputs from the references [167,172–174] and [http://www.fuelcellstore.com/toray-carbon-paper-060/] and, as demonstrated in the study, the results strongly depend on the electrochemical area available and the Platinum agglomerate radius. The output of the models is a Voltage Degradation Rate (VDR), which is a percentage value concerning the initial voltage value at the same boundary conditions (temperature, pressure, current, relative humidity, etc), calculated in Equation 31:

$$VDR\% = \left(1 - \frac{V_{cell}^{N}}{V_{cell}^{N-0}}\right) * 100 \qquad \textit{Equation 31}$$

In the first model, a parametric study is performed at the current density of 0.8 A/cm^2 for 1000, 2500, 4000, and 5500 numbers of cycles (N) under standard conditions (60 °C, relative humidity 100%) and the results are validated with the experiments of references [159,167]. In

the second, a cyclic load protocol is implemented through a cyclic square-shaped voltage signal with maximum and minimum voltage of V_{max}=1.2 V and V_{min}=0.6 V; a cycle is repeated every Δt=60 seconds and a sensitivity analysis is performed to rank the most influential parameters on the VDR%: temperature, Relative Humidity (RH), pressure, the minimum and maximum voltage of cyclic load protocol. The results are summarized in the following table:

Table 9: Rank the most influential parameters on the VDR% according to [153].

Rank	**Parameter**	**Range studied**	**Optimum value**	**Change in the VDR%**
1	T [°C]	60-80	60	34,53-14,27% after 2500 cycles
2	V_{min} [V]	0,2-1	1	27,12-12,41% after 5500 cycles
3	RH [%]	50-100	50	14,27-8,57% after 5500 cycles
4	V_{max} [V]	1-1,2	1	14,27-10,27% after 5500 cycles
5	P [atm]	2-4	4	10,51-9,10% after 5500 cycles

In the study by Thangavelautham et al. [175], the lifetime of a PEMFC was compared, through the application of a degradation model that they developed, under different stressing operating conditions. The model allowed to calculate the effect of voltage oscillation amplitude (Figure 23) on residual cell life.

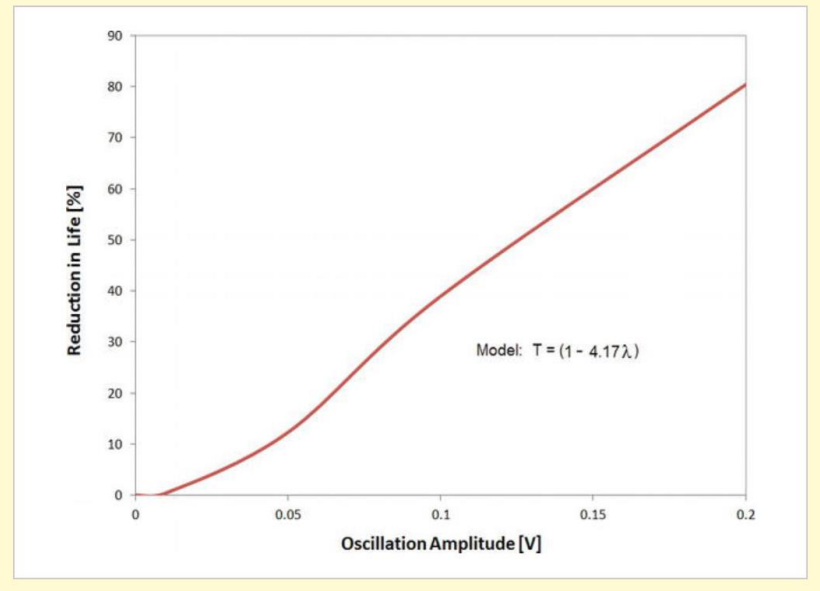

Figure 23: Percental reduction in PEMFC useful life depending on the oscillations verified on cell potential during operation, according to reference [175].

The results show that as the amplitude of voltage oscillation increases, the previewed life reduction is increased, pointing out that constant load operation is less affecting the predicted lifetime of PEMFCs.

Due to the operative constraints in load intensity and variation, hybrid systems made up of a PEMFC coupled with a battery are under investigation as they show many advantages, especially in automotive applications, to mitigate the effects of harmful operative states on the MEA. Adopting this solution, the useful life of the system can be prolonged: a Power Management System (PMS) must supervise the load sharing between the components; its strategy can balance the load demand and protect the PEMFC technology from catalyst degradation. The studies presented in the literature show a similar approach, which is to let the FC work as much as possible at a constant load while the battery has the role of covering the load peaks – when they overcome the FC power – while it is charged by the FC when the load request is lower than the FC power rate [31,33,34,176,177].

Table 10 contains the values of degradation associated with operating conditions of low power operation (idling), high power operation, transient loading, and start and stop cycles. These values have been employed in a study by Fletcher et al. [131] to implement a degradation model. Of course, the values can vary depending on the technology and the assumptions on boundary conditions and magnitude of low/high/transient operation; however, it is important to note that results agree with the ones reported in [171] on the harmful impact of Start-Up/Shut-Down (SU-SD) cycles: the degradation effect – measured in terms of voltage decay rate – associated to one SU-SD cycle compares in fact to two hours of operation at low power (and thus high cell potential).

Table 10: PEM fuel cell degradation rates (per cell) under different operations, according to reference [131].

Operating conditions	**Degradation rate**
Low power operation	10.17 μV/h
High power operation	11.74 μV/h
Transient loading	0.0441 μV/ΔkW
Start/stop	23.91 μV/cycle

Considering that usually around 10 seconds are needed to complete the SD procedure, and that – as reported in [149] – a PEMFC installed on an FCEV could be exposed to these cycles around 38500 times in its lifetime, it results that the technology could in normal operation be subjected to this condition for more than 100 hours during its lifetime [155]. This enhances the importance

of implementing a good SU-SD procedure via the control system, to mitigate its effect on materials' degradation.

During SU, a local gas mixture is formed at the anode, and it is usually called hydrogen/air or hydrogen/oxygen interface: an amount of air permeates from cathode to anode when the cell is not operating and is therefore mixed with hydrogen during the start-up phase. Hydrogen/air interface leads to a reduction reaction of air in the anode, generating a high potential and leading to the corrosion of carbon carrier in the cathode catalyst layer: this phenomenon is called reverse current. Platinum particles fall off the catalyst surface, reducing MEA's active area, and therefore the performance of the FC gets worse. In addition, the uneven distribution of reactive gas – consequent of the air permeation to the anode – can lead to fuel cell degradation due to local starvation. Even during SD, a hydrogen/air interface is created, due to air permeation and diffusion. The high interfacial potential generated can oxidize the catalyst's carbon support to carbon dioxide or even to carbon monoxide, which will disable the platinum catalyst. These processes are the major cause of performance degradation of the PEM fuel cell system during the SU-SD process [178].

SU-SD can be unavoidable, especially if the PEMFC technology will be installed on transport applications; therefore, some studies focused on mitigation strategies for SU-SD cycles. Generally, these strategies aim to avoid the creation of the hydrogen/air interface and to limit the consequent cell exposition to high potential values, through:

- Alternative catalyst support materials, more resistant to corrosion or without carbon (i.e., indium tin oxide).
- Electrical short, to eliminate the high potential developed at the cathode.
- Exhausted gas recirculation, to consume the residual oxygen in the cells.
- Use of an external auxiliary load to help the discharge of residual gas inside the cell and inhibit high potentials.

The use of an auxiliary "dummy load" has indeed successfully been employed by different automotive companies [178]. They demonstrated significant mitigation of carbon corrosion with the application of the dummy load under all conditions, especially during the shut-down procedure. This could be explained by the promoted additional oxidation of hydrogen during the displacement of the hydrogen/air interface.

Table 11 summarizes the main results of the literature review on the degradation mechanisms that can be verified in a PEMFC:

Table 11: Summary of the main causes and effects of the degradation of membrane and catalyst in the PEMFC.

Degraded component	**Process**	**Cause**	**Effects**
Membrane	Mechanical degradation	Exposure to shock/vibration	Pinholes formation, cracking
		Incorrect water presence	Reduction of membrane active area, local temperature increase (hot spots), membrane cracking
	Chemical degradation	Exposure to ionic compounds	Reduction of active sites and efficiency of proton exchange
		Exposure to free radicals	Reduction of active sites and efficiency to proton exchange, chemical attacks to the polymer
	Mechanical + chemical	Cyclic load: unstable temperature and humidity	Swelling and shrinking of the membrane leads to pinholes formation and cracking; increase in free radicals presence and chemical attack
Catalyst	Mechanical degradation	Incorrect water presence	Sintering and migration of Pt molecules, reduction of the active area
	Chemical degradation	Contaminants presence	Development of chemical bonds between Pt and contaminant, reduction of active sites
	Mechanical + chemical	Cyclic load: unstable temperature and humidity	Enhancement of Pt sintering and migration, reduction of the electrochemically active area

3.3. Results of the literature review: definition of a degradation map for catalyst poisoning

While it is important to limit the inlet of contaminants, it may be difficult due to the intrinsic properties of hydrogen and air employed as the fuel. This is why it is crucial to quantify the effect of contaminants during the time and to distinguish the consequences implied by the ones deriving from the operative conditions applied.

Many studies have demonstrated that the catalyst can be poisoned by external contaminants – present in the hydrogen if produced from fossil resources, and in the air if it is taken from polluted areas such as traffic urban areas or engine rooms – which then enter the fuel cell through the anode and/or the cathode inlets [107,124,179–199]. If catalyst degradation is verified, the achievable cell voltage can decrease permanently, causing a significant performance loss. The results of the literature review on catalyst poisoning shown in this Section have merged with the results available in the international scientific research and State of Art (SoA) on catalyst degradation by poisoning, allowing to obtain the generic effects on the

cell voltage. Literature results have been collected, analyzed, and compared, aiming to define an analytical tool to predict the cell voltage degradation depending on the environmental conditions due to reactants.

Hydrogen quality must be high and compliant with different international standards: thirteen gaseous contaminants must be monitored according to ISO 14687:2019 [200] (Table 6), SAE J2719:2020 [201], and EN 17124:2019 [202]. The common substances that are most dangerous to the catalyst at the anode side are carbon monoxide (limit: 0.2 ppm), sulphur compounds (limit: 0.004 ppm), ammonia (limit: 0.1 ppm), nitrogen compounds, and hydrocarbons in general (total limit: 100 ppm) [189,203]. The most detrimental pollutant that may reach the CL through the cathode side is in general the air contaminants (the ones found in traffic urban areas such as particulate, naphthalene, acetylene, ozone) as well as carbon, nitrogen, and sulphur oxides [193,195,204–208]. According to the United States Environmental Protection Agency (EPA), the nitrogen and sulphur dioxide presence in the air has been following a decreasing trend during the last 40 years, with an average concentration nowadays respectively between 0.050-0.035 and 0.035-0.010 ppm [209]. As regards sulphur dioxide, its average concentration in the air could already be detrimental to the CL, considering the related restrictions applied to the hydrogen gas. Yet, some concentration peaks can be verified in traffic areas, also depending on the environmental conditions (wind speed, precipitations). This is, in particular, relevant for other pollutants, such as carbon monoxide, which can reach a concentration up to 3.1 ppm in traffic areas during rush hours [210], while its content limit in hydrogen gas is set at 0.2 ppm.

Since the main component of the CL is the same, the most dangerous poisonings components are similar on the two cell sides. Moreover, the air contaminants may also permeate through the membrane and reach the anode's catalyst, increasing the effects of chemical degradation due to contamination and partially nullifying the strict regulations on hydrogen quality. Ionic substances – such as chlorine – should be avoided in the reactants' flows, too. However, they are usually more detrimental to the polymer membrane, as they tend to create bonds with the end part of the membrane's acidic chains and are therefore not deepened in this study.

While hydrogen quality is accurately monitored before the use in PEMFCs, on the other hand, it is more difficult to control the quality of air entering the cathode, considering that it strongly depends on the application and the use context (i.e., vehicles, shipping, stationary applications). This results in no internationally shared standard definition of air quality for PEMFC.

Many scientific reports have studied the effect of specific contaminant species on the degradation of the catalyst, but poisoning studies mostly consider just one species at a time. Also, the effect of contamination coupled whit dynamic operating conditions is yet poorly

investigated in the literature, while it is a relevant topic: contaminants show different effects depending on operating temperature, pressure, potential, exposure time, contaminant concentration, etc. This confirms that research is still needed to make assumptions close to reality. Finally, contamination studies in the literature never follow a testing protocol. This increases the difficulty of defining a trend in the effect of a specific poisoning compound and of comparing it to others.

While the effects of catalyst contamination can be similar on the two cell sides, they instead have a very different intensity depending on the test conditions. Among the most influencing concurring parameters to CL contamination, recent literature has underlined the relevant effect of exposure time, contaminant type, contaminant concentration, and current density. For this reason, the results shown in this Section have been obtained by focusing on these four aspects linked to CL degradation by five contaminants: CO, H_2S, NH_3, NO_2, and SO_2. Among the results available in the literature, only the ones related to a single PEMFC under stress tests have been considered, to obtain a more reliable comparison between results. On the other hand, as contaminants and materials are similar at the anodic and cathodic sides, and considering the membrane permeability to the contaminants, these results have been analyzed together. Both AST and Long-Lasting Tests (LLT) have been considered. The firsts (which involve high contaminant concentrations and short time) are usually more convenient from the economic and time demand point of view; however, they differ from real operative conditions and can give misleading information. Indeed, Platinum poisoning after a certain time tends to reach an equilibrium point, where associative and dissociative reactions with the contaminant are almost even. Thus, the degradation effect results smoothed if observed in the long term. However, both AST and LLT are considered in this Thesis, to identify the minimum time a test should last.

To understand the effect of contaminants under different test conditions, a deep literature investigation of experimental results has been carried out. Different articles have been found, which reported the results of experimental activities concerning CL poisoning effect quantification. The presence of CL degradation can be usually detected by a voltage reduction. Therefore, to estimate the degradation level, it is useful to evaluate the voltage reduction measured at the same current density. For this reason, only the articles containing the evaluation of voltage reduction have been considered for the present work, and the authors which had instead defined a current reduction at a given voltage value, difficult to be compared, have been excluded.

The Equations hereby described (from Eq. 32 to Eq. 36) are the resulting method proposed by the Author to quantify degradation and make it comparable among different contaminants while

considering the operative conditions (contaminant concentration, exposure time, current density).

On a first attempt, a percentage voltage decay V_D has been computed for the results found in the literature. This is obtained with Equation 32, comparing the baseline cell voltage defined in the respective publication to the cell voltage measured after the stress test:

$$V_D = 100 \cdot \frac{V_{baseline} - V_{after\_test}}{V_{baseline}} \qquad \textit{Equation 32}$$

Where:

- $V_D = Percentage\ Voltage\ Decay$ [%].
- $V_{baseline} = Initial\ Cell\ Voltage$ $[V]$.
- $V_{after\_test} = Final\ Cell\ Voltage$ $[V]$.

The voltage decay V_D has been initially employed to analyze results concerning a single contaminant provided to the PEMFC at a constant concentration and to check the influence of exposure time and current density on the CL degradation. However, the V_D value resulted in very different and non-comparable results that are obtained at different exposure times, neither within tests that employ the same contaminant.

To make AST and LLT results comparable, an Average Voltage Decay Rate $V_{DR\text{-}Avg}$ has been defined from the voltage decay V_D divided by the exposure time. $V_{DR\text{-}Avg}$ is calculated in the following way:

$$V_{DR\_avg} = \frac{V_D}{\Delta t} \qquad \textit{Equation 33}$$

Where:

- $V_{DR\_avg} = Average\ Voltage\ Decay$ $\left[\%/_h\right]$.
- $V_D = Percentage\ Voltage\ Decay$ [%].
- $\Delta t = Test\ duration\ [h]$.

This value can be used as a reference to compare the results of studies at different durations available in the literature. However, if an AST is implemented for a time shorter than 1 hour, the V_{DR_avg} value can be misleading resulting in values higher than 100%. These values are not consistent, but it is due to the voltage decrease that can be very strong in the first minutes of exposure to the contaminant due to the kinetics of the reactions affecting the CL. This fact underlines the necessity of longer stress tests. The $V_{DR\text{-}Avg}$ has been calculated for all the results found in the literature, allowing a general comparison among the five contaminants and their effect on cell voltage.

Nevertheless, the V_D and $V_{DR\text{-}Avg}$ obtained did not allow the definition of a trend to describe the degradation effect at different contaminants concentrations, exposure times, and current density. To have a more global view of the CL degradation phenomenon, and to account for more than one factor at the same time, it has been necessary to define new parameters. The first one is the Coulomb density C_D, and it is obtained through Equation 34. The Coulomb density allows to consider both the current density at which the experimental test is developed and the test duration:

$$C_D = I_D \cdot t \qquad \textit{Equation 34}$$

Where:

- $C_D = \ Coulomb\ density\ \left[{C}/{cm^2}\right]$.
- $I_D = current\ density\ \left[{A}/{cm^2}\right]$.
- $t = \ test\ duration\ [s]$.

The last parameter defined has been named as Reduction Effect (RE). This is an indicator of the contaminant mass that reaches the fuel cell, and it is obtained by Equation 35:

$$RE = C_D \cdot C_{conc} \qquad \textit{Equation 35}$$

Where:

- $RE = \ Reduction\ Effect\ \left[{C \cdot ppm}/{cm^2}\right]$
- $C_D = Coulomb\ density\ \ \left[{C}/{cm^2}\right]$
- $C_{conc} = \ Contminant\ concentration\ \ [ppm]$

The RE can quantify the degradation of the CL in terms of $V_{DR\text{-}Avg}$ depending on the operative conditions (concentration, time, current density).

Table 12, Table 13, Table 14, Table 15, and Table 16 resume the most interesting results for V_D and $V_{DR\text{-}Avg}$ calculations, obtained starting from literature values. These values confirm that, for all the 5 contaminants investigated, there is a link between the intensity of degradation and the current density. This is as well visible in Figure 24 (which contains results for CL poisoning with 10 ppm CO) and it is following the fact that, at a higher current density, the reactants flow is increased and so is the amount of contaminant reaching the CL. From these results, it is also possible to observe that a higher contaminant concentration has a more detrimental effect on cell voltage, even in LLTs. Therefore, even if in the long term the CL kinetics of contamination reaches equilibrium, a higher concentration results in more impact. Yet, the results of AST have

an impact on both V_D and $V_{DR\text{-}Avg}$ which can reach a 1 or 2-orders magnitude difference. Publications found in the literature are generally difficult to be compared, as the absence of test protocols (temperature, duration, contaminant concentration, load profile) does not allow to exclude some of the variables which instead – as visible from the Tables reported in this work – have a strong influence on cell voltage.

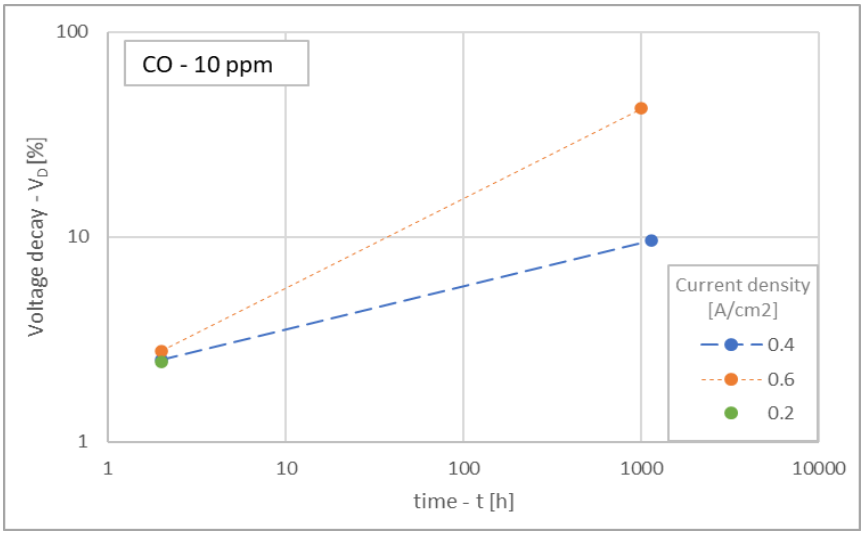

Figure 24: V_D for 10 ppm CO contamination at different current densities and exposure time.

Results for CO contaminations shown in Table 12 are obtained with a pollutant concentration always higher than the imposed limit indicated in ISO 14687-2 (0.2 ppm) and higher than the peaks that can be registered in traffic urban areas (3.1 ppm). These tests are in general more detrimental at higher current density and longer exposure time, but in the longer duration, the voltage loss seems more significant for operation at a higher current density. The chemical bonding reactions between the catalyst and the poisoning compound appear more frequent at first, then an equilibrium is likely to be reached: this could explain the greater average voltage decay rate for AST.

Table 12: Degradation associated with carbon monoxide contamination in literature results.

Concentration of CO [ppm]	**Time [h]**	**I_D [A/cm^2]**	**V_D [%]**	**$V_{DR\text{-}Avg}$ [%/h]**	**Reference**
10	2	0.2	2.45	1.23	[211]
10	2	0.4	2.51	1.26	[211]
10	2	0.6	2.78	1.39	[211]
10	1145	0.4	9.6	0.01	[212]
10	1000	0.6	42.2	0.04	[212]
50	1	1.2	23.39	23.39	[211]
100(*)	0.6	1.2	93.57	160.42	[211]

100(*)	0.3	0.2	66.21	198.65	[205]

For what concerns hydrogen sulphyde (Table 13), literature results have been found only for anode contamination, as H_2S is not usually present in the air stream. Its tested concentration is also always higher than the allowed amount in the hydrogen stream (0.004 ppm). However, the results evidence that it causes a higher voltage decay than CO at similar exposure time and concentration (see tests at 18 and 30 ppm of H_2S compared with the results of 50 ppm CO). Nevertheless, results for LLT are lacking in the literature and it is therefore impossible to make a comparison to other contaminants at longer exposure times. Observing the results from references [213] and [214] it can be concluded that the effect of current density is not negligible, and a higher current density has a more detrimental effect.

Table 13: Degradation associated with hydrogen sulphide contamination in literature results.

Concentration of H_2S [ppm]	**Time [h]**	**I_D [A/cm^2]**	**V_D [%]**	**$V_{DR\text{-}Avg}$ [%/h]**	**Reference**
1.15	25	0.1	47.76	1.91	[213]
1.5	6	0.8	94.98	15.83	[214]
1.95	15	0.5	68.73	4.58	[213]
11.73	15	0.1	61.12	4.07	[213]
18	1	0.6	32	16	[215]
30	1	0.6	66	66	[215]

Contamination by ammonia can be a relevant issue in the medium-long term perspective of using it to store hydrogen. Its limit is set at 0.1 ppm in the hydrogen gas (Table 6), and the experimental results in the literature regard tests with higher contaminant concentrations provided both at the anode [216] and the cathode side [188,217]. It causes a voltage decay that is on average in between the one caused by CO and the one caused by H_2S poisoning, and the effect is enhanced at higher current density tests.

Table 14: Degradation associated with ammonia contamination in literature results.

Concentration of NH_3 [ppm]	**Time [h]**	**I_D [A/cm^2]**	**V_D [%]**	**$V_{DR\text{-}Avg}$ [%/h]**	**Reference**
1	330	1	5.97	0.018	[188]
1	330	0.75	4.96	0.015	[188]
1	330	0.5	4.11	0.012	[188]
2	330	1	4.98	0.071	[188]
10	1	0.7	10	10	[217]
200	1.6	0.1	65.06	20.96	[216]

The NO_2 contamination results found in the literature show a contaminant concentration lower than the limits for total nitrogen compounds in the hydrogen flow (100 ppm) and higher than the one found in urban areas (below 0.05 ppm). While reference [217] analyses the effects of nitrogen dioxide supplied at the anode, references [218] and [219] face the cathode contamination by air impurities. Short tests indicate that NO_2 exposure can cause a higher voltage decay than CO and NH_3, but the effect still seems lower than the one caused by H_2S if the 1-hour tests at 10 ppm concentration are compared.

Table 15: Degradation associated with nitrogen dioxide contamination in literature results.

Concentration of NO_2 [ppm]	**Time [h]**	**I_D [A/cm^2]**	**V_D [%]**	**V_{DR-Avg} [%/h]**	**Reference**
1	100	0.5	10.45	0.104	[218]
2.5	24	0.6	7.97	0.332	[219]
5	12	0.6	12.31	1.026	[219]
10	1	0.7	20.00	20	[217]

With regards to sulfur dioxide contamination, all the references for this case are dealing with cathode exposure to the poisoning compound. All the examples found in the literature are comparable in terms of contaminant concentration, exposure time, and current density, and the results evidence that contaminant concentration is not directly linked to the voltage degradation: indeed, the voltage decay is lower for the 46-hour test with 2.5 ppm SO_2 in the supplied air [219] than for the test with 1 ppm developed for 50 hours [220]. This happens despite the similar current density implemented during the tests (0.6 A/cm^2). Therefore, there may be other parameters that influence the voltage decay which have not been included in the present analysis – such as operative temperature and relative humidity. This topic needs further development in future studies.

Table 16: Degradation associated with sulphur dioxide contamination in literature results.

Concentration of SO_2 [ppm]	**Time [h]**	**I_D [A/cm^2]**	**V_D [%]**	**V_{DR-Avg} [%/h]**	**Reference**
1	50	0.6	27.82	0.556	[220]
1	100	0.5	35.29	0.353	[218]
2.5	46	0.6	18.84	0.410	[219]
5	23	0.6	28.26	1.229	[219]

The first conclusion is related to the contamination test duration: AST has the aim of saving time and economical resources and thus they expose PEMFCs for very short times to contaminants concentrations that are not found in real operative conditions. The results of this

type of test can be misleading and can give unreliable information on the cell's durability in standard operative conditions. According to the experimental results found in the literature, a minimum duration of 50 h is needed in a stress test to estimate reliable cell durability. Moreover, the contaminant concentration must be coherent to the one that can be verified in real applications (i.e., urban areas concentrations for FC cars, FC-rooms concentrations for shipping, etc.).

As regards the degradation prediction of a PEMFC exposed to a contaminated reactant flux, the computation of the RE can give useful information. RE can consider at the same time all the significant parameters involved in CL contamination and degradation (concentration, time, current density). Thanks to results found in the literature, it has been possible in the context of the present Thesis to individuate a trend that links RE – which can be computed for real-case as well as laboratory tests – to the parameter $V_{DR\text{-}Avg}$.

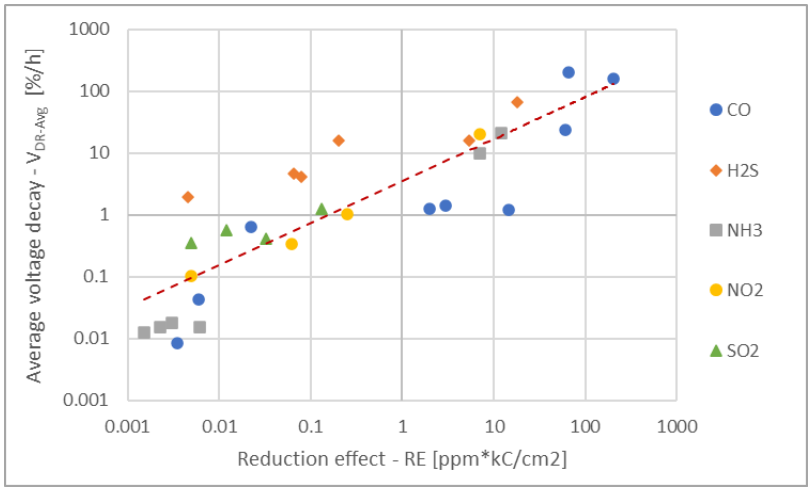

Figure 25: Trend of the RE for the literature results investigated.

This result, shown in Figure 25, is consistent with the data available in the literature; it underlines – for all the contaminants investigated in this study – the enhancement of the Average voltage decay rate at an increasing RE, with the following relation:

$$V_{DR\_avg} = a \cdot RE^{b} \qquad \textit{Equation 36}$$

Where:

- $V_{DR\_avg} = Average\ Voltage\ Decay\ \left[{}^{\%}/_{h}\right]$.
- $RE = \ Reduction\ Effect\ \left[{}^{C \cdot ppm}/_{cm^2}\right]$.
- $a = 3.5;\ \ b = 0.68$.

As indicated by Equation 36, the relationship between the average voltage decay and RE is a potential function (as clear by Figure 25, where both axes are logarithmic). This output is also confirming the results as well described in the literature, defining Sulphur-compounds as the most detrimental contaminant to the PEMFC's state of health.

These results have been described in a dedicated publication [221]. Further development of this research will include collecting additional experimental outputs to increase the reliability of the relation here presented. Moreover, this analysis approach can be addressed to the single contaminant species and to other degradation sources, such as flooding or dehydration issues linked to the presence of free radicals that may damage the polymeric membrane.

4. Experimental validation of the PEMFC technology: test protocols definition and test campaign on the HI-SEA Laboratory

4.1. International regulations for the installation of PEMFC systems on maritime applications and testing protocols for FCS on shipping: FC-PROMATE Project

No dedicated regulations for the installation of FC systems onboard maritime vessels currently exist. Therefore, to have a broad overview, the Author has reviewed the available existing legislations defined by the CS for fuel cell installations, that concern their operational conditions on vehicles. Besides, the Author has considered the aspects related to naval regulations for what concerns environmental conditions onboard.

The outcome of the study of the available legislation, as described in Section 1.5, is the definition of a test list to assess different conditions that a PEMFC system can face on a maritime vessel. This is in fact part of the European project FC-PROMATE, currently under development. The main project outputs are: i). the list of experimental tests necessary to define the FCS suitable for the installation onboard – already developed by the Author; ii). The implementation of tests in the Joint Research Center (JRC) in Petten (NL), and a consequent thorough data analysis to study the influence of operative and environmental parameters on the PEMFC outputs – currently under development by the Author.

The tests can be divided into six different typologies:

- Environmental.
- Operative.
- Emissions.
- Normal conditions.
- Failure conditions.
- Routine tests.

Once the dedicated test protocols necessary to be completed before the FCS installation onboard are individuated, the different available FC technologies should be tested following the outlined procedure. In this way, it is possible to assess if the commercial technology investigated is

suitable for onboard operation. Besides, the results of test protocols can identify the best FCS among the available ones.

To prove the effectiveness of the test protocols defined, they have been implemented on the FCS evaluated for the installation onboard the Zero Emission Ultimate Ship (ZEUS) by Fincantieri, a research vessel under construction designed for the TecBia project. ZEUS will be powered by a PEMFC system in a hybrid configuration (batteries and diesel engines are installed as well). To develop the tests, an experimental test rig has been designed and built by BluEnergy Revolution (BER [222]), an emerging company operating in the field of hydrogen applications on marine vessels, with the support of the Author. BER also designed a dedicated platform able to withstand 500 kg and to offer two different inclination degrees: 30 and 45°. This test rig is crucial to estimating the effects of static inclination on the FCS performance.

Table 17 summarizes the experimental tests that have to be carried out on the FCS to evaluate its suitability for maritime applications. The depicted tests have been in fact partly reproduced in BER's test rig on different FC systems, with the support of the Author in the development of tests as well as in data post-processing, producing the results that are shown below (namely FCS Efficiency, Polarization curve, Operative profile, Static inclination tests). Another part of the tests has been implemented in the testing facility of the JRC in Petten. Here, the Author has overviewed the activities, choosing the galvanostatic operation mode and the environmental conditions to be set in the climatic chamber, and is currently working on data post-processing to define the effect of the experimental campaign on a chosen PEM FCS. This work is under development and will not be part of the present Thesis.

Table 17: Experimental tests performed.

Typology	**Test description**	**Regulation**
Environ-mental tests	Cooling temperature: ±2°C from setpoint	RINA PartC, Vol II, Sec2
	Static inclination: startup+constant load at 30°	IACS UR E-10
Operative tests	Efficiency: calculated at 25%, 50%, 75% and 100% of nominal power	EC 62282-3-200
	Power response (electrical and thermal, time needed), minimum to nominal power, and reverse	EC 62282-3-200
	Start-up/shutdown: time response of the net electrical power	EC 62282-3-200

Emissions tests	Maximum noise: during operation and in background with FCS off	EC 62282-3-200
	Maximum vibrations: during operation and background with FCS off	EC 62282-3-200
	Exhaust reaction water: quantity and quality	-
Normal conditions tests	Polarization curve	-
	Constant load (minimum time: 15 minutes)	-
	Typical navigation profile simulation	-
Failure conditions tests	Emergency shutdown: time needs to conclude the procedure	EC 62282-3-200
Routine tests	Visual inspection (agreement with technical schemes)	IACS UR E-10
	Voltage variation measure	-
	Gas leakage assessment test (on FC stack)	-

Here below, more details are supplied for what concerns the most important tests of the routine and the results of their application to the FCS in BER's test rig. The results of the application of the tests are related to the commercial FC technology that was eventually chosen for the installation onboard ZEUS. A description of the FCS tests performed by BER, and the results obtained, are described below and in the next figures (Figure 26 to Figure 33). Results are original and have been reported in a dedicated publication [133].

FCS efficiency

According to [68], the efficiency should be calculated based on the Higher Heating Value (HHV) of hydrogen, and the calculation requires the following measures:

- Hydrogen inlet flow rate.
- Heat supplied/absorbed externally.
- The flow rate of the oxidant (air) entering the system.
- Electrical power absorbed by auxiliaries.
- Electrical power generated by the system.

Besides, the efficiency test should be conducted following the procedure:

- Start the system and require constant power.

- Verify that the system operates in stable conditions, i.e., within the limits of variability imposed by the [68] regulation.
- Measure the parameters necessary for the calculation of efficiency for no less than 1 hour.

The electrical efficiency η_{el} of the system can be therefore calculated by using the following formula:

$$\eta_{el} = \frac{P_n}{P_{in}} * 100 = \frac{\left(P_{el,out} - P_{el,aux}\right)}{\left(P_{fuel,in} + P_{air,in}\right)} * 100 \qquad \textit{Equation 37}$$

Where P_n is the net electrical power generated by the system, and P_{in} is the total power input to the system. The thermal efficiency of the system is calculated as:

$$\eta_{th} = \frac{P_{HR}}{P_{in}} * 100 \qquad \textit{Equation 38}$$

Where P_{HR} is the recoverable thermal power output from the system, and it is obtained by the following equation:

$$P_{HR} = \dot{m}_{HR} * c_{HR} * (T_{HR1} - T_{HR2}) \qquad \textit{Equation 39}$$

knowing the mass flow $\dot{m}_{HR}$ of the cooling fluid [kg/s], its specific heat c_{HR} at given temperature and pressure [J/(kgK)], and the temperature difference $(T_{HR1} - T_{HR2})$ between entrance and exit of the system under consideration.

In order to compare the performance of FC systems, it is necessary to normalize the dimensions on which carry out the comparative study. The comparative analysis mainly concerns the performance in terms of voltage and current ranges, as well as system efficiency. The latter is given by the net system power output divided by the gross power input, which accounts for the power absorbed by auxiliaries. Since the powers absorbed by the BoP have different levels of uncertainty and changes depending on the components installed, to make the analysis meaningful it was chosen to proceed with the calculation of the electrical performance measured concerning the stack, excluding the consumption of the BoP. Figure 26 shows the trend of efficiency depending on current density, as calculated from the experimental data.

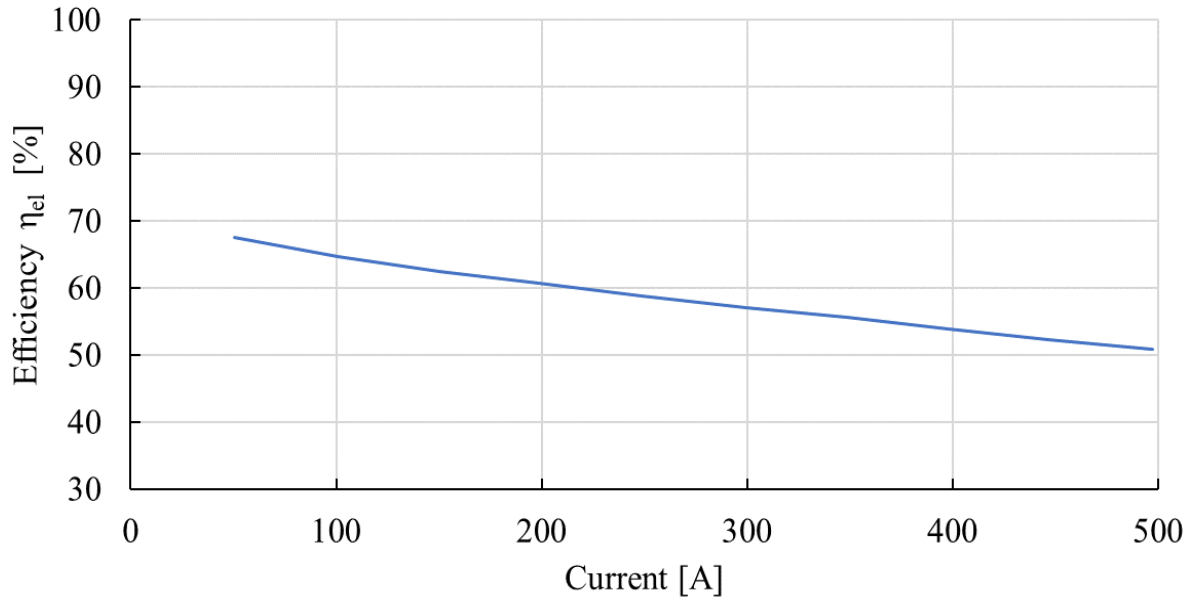

Figure 26: Electrical efficiency of the FCS tested.

Polarization curve

Experimentally reproducing a polarization curve implies that an FC (single cell or stack) will be subjected to the operation at subsequent current setpoints, from zero to the nominal value and back to zero. This procedure allows the operator to draw for the tested device the V-I curve, which varies slightly for FC technologies by different manufacturers. In general, the goal of measuring the polarization curve is the determination of MEA's performance in terms of cell voltage and power density considering the current density as a reference. The residence time of each set-point should be long enough to ensure the stabilization of cell voltages in ±5 mV in a time range between 2 and 15 minutes, except for the OCV measure, which must not exceed one minute of stay. The set-points proposed by the EU Harmonised Test Protocols for PEMFC-MEA Testing in Single Cell Configuration for Automotive Applications [223] are summarized in Figure 27: the y-axis represents the current density at which the FC must be tested, while the x-axis indicates the subsequent test steps. This harmonized test protocol is designed for single-cell tests and for this reason the possibility to make slight changes to the protocol is allowed, in order to apply it in the best possible way to the characteristic limitations of the individual FC modules: minimum operating electrical power, longer possible operation at minimum power, etc.

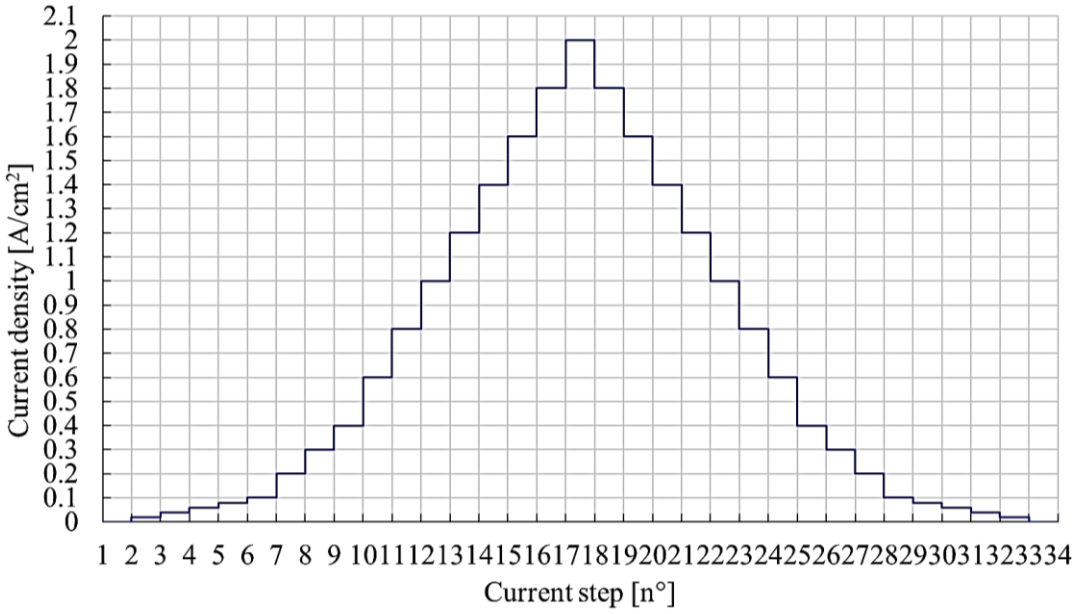

Figure 27: Setpoints for the polarization curve testing [223].

Figure 28 shows the experimental V-I points collected during the dedicated tests (blue dots), compared with two reference curves named "FAT", which stands for Factory Tests. The yellow and orange lines represent in fact the results of the FATs that have been implemented by the FCS supplier, and which are given together with the specifics of the system. The two curves represent respectively the implementation of the first half of the current profile shown in Figure 27 (orange line), and the second descending half (yellow line). It is possible to notice from Figure 28 that FAT's results and the ones obtained inside BER's test rig are similar; the slight difference is mainly due to the lower temperature of the FCS (air, cooling fluid, components) during the test.

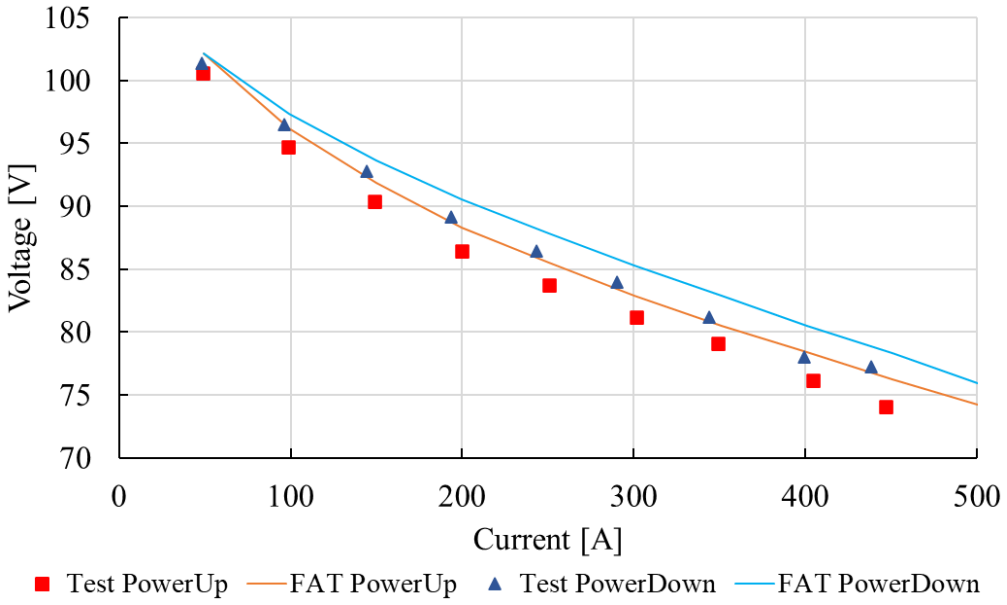

Figure 28: Polarization test results.

Operative profile test

To verify the adequacy of the performance of the FC module in a real on-board application, part of a typical naval cargo load energy demand profile – agreed with Fincantieri – is considered. This profile can be divided into two parts: the first one, where first some increasing and later some decreasing load steps are present, represents the dynamic load that can be required during maneuvering. The second one simulates navigation after maneuvering inside the port, where the system works for a longer period at constant load and 100% of its capabilities. It may represent the load request during navigation at constant speed for propulsion, or the case where the system is employed as an auxiliary to cover the hotel load. The profile can be obtained thanks to the implementation of the electrical control of the systems (including the FC and DC/DC module coupling).

Figure 29 shows the shipping load profile cited, to be applied to the PEM fuel cell systems under consideration for 4300 seconds.

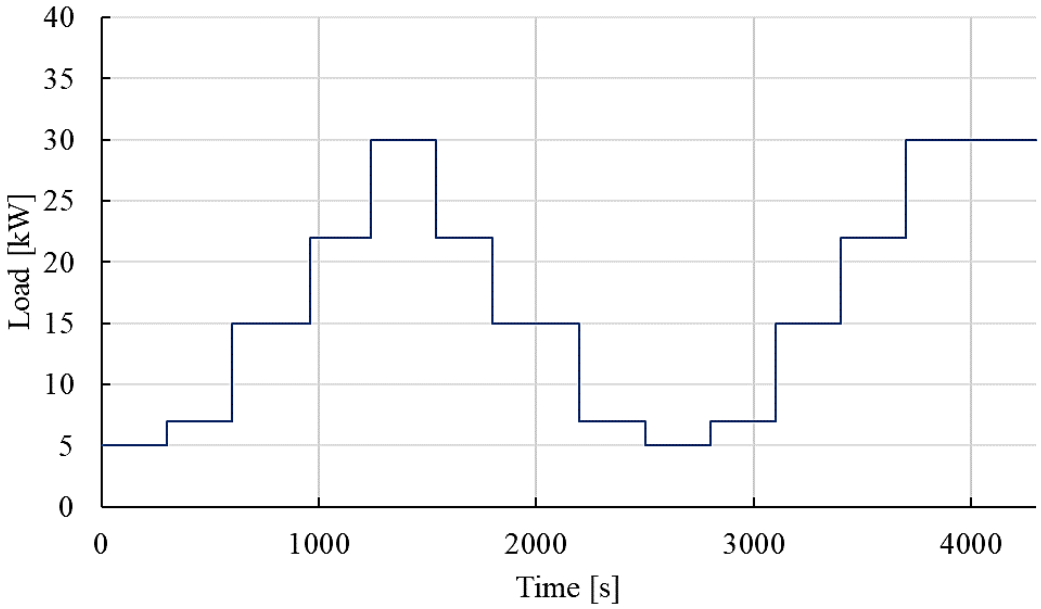

Figure 29: Shipping load profile assumed to be tested on the FCSs.

Unlike tests in stationary and dynamic conditions, the operating profile represents a mix that can positively or negatively affect stack performance. The tests have been conducted in ideal conditions, to evaluate the global average performance of the FC system during the implementation of the operative profile. In Figure 30, it is reported the trend of the electrical power output – P_{el} – and of the thermal power – P_{th} – exchanged by the cooling circuit during the development of the naval profiles tested. The load request is always guaranteed, while the thermal power follows the trend of the electrical power output and is always managed correctly by the cooling loop. The FC stack voltage reaches a stable value during the implementation of

each load step, despite the short time. This is especially appreciable at the end of the test, where a high and constant load is requested after the more stressing dynamic load, demonstrating that the FCS can withstand a similar load profile.

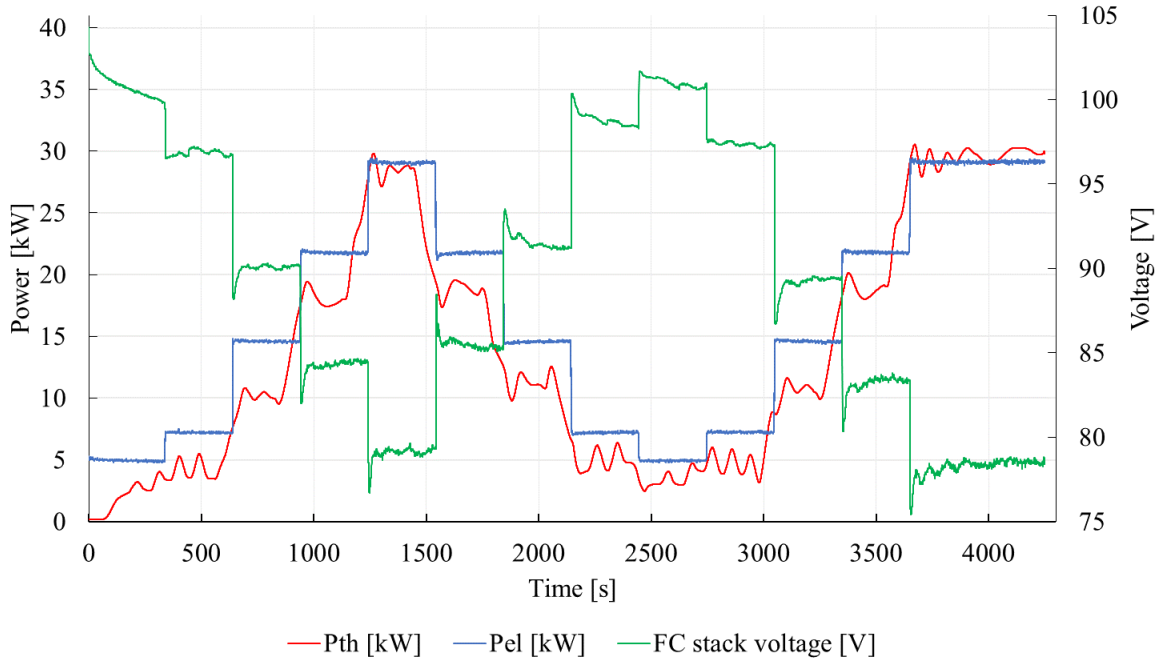

Figure 30: Operative profile test results.

Static inclination test

To assess the ability of the FCS to work while inclined, it has been installed and tested under static load conditions on the Test Bench developed by BER (Figure 31).

The angle of inclination tested was 22.5°, and the load request during this part of the assessment was constant for a prolonged period (around 20 minutes), to verify the good operation of the system in this condition. The main concerns that may arise from this type of operation are linked to the efficient delivery of the reactants and cooling flows to the FCS.

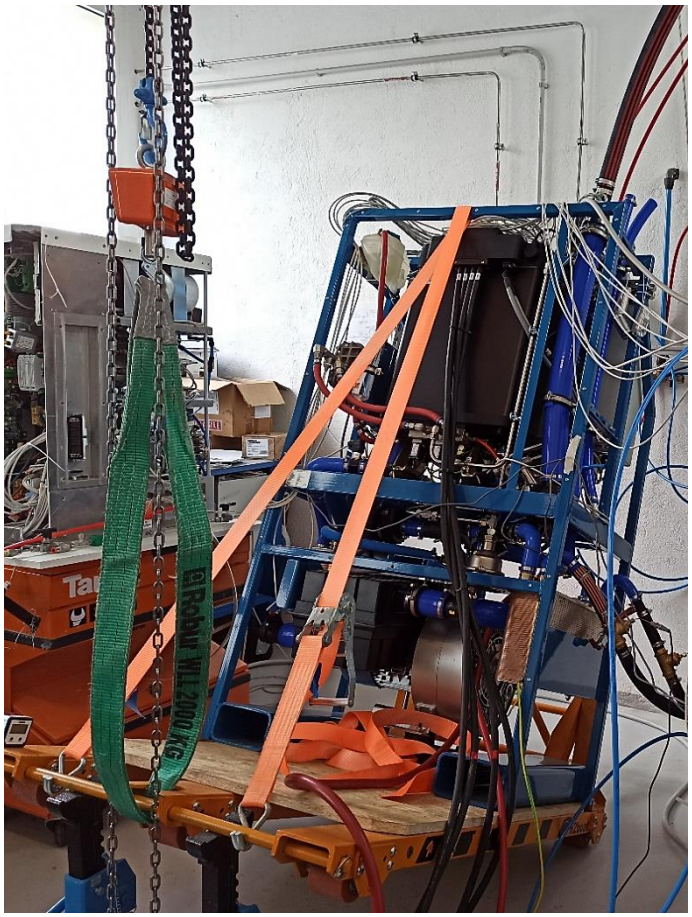

Figure 31: Static inclination platform developed by BER.

The results of this test are compared with the implementation of the same load profile on the non-inclined stack in Figure 32 and Figure 33:

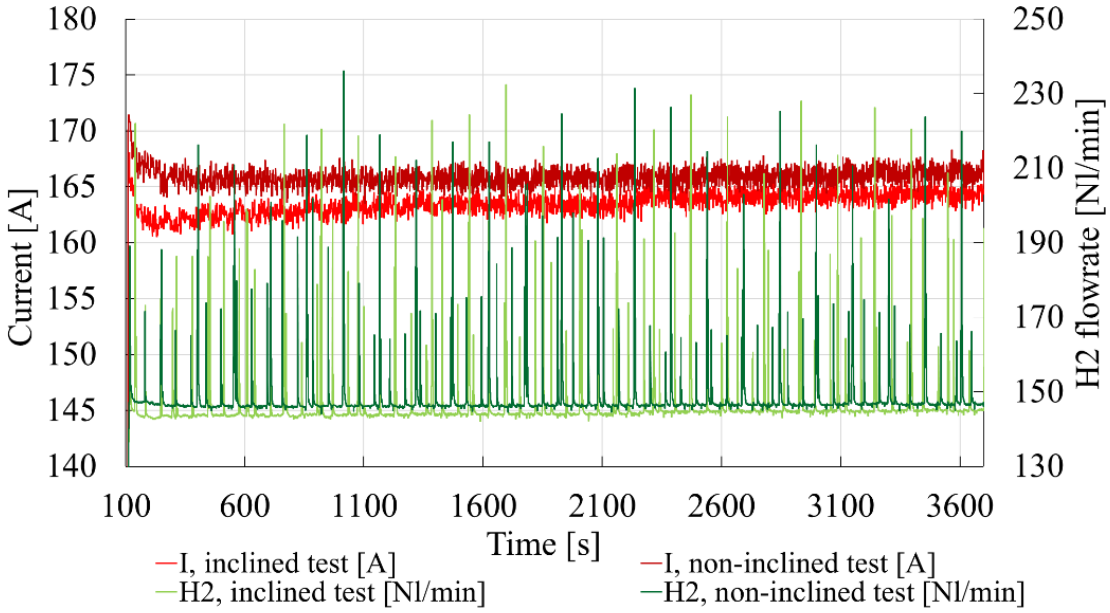

Figure 32: Static inclination test results - current and hydrogen flowrate.

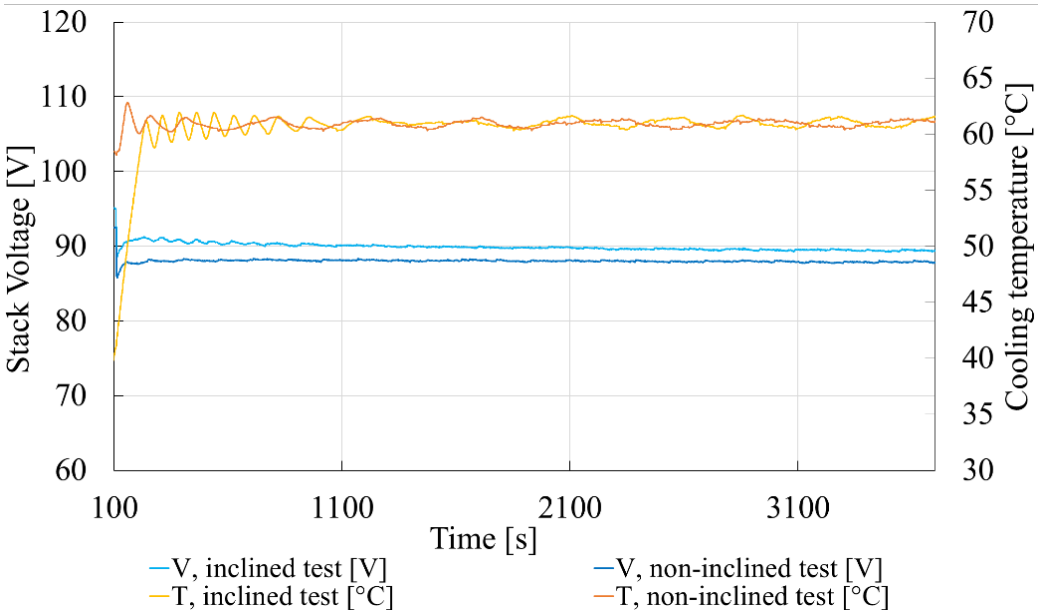

Figure 33: Static inclination test results - cooling temperature and stack voltage.

During these tests, the specific consumption, the efficiencies of the system, the analysis of the purges, the temperatures and operating pressures of the FC system, the temperatures and flow rates of the cooling output to the FC system, the measurement of water produced at the cathode, and the measurement of the water purged at the anode have been defined. No abnormal operating conditions have been encountered, confirming the good setting and operation of the stack control system which automatically manages the cooling, the airflow rates, and the current supply ramp. The constant load has been maintained for a long time without major fluctuations but, most important, no difference in the stack voltages has been measured, proving that the humidity management of the system is optimal.

In conclusion, the review of existing legislation regarding operational requirements for FC on vehicles and environmental conditions onboard ships has brought to the definition of a testing routine. The latter has been suggested to be taken as a reference by the international naval registers. The collaboration of the University of Genoa with the RINA in the context of the FC-PROMATE project will lead to the approval of the test procedure for the definition of internationally shared standards. The definition and implementation of the test routine allowed to individuate the best commercially available PEMFC technology to be installed onboard the ZEUS research vessel, which is the main outcome of the TecBia project. The PEMFC system supplier has in fact been defined thanks to the comparison of results of the testing routine, namely FCS Efficiency, Polarization curve, Operative profile, and Static inclination tests. More tests are under implementation at the JRC laboratories, overviewed by the Author who is also taking care of the data post-processing and interpretation.

4.2. The HI-SEA Laboratory

Given the rising interest in PEMFC systems for maritime applications, the University of Genoa and Fincantieri developed the Hydrogen Initiative for Sustainable Energy Application (HI-SEA) Joint Laboratory, a 240-kW system based on 8 PEMFC automotive modules Orion® (30 kW each) supplied by Nuvera Fuel Cell with the goal to scale-up the existing technology and assess the on-board integration [44]. Fincantieri is the main Italian shipbuilder and is starting a path toward the construction of zero-emission vessels in the next years [67]. The HI-SEA Joint Laboratory represents the first large-scale PEMFC test rig especially dedicated to the study of FC for marine applications. The goal of the laboratory is to define the best design for a modular FC system for ship applications able to guarantee the maximum life span of FC stacks, without omitting performance. The HI-SEA Project has been the heart of the work developed by the Author in the context of this Thesis. In fact, the Author has been responsible for the definition of the experimental activities and experimental data post-processing during 2018-2022 that brought to: i.) understanding of previous issues verified on the system; ii.) reactivation of the system; iii.) definition of a recovery procedure; iv.) refitting of the Balance of Plant components; v.) final commissioning of the system and assessment of its employability for operation onboard a ship.

The first and main objective of the FCS test rig, previously developed during the TESEO Project (2014-2016) [224], was the definition of the best design and size of a modular PEMFC system for ship applications. The goal was achieved towards the development of a highly flexible system able to demonstrate the feasibility of the technology in a simulated relevant environment, namely a ship fuel cell room. The HI-SEA system commissioning started in 2018, brought to the installation and recovery from inactivity [225] of the 8 PEMFC stacks, with a procedure similar to what was reported by Yap et al. [226] and which will be described in Section 4.3.2.1 [227]. Then the FCs power plant was tuned (Section 4.3.3) [228] to prepare the experimental campaign for studying the power plant's behavior under different marine operative conditions (Section 4.4) [45]. The initial state of health of the cells was in fact poor due to wrong test conditions during project TESEO and inactivity between 2016 and 2018. Therefore, some changes to the control system were necessary to operate the system: for example, it was necessary to increase the cathodic air inlet mass flow rate – especially at low current operation – to enhance cell voltage and allow test development. This is in line with the results of reference [229,230], where performance at low current is increased by employing a higher air mass flow rate.

The FCS is installed in the Innovative Energy Systems (IES) Laboratory inside the Savona Campus (Figure 34), partly inside the 10-meter container that simulates a dedicated machinery room, following typical redundancy principles of ship architectures [231] that brought to a configuration of two symmetrical branches (branch01 and branch02), electrically connected in parallel.

Table 18: HI-SEA system technical data.

Max H_2 mass flow rate	14.4 [kg/h]
Max H_2 Pressure	10 [bar]
Max Air flow rate	12.3 [Nm^3/min]
Max Air Pressure	10 [bar]
Output Voltage	500 [Vdc]
Output Current	600 [A]
Power	240 [kW]

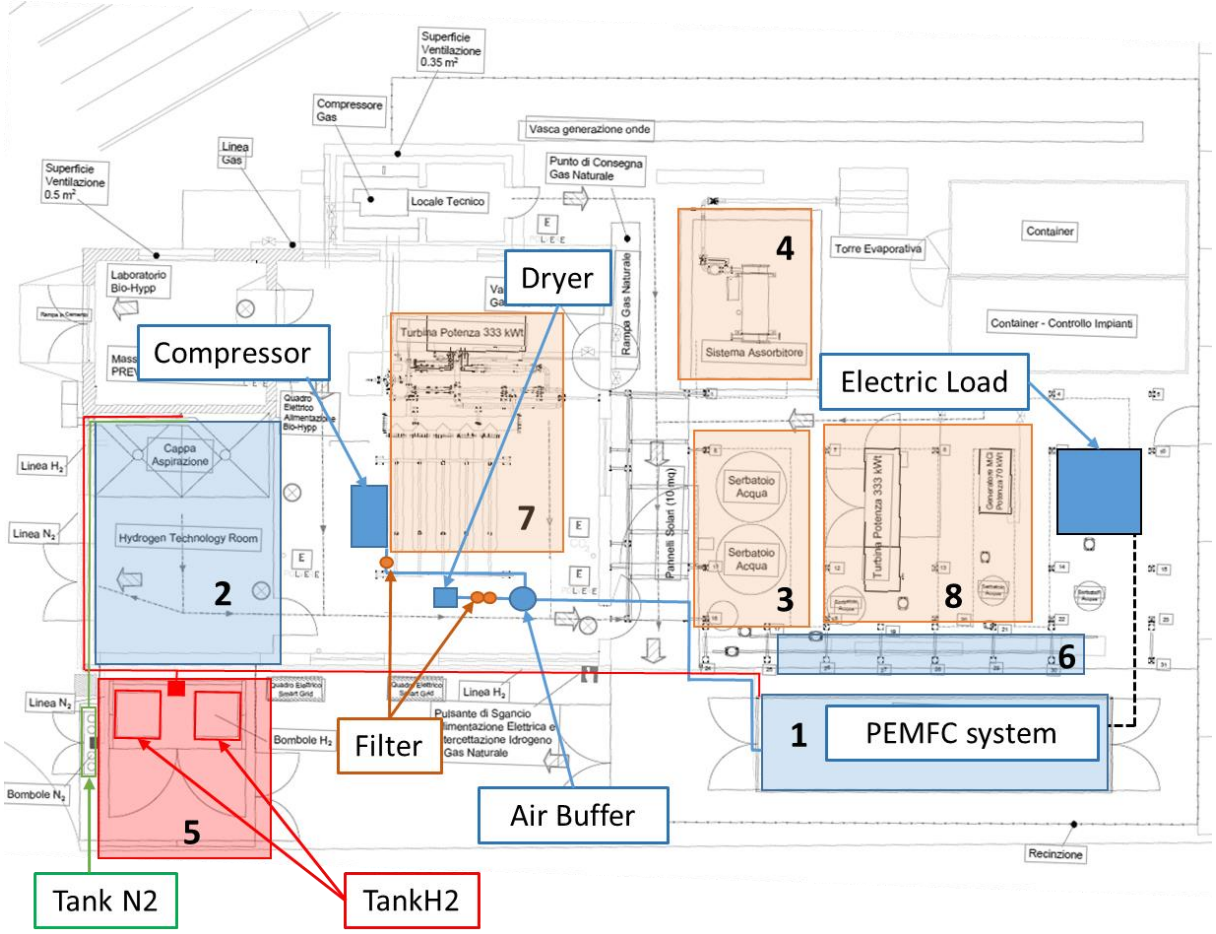

Figure 34: The IES Laboratory and location of components of the HI-SEA system.

Each branch is composed of four Fuel Cell Modules (FCM01 to FCM04 on branch01, FCM05 to FCM08 on branch02), electrically connected in series, a dedicated cooling system, and power conversion components.

The HI-SEA container is shown in Figure 35.

Figure 35: The HI-SEA PEMFC system, view of the container – outside and inside.

4.2.1. Main components

The P&ID of the system is shown in Figure 36. Hydrogen is stored in pressurized tanks, and because of its high flammability and explosivity, safety issues are an important aspect. Risks are minimized using a box, in which two groups of tanks are safely stored and naturally ventilated that could contain an explosion. Pipelines exiting from the box are made by inox steel 316L and provide hydrogen to the HI-SEA laboratory and the H_2 Lab, a test room for stacks up to 30 kW, and for tests with Metal Hydrides. Inside the hydrogen-tank box are a control panel for a first pressure reduction from 200 to 30 bar and a second that allows to vary the pressure in the interval 0-30 bar. The HI-SEA inlet pressure varies in the range of 7-12 bar, and the inlet pressure H_2 Lab is lower.

Close to the hydrogen gas box, there is the Inert box that contains pressurized Nitrogen. This gas is used to guarantee safe work conditions and to pressurize the system in case of maintenance or long periods of inactivity. In this case, after closing the H_2 valves that control distribution from the box, the system would be ventilated for about two minutes before N_2 is pressurized inside pipes and H_2 is removed by the system.

The air supply line has been designed to feed the fuel cells of the HI-SEA plant. All components related to the air supply line are installed inside the IES Laboratory, to ensure greater protection against atmospheric agents and consequently a longer useful life. Air provided to the plant must

be appropriate in terms of flow rate, pressure, and quality, without pollutants and with a specific level of residual moisture. Pipeline material is aluminum to guarantee a high quality of air, in terms of purity. A remote sensor and an analogic pressure sensor have been installed on the air supply line; condensation is removed with a dedicated line outside the laboratory. There is the possibility of adding a relative humidity sensor. Cathode air is stored into accumulation volumes, then it passes through the dryer and finally through the shut-off valve at the inlet of the container. A portion of air is used also in the H_2 Lab.

During the operation, the plant produces a total thermal power that ranges from 0 to 240 kW_{th} dissipated by a suitable cooling circuit designed in two circuits:

- Internal or primary circuit.
- External or secondary circuit.

The heat released by the eight fuel cell stacks is removed by the primary circuit, which is integrated into the container. It is made up of a couple of circuits, one for each of the two branches of the system, and each one cools down four fuel cell stacks found on the same branch. The cooling fluid, as recommended by the fuel cell producer, must have precise values of conductivity for the security of cell membranes. For this reason, two conductivity sensors have been added to have real-time monitoring. In each branch, there is a plate heat exchanger that allows the heat exchange between the primary and secondary circuit, and heat is dissipated with a fan-cooler of 300 kW.

The system has also a three-way valve that allows regulation of water flow rate and, consequently, the control of output water temperature and the regulation of the fan-cooler rotor (managed by the inverter).

The secondary circuit is equipped with eight RTD type Pt100 with four wires, two flowmeters, and two output analogic signals to control the three-way valve.

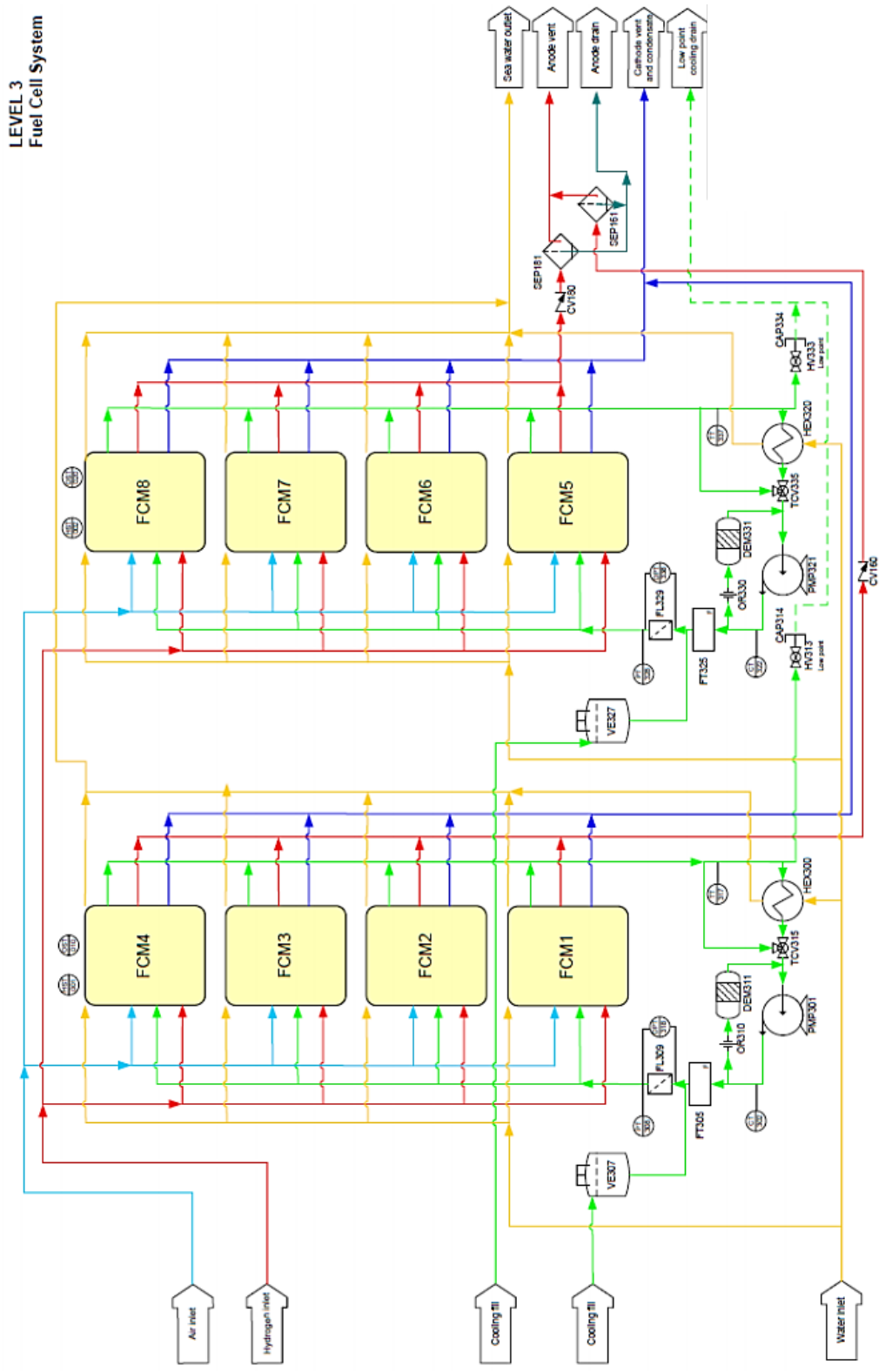

Figure 36: P&ID of the HI-SEA system – air, hydrogen, and cooling lines.

Single and triphasic electrical connections were already available in the IES laboratory in Savona. Thus, the internal connections to feed the HI-SEA laboratory are available. The main system in the DC line consists of the electrical dissipation plant, which has a switch, the electrical load, a power supply line for the load's PLC, a line connecting the electrical resistors

to the container HI-SEA and finally an Ethernet connection for remote control of the load's PLC from the container.

Container HI-SEA's supply line is fed by three different lines at 380 V that start from the laboratory and reach the electrical panel inside the container. The first line is the non-preferential one and it starts from a switch located inside the container. The second line is connected to an Uninterruptible Power Supply (UPS) to always get current. The third line is the AC/DC one, with a different supply.

The final BoP, summarizing, includes:

- Compressed hydrogen storage (50 tanks, storage pressure 200 bara).

Table 19: Characteristics of the pressurized hydrogen storage tanks.

Number of tanks	50
Disposition	Vertical
Capacity [l]	40
Geometrical capacity [m^3]	0.04
Mass content [kg]	0.656
Volumetric content [Nm^3]	8
Pressure [bara]	200
Length [cm]	165
Width [cm]	20,3Ø
Height [cm]	180
Weight [kg]	51

- Hydrogen, air, and cooling pipes volume and pressure, design dependent.
- Hydrogen pressure regulator valve (7-10 bara), installed between H_2 tanks and FCS.
- Industrial compressor (Ceccato model DRE 100 8,5 CE 400 50, 8000 Nl/min at 3-12 bara) for the whole air adduction line, feeding the 8 Air Mass Flow Controllers (MFC) with dynamics different from the fast FC's ones.
- Dryer and filters, installed between the compressor and the FC stacks, to eliminate water content in the cathodic flow and keep a good membrane humidity.
- Cathode inlet pressure stabilizer, before each stack's MFC, to regulate the pressure before the MFCs and create more suitable operating conditions for them.
- Air MFCs to control the air mass flow rate on each PEMFC module to simulate the performance of blowers with different specifications.

- Cathode outlet manual valves, installed on each PEMFC module, to control the stack cathode pressure and test different pressurized FC conditions.
- DC/DC converters (300-500Vdc in and out, 500A), one for each branch, able to regulate the outlet voltage or the outlet current. To allow parallel branch operation during voltage-control operation, a current division control board was introduced.
- An AC/DC rectifier (60 kW, 300-500 Vdc out, 110 A) to simulate a battery pack.
- A Two-stage cooling circuit:
    - Internal (or primary), flow cooling control through a pump, temperature control by means of a three-way valve on the external circuit heat exchange, and a flow control valve at the inlet of each PEMFC module.
    - External (or secondary), flow cooling control, and temperature control: the external system was always set to a fixed temperature to simulate seawater's constant temperature source.
- A modular resistive load controlled via the PLC of the system, to dissipate the power produced during tests. It allows the testing of different operative profiles through the insertion of different resistors depending on the load to be dissipated.

Table 20: Characteristics of the resistive load.

Parameter	**Value**	**Units**
Max Current	1000	A
Max Power	260	kW
Power step	1	kW
Max power step	60	kW
Max current step	100	A

The Nuvera's Orion® PEMFC technology, assembled in 2014, has metallic bipolar plates and an open flow field, to increase the active area of each cell's MEA. The anode is Dead-end and the anodic flow is recirculated, therefore anodic purges are planned to eliminate impurities and water accumulated during operation and to avoid excessive FC degradation [232]. The main parameters that characterize the FC stacks have been reported in Table 21:

Table 21: Orion Product Specifications - Industrial Motive Power.

Continuous Rated Power, Net [kW]	30
Configuration/Orientation	Mono-Stack/Horizontal or Vertical
Rated Maximum Power [kW]	36
Rated Maximum Current [A]	450

Maximum Voltage [V]	141
Minimum Voltage [V]	72
Length [mm]	326
Width [mm]	280
Height [mm]	210
Dry Weight [kg]	34
Ambient Operating Temperature [°C]	-40 to +60
Anode Management	Passive Recirculation

The number of cells in series and their active area are confidential data by Nuvera and therefore they are not reported in the Thesis. The FC stacks are auto hydrated, which makes thermal management crucial to maintain a good humidity equilibrium inside the cells, but it gives the advantage of saving space on board [233]. Moreover, for humidity management, a dryer is installed between the industrial compressor and the stacks, to eliminate water content in the airflow. Temperature control relies on operative current; the inlet and outlet temperature of the cooling fluid on each FC stack is controlled depending on the measured current.

4.2.2. Control system and measured parameters

The control system consists of a supervision system and a local panel which contains the Programmable Logic Controller (PLC), an I/O field, the power supply, and all auxiliary accessories for the management of communication lines; it also manages the Human-Machine Interface (HMI) and it collects the data of the main system's parameters, executing automatic controls and communicating the acquired data to the HMI, which then reveals the possible presence of improper values, causing a correspondent alarm. Based on the severity of the alarm, an emergency system shutdown can be triggered. The HMI main window (HOME) is shown in Figure 37: it gives an overview of the main system connections (FC stacks, air, and hydrogen lines, DC/DC converters, resistor bank, cooling loop) and of the main parameters that are monitored during the online operation. In case an alarm is generated, the operator will get a notification via the bell icon on the top left corner of Figure 37, which also explains the cause of the alarm.

Figure 37: Control system HMI, "HOME" window.

The other windows are dedicated to the control of more specific parameters and the alarm thresholds and are:

- Equipment Manual Override Switch.
- Analog signals setup; Analog alarms setup.
- Operative sequence parameters.
- Regulation algorithm parameters.
- PIDS management.
- Stack overview.
- Resistor bank load profile.

These windows allow the operator to monitor the main parameters of the system during operation, choose the manual or automatic control for secondary components, set the alarm levels, and manage the resistive load to allow different profile tests.

Among the tasks assigned to the system, the control and regulation of the fuel cells' circuit are very important; the software is designed to control up to eight FC stacks at a time. One of the most important parts of the control system is the Cell Voltage Monitoring (CVM) since cell voltage is an important indicator of the performance as well as of the state of health of the cells [80,83,234,235]. The CVM acquires the voltage value of each cell in the stacks while it saves and communicates to the control system – indicated below each FC stack, as shown in Figure 37 – the following data:

- Minimum cell voltage (V_{min}): the lowest voltage value measured in a stack, and the ID of the cell where it is measured.

- Maximum cell voltage (V_{max}): the highest voltage value measured in a stack, and the ID of the cell where it is measured.
- Average cell voltage (V_{avg}): obtained by dividing the total stack voltage by the number of cells.

Another crucial aspect of the control system is the management of the cooling circuit. The most suitable operating temperature has been set by the FC supplier to keep the ideal relative humidity on the membranes. In fact, the FC stacks do not have an external humidification system at the cathode or the anode side, and the membrane humidity is regulated through accurate cell temperature management and cathode airflow control, as suggested in the literature [233,236,237]. The maintenance of the correct cell temperature is ensured by the cooling circuit, which regulates the cooling flow temperature and mass flow rate, removing the excess heat from the cells by means of a heat exchanger. The temperature control relies on the operative current measured. Table 22 resumes the control variables in the HI-SEA FCS and the equipment through which their control is implemented.

Table 22: Controllable variables in the FCS.

Line	**Variable**	**Control**
Anode	IN pressure	Pressure Regulation Valve
	OUT Flow (H_2 purge)	Pressure Regulation Valve
Cathode	IN pressure	Pressure Regulation Valve
	OUT pressure	Manual Valve
	Pipe pressure	Compressor
	Pressure stabilizer	On/Off
Cooling I stage	Flow	Pump
	OUT-IN temperature	FCM flow control valve
	IN temperature	Heat Exchanger with three-way valve
	Pipe cooling pressure	-
Cooling II stage	Flow	Pump
	IN temperature	Chiller control
Electric FC	OUT voltage	DC/DC
	OUT current	DC/DC
	DC/DC	On/Off

Electric battery	OUT voltage	AC/DC
	OUT current	AC/DC
	AC/DC	On/Off
Power	Power profile	Resistance El. Load
	Resistance profile	Resistance El. Load

4.2.3. Shipping environment simulation

Since the objective of the HI-SEA system is to assess PEMFC for maritime applications, BoP components are chosen to aim to simulate the ship environment. Therefore, the test rig has been designed and installed inside a 10-meter container in order to be easily integrated inside the ship infrastructure (Figure 38). To allow the investigation of the best electric and fluid architecture, a mixed configuration has been adopted connecting in parallel two symmetrical branches composed of 4 PEMFC stacks Nuvera Orion® in series (branch01: FCM01, FCM02, FCM03, FCM04; branch02: FCM05, FCM06, FCM07, FCM08). Each stack has been integrated with BoP components. The BoP components and configuration have been chosen to represent a possible integration of the FCS onboard a ship.

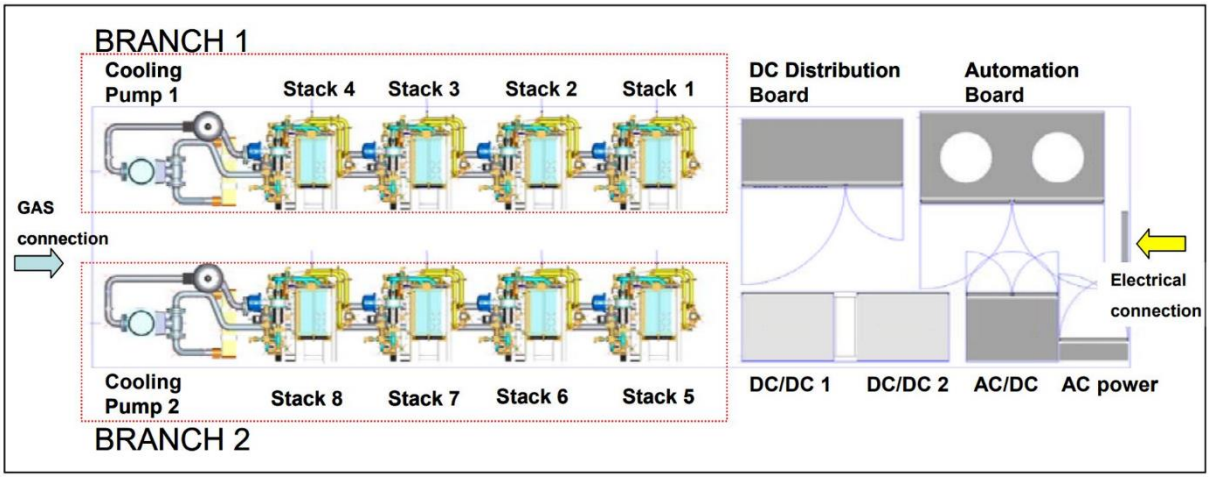

Figure 38: FCS test rig configuration.

Indeed, an MFC controls the cathode inlet airflow, to simulate the behavior of different blowers' specifications.

The air adduction line has been designed as a single one: an industrial compressor provides the 8 FC stacks with an air mass flow up to 8000 Nl/min at 4 bar. Its characteristics make it not able to comply with FC's fast dynamics, but such a standard component was chosen to simulate the exploitation of the compressed air line already existing on a ship to feed the fuel cells, becoming part of the FCS BoP itself.

Each branch is electrically autonomous, with a dedicated DC/DC converter that is compatible with the voltage of 3 or 4 connected stacks, enabling the simulation of a single stack fault on each branch and the control of the output voltage and current. It can also be bypassed. In this case, the FCS is directly connected to the modular resistive electric load, which can work at constant power or constant resistance. Thanks to the resistive load, different operative profiles can be tested to investigate the possibility of utilizing PEMFC systems to power auxiliaries and/or propulsion. During the experimental campaign, the resistive load control was set at constant power.

Finally, each branch has its primary circuit that relates to the singular secondary one, filled with fresh water at a constant temperature, that simulates the heat exchange with the seawater using controlled chillers, that maintain a constant cooling temperature of around 15-20°C. This enables the study of the feasibility of a scaled-up FC ship installation exchanging heat with seawater.

4.3. HI-SEA system commissioning

4.3.1. Analysis of cells rupture on FCM02

The PEMFC test rig of the HI-SEA Joint Laboratory was originally designed and tested inside the context of the TESEO project, which concluded in 2015 [224]. This project was carried out by the University of Genoa in collaboration with the Italian National Research Centre (CNR), Nuvera Fuel Cells, and Fincantieri. Due to the lack of experience and BoP effects underestimation, the original data acquisition system was unable to save data when the system's stacks were not in operation, a crucial factor since, as it will be shown, the final cause of the damage of one of the FC Module (FCM) is related to its wrong management during the non-operative phase. The objective of this work is to identify and understand the reasons for the rupture of 16 cells composing one of the system stacks, which happened on October 21st, 2015, during the final test of the project. The aim is to avoid the occurrence of analogue issues in the future.

Via the control system, Operative sequence parameters (FC stacks related parameters) can be modified as well as Regulation parameters (BoP related parameters) and the Alarm parameters (see Section 4.2.2). The automatic control enables to perform running tests within definite control ranges. If more flexibility is required, the Manual Override Switch (MOS) control can be activated to manually control many parameters. This procedure enables testing single components or overriding control problems, but if not well managed it could bring system malfunctioning and potential damage. During the TESEO project, MOS was in fact employed

to operate on the MFC installed at the inlet of the cathode line. It was necessary to adopt the MOS for FCM02, as the correspondent MFC device had a control issue that was causing the impossibility to run the stack normally, also leaving the valve slightly open when not requested. Only through the Manual Override Switch configuration, the controller could be closed. A relevant aspect of the control system was the data collection and saving, which was made only when the system was in operation: the data backup of each FCM was activated only when the stack was under current conduction, or rather when the current was passing through the cells. This configuration was implemented to facilitate data analysis but resulted in wrong and dangerous. Moreover, important data were not acquired like cooling conductivity or actual air mass flow.

During the test campaign, on the 21st of October 2015, the PEMFC test rig was operated to demonstrate its functioning to reach the maximum nominal power of 240 kW. For this reason, the 8 PEMFC stacks were turned on and controlled partly under MOS configuration in order to override the operative problems on the components that emerged during previous tests, that couldn't be repaired within the final tests. In particular, the air MFC of the FCM02 showed anomalous behavior that required the MOS configuration. Even so, the controlled air valve could not be completely closed when the control system was energized. Unfortunately, the problem was not noticed, also because of the data acquisition strategy that was adopted at the time. After a few hours of operations during the morning to prepare for the final test, the PEMFC test rig was turned off for 3 hours during which the airflow on FCM02 was active due to MOS activation probably. Afterward, it was turned on again for the final test that brought to the damage of stack FCM02. Even though the first hypothesis was that the FCM had been affected by starvation, later inspections would show that the cells did not experience hydrogen starvation but suffered from MEA ionic conduction problems mainly, together with a series of other system wrong management issues.

During the test, there was a discrepancy in the stack performance after a few hours of operation, which was probably due to the drying of the membrane generated by a prolonged airflow to the stack during no operation. The next figures explain the sequence that brought the damage during the test.

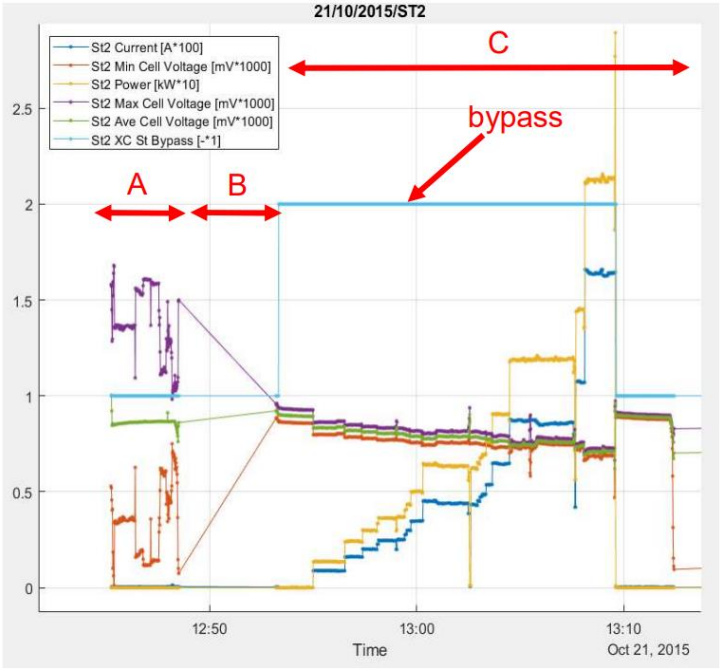

Figure 39: FCM02 performance before the damage. St2 stands for FC module 2; XC is the FC module's electrical contactor.

It is possible to distinguish three different zones in Figure 39:

- No electrical current through FCM02, data acquisition is active as a result of a failed startup procedure (zone A).
- Data acquisition off, no other stack active in Branch 01, no current is circulating (zone B).
- FCM02 working and in operation with closed bypass (conducting) (zone C).

FCM02 remained not in operation for about 3 hours, during which with all probability the cathode air mass flow was left open. The prolonged air flux on the hot membrane brought a drying phenomenon [80,101,226,238–240]. Moreover, the high temperature imposed on the FCM02 by the branch cooling system, on which were operating FCM02 and other stacks of the same branch, favorited the evaporation of water from the membrane [77,81,241–244]. Indeed, the primary cooling circuit (that connects the branch stacks to remove the heat by means of the secondary circuit towards a heat exchanger) was defective due to the malfunctioning of the three-way valve that was supposed to regulate the FC inlet cooling temperature. In order to run the system for the final tests, the three-way valve was left always open, and the temperature control was done by the secondary circuit, with a long response time, that brought to the general operation of the stacks at higher temperatures. The results of the wrong BoP management are visible in Figure 40: the electrical current was drawn from FCM02, but a limited current ramp resulted in an abnormal low cell voltage that was immediately followed by a large divergence between the minimum and maximum cell voltage.

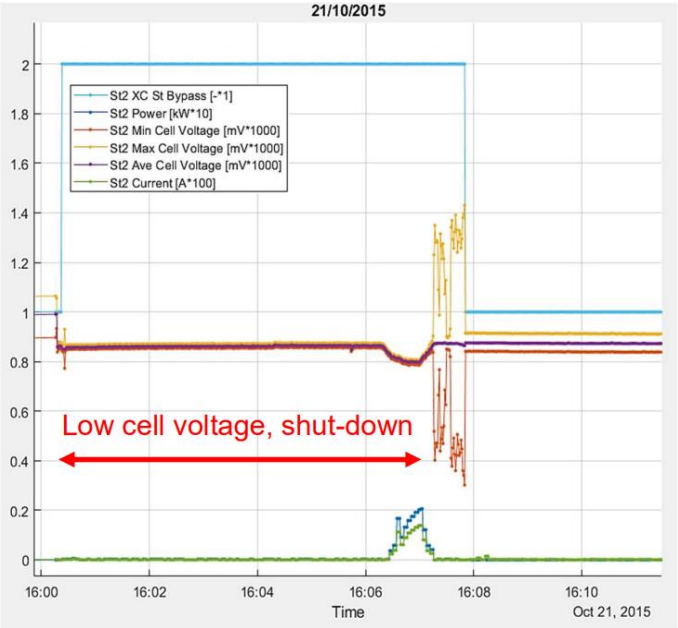

Figure 40: Anomalous cell voltage in FCM02 although the current ramp is limited.

A few minutes later, FCM02 was inserted in conduction when the flowing current was already high on the system branch. In Figure 41 it is possible to distinguish:

- Load cycle, an indicator of stack malfunction that brought to the module disconnection (zone D).
- Branch 01 was put under work while FCM02 was not online (zone E).

FCM02 was put online while the current was about 80 A, creating hot spots on the membrane that brought to the rupture of 16 cells distributed at different points of the stack.

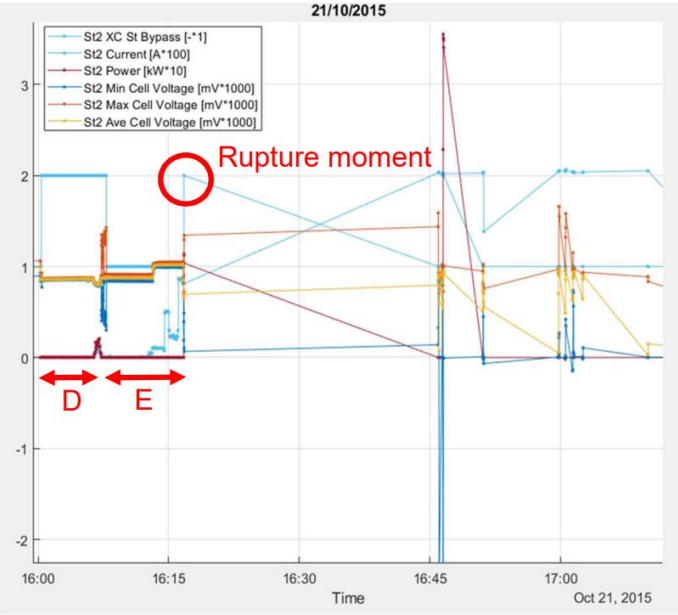

Figure 41: Rupture of cells in FCM02.

At the end of the project, the stack was dismounted and analyzed by the fuel cell provider (Nuvera Fuel Cell). 13 cells were found broken while the other 3 were damaged. The combination of hot spots on the membrane, high current, and high water conductivity brought to the perforation not only of the membranes but also of the metallic bipolar plates. This was testified also by the presence of metallic residuals in both the anode water pure collector and in the cooling system filters. The damaged cells and bipolar plates were removed, and the remaining cells were stacked again, proving the robustness of this technology. This is shown in Figure 42, which has been drawn in a dedicated test after the reassembling of FCM02.

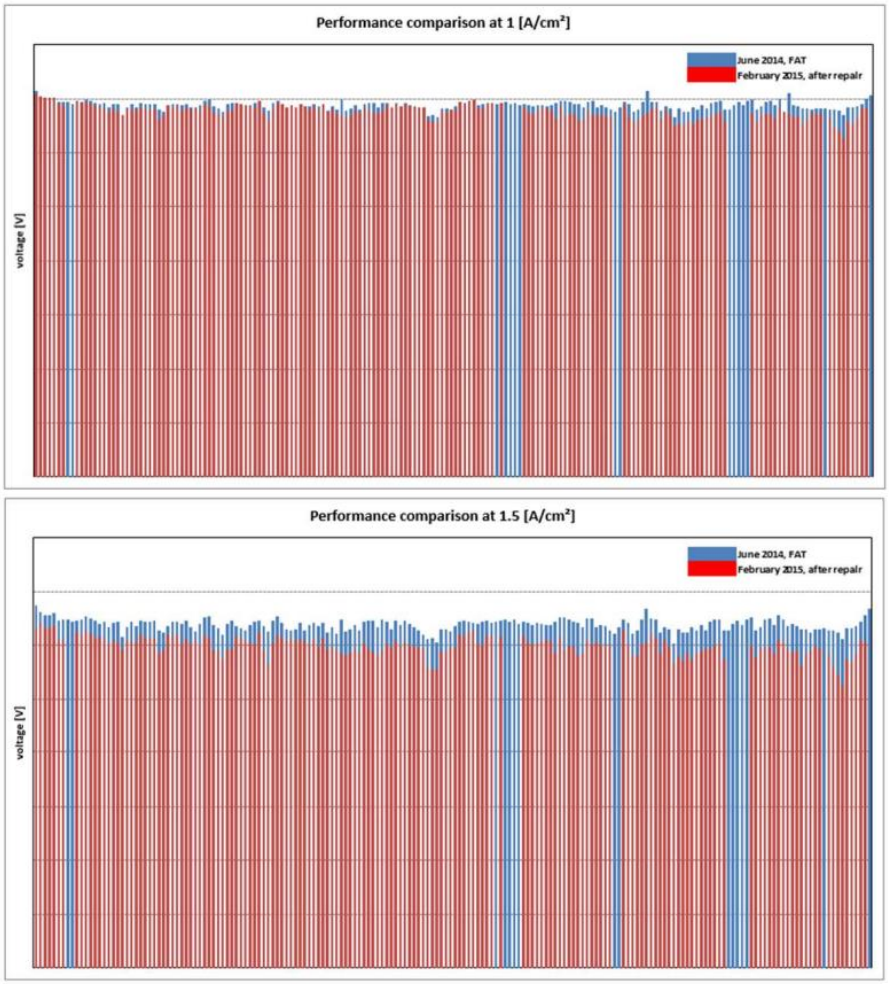

Figure 42: Cell voltage comparison before (blue lines) and after damage (red lines) on FCM02 – 1 A/cm^2 and 1.5 A/cm^2.

Today the FCM02 is working along with the other stacks while in the HI-SEA Laboratory new studies are under development to define and implement diagnosis strategies to prevent flooding and drying phenomena on the stacks again, assessing the relation between anode and cathode pressure drops, cathode airflow and cooling temperature. An assessment of the facts that led to the damage was done together with a new experimental campaign, to show the consequences of cells rupture on the global performance of the remaining cells in FCM02. The final consequences of the damage on FCM02 can be resumed in:

- Global 2% cell voltage reduction after the recovery process was verified.
- 16 cells were removed due to damage to the membrane and the bipolar plate.
- No other hardware modification is required.

The results of the damage assessment have brought to other research activities in the HI-SEA Joint Laboratory related to this problem:

- Drying phenomena online diagnosis strategies assessment.
- HMI alarms based on cross-data.
- Recovery procedure to drying/flooding phenomena development.
- New thermal management control strategies implementation.

At the end of the TESEO project, the following observations were made with related countermeasures (system modifications) application:

- *Cooling water conductivity*. At the end of the project, the cooling water was analyzed and found with conductivity values higher than the accepted value, 5 µS/cm. The problem was related to the use of inappropriate glycol.
- *Standby monitoring (air to the cell)*. The lack of airflow measure of the stacks didn't permit the identification of a faulty air MFC.
- *FC module insertion in series*. When a series of fuel cell stacks is supplying high currents, the insertion of a stack must be avoided in order to prevent possible FC damage.
- *Purge system synchronization*. If the purge pipes of various operating stacks are combined into a single pipe, the former should be properly dimensioned, or the stacks' purge time should be correctly synchronized in order to avoid the counter pressure.
- *Electric load control for simulation*. The electric load resistance should be properly sized and controlled to simulate an electric load without falling into control interference between the DC/DC converter and the electric load.
- *Hydrogen inlet pressure*. In order to deliver the same anodic pressure to the stacks, a collector pipe was installed.

Moreover, several parameters have been added to the monitoring system of the new HI-SEA installation to enhance the interpretation of phenomena. This work has been described in a dedicated conference paper [245].

4.3.2. Reactivation of the HI-SEA system

TESEO Project allowed investigating of the use of PEMFC for the development and demonstration of an electrical generator of 240 kW output power for shipping. Indeed, it started the path towards the definition of the best design for a modular FC system to guarantee the maximum life span of FC stacks without omitting performance. After the end of the project, however, the stacks were left inactive for almost two years before being employed in the HI-SEA Laboratory. As inactivity is linked to many issues, mainly membrane dehydration [238], stacks were at first in poor conditions and it was necessary to find out an effective recovery procedure: the prolonged inactivity exacerbated the effects on voltage due to the natural degradation and dehydration that the lack of operation implies on PEMFCs [119,246].

Thanks to some dedicated experimental activities, the Author could notice that the voltage gained a benefit from the enhancement of the airflow to the FC modules. Therefore, the situation, at first, led to the decision to increase the airflow rate with respect to the original design settings to reach a higher voltage, in accordance with the Nernst equation [247] and with the approval of the FC supplier. This choice had a good effect in the first moment. On the other hand, though, the airflow exerts a drag force onto the polymer membranes, giving a further contribution to dehydration [80,101,238]. As Nuvera Orion® stacks are auto hydrated devices, it is very common to have problems linked to the amount of water contained in the membranes: it all depends on a delicate link between the temperature of operation, and partial pressure of reactants, and environment conditions [81,83].

Voltage is among the most important parameters to ensure the state of health when operating a PEMFC [80]. As introduced in Section 4.2.2, stacks in the HI-SEA system are provided with a CVM system that acquires, amplifies, and digitalizes the signals from each one of the almost 200 cells per stack. Data are collected and elaborated by a PLC that saves, among others, values of the average (V_{avg}), maximum (V_{max}), and minimum (V_{min}) cell voltage. The data analysis linked to V_{min} was crucial at the beginning of the experimental campaign to hint at issues linked to inactivity and dehydration, and at the end of it to suggest that recovery was effective. The acquired voltage was in fact compared with Factory Acceptance Tests (FAT) performance and with the results of the stack voltage model developed on Matlab-Simulink [228]. Before recovery, stacks could reach half the nominal power, showing significantly low voltage values and strong instabilities. Increasing the airflow rate with respect to the original design settings allowed reaching higher voltages, and exploring the entire operative range of FC stacks. This condition highlighted the main problems that have been faced thanks to the recovery procedure.

This procedure is focused on thermal management, aiming to restore the original performance by establishing back a good membrane humidity level on the dehydrated polymers following other recovery procedures shown in [119].

4.3.2.1. Result of the reactivation: development of the recovery procedure

The recovery procedure has been designed by the Author thanks to the post-process of experimental data, a dedicated literature review, and a discussion with Nuvera's technicians. In fact, it is known that inactivity leads to dehydration – which chemically affects the stability of the membrane, as explained in Section 3.2.1 – and that, at a lower temperature, more water can be condensed and absorbed by the membrane. Therefore, some successful attempts have been implemented in the system to lower the cooling temperature setpoints. In that condition, the cell voltage would show an increasing trend and Nuvera's technicians confirmed the link with the enhancement of liquid water amount. Finally, the recovery procedure has been precisely defined by the Author.

During the experimental campaign, three main phases have been defined for the recovery:

- *Recovery Phase 1*: it is focused on the reestablishment of a correct humidity level in the membranes.
- *Recovery Phase 2*: aims to assess the optimal temperature of operation, depending on the relative humidity that the cells have reached after Phase 1.
- *Recovery Phase 3*: once the membrane's humidity and the operative temperature are assessed, in Phase 3 the nominal power is achieved with each stack, also ensuring a stable cell voltage in this configuration, and reducing, if possible, the air excess at the cathode flow.

The implementation of the recovery procedure has been possible thanks to the resistive modular load, that was controlled in power configuration: the internal PLC of the machine elaborates the number of resistors to be applied as a function of voltage and power set-point, using an established set of resistors, enabling a 1 kW step control.

It is important that the procedure is applied to one FCM per time, to reach the best performance with that device before exposing it to interactions with the rest of the system as, for example, the cooling circuit is the same for each stack in the same branch. With a single cooling circuit for the entire branch, it would in fact be impossible to set the best fitting temperature of the cooling fluid for just one FCM, as the settings will be valid for all stacks on that branch. Nevertheless, the procedure can be applied to the same FC stack more than once – if the results of the first application are not satisfying enough – and on different days.

The procedure applied successfully to the 8 FCMs, is described in detail in the following.

Recovery Phase 1:

- The stack is turned on; if there are no damages in the system or in the FCs themselves – to be checked out, in case –, it will enter the online status and be ready to drain current.
- The user begins to impose an increasing load to the FC stack, implemented thanks to the resistive load (minimum increase: 1 kW/min).
- The stack is brought to the maximum reachable power with a rapid load ramp. The maximum power is defined as the last condition with stable cell voltage that the stack can sustain without incurring a "*Low Low Cell Voltage*" (LLCV) alarm due to further current requests.
- If the cell voltage starts to be unstable or to decrease, the maximum achievable power is reached, and the load should be decreased to the previous stable setpoint, therefore operative conditions will be set on lower power output, to be maintained for another minute.
- The objective in this phase is to reach half of the nominal power. In the attained condition there is a balance between water produced and water evaporated or removed by drag forces.
- The stack should be left to work in this setup for 20 minutes: as water production and removal are balanced, the polymer membrane has time to get correctly hydrated. During this time, minimum and average cell voltages should be monitored and are supposed to slightly increase, to get more stable and also to reduce the distance between them.
- Recovery Phase 1 is completed.

Figure 43 shows the application of Recovery Phase 1 to FCM06. During the development of the test, the load is gradually increased by the user through the resistive load control. In the beginning, minimum, average, and maximum cell voltages tend to get closer, but after a certain point minimum cell voltage undergoes several significant and sudden variations. At the beginning of the process, almost all the stacks could reach a maximum stable voltage at about half of the nominal power, around 10 to 15 kW. In Figure 43 it is possible to observe the achievement of the maximum power associated with a stable voltage with FCM06; after, the voltage started to oscillate and thus the power output is looped between 12 kW and 13 kW. The stack was kept in these conditions for 20 min, as foreseen by Recovery Phase 1: this helped to reduce the intensity of minimum cell voltage variations.

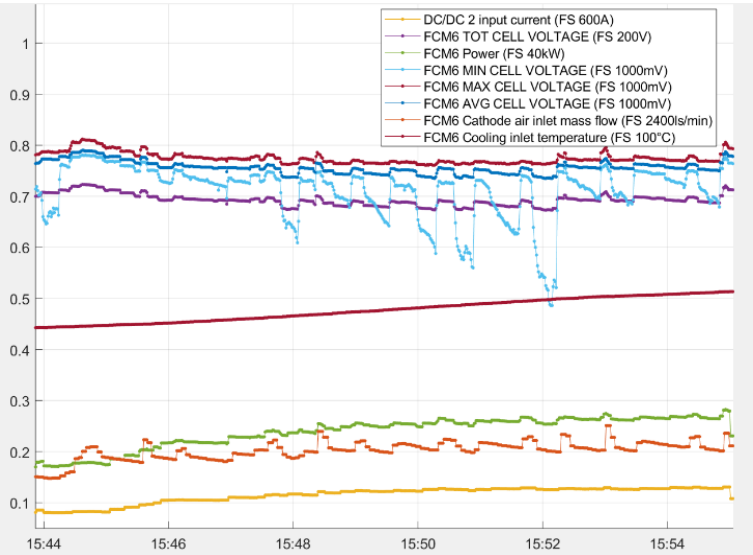

Figure 43: Application of Recovery Phase 1 to FCM06.

<u>Recovery Phase 2:</u>

- The operative stack inlet cooling temperature is decreased by 3°C: a lower operative temperature inside the cells of a stack results in a higher water condensation rate on the membranes, countering dehydration.
- The stack is operated with a lower temperature as long as the average cell voltage does not start to slightly decrease; at this moment, the operative temperature can be set again to standard values suggested by Nuvera to avoid membrane flooding. In the new conditions, it is expected that minimum cell voltage continues increasing, getting closer to the average one, and globally it should get more stable.
- If the decreased stack cooling inlet temperature does not bring a beneficial response in terms of cell voltage, or it even worsens, this can be interpreted as the starting signal of a flooding condition. In this case, the opposite strategy is tested by increasing the cooling inlet temperature setpoint by 3°C. If the stack operated at a higher temperature shows increasing cell voltages, the higher temperature is maintained until the voltage gets stable or starts again to diminish.
- Recovery Phase 2 is complete.

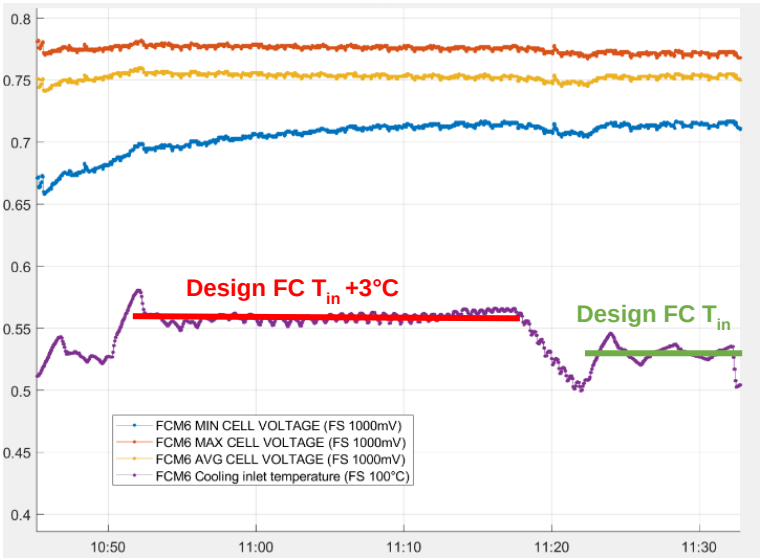

Figure 44: Application of Recovery Phase 2 to FCM06.

Figure 44 shows the application of Recovery Phase 2 to FCM06. In order to recover the correct membrane humidity, the second phase of the procedure consists of the modification of the FC inlet cooling temperature setpoint to higher and lower values, in the range of ±3°C. In fact, since the initial cell voltage is low, the temperature is increased by 3°C with respect to the design value. Therefore, cell voltage increases during 20 minutes of the test. Then, it starts to decrease again, and the temperature is brought back to the design value. As expected, the decreased temperature brought beneficial effects to cell voltage, meaning that weakness was since the membranes were suffering from dehydration. In certain cases, Recovery Phase 2 has to be applied to a stack more than once. In fact, ambient and working conditions (temperature, humidity) could bring the appearance of the opposite phenomena to the initial problem. In Figure 43, the effect of the 3°C increase in temperature on the minimum cell voltage is beneficial for the first 15 minutes, solving a previous excess water condition in some cells. Average and maximum cell voltage instead undergo a feeble decrease: this confirms that only part of the cells in FCM06 was suffering from excessive humidity. After 15 minutes, minimum cell voltage begins to decrease too, due to the outset of a dehydration process. Therefore, the temperature setpoint is brought back to its design value, taking to a further slight increase in minimum cell voltage.

Recovery Phase 3:

- After Recovery Phases 1 and 2 are completed, a gradual increase in the power output can be requested, following the 1 kW/min strategy or by making a further step in the power requested only when the minimum cell voltage gets more stable. In this phase,

the stack is brought to the nominal power output, and it is left to operate at nominal conditions (with all the original design settings) for 15 minutes.

- After this time, a complete shutdown procedure is performed, and the recovery procedure is considered concluded.

Figure 45 shows the final part of Recovery Phase 2 and then the application of Recovery Phase 3 to FCM06.

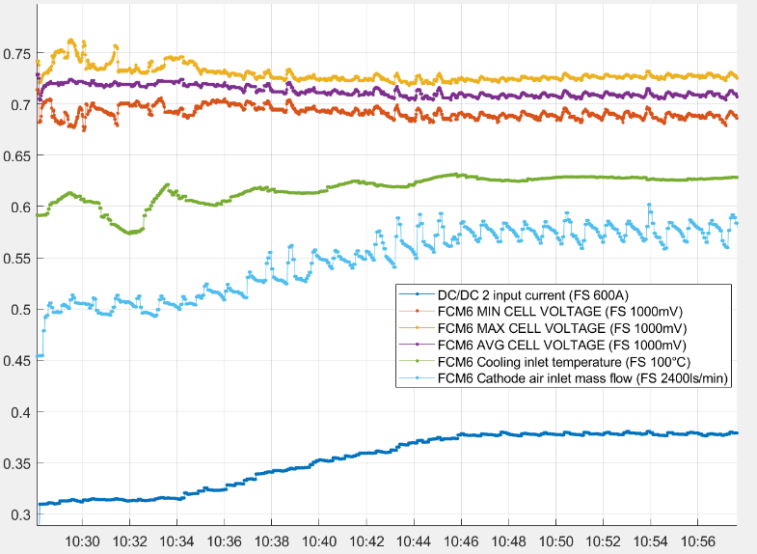

Figure 45: Application of Recovery Phase 2 and 3 to FCM06.

As cell voltage is showing a stable behavior at 15 kW and as the temperature is considered correct with respect to the water content in the membranes, the load is gradually increased. During this phase, particular attention is paid to the presence of instabilities in minimum cell voltage: the user could prefer to linger on a certain load until he/she is sure that a rise in the power request will not affect the voltage stability. The application of the recovery procedure to each one of the 8 FCMs brought a higher strength in cells despite the long inactivity time, as demonstrated by more stable cell voltage values (minimum, average and maximum ones).

The 30 kW-stacks recovery procedure developed in the HI-SEA Laboratory, deduced from a dedicated experimental campaign, can be summarized with the scheme in Figure 46. This recovery procedure gives back the FC stacks a good performance and it increases voltage stability by restoring an adequate humidity level in the membranes. It can be usefully adopted in case of low performance after any thermal or water management issue. This comprises a wrong operation of the system and longer or shorter inactivity time; it can simply be implemented before starting the new tests, to ensure a good relative humidity in the membranes. The process that led to the definition of the procedure and its application has been described in a dedicated publication [248].

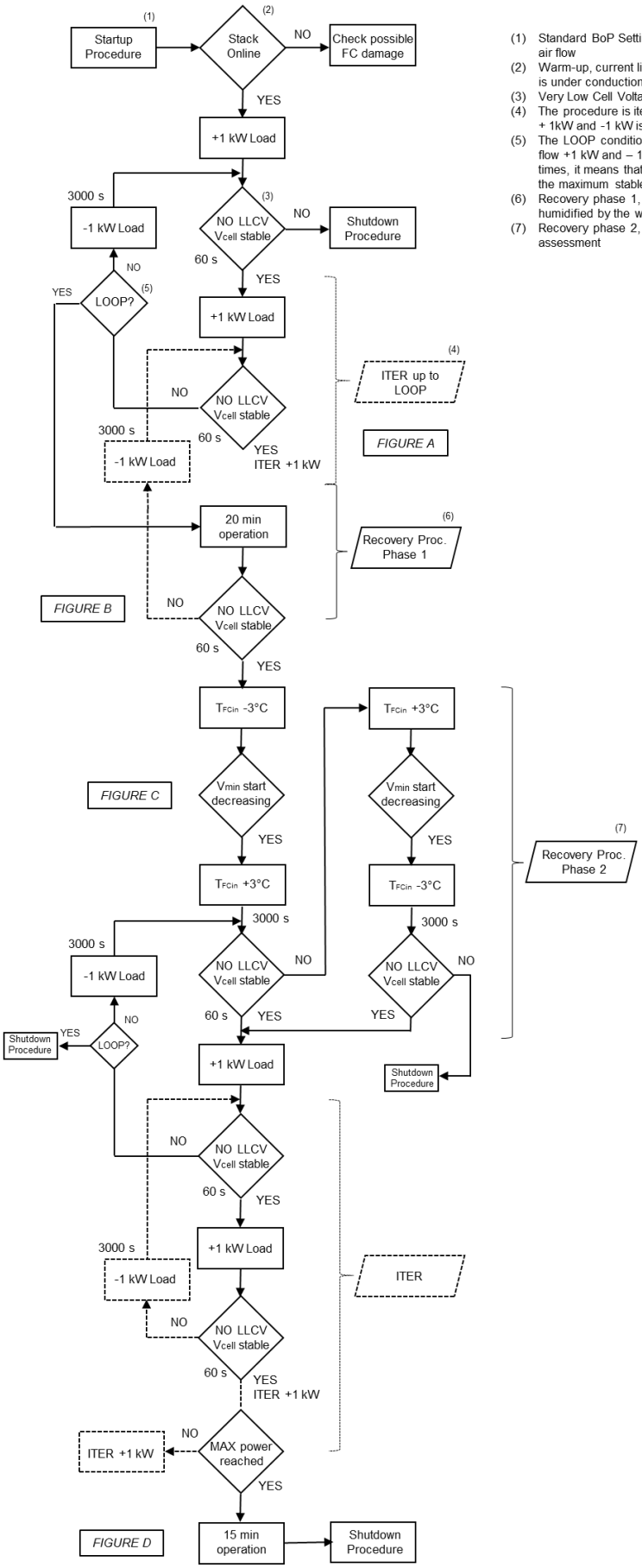

Figure 46: Recovery procedure block diagram.

4.3.3. Assessment of the BoP's influence and adequacy

The HI-SEA plant has undergone different tests from 2018 to 2021. As explained in the previous Sections, at the beginning of the campaign the system was unable to operate over half of the nominal power (0 to 15 kW per FC stack), due to sudden alarm signals and emergency shutdowns, mostly linked to low cell voltage values. The experimental campaign allowed the Author to individuate critical aspects in the original design of the BoP thanks to testing data post-processing. Therefore, the Author proposed to apply some changes to the system configuration. This operation eventually brought to obtain a system able to operate in the whole expected range. This has been possible also thanks to the design of the recovery procedure for the FC stacks. Finally, it has later been possible to study the system's behavior under different conditions. The most significant issues that caused the need of bringing modifications to the system's BoP are hereby described. The main findings are part of a dedicated publication in a scientific journal [43].

The preliminary assessment allowed in fact the identification of the defective elements in the BoP, the most critical ones being the cooling and the cathodic circuits. The application of changes allowed to solve them, and the benefits of the new BoP and the new performance have been assessed:

- Directly: after modifications, the system managed to operate in the whole range (0 to 30 kW per FC stack) with reduced instabilities and drops in cell voltage.
- Through a stack voltage model: analysis of polarization curves pre- and post-BoP changes, compared also with the stack voltage model outputs and FATs results.

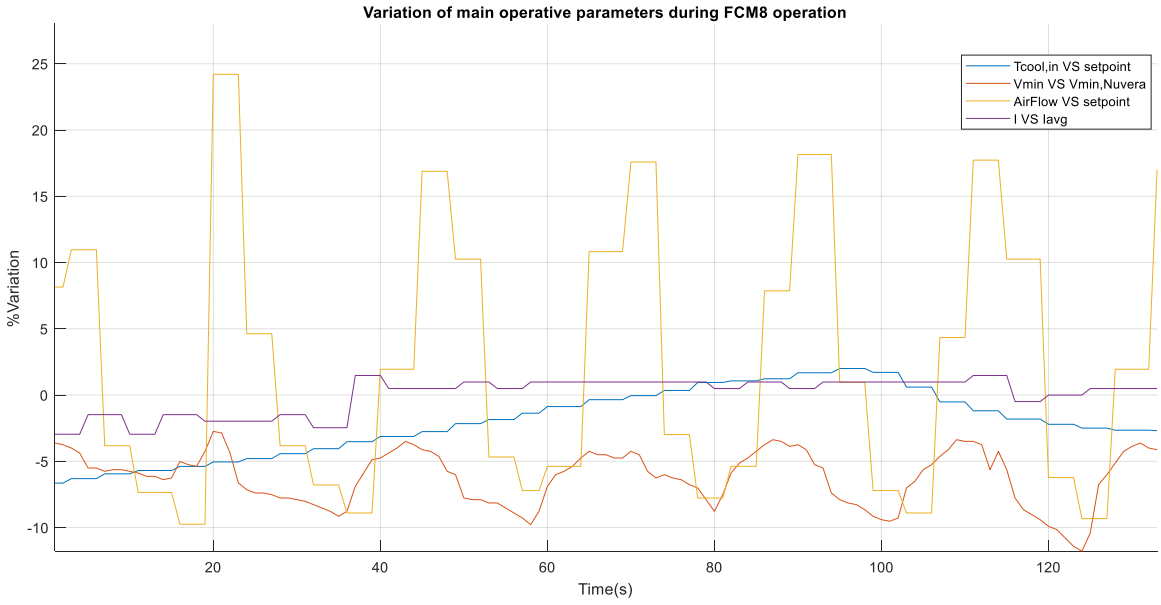

Figure 47: Manual temperature control and air supply line instabilities during operation with the initial BoP configuration.

4.3.3.1. Cooling circuit

Individuation of critical issues in the system's configuration

Nuvera Orion® stacks are auto hydrated systems based on anode recirculation and temperature control. Therefore, temperature control is crucial for water management in the membranes, with consequences on degradation (mechanical to electrochemical). On the one hand, a temperature higher than the setpoint has a positive effect on the kinetics of the oxygen reduction reaction [249] and, in the case of flooding, it contributes to excess liquid water evaporation [242,250]. On the other hand, excessive water removal decreases the protonic conductivity of the membrane. A good cooling circuit control is, therefore, crucial to avoid a loss of proton-conductive active area [77,83], ensuring a good performance: the cell's temperature must follow the trend of current density across the stack. This became even more evident during the experimental campaign.

Both the cooling inlet temperature and the temperature difference between the cooling inlet and outlet are monitored during operation. In the first system configuration, the FCM cooling inlet temperature control relied on the manually regulated secondary cooling circuit, which opened, or closed depending on the temperature reached the cooling inlet side. Figure 47 shows an example of a test with the initial absence of automatic regulation in the cooling circuit temperature. The main operational parameters are reported in percental values concerning setpoints. During the tests, when temperature overcame the setpoint value, the operator had to manually modify the settings of the cooling circuit to bring the temperature to a suitable value for the circulating current. This control was not precise, demonstrating consequences on the performance of the FCMs: minimum cell voltage is between 3 and 12% below the predicted value by Nuvera and it shows strong oscillations. Besides, the control of the air mass flowrate was strongly unprecise, as visible in Figure 47 (yellow line), causing significant cell voltage instabilities. The consequences could not be neglected, and therefore some changes to the cooling line have been applied, as described in [43].

Changes applied

One automatically controlled three-way valve has been installed on each branch of the system and a PID controller has been tuned to regulate the heat exchange between the primary and the secondary cooling circuits, depending on the current across stacks and on the correspondent temperature set-point (measured at the stack cooling inlet). Figure 48 and Figure 49 show two polarization curve tests on the same module (FCM05). The tests are carried out according to the procedure depicted in [223]: starting from the minimum load, it is therefore increased up to

the maximum value and then decreased back to the minimum one. A second ramp is implemented to assess the repeatability of results.

In Figure 48, the parameters of the PID controller are not optimized and temperature results non-uniform at constant load, while in Figure 49 they are correctly implemented. The effects of temperature variations on cell voltage are evident in Figure 48: when the cooling inlet temperature (purple line) oscillates around its setpoint value (green line), the stack voltage undergoes strong oscillations (blue line) which sum up to the ones caused by the airflow rate (yellow line), creating more global instability.

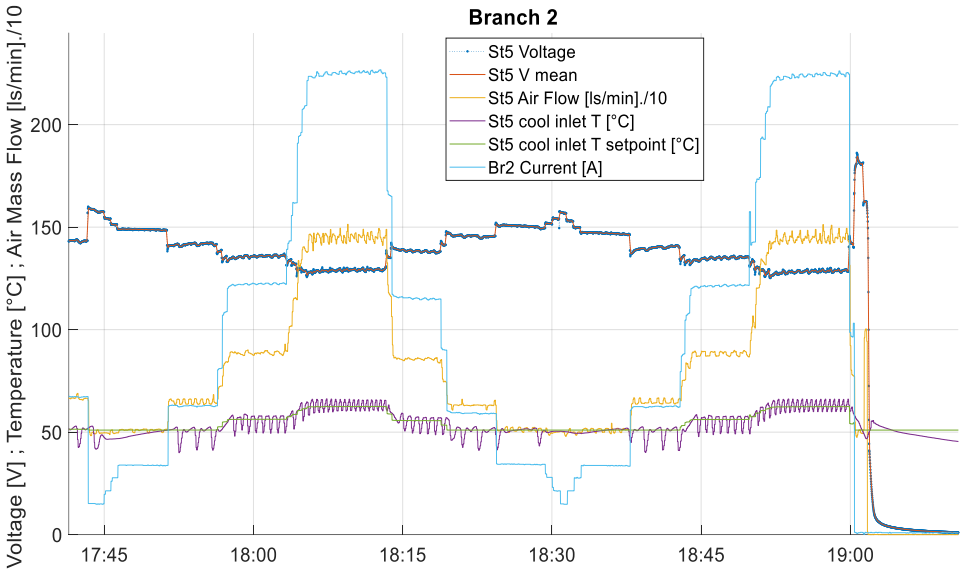

Figure 48: Operational profile with non-optimized PID setting for the 3-way valve control.

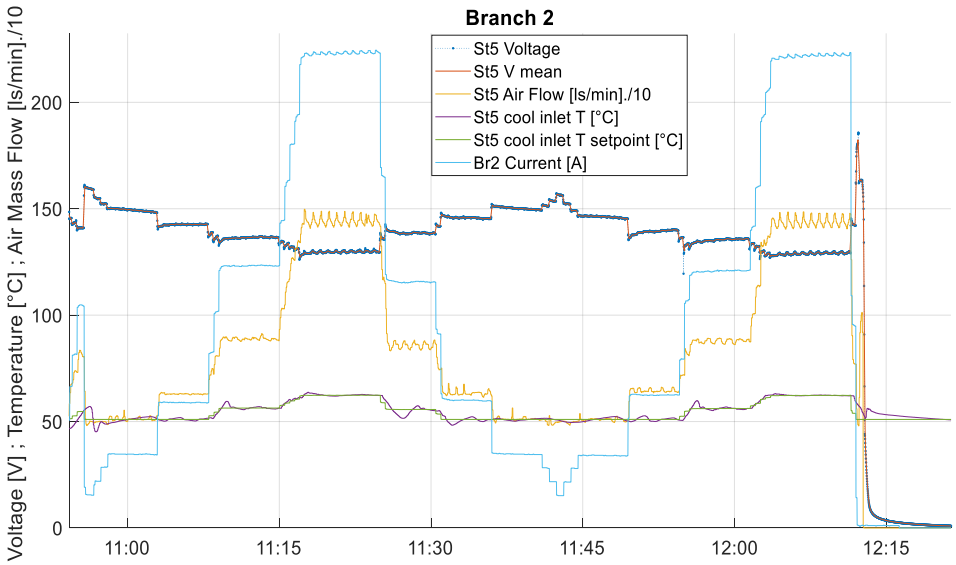

Figure 49: Operational profile with optimized PID setting for the 3-way valve control.

In Figure 49, the remaining stack voltage instabilities are instead mainly due to the airflow variations, since temperature, regulated through the 3-way valves, is stable at constant load operation.

The installation of 3-way valves has brought significant benefits. Their automatic regulation is fine enough to have the stacks' cooling inlet temperature coherent with the setpoint established by the FC supplier. This is true both at constant load and during load variation and it helps to avoid thermal issues linked to water management in the polymer membranes. Moreover, the automatic regulation allows good stability in temperature such that the cell voltage and current can benefit, too, from the changes. They in fact have become more stable than in the previous case. This BoP modification enabled running the FC stacks in the complete range predicted by the FC supplier, without verification of alarms linked to the improper temperature difference across a stack nor linked to an improper cooling inlet temperature with respect to the setpoint. This kind of alarm is indeed not to be underestimated and can even bring to FC emergency shutdowns.

The installation of 3-way valves has also opened the door to different kinds of tests, as through the control system it is possible to change in a certain range the temperature setpoint values in the cooling circuits. Through a temperature-focused test campaign, it has been possible to develop operative strategies and the dedicated procedures for the recovery of Nuvera Orion® 30 kW stacks in case of problems deriving from inactivity or incorrect water management, as described in Section 4.3.2 [227].

4.3.3.2. Cathodic circuit

Individuation of critical issues in the system's configuration

The issue linked to cathodic airflow management was first faced during the system design phase: the system scale-up from one to multiple FC stacks has seen the employment of non-standard equipment – one single industrial compressor for 8 FC stacks, while the air compressor is usually a dedicated component designed for a single stack and selected depending on dynamic characteristics.

The main problem in the initial system configuration was linked to the wrong airflow management during load variation and to the slowness in adaptation to a new airflow rate setpoint value. This resulted in high instability and delay in delivering the needed amount of oxygen to the FCs, up to preventing the correct operation of the system both at medium-high constant loads (10 to 15 kW) and when increasing the load. A wrong airflow control system can cause different problems to the FC modules, particularly to the polymer membranes, and

should not be underestimated. High and sudden peaks in air delivery to a stack can cause mechanical stress and create pinholes, as described in Section 3.2.2, thus gas crossover and local oxygen-hydrogen direct reactions, which increase the temperature in the membranes of PEMFCs creating hot spots and further stress [239]. Also, air flow contributes to water removal from the membrane through drag forces [240]. Uncontrolled water removal is dangerous as it leaves the membranes dehydrated, causing embrittlement and a decrease in efficiency [80,97]. Operation with a dehydrated cell leads to instantaneous and long-term irreversible degradation [97]. The effect of dehydration is in this case aggravated by poor thermal management, which makes it even more crucial to dispose of a good temperature control system in the power plant [251].

Figure 47 shows also the significant initial instability concerning the airflow rate during operation (yellow line): not only during the load-increasing phase but also during constant load operation there are strong fluctuations affecting cathode air inlet mass flow. The variation of the airflow from the setpoint for the depicted test, as reported in Figure 47, can reach peaks ranging from +24% and -11%. Cooling circuit and cathodic circuit issues were responsible for difficulties or even prevention in the operation of the system; they were damaging the system and were lowering its performance, as visible by the minimum cell voltage if compared to the predicted value: this difference can be up to -12% (Figure 47, orange line). Indeed, all the tests demonstrated a strict link between air, temperature, and cell voltage oscillations, which led to low cell voltage values and emergency system shutdowns.

Changes applied

To face the slowness in adaptation to a new setpoint, the general instabilities, and the wrong airflow management during load variation, a pressure regulator set at 3 bar has been installed before each air MFC at the cathode inlet side, for each FCM. This operation helped in reducing and stabilizing the pressure of the air flowing from the industrial compressor (working in a range from 7 to 10 bar) towards the MFC. Such a more convenient pressure at the MFC inlet brought benefits to the device performances, which could show a faster response in adapting the airflow rate to the setpoint, depending on the current. The output of the MFC was also observed more stable at constant load operation, mitigating the effects of frequent starts and stops of the industrial compressor, especially at lower loads. This result shows that it is possible to operate Nuvera stacks with different compressors and different air supply line controls (single central compressors against one compressor for each stack). Basic components are enough to adapt the compressor's flow to what is needed by the FC stack.

During the experimental campaign, a discrepancy emerged between the components installed in the system and the original P&ID of the plant. In fact, an orifice for each FC stack was reported but missing. The orifices should have been installed at the cathode outlet, in every stack, to create backpressure, which is good to improve the FC performances. It increases the stack pressure and thus the operative oxygen partial pressure, enhancing FC voltage according to the Nernst equation [240]. Also, having a controlled pressure at the cathode reduces the stress on the membrane which is a very sensitive component: anode and cathode pressures should be similar to avoid damage to the membrane [252,253]. Therefore, a ball valve was installed and regulated referring to the values of cathode outlet pressure depicted in test results supplied by Nuvera. This recreated the backpressure. The insertion of the valve gave a further contribution to compensating for the instability of the cathode inlet air flow rate generated by the industrial compressor while increasing the performance of the stacks.

These two changes – the insertion of a pressure regulator before the MFC at the cathode inlet and the insertion of a ball valve to create backpressure at the cathode outlet – were first implemented only on FCM07. The actual benefits of these changes were observed by letting FCM07 and FCM06 (with the same performance, laying on the same branch) operate for 15 minutes at the same time, with the same current and external conditions. Such modifications led to a first performance improvement. During the test, the airflow rate resulted more stable in FCM07 with respect to FCM06. Figure 50 shows that FCM07 has a better performance thanks to the applied changes. The effect of a quite stable air flow rate and the backpressure is immediately visible on cell voltage: the minimum cell voltage depicted in Figure 50 is more stable in FCM07 than in FCM06, as well as more similar to the value depicted by the FC supplier and with slighter oscillations. Therefore, the same changes have been applied to all the FCMs of the HI-SEA Laboratory. The values of minimum cell voltages in Figure 50 are reported in percental values with respect to what was predicted by Nuvera FC.

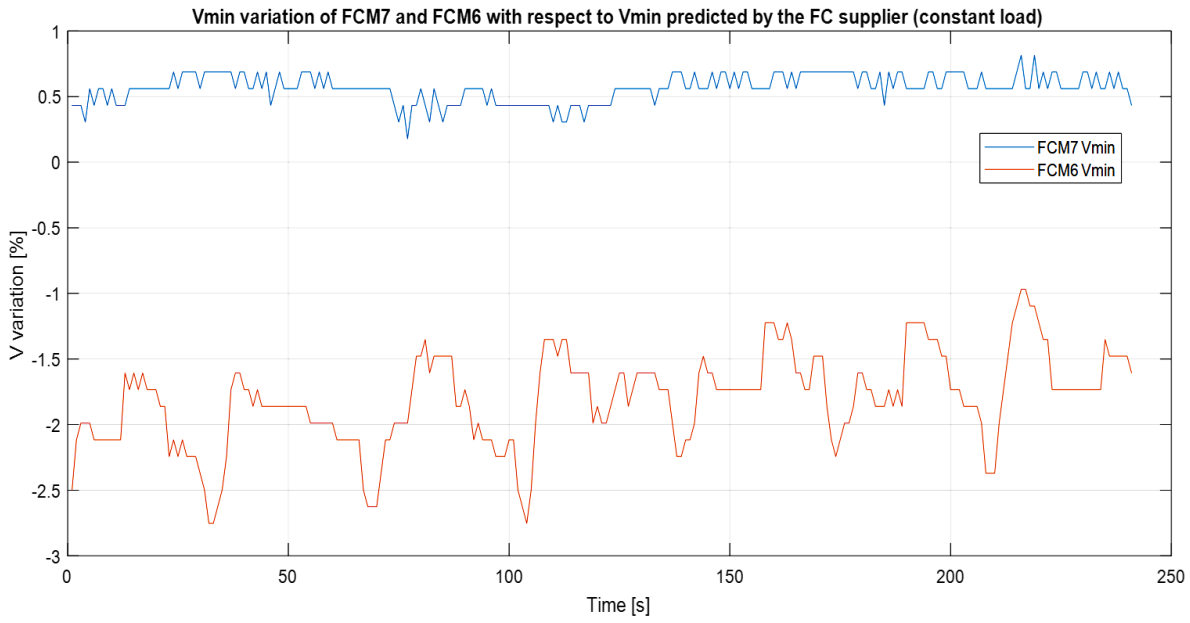

Figure 50: Benefits from the insertion of backpressure and pressure regulator before MFC in FCM07.

Thanks to the improvement of the airflow rate stability, the insertion of cathodic backpressure, and to the inclusion of the 3-way valves for cooling temperature regulation in the system, it has been possible to explore the entire operative range, while previously only a half of it could be reached.

4.3.3.3. Benefits of changes to the BoP configuration

All the stacks installed in container HI-SEA have been tested, after their construction, in FATs shared by the supplier, Nuvera FC. The resulting polarization curves are defined starting from the OCV until the achievement of the maximum operative current. FAT characteristic curves are analog for all the 8 FCM in the HI-SEA system. This has been verified also experimentally: through the setting of the resistor bank, it is always possible to reproduce the polarization curves at similar current densities for each FC module. Increasing and subsequent power steps are therefore set for the test, which starts when the system has reached proper working conditions related to operative temperature; each step is kept for some minutes. The experimental curves can be compared with FATs to evaluate the performance of the FCs after the BoP changes. The performance of the FC stacks has been also analyzed by employing a stack voltage model based on Matlab-Simulink, developed in a previous Ph.D. Thesis by a researcher of the University of Genova [254]. The model has different interacting sub-models (Figure 51). It takes as inputs the boundary conditions measured during operation: stack inlet and outlet cooling temperatures, reactants inlet and outlet pressures, reactants mass flowrates, and current. Therefore, based on

the calculation of Nernst's potential and on the computation of losses with the approaches described in Section 2.2.5, it gives the cell voltage as the output.

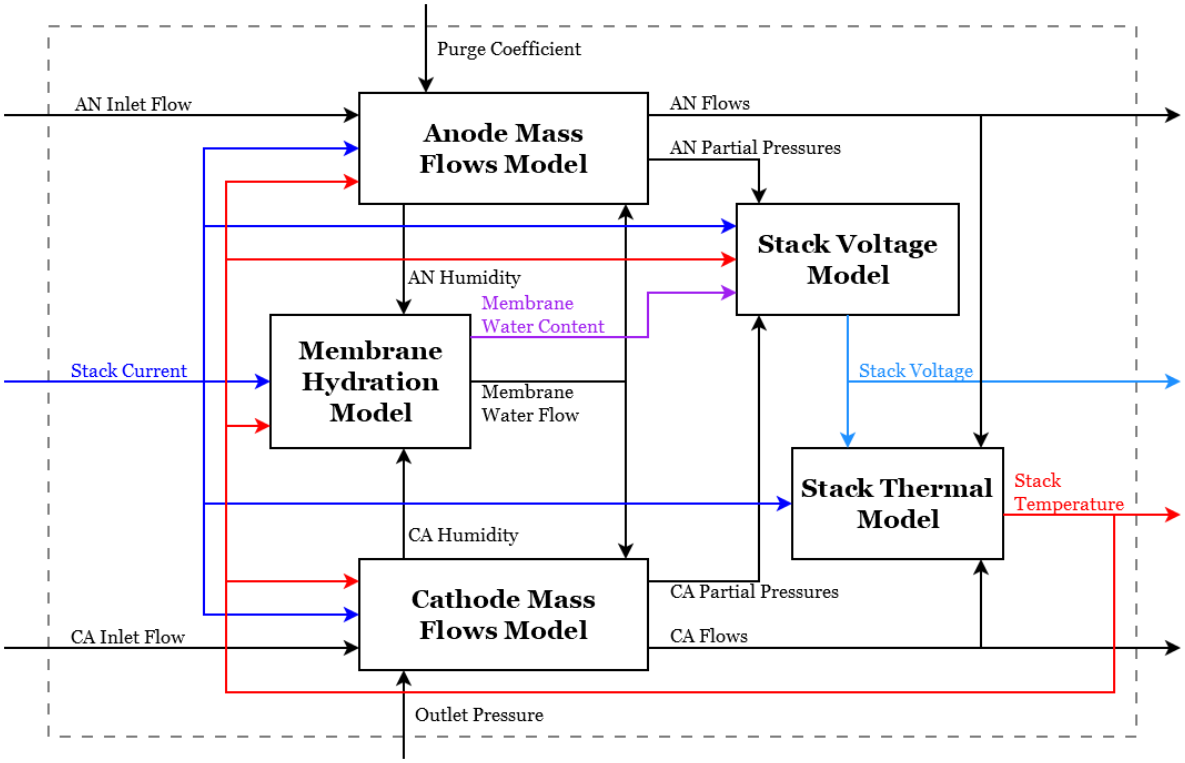

Figure 51: Fuel Cell model and interacting sub-models [254].

Both FATs and model outputs reporting average cell voltage can be compared with experimental results. Thanks to the implementation of the polarization curves tests, it has been proven that the trends of the 8 FCMs curves agree.

At the beginning of the experimental campaign, it was not possible to reach the maximum operative current, due to the BoP issues, and the general performance was poor. The polarization curves were reproducible up to almost 15 kW instead of 30 kW (Figure 52a). In this case, the experimental values of maximum, average and minimum cell voltage were well below both FATs results (purple line) and the stack voltage model's outputs (green circles) under those operative conditions. Moreover, as one-third of the nominal power was reached, the sum of instabilities – generated mainly by the cooling and the air supply lines – was reflected in the system, perturbating the values of cell voltage: the distance between experimental average cell voltage and FATs average cell voltage increases with current, and experimental minimum cell voltage becomes more divergent as current increases. Minimum cell voltage could even become low enough to cause emergency shutdowns of the system.

After the implementation of changes to the cooling and the air supply lines, polarization curves were newly reproduced for the 8 FCMs. This underlined the benefits brought by the changes to the BoP (Figure 52a and b): finally, it is possible to test FCMs performance in the entire range

of operation, up to the nominal power of 30 kW, while maintaining good stability in cell voltage values – up to two-thirds of the operative range. After that, the appearance of oscillations is due to the strong influence of the industrial compressor, which has more frequent starts and stops that cause pressure variation when the air request increases, at high currents. In fact, in Figure 52a and b, all the experimental values acquired during the test are reported, to underline the benefits of the system assembly as well as its remaining instability, especially at currents higher than 70% of the operative range visible on the x-axes. Thanks to the improvements to the BoP, and the application of the recovery procedure described in Section 4.3.2.1, it has been possible to improve the FC performance up to FATs predictions. The results of the stack voltage model (green circles) overlap FATs results (purple solid line) – confirming a good validation of the model – and agree with the experimental values of maximum, average and minimum cell voltage (blue, orange, and yellow dots, respectively). The slight transposition of results of the experimental campaign with respect to FATs may be caused by different operative conditions. Indeed, the temperature at which the supplier runs FATs is unknown, but as a fact, it is a very significant parameter that influences the performance of fuel cells.

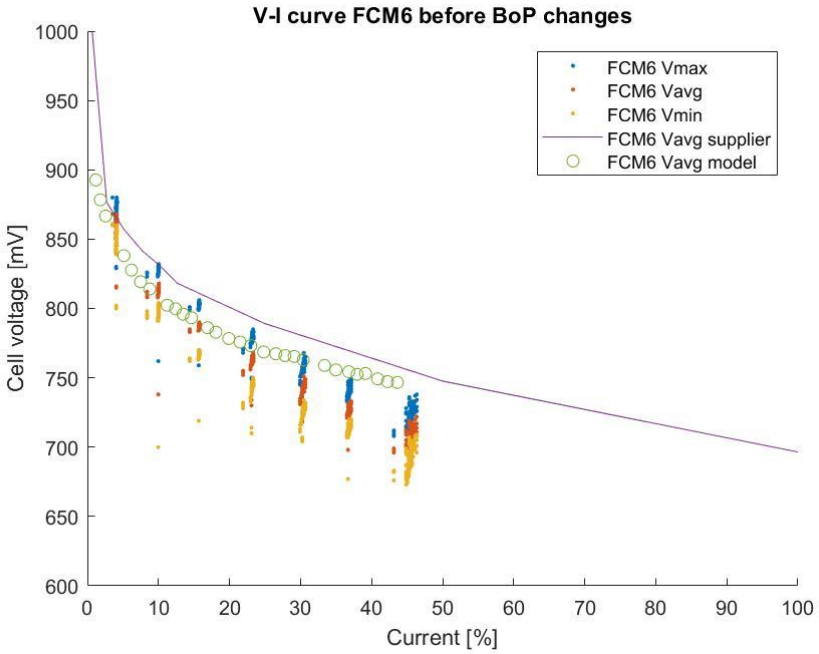

(a)

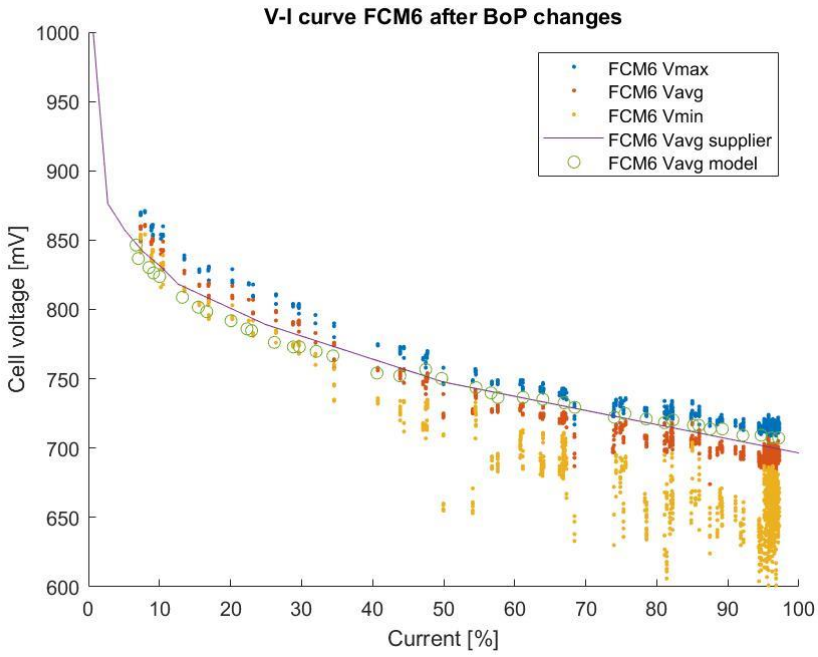

(b)

Figure 52: Polarization curves for FCM06 (a) before and (b) after BoP changes.

4.4. Experimental assessment on adequacy of the FCS to the operation on board a ship

The hereby described part of the experimental campaign is dedicated to assessing the performance of the whole FCS against different operative profiles that can be found onboard a ship. Before the tests were conducted, the air flowrate has been enhanced (+82% on average) with respect to the original settings, especially in the lower operative range of the stacks, to improve the PEMFC performance at partial loads in accordance with [229] that was lowered by natural aging of the FC stacks. This operation was done with the agreement of the FC supplier.

The system has been tested in stationary and dynamic conditions, with an operative profile agreed with Fincantieri, and with and without the DC/DC converter presence in order to assess the static and dynamic performance of the system in different configurations. Since one of the 8 PEMFC stacks has a lower cell number, as described in Section 4.3.1, the two branches have a slightly different voltage [245]: thus, the possibility of issues in load management is investigated as well in this Section.

4.4.1. Static operation

Tests with stationary power load were conducted for each FCM, for each branch, and the whole system (with the two branches working in parallel). Tests were repeated three times, to verify

the coherence of the results. Three different power outputs have been required, corresponding to 10, 20, and 30 kW related power per single stack. Each experiment had a duration of 20 minutes. The main objective of this test is to verify the good assembly of the FC stacks in a complex system that integrates industrial auxiliary components and to assess the ability of the FCS to satisfy a constant power request during a significant time horizon, with no losses in performance. This operative condition simulates the behavior of the FCS to provide, during the whole navigation time, constant power for cruise speed propulsion, or constant power for the hotel load requirements in case of larger ships. If the whole setup is correct, it is expected that the produced power will be constant over time as well as the performance.

The stationary load test has been conducted on all the FC stacks, and it has been developed at three different loads. Results obtained for stacks in branch01 are comparable to the ones achieved for branch02, therefore only part of the results are hereby graphically represented. Figure 53 shows the results of a long-lasting test on FCM04 (at 10, 20, and 30 kW, respectively). It is possible to appreciate that the voltage, in particular the minimum cell voltage (V_{min}), is slightly decreasing over time in the test developed at 10 kW: this effect is probably related to the membrane drying phenomenon, caused by a non-optimized temperature and humidity control during a long operation at 1/3 of the nominal stack power. Partial load operation, tested in this part of the study, is known to be a stressful operative condition that may bring a loss of performance due to a stronger degradation of the MEA [153–155]. In this particular case, the voltage decrease is due to the thermal management in the actual system's configuration. In fact, as described in Section 2, the air flowrate at partial load is higher than the one originally set by the FC supplier; such an increase in the air flowrate was necessary to rise the stack voltage [247] and to allow operation with the aged stacks. On the other hand, an increased air flow rate can exert stronger drag forces onto the membranes, affecting the cell's relative humidity and causing dehydration [101,238], thus a voltage decrease in the 10-kW test. It is worth noting that, observing the results of stationary load tests at 20 and 30 kW (Figure 53), cell voltage does not decrease. Indeed, the boundary conditions of these tests are more similar to the original ones set by the FC supplier and do not affect the relative humidity.

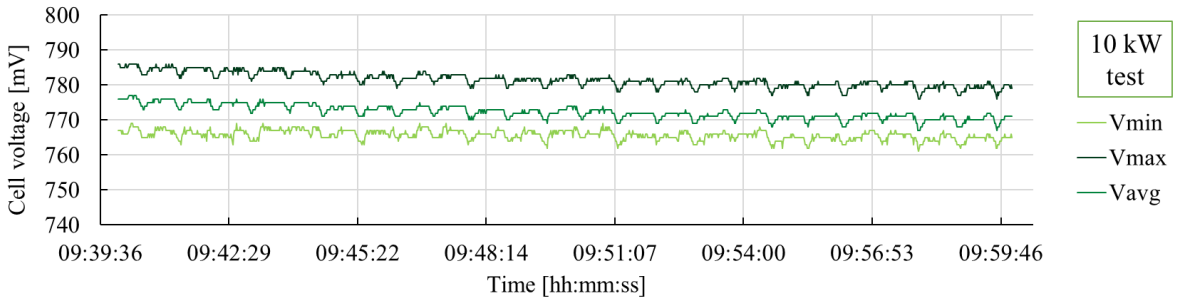

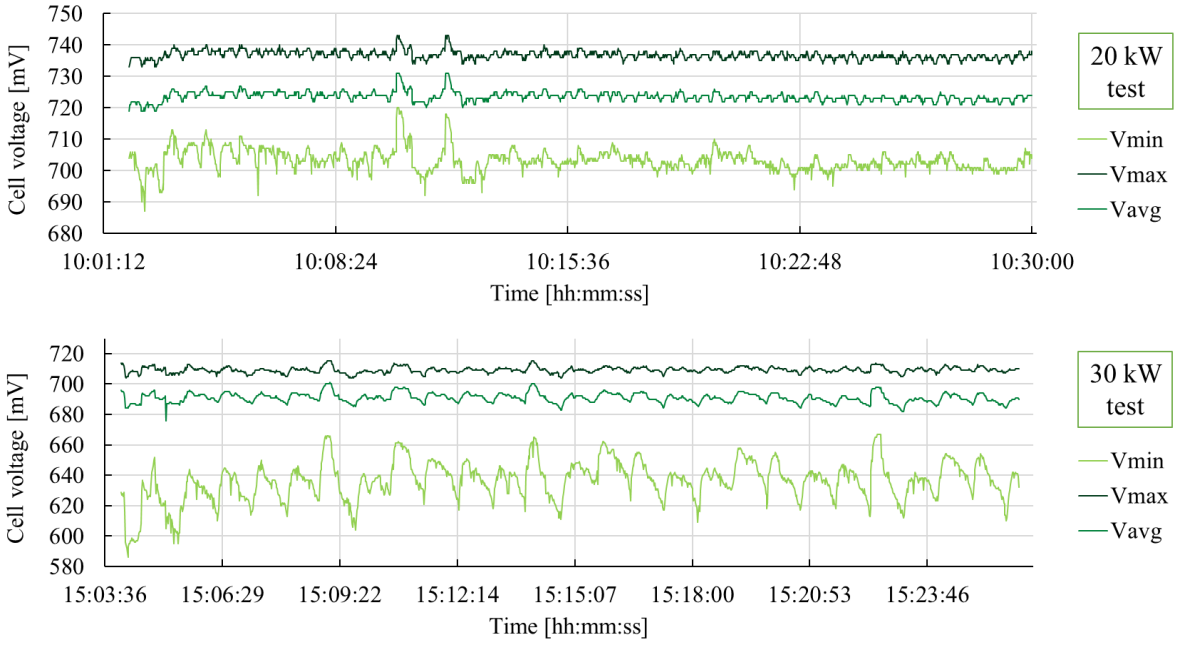

Figure 53: Effect of stationary load on cell voltage at 10, 20, and 30 kW (FCM04): global voltage decrease at 10 kW and voltage instability at 20 and 30 kW.

Nevertheless, due to the system's configuration, and especially to the air supply line setup, the influence of the frequent starts and stops of the industrial compressor on cell voltage can be observed especially in 20 and 30 kW tests: oscillations in the air flow rate deriving from the compressor are only partly compensated by the pressure regulators and by the MFCs. Therefore, it is not possible to totally delete its influence. Yet, the effect of the compressor does not have significant consequences on the performance of the FC stacks, demonstrating that such a component can be employed despite its dynamics being different from the FC ones. In fact, the cell voltage is unstable but does not show a decreasing trend.

Some instabilities are also related to the presence of anodic purges. Keeping in mind that the purging occurs when there is an accumulation of nitrogen and in this instant of accumulation the hydrogen is diluted in a higher way and thus the system requires more fuel, the curves of variations of reactants have also been analyzed, looking for a possible similarity of the repetition time to the purging time. Also in this case, from the graphs in Figure 54, it is possible to note that the timing of the hydrogen inlet pressure peaks (average time value between peaks is 33.75 seconds on the four test cases reported) and of the purging (valve closed during the 30s, then open during 5s) studied are similar. Moreover, Figure 55 shows a correlation in terms of time also for what concerns the hydrogen mass flowrates (average time between peaks is 35.32 seconds on the four test cases reported) and the periodicity of the purging. The influence of anodic purges will be further studied in future dedicated test campaigns.

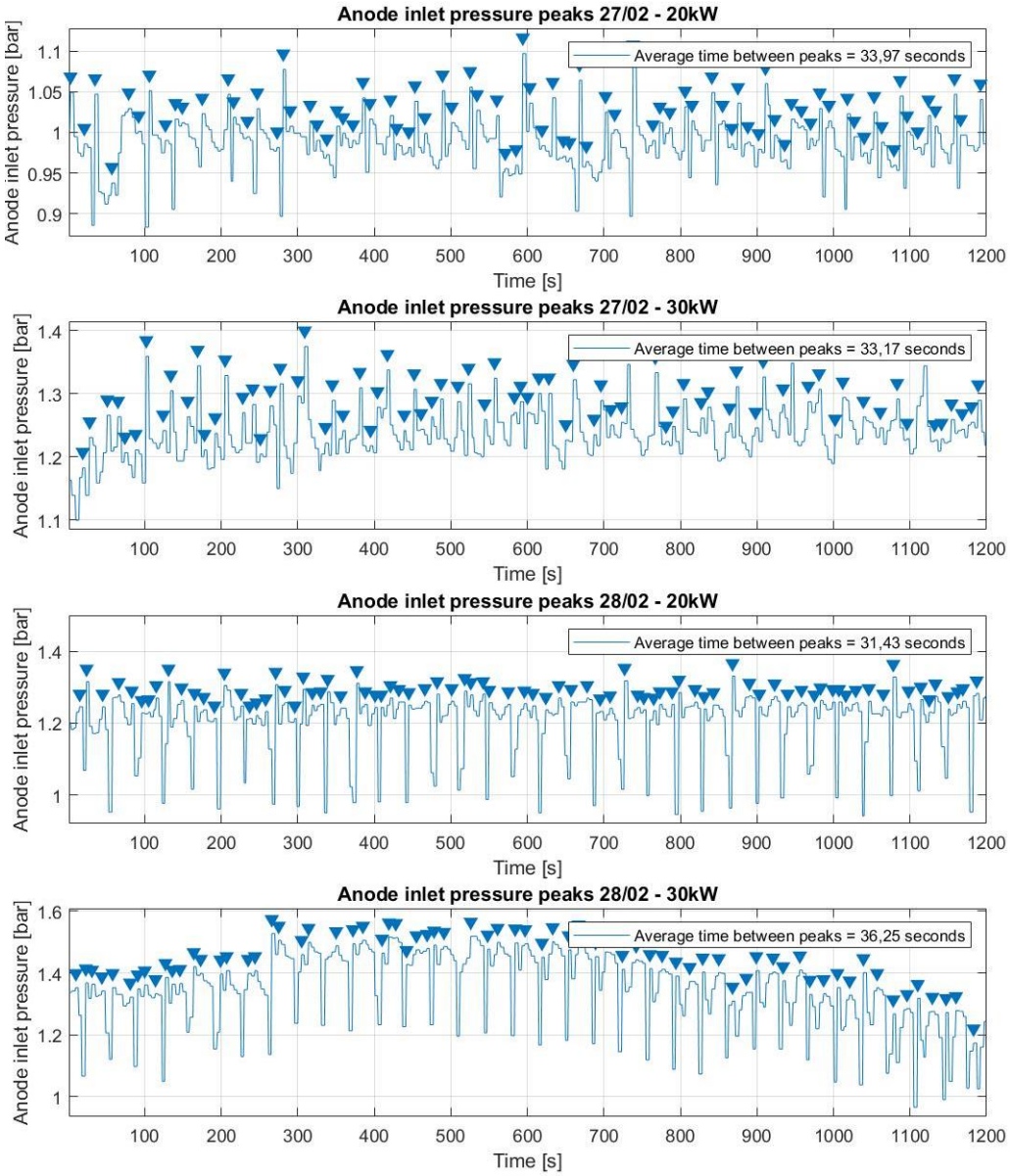

Figure 54: Anodic inlet pressure peaks at 20 and 30 kW power output per FC stack.

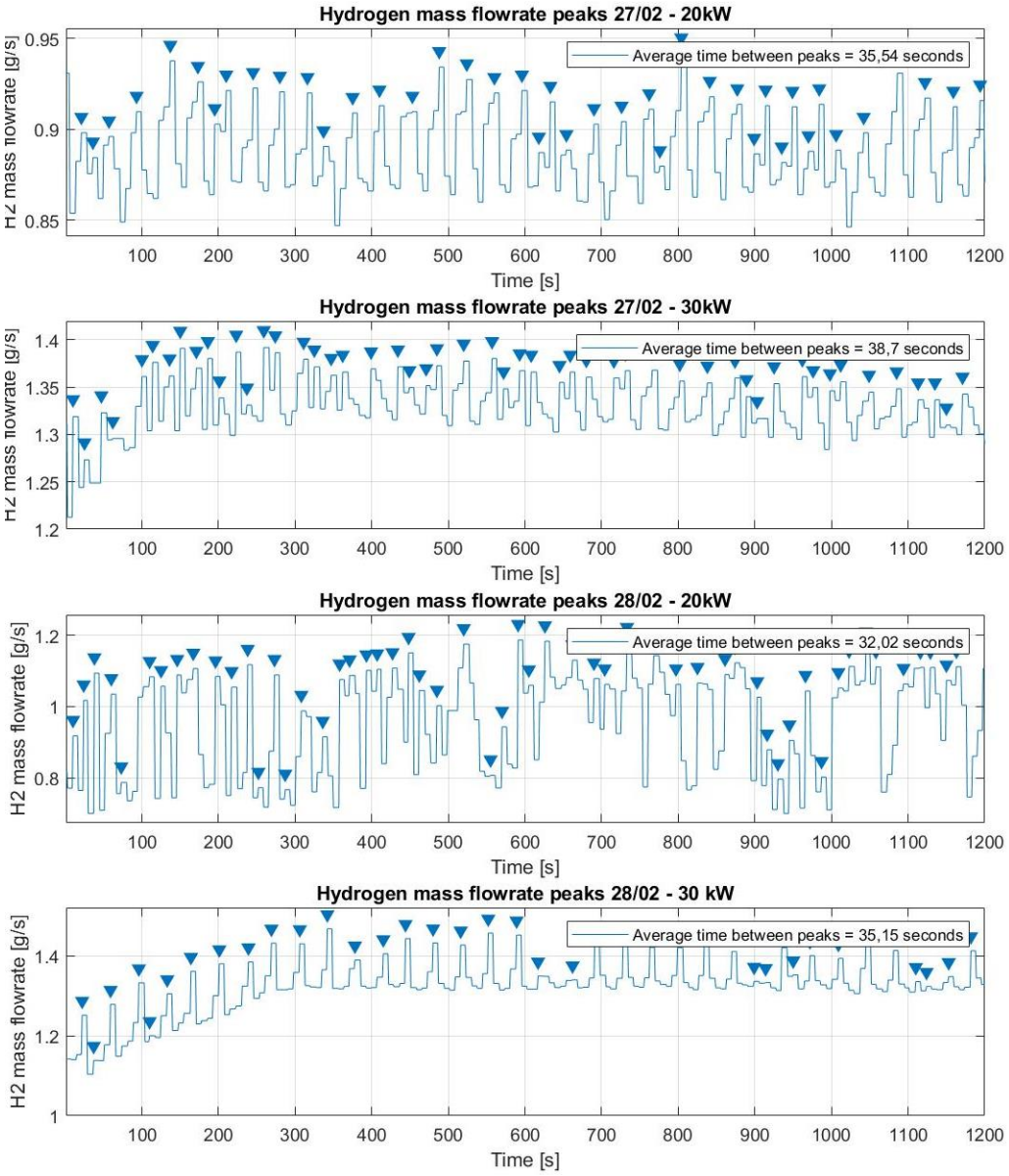

Figure 55: Hydrogen mass flowrate peaks at 20 and 30 kW power output per FC stack.

4.4.2. Dynamic operation

Tests with dynamic power load were carried out for each FCM, each branch, and parallel branch configurations. The dynamic testing routine was designed with sudden power demands to the FC stacks, to verify the presence of differences in the dynamic FC performance between the one depicted by the FC supplier and the real one, obtained by inserting the FC modules in a complete system. The baseload to implement dynamic load tests is initially set at 1 kW, and the aim is to define the maximum power increase (requested to each FCM) that does not generate alarms in the system. Once the maximum power increase is identified for the 1-kW baseload, the latter is increased and the test is repeated (1, 5, 10, 15, and 20 kW power output referred to each stack are employed as baseloads and tested). This test is important to assess the ability of

the FCS (BoP included) to withstand load variations and to verify the time needed by the system to readapt to the new power request. The ability to follow load variations efficiently is a very important characteristic for an FCS in real conditions, and it may influence the choice for the sizing of the battery – if it is needed to implement a hybrid system – as well as the choice of specific BoP components.

As the FC supplier predicts the ability of the stacks to follow current ramps up to 200 A/s, this type of test aims to identify the FC dynamic performance in the HI-SEA system configuration. Therefore, the system is required to withstand sudden load increases, identifying the maximum one that can be reached. The results of the dynamic tests show the high sensibility of the stacks to the cathodic air flowrate setup as it is designed. The maximum power increase depends on the baseload, and it is possible to demonstrate that the HI-SEA system is performing better in dynamic load tests when it is operated at low currents. The limiting parameter in dynamic conditions is given by the cathode air flowrate, which takes excessive time to adapt to a new load request. The higher success rate for dynamic load tests is obtained when the test starts at a lower power baseline, since – as explained in Section 4.3 – the enhanced airflow rate results in a favorable boundary condition. In this case, the system manages to tolerate a short delay in adapting the air flow to the new request. On the other hand, when the baseload power is higher the air flow rate is closer to the original setpoint given by the FC supplier; in this case, a delayed reactant's increase cannot lay on a previous excess of air, and very short air starvation is verified. This causes low cell voltage and can eventually lead to the emergency shutdown of the system. While for single stacks with a dedicated blower this problem is directly related to the blower performance, a system integrating more stacks requires a well-designed BoP and, in any case, suffers from high dynamic power loads. Figure 56.a indicates the percental increase in the air flowrate that has been implemented in the system with respect to the original values, considering all the baseloads tested, while Figure 56.b shows the different power increases managed by the system in dynamic load tests, referred to as the power increase that can be reached by the single FC stack, obtained at the baseloads indicated on the x-axis. It is possible to see that the two parameters have the same trend, confirming their close correlation.

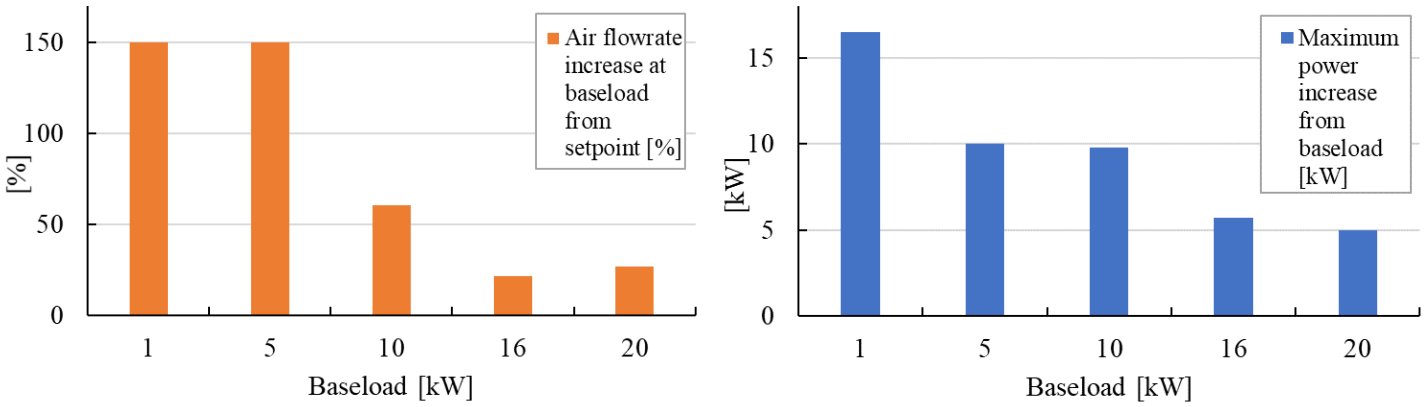

Figure 56: a. Air flowrate percental increase with respect to the original setpoint value at different baseloads; b. Power increase reachable by the FC modules at different baseloads.

Figure 57 shows dynamic load test results for FCM03 for the 1-kW baseload. The stack is initially required to ramp up from 8 to 135 A over 1 second; the air flowrate follows the load variation within a short time and the test is successful. In a second time, it is required to increase the current from 8 to nearly 160 A, which in terms of stack power output is equivalent to an increase from 1 to 17.5 kW: FCM03 approves the test despite the delay time that the air flowrate takes to be adapted, considering also that some intermediate steps are verified. This is the maximum power increase that the system could withstand starting from a 1-kW baseload. A higher increase could not be required to the system due to a prolonged delay of the air flowrate adaptation, which causes low cell voltage alarms and emergency system shutdown.

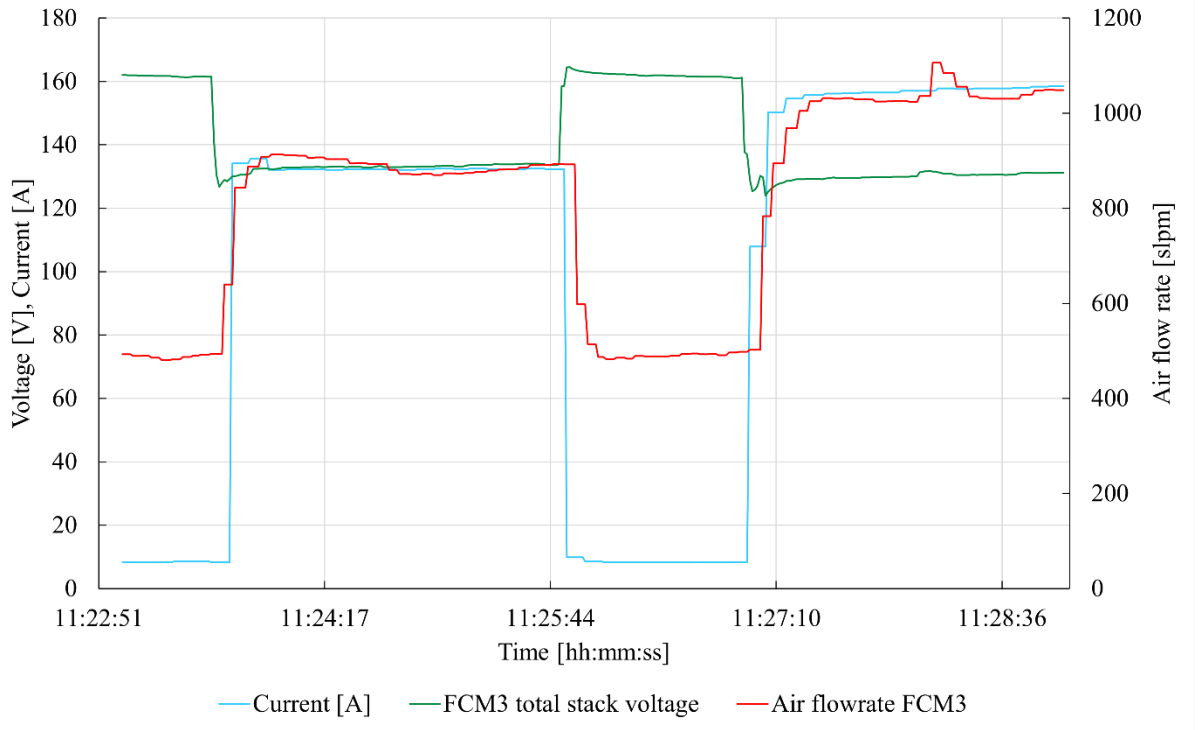

Figure 57: Two moments of dynamic load test on FCM03: 8 to 135 A and 8 to 160 A.

4.4.3. Load profile requirement

The operative profile defined together with Fincantieri (profile A in Figure 58, red line) can be divided into two parts:

- The first part, where subsequent current steps are implemented until the nominal conditions are reached; then, the system is kept working for a longer time, to simulate steady-state operation during the navigation phase or to feed the hotel load.
- The second part of the profile aims to simulate maneuvering; originally this condition was implemented through a sinusoidal trend where the current output ranged from 90% to 33% of its nominal value. However, the original operative profile A (red line) had to be simplified in this part due to the constraints in the control of the modular resistive load through the control system.

Therefore, a more conservative profile was defined, too: profile B (Figure 58, blue line) shows slighter current increases and avoids the sinusoidal trend in the second half of the profile. It is still a good example of alternating constant load and dynamic load, which is verified in real operation. Figure 58 shows the current output requested for each parallel branch during the test. Each test lasts 32 minutes and, during this time, it is expected that the system manages to switch between the two parts of the operative profile without significant losses in performance or incurring alarms.

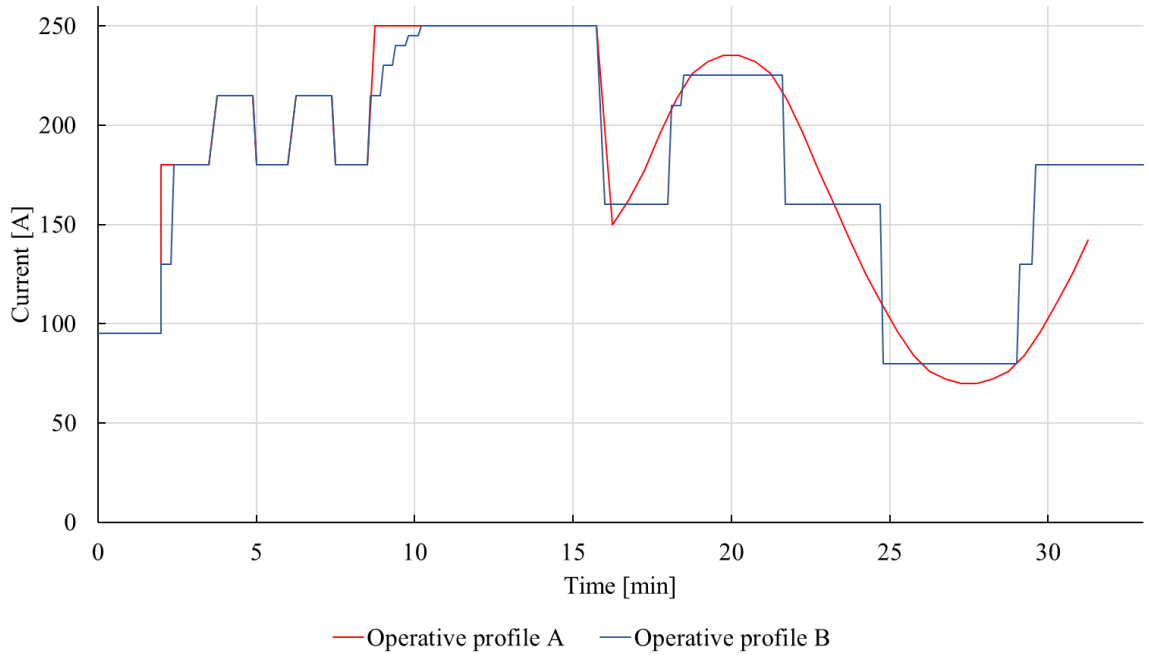

Figure 58: Operative profiles A and B.

After assessing the ability of the system to withstand constant load requests, and after individuating the maximum load variation that can be safely required to the stacks depending on the baseload through the dynamic load test (Figure 56.b), the maritime operative power profile B (Figure 58) was chosen for the test, as it is more suitable to the FCS possibilities. It has been tested both on a single branch and in a parallel branch configuration. Since the power steps of profile A (red line) resulted in fact too high for the actual system configuration, profile B (blue line in Figure 58) is tested and the results are reported in this section. This decision was taken to avoid the occurrence of emergency shutdowns that would have prevented the completion of the test. The results of the operative profile test, implemented on a system configuration that represents fault conditions (3 FCM active on branch01, 4 FCM active on branch02), are reported in Figure 59. The test is concluded successfully, and the load request is always satisfied by the system. As in the static load tests, the influence of the compressor at high power operation on the airflow rate is reflected in the values of FC stack voltage. Nevertheless, the test is completed, making it possible to assert that the system can comply with the operative profile proposed, without negative consequences on the FC stacks' performance. The hydrogen mass flowrate trend follows the load profile (Figure 59.a, black line); the temperature of the cooling line is properly controlled during the whole test, on both branches (Figure 59.a, red lines). DC/DC converters are bypassed in this test, and the FCS is directly connected to the resistive load, in fact, branch voltage outputs (Figure 59.b, orange lines) show the same values, variable depending on the current. It is worth noting that the current on branch01 is lower than on branch02 (Figure 59.b, blue lines): in fact, as a fault condition is simulated, the voltage equalizes at the output of the two parallel lines, and branch01 must work at lower current to maintain the voltage value, compensating the absence of one stack in the electrical series. The lower current also justifies the slightly lower temperature on the cooling temperature on branch01 (Figure 59.a). This test demonstrates that the system can withstand the operative profile even in case of faulty conditions, thanks to its architecture based on the redundancy of the lines.

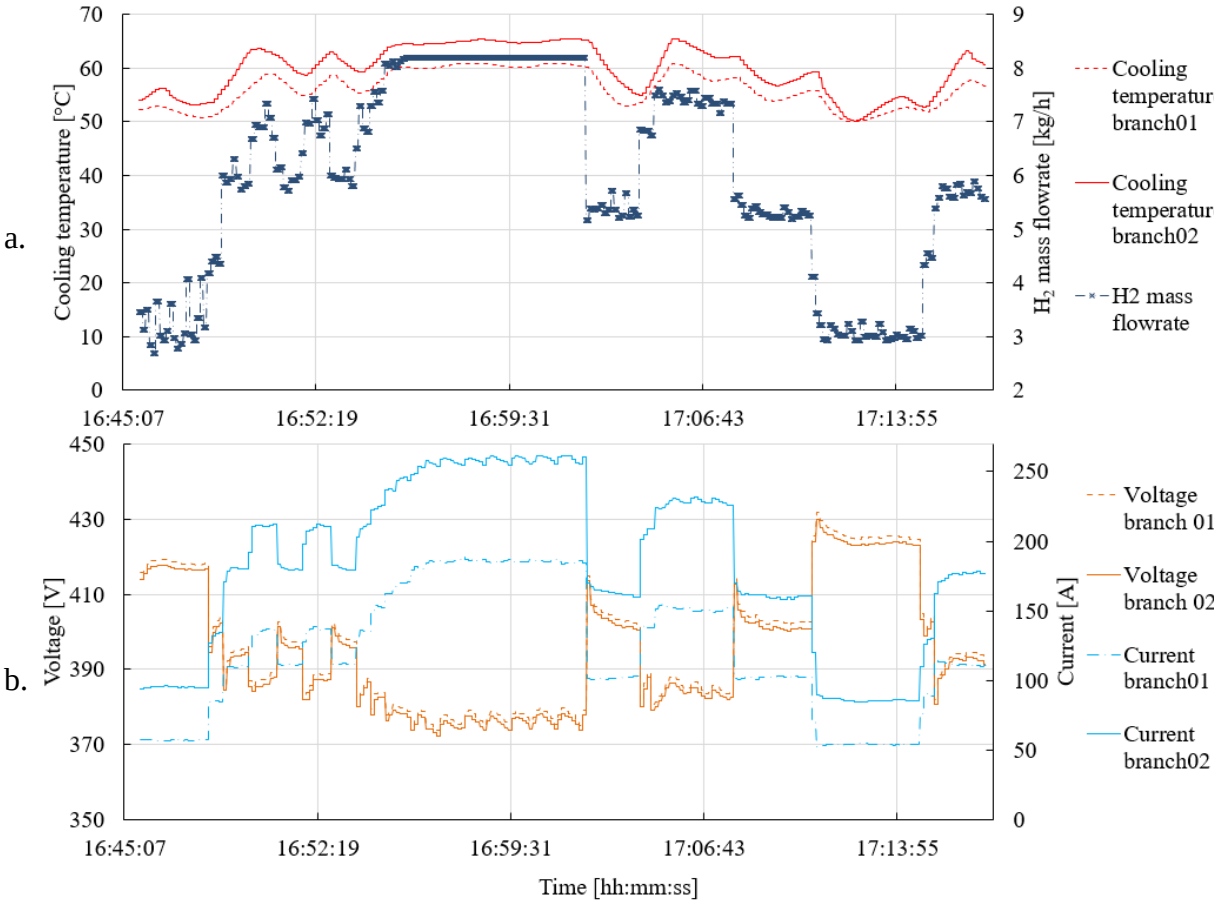

Figure 59: Operative profile test on the FCS without DC/DC insertion: a. cooling temperature on branch01 and 02, and total hydrogen mass flowrate; b. voltage and current on the two branches.

4.4.4. Operation of parallel branches

The test results assess that the HI-SEA system can withstand different load profiles even in parallel branch operation. However, in all the described results the DC/DCs were bypassed. It is important to test the correct operation of the system including the voltage converters, as the FCS may be part of a more complex system and need to interact with other components via a DC bus. Therefore, this condition is hereby described.

The original load-following stacks control (voltage control), implemented using a standalone DC/DC on each branch without a Power Management System (PMS), did not allow the branches to work in parallel and generated instabilities in load sharing, as shown in Figure 60: the current was conducted only by the branch whose DC/DC had the highest output voltage, making it impossible to reach a stable condition and causing a discontinuous and stressful condition to the FC modules.

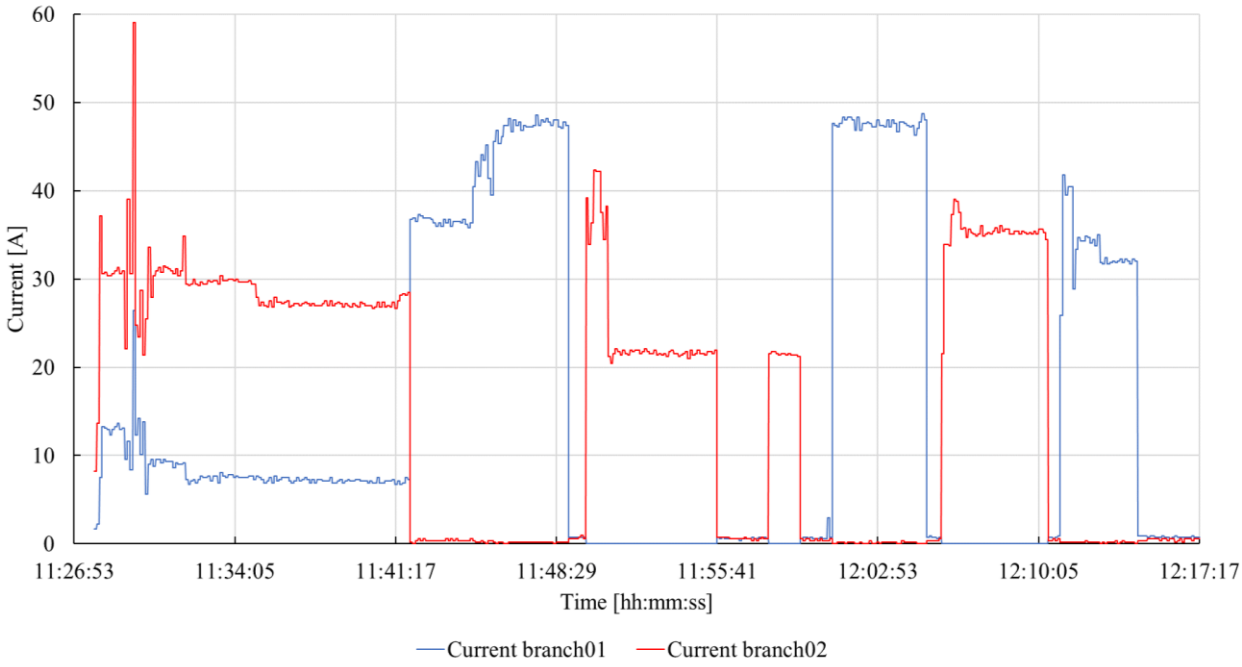

Figure 60: Switching of the load between the two branches in absence of PMS for the DC/DC output control.

Therefore, a PMS has been installed on the two DC/DCs to equalize the branches' output voltage and to improve the system performance in parallel operation. The use of the DC/DCs coupled with the PMS and a load-following voltage control strategy allows to have the same output voltage on the two converters and then to communicate with the resistor bank at the same voltage conditions. Figure 61 shows the results of a load ramp-up test implemented with the two branches operating in parallel at partial load (three FC modules active per branch) and with the DC/DC converters included. The current is increased gradually and simultaneously on the two branches, and the total power output increases from 0 to 180 kW. The current ramp proceeds more slowly than the possibilities checked in the analyses reported in Section 4.4.2. Such a choice is due to the interest of the Author in verifying the stability of the system in the specific configuration that includes the DC/DC converters.

The ramp has been implemented in the system through manual control of the modular resistive bank. If the converters are bypassed, their input and output voltages should remain unchanged across these devices, as verified in Figure 59 during the operative profile test. In the case analyzed hereby, the input voltage to each DC/DC converter depends on the sum of the voltage by the FC stacks on the same branch, that are in electrical series. The DC/DC output voltage, on the contrary, must remain constant on the chosen setpoint value, despite the input voltage variations. The trend of DC/DCs voltage outputs in Figure 61 confirms the correct operation of the converters when included in the system: the output voltage is properly regulated as the load changes, and it remains constant and equal for the two branches. The load is hence equally split

between branches, despite a slight performance difference, as the DC/DC input voltage is lower for branch01, as well as its current, due to different aging from branch02. Eventually, the insertion of the PMS is relevant to ensure a good operation in this configuration.

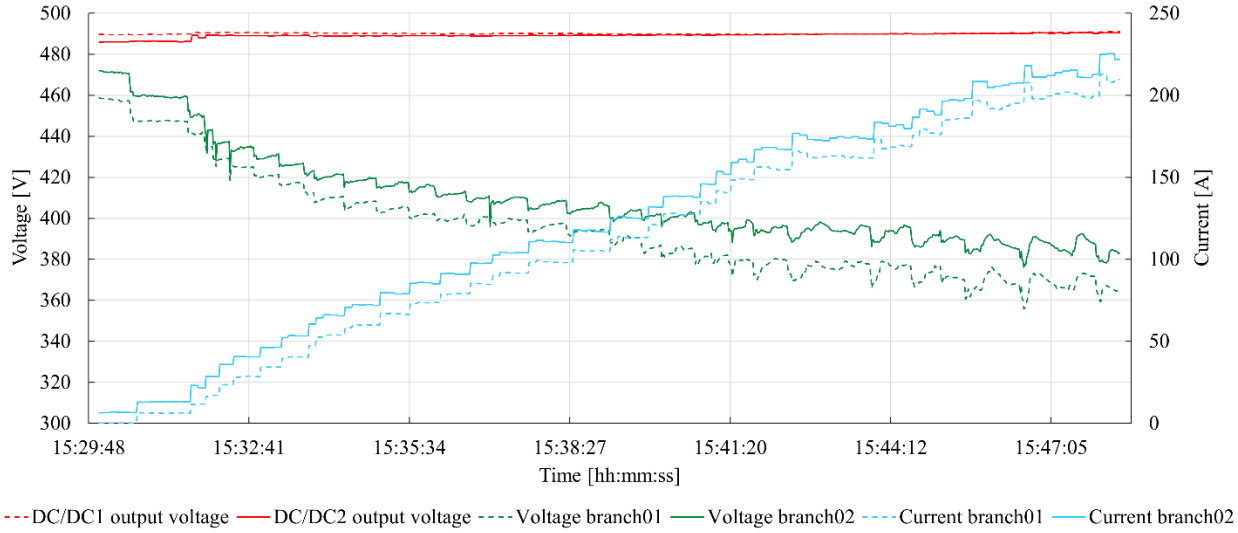

Figure 61: FCS operation with DC/DCs inserted: voltage (branches and DC/DCs outputs) and current, power ramp from 0 to 180 kW.

The results described above are part of a dedicated article that has been accepted and therefore is currently to be published in a scientific journal.

5. Design of Experiment approach to data analysis

The HI-SEA system has eight PEMFC stacks, sized 30 kW each for a total power installation of 240 kW, that have been tested with two aims: drawing guidelines for the best system design onboard ships, and deepening the know-how on the experimental management of the technology. During the tests, as described in Sections 4.3 and 4.4, it was possible to observe the reciprocal influence of some parameters, which may affect the system efficiency.

Since the results of the experimental campaigns carried out in the HI-SEA laboratory underlined a persistent instability of some parameters of the system, the latter has been studied in detail. Indeed, the BoP of the FCS is designed to prioritize the representation of an onboard installation and to study the interaction between the auxiliaries and the FC Modules (FCM). However, it has been verified that the chosen configuration does not perfectly suit PEMFC fast dynamics [43]: this can be reflected in the FC voltage, which shows instabilities coherent with the ones measured in other input parameters – i.e., cooling temperature and air flow rate. Therefore, the present analysis aims to define the typical range of variation of the input parameters of the system and thus estimate their effect on the FC performance and the output voltage stability. The results can help to design a monitoring tool that detects rapidly and efficiently any anomalies in the parameters evaluated by the control system. Besides, understanding the optimum value of input parameters (i.e., air flow rate and cooling temperature) can improve the definition of their setpoints ensuring a more desirable value of the objective function (i.e., stack voltage).

The present Section will deepen the analysis carried out in reference [255] and will describe the results of a further study (which is part of another publication submitted to the International Journal of Hydrogen Energy and currently under review) thanks to the results of a new dedicated test campaign. To understand the interactions in the system, the tests have been developed operating the FCM in three different power outputs. The obtained data have been analyzed employing a statistical investigation to quantify the cell voltage variation correlated to the values of cooling temperature and airflow rate. This has been possible thanks to Design Expert (DE), a software developed by Stat-EASE, Inc. Through Design Of Experiment (DOE) and ANOVA techniques, it is possible to evaluate the significance of input variables in the FC system and their interaction. The experiment under consideration is characterized by non-controllable factors, the cause of disturbances that induce further variability in the response. Thus, to assess the presence of outliers and to analyze the significance of the parameters

involved, an analysis of variance has been performed, and finally, it was possible to build a regression metamodel of the response.

5.1. Design Expert and Regression Approach

The Design of Experiments (DoE) is a statistical approach to the optimization of processes that allows varying several factors simultaneously to explore the domain of investigation to identify optimal values. Some objectives of the experiment can be:

- Determine which variables have the most influence in response.
- How to adjust the variables to optimize the response.
- How to adjust the variables to minimize the variability of the response.

DoE is an active statistical method because a series of tests are done on the process, making changes in the inputs, and observing the corresponding changes in the outputs; this produces information that can lead to an improvement of the whole process. DoE methods can be very useful in putting the process under statistical control. It can be difficult to bring the process back under control unless it is known which input variables matter the most. Experiment programming methods can be useful in identifying these influential input variables [256].

Experiment planning is a critical tool for improving a process and developing new processes. The timely application of these techniques can lead to:

- An increase in the volume of product.
- A reduction in variability and more precise respect for project specifications.
- A reduction in development times and total costs.

DoE plays an essential role in project activities when developing new products or improving existing ones. Some DoE applications include:

- Comparison of project configurations.
- The evaluation of alternatives on materials.
- The determination of the key parameters in terms of influence on performance.

The key terms of the DoE are hereby described.

Factor or parameter

Any characteristic quantity of a physical and technological phenomenon that affects its performance can be defined as a Factor (or parameter). With respect to the context of the experiment, the factors are divided into two types:

- Controllable: these are the factors for which it is possible to define the *a priori* values, as input to the experiment itself. Furthermore, the controllable input factors of a process

can be both qualitative (type of reagent, packaging material, etc.) and quantitative (% of additive, the quantity of oxidant, etc.)

- Not controllable: these are those factors that can change during the operation of the process but are not part of the controlled variables (by constructive or operational choice or by objective impossibility).

Levels

A Level indicates each value of the factor or parameter considered, concerning units of measurement and measurement methods for physical quantities, technical or construction choices, or to indexes of merit in the case of parameters that cannot be directly measured. The experiment must be designed before its execution, generally, the following is established: i.) the appropriate response to the problem under investigation; ii.) Factors and Levels to be used in the experiment and that are expected to influence the response; iii.) the existence of a trade-off between the number of Factors or Levels and times or costs of the experiment; iv.) the number of trials or replicates per treatment (n). Usually, a balanced experiment is preferred, i.e., with the same number of tests for each treatment.

Important concepts in DoE are randomization, replication, and block execution. Randomizing both the order of execution of the tests and the assignment of the experimental material to the treatments allows for mediating the effect of the uncontrollable factors present that will affect the various treatments uniformly. Carrying out more than one independent test for each treatment, i.e., replication allows to improve the accuracy of the estimation of the effect of the factors and at the same time to reduce the estimation of the error and the background noise, since the standard error of the sample mean is equal to the population mean square deviation σ, divided by the square root of the replication number $\sqrt{n}$. While the block is a known and controllable disturbance factor that almost certainly produces an effect not relevant to the experiment on the response. If the disturbing factor is neither known nor controllable, randomization is the only solution. Therefore, the guidelines for the planning and analysis of the experiments can be summarized as follows:

- Identification and formulation of the problem.
- Choice of Factors, Levels, and intervals.
- Identification of blocks and covariates.
- Selection of the response variable.
- Choice of the experimental plan:
    - Determination of the number of replicas.

    - Assignment of experimental material to treatments.
    - Definition of the order of execution of the tests.
- Carrying out the experiment.
- Statistical analysis of data using ANOVA (Analysis of Variance) methods.
- Conclusions and recommendations (possible planning of a new experiment based on the results obtained).

The ANOVA

The ANOVA is a data analysis technique that allows for to verification of hypotheses relating to the differences between the means of two or more populations and evaluates the relative importance of the different sources of variation in the observed variability. During an experiment, sources can be:

- Systematic sources of variation, under the investigator's control, i.e., the data sets of input factors.
- Sources of random variation such as intrinsic stochastic variability, environmental conditions, and measurement errors.

The analysis of variance more specifically is a parametric statistical technique. Therefore, it is assumed that the variable of interest is normally distributed in the population and that the two samples are randomly extracted from the population; besides, the sample size is a significant issue and, in the comparison between several samples, the variances must be homogeneous.

ANOVA models can be classified according to the number of variables and the type of variables:

- Models that envisage a single independent variable are defined as one-way or monovalent designs.
- Models involving two or more independent variables are called factorial designs or factorial designs.
- Models that provide for a single dependent variable define a univariate analysis of variance.
- Models that include two or more dependent variables define a multivariate analysis of variance (or MANOVA, Multivariate Analysis of Variance).

Experimental error

For non-deterministic systems, even though the same input factors $x1$ are provided, the same response y is not generally obtained (Figure 62), in fact, there may be disturbing factors attributable to different causes.

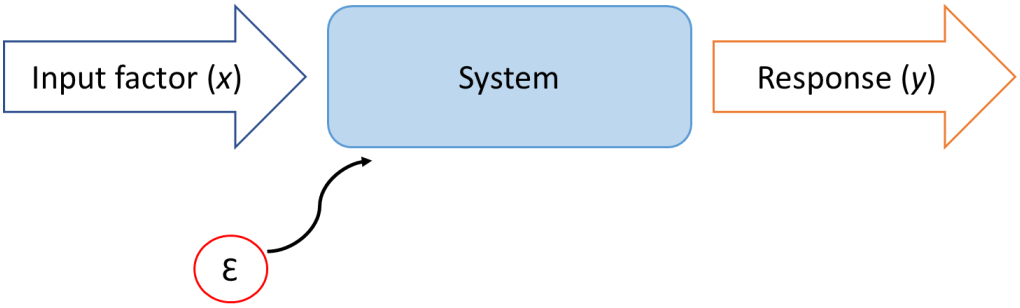

Figure 62: Non-deterministic system representation.

It is therefore necessary to determine the experimental error. The errors ε_{ij} are normally and independently distributed random variables of zero mean and constant variance, but not known a priori. In experimental practice, the two assumptions may not be respected with sufficient precision, so they are checked through the analysis of residuals. The residual analysis takes place through the following steps:

- Verification of the hypotheses of distribution of the experimental error as a NID (0, σ^2) by using a normal probability diagram (Figure 63).

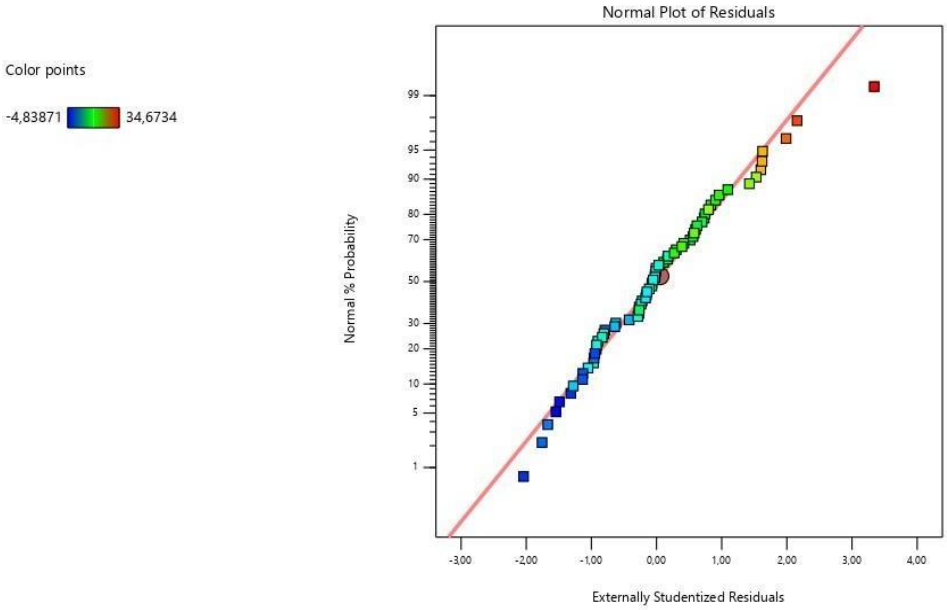

Figure 63: Normal probability diagram (Elaborated via DE version 12).

As for the reading of the diagram, moderate deviations from normality do not significantly affect the ANOVA. While if one or more residues are found to have a much larger value than the others, defined as outliers, their presence can seriously distort the ANOVA and require careful investigation. Often this depends on calculation errors; if this were not the case, an outlier could provide more information than all the other data. therefore, it must not be neglected until it is subjected to accurate statistical verification.

- Verification of the assumption of independence of errors or lack of correlation of

experimental data over time. Any violation of this assumption is considered serious, for which randomization is used. From the operative point of view, the verification of the assumption is carried out with the graph of residuals in the test runs or time (Figure 64).

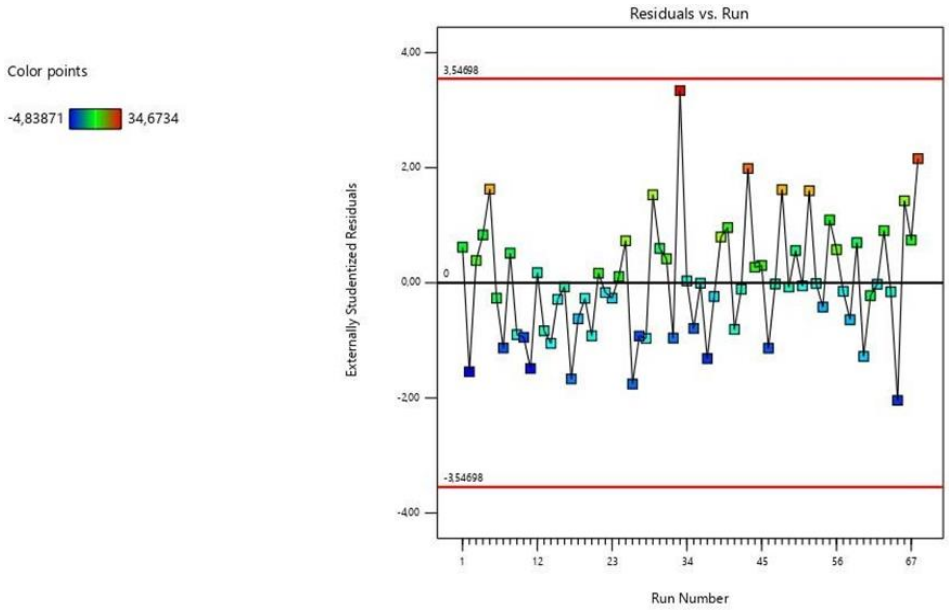

Figure 64: Graph of the residuals depending on the test runs number.

- Verification of the constancy of the variance of the observations, that is, of the error. This analysis is carried out on a residual-response plane on which the residuals concerning the responses must appear to have no structure (Figure 65), i.e. by imagining that the most extreme points for each level of the represented factor are connected by vertical lines, the length or amplitude of the lines should be uniform. In the reported case there is no uniformity.

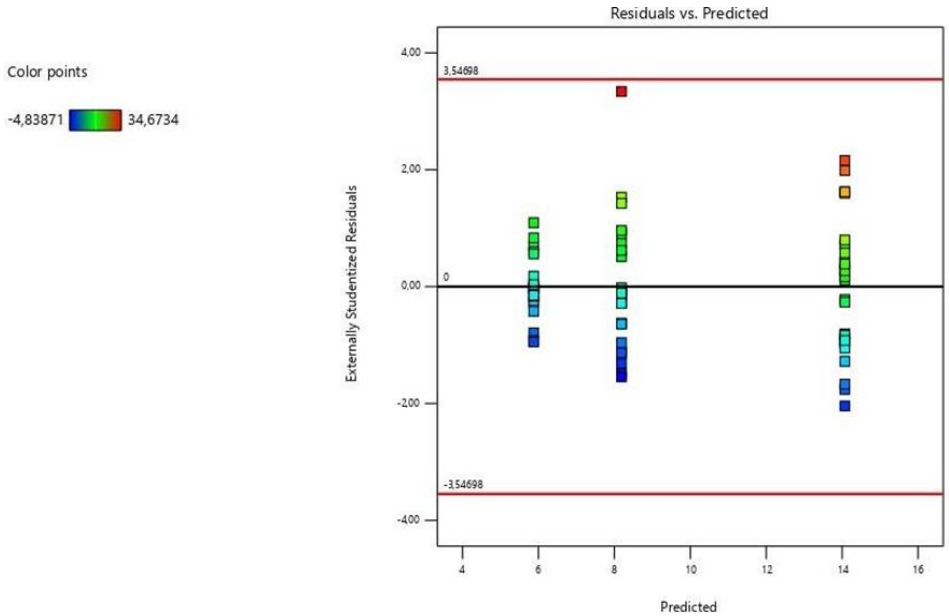

Figure 65: Residual-response plane.

From a mathematical point of view, for the analysis of variance, a test named "F" is carried out. Initially, the null hypothesis H_0 must be formulated, which usually provides for the statistical equality of the means under the "a" number of treatments μ, meaning that the belonging to a particular group has no influence on the results, that the data of all groups come from the same population, and that the differences observed between the groups are due only to the sources of random variation; the alternative hypothesis is its negation. The mathematical formalization of this concept can be expressed as:

$$H_0: \mu 1 = \mu 2 = \cdots = \mu a \qquad \textit{Equation 40}$$

$$H_a: \mu i \neq \mu j \text{ for at least one } i \qquad \textit{Equation 41}$$

To verify the test F according to the model considered, it is necessary to calculate:

- The averages of treatments, blocks, and effects, and the large average.
- The sum squares i.e., the total variations, treatments, blocks, and effects.
- The mean squares, i.e., the mean variations through the relationship between variations and degrees of freedom.
- The summary F_0 i.e., the ratio between the mean squares to conduct the F test and deduce the conclusions.

Finally, it is possible to proceed with the graphic representation of the interaction between the different input factors.

5.2. Scope of the analysis and input and output variables identification

In stochastic systems, such as the HI-SEA PEMFC system under consideration during the experimental campaign, specific statistical techniques are used to determine the effect that input parameters have on the output variable (objective function). The DoE techniques aim to determine the influence on a selected objective function for one or more independent variables (named factors), varying among different levels or treatments. The significance of such factors is determined through statistical analysis of data using ANOVA (Analysis of Variance) methods [257,258]. This process is carried out to establish which factors determine a significant variation of the objective function in the HI-SEA system. The experiment is also characterized by uncontrollable factors, which are the cause of disturbances or background “noises”, which induce further variability of the response.

An important evolution of DoE is the so-called Response Surface Methodology (RSM) which aims to define the optimal design (the grid of candidate points in the experimental region) in order to build regression models for the objective function.

To fit a first-order regression model, the RSM identifies as the best experimental design the Two-Level Factorial Design. To fit second-order regression models, the Central Composite Design (CCD) or the Face-Centered Central Composite (FCC) design are adopted. The statistical analysis and graphical analysis of the data developed for this part of the Thesis were performed by using Design Expert (DE) software (Version 12.0, Stat-Ease, USA). Design-Expert software provides test matrices for screening up to 50 factors at a time. The statistical significance of these factors is established with variance analysis and graphing tools that help identify the impact of each factor on desired outcomes, revealing anomalies in the data if any.

During the development of experimental tests on the HI-SEA system, different parameters can be collected. The postprocessing of these data can be employed to create a regression model of the system, like the ones developed in previous studies such as [259–268].

As explained in Section 4.2.2, the control of the HI-SEA system consists of a supervision system and a local panel that contains the PLC, an I/O field, power supplies, and all auxiliary accessories for the management of communication lines; the supervisory computer interfaces to the PLC and performs the monitoring and historicization of all process variables, also implementing all the procedures to provide standard security levels for the access to the information. The PLC performs the interfacing, management, and coordination of field devices, using when necessary different communication standards. One of the tasks assigned to the system is to control and regulate the control circuits of fuel cells; the software is designed to control up to 8 stacks, however, the operating logic of all stacks is perfectly identical to each other. One of the most important parts of the control system is the CVM. As cell voltage is a very important indicator of the performance as well as of the state of health of cells, this value must be carefully handled and considered. The CVM chosen by Nuvera Fuel Cells acquires every second the voltage value of each cell in the stacks; therefore, it saves and communicates to the control system – for each FC stack – the following data:

- Minimum cell voltage (V_{min}): the lowest voltage value measured in a stack, and the ID of the cell where it is measured.
- Maximum cell voltage (V_{max}): the highest voltage value measured in a stack, and the ID of the cell where it is measured.
- Average cell voltage (V_{avg}): obtained by dividing the total stack voltage by the number of cells.

Another crucial aspect of the control system is the cooling circuit. The most suitable operating temperature has been set by the FC supplier to keep the ideal relative humidity on the membranes. The maintenance of the correct cell temperature is ensured by the cooling circuit,

which regulates the temperature and mass flow rate of the cooling flow that removes the excess heat from the cells by means of a heat exchanger. The regulation is led by the measured current. The current leads as well the regulation of the reactants' flowrates: it in fact acts on the cathodic inlet air which, as seen in Sections 4.3.3 and 4.4.1, shows some intrinsic instabilities that cannot be avoided. The same is verified for the cooling circuit.

The present analysis aims to apply the Design of Experiment approach to assess the effect of different variables, i.e., cooling temperature, current variations, and air mass flow rate, on stack voltage. These input variables have therefore been classified as the independent variables (factors) of the study. The results obtained gave some hints to identifying the most influential operative parameters that determine the global efficiency of the system, which are taken as the starting point for the present study. The stack voltage values are afterward employed in a regression analysis as the output variable (objective function), to evaluate the influence of the aforementioned parameters on the global FC performance.

The use of the software Design Expert allows to draw the survey domain, the regression model, and the confidence intervals of the stack voltage for the case study and can become the reference for the creation of a precise performance monitoring system for the PEMFC installation: if the stack voltage lays out of the confidence intervals, anomalies can be rapidly detected, reducing significantly the operation in stressing conditions that can affect the state of health of the PEMFCs.

5.3. Test definition

The initial analysis has been carried out employing a dataset available from a previous test campaign. This approach was a preliminary one, chosen to verify the possibility to apply the DoE approach to the existing system. In this case, the current has been considered as an input variable, also to verify its stability at constant load; the second input variable considered for the preliminary analysis is cooling temperature. The effect of the instability of these input variables on the objective function, stack voltage, has been studied. The preliminary results encouraged the authors to deepen the analysis and evaluate the influence of the operative conditions on stack voltage by utilizing a more detailed and dedicated test campaign. Therefore, cooling temperature and air mass flowrate have been considered as the input variables during the development of the dedicated test campaign, while, since the first analysis assessed good stability of current, the latter has not been considered as an input variable in the next part of the study. The stack voltage has been set again as the output variable. In normal operation, the voltage follows a well-known trend that depends on the current density. The generic

polarization curve (Figure 14) describes the typical correlation between current and voltage in a PEMFC. Due to the different losses – namely Activation, Ohmic, and Concentration losses [269] – the voltage tends to decrease with the increasing current, but with a different slope depending on the value of the latter.

For this reason, for the statistical analysis of the HI-SEA system, it was chosen to develop constant load tests, to avoid incurring misleading voltage variations due to different load requests and not to the system's instabilities under investigation. The constant load tests usually have the objective of verifying if the system is adequate for the operation. Although the operating conditions are static, some intrinsic instabilities are still present, as shown in reference [43]. The ANOVA approach can therefore verify the consequences of those instabilities on the objective function – i.e., the stack voltage.

The constant load tests have been implemented at different loads: 10, 20, and 30 kW power output per stack in the HI-SEA system. These tests should be considered independent of each other since the setpoints related to the input variables depend on the current and therefore are different. For this reason, the tests at different power outputs are not directly comparable. The choice related to the three different loads was made to investigate the whole operative range indicated by the FC supplier and to ensure good performance without excessive stress to the FC due to instabilities of the input variables. Besides, each test has been repeated three times to ensure the repeatability of the results. After the development of the tests, the acquired data has been post-processed and analyzed via the DE software. To investigate the total stack voltage as a function of the input variables, the following steps are taken:

- First, current and cooling temperature and therefore air flowrate and cooling temperature are considered as the quantitative independent variables to be analyzed.
- Maximum and minimum values of the independent variables are identified.
- Total stack voltage is considered the objective function.
- The presence of outliers is issued, as they can distort the results of the analyses.
- The software DE evaluates the significance of the analyzed variables and builds a representative regression model.
- The ANOVA allows the evaluation of significative and non-significative terms (p-value > 0,05).

This process has been applied to all the stacks, whereas only the results related to one stack of the system (FCM07) are reported. For what concerns the preliminary analysis, only results for an output power of 20 kW are reported, considering the average quadratic deviation relative to

the stack voltage. For the second part of the analysis, the results are reported for the same FCM07 operating at the three different power outputs (i.e., 10, 20, and 30 kW). Two DE output figures per test will be reported in Section 3.2, to prove repeatability. The goal, therefore, is to study the trend of the stack voltage, while monitoring: first, the current and cooling temperature (preliminary analysis), and therefore cooling temperature and air mass flow rate in the second part of the analysis (constant load tests).

For each test, two ranges for cooling temperature (*TT*) and three ranges for the airflow rate (*QM*) have been considered as detailed in Eq. 42 and 43, and they will be reported in the dedicated Table 1, 2, and 3.

The ranges thus identified were chosen as the Levels for the independent variables. Levels are chosen equal in all the tests implemented at the same load, to make them comparable. Once the Levels for each factor and the boundary values are defined, a table is created to contain all the possible combinations of experimental values measured in the tests.

$$TT_{interval} = \frac{TT_{max} - TT_{min}}{2} \qquad \textit{Equation 42}$$

$$QM_{interval} = \frac{QM_{max} - QM_{min}}{3} \qquad \textit{Equation 43}$$

5.4. Results of the DoE approach

5.4.1. Effect of temperature instability

As described in Section 5.2, current and cooling temperature are considered the input variables in the preliminary investigation. After analyzing the influence of the cooling temperature via the DE software, a regression model is built. A response surface method has been carried out at first applied to historical data using only current and cooling temperature as input parameters, to build a predictive model at different power setpoints.

The three main outputs of the preliminary analysis are:

- The survey domain, represented in Figure 66: relative to the total cell voltage, it shows the contour lines and, depending on the red or blue color, it gives an indication of the increase or decrease of the objective function (voltage) linked to the parameters change (current and temperature).

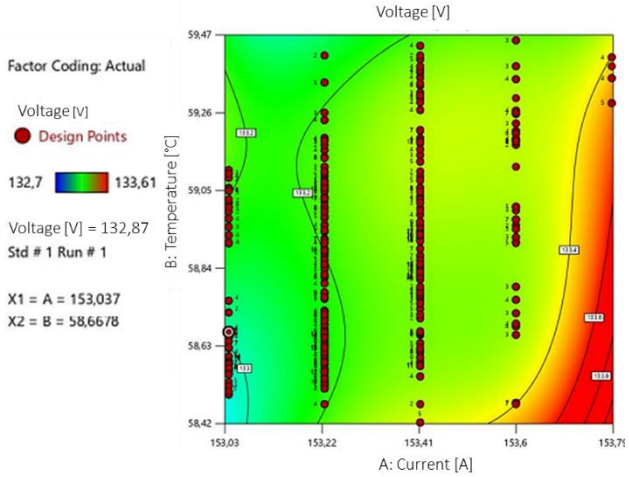

Figure 66: Survey domain of total stack voltage, FCM07, 20 kW.

- Response surface, represented in Figure 67: for each investigation domain, Design Expert builds a response surface based on historical data that represents the behavior of the output variable as a function of the input factors in the investigated ranges. The surface is represented through a 3D graph. For this analysis, it must be considered that the sampled data, being collected during the tests on the HI-SEA system, can make the experiment result unbalanced. This means that in the domain there could be some areas where no experimental responses are available, and where an incorrect approximation of the response is verified leading to an unreliable response surface at those points. To delimit the problem, an appropriate domain cut can be made in order to analyze only the area where the experimental data are located, in order to make the statistical analysis more reliable.

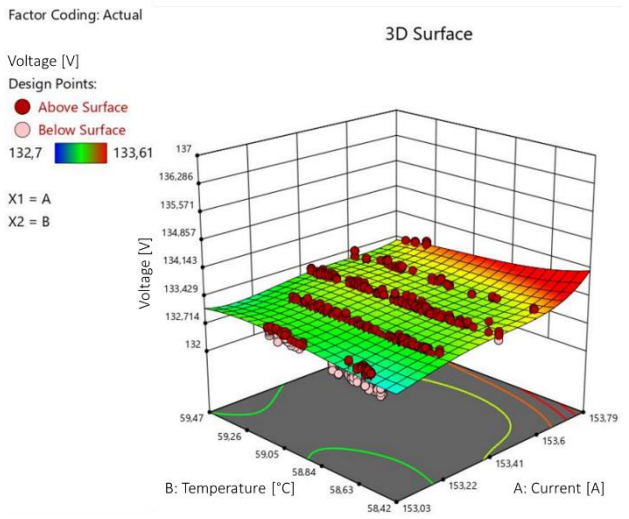

Figure 67: Response surface, FCM07, 20 kW.

In this case, no imbalance areas to be cut have been identified.

- Confidence interval, represented in Figure 68 and Figure 69: once the most suitable response surface has been identified, three types of confidence intervals are analyzed, the confidence interval on the mean response (CI), the prediction interval on the future response (PI), and the tolerance interval (TI). CI contains the mean value of the dependent variable, PI contains the value of the dependent variable for a single new observation given specific values of the independent variables and the latter TI represents, the spread of the individual data points around the population mean. Figure 68 and Figure 69 show the three types of intervals using a confidence level of 95%.

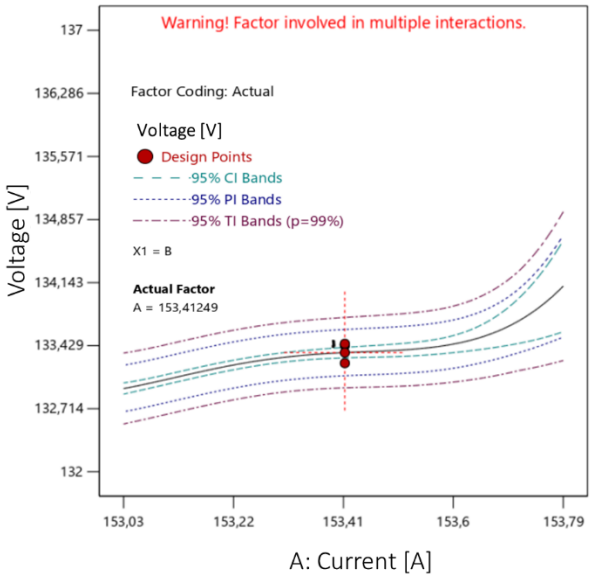

Figure 68: Confidence interval for total stack voltage, FCM07, 20 kW; current is set at 153,41 A.

For each domain, one single current value is set, as the variations for this parameter are negligible, demonstrating good stability during tests. The residual instabilities are mainly due to the control of the resistive load that is part of the HI-SEA system, by which the power output is dissipated. The current value for the confidence interval is set at 153.41 A, as this value was the most frequent one during the tests at 20 kW. As regards the cooling temperature, it is set at 58,42 °C, corresponding to the most measured value assumed during the tests at 20 kW. The lines in Figure 68 and Figure 69 represent the trend of the total voltage of FCM07 and its confidence intervals for a 20 kW power output.

These maps can be the starting point to developing a precise monitoring system: when voltage is measured, if it lies within the confidence interval thus the system is operating correctly. Otherwise, a warning is reported as some anomalies may be ongoing, and the cooling temperature value is immediately checked to assess if it is related to the voltage anomaly. The present results have been described in [255].

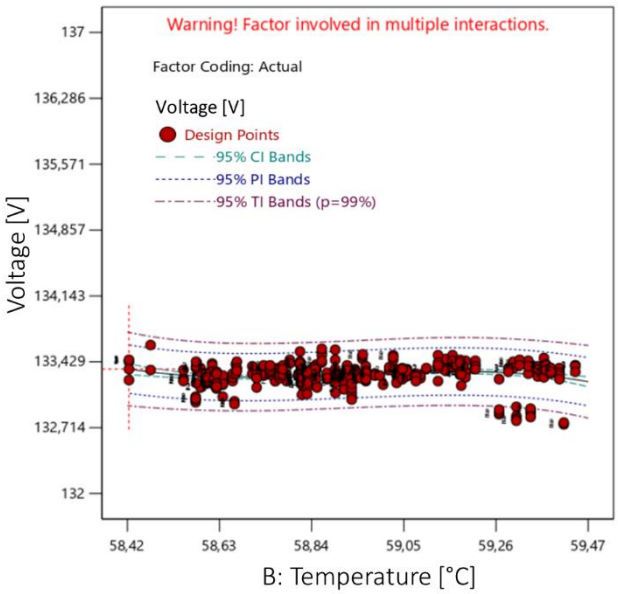

Figure 69: Confidence interval for total stack voltage, FCM07, 20 kW; cooling temperature is set at 58,42 °C.

5.4.2. Effect of airflow rate instability

Constant load tests are implemented as well to study the effects of airflow rate instabilities on cell voltage. As a general consideration, it must be considered that the values of stack current and voltage are as reported in Table 23:

Table 23: Power, current, and voltage values for each stack at the three different test conditions.

Power [kW]	Current [A]	Voltage [V]
10	70	141
20	156	130
30	250	122

As seen in the previous Sections, the three parameters reported can show variations during the test development. Current has some instability due to the control of the resistive load: the system does not allow galvanostatic operation, and the external load is controlled in power mode. On the other hand, voltage has instabilities due to the influence of auxiliaries and the aging of cell components. However, current instabilities can be neglected and therefore stack voltage can be studied as the objective function, linking its trend to the influence of input variables. Besides, each power condition is to be considered separately, to correctly compare the results.

The results of the RSM analysis of 10, 20, and 30 kW tests are hereby shown. To the repeatability aim, each test is repeated three times.

10kW tests

The software automatically performs all calculations: ANOVA, residuals, and Least Significant Difference (LSD) test; therefore, it is possible to detect the presence of outliers to be eliminated from the project to continue with the variance analysis. From Figure 70 it is possible to highlight that there are no design points that go beyond the two red lines that represent the limits of the confidence interval.

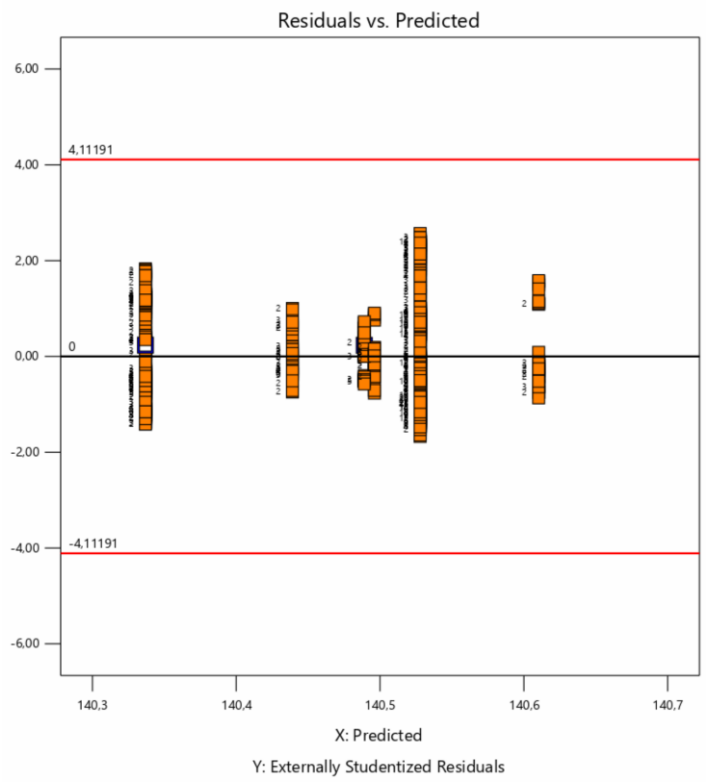

Figure 70: Residuals for the 10 kW tests.

If there are points that are outside the confidence interval, represented by the red lines, they are removed, and the test is carried out again from the beginning until points that do not fall outside this interval are found.

The analyses performed were based on multilevel factorial designs considering two factors: air flow rate and cooling temperature. For airflow rate three levels have been considered, while for the cooling temperature two levels have been identified, leading to a total number of investigated experimental combinations equal to six. Factor levels were associated with appropriate ranges of the variability of the two factors analyzed as reported in Table 24, Table 25, and Table 26 (for respectively the 10, 20, and 30 kW tests). Tests have been repeated three times each, to ensure repeatability of results.

Table 24: Airflow rate (QM) and cooling temperature (TT) intervals (10 kW tests).

Levels	Air flowrate [slpm]
Level 1	662.33 – 671.83
Level 2	671.83 – 681.33
Level 3	681.33 – 690.83

Levels	Cooling temperature [°C]
Level 1	48.56°C – 50.53°C
Level 2	50.53°C – 52.50°C

Table 25: Airflow rate (QM) and cooling temperature (TT) intervals (20 kW tests).

Levels	Air flowrate [slpm]
Level 1	1085.70 – 1096.95
Level 2	1096.95 – 1108.20
Level 3	1108.20 – 1119.45

Levels	Cooling temperature [°C]
Level 1	56.66°C – 57.70°C
Level 2	57.70°C – 58.73°C

Table 26: Airflow rate (QM) and cooling temperature (TT) intervals (30 kW tests).

Levels	Air flowrate [slpm]
Level 1	1530.75 – 1540.75
Level 2	1540.75 – 1550.75
Level 3	1550.75 – 1560.75

Levels	Cooling temperature [°C]
Level 1	62.83 – 63.58
Level 2	63.58 – 64.33

From the analysis of variance (Table 27), all parameters involved are classified as significant: cooling temperature (factor A), Air flowrate (factor B), and their interaction (factor AB).

Table 27: ANOVA table relative to the 10 kW tests.

Source	Sum of Squares	df	Mean Square	F-value	p-value	
Model	7.57	5	1.51	12.18	<0.0001	Significant
A-TT	5.83	1	5.83	46.9	<0.0001	
B-QM	1	2	0.5003	4.03	0.0181	
AB	1.25	2	0.6246	5.03	0.0067	
Pure Error	147.39	1186	0.1243			
Cor Total	154.95	1191				

The different rows in Table 27 can be described as follows:

- The first column of the table shows the factors considered in the project and, when possible, also their interactions.

- The second column shows the “Sum of Squares” (SS).
- The third column contains the degrees of freedom for each factor.
- The fourth column shows the "Mean Squares" (MS).
- The fifth column called *F*-value shows the summaries of F_0 for each factor.
- The sixth column was used to calculate the p-values which will be used to understand which factors are significant and which are not for the project concerning the response factor.

Specifically, the calculated p-value is compared with the significance α in the case under investigation α = 0.05; the factors with a p-value less than 0.05 are significant, otherwise, they are not significant. If one or more interaction factors are not significant, they are added to the error. From the analysis of variance, both the TT (A) and the QM (B) and the interaction (AB, between QM and TT) factors appear to be significant.

Analyzing the effects of the factors in Table 27, it results that the Sum of Squares related to *TT* is equal to 5,83, *QM* is equal to 1 while the one related to AB is 1,25, demonstrating how much the cooling temperature affects the system under investigation.

By calculating the Least Square Difference (or LSD), it is possible to verify the presence of a significant difference among the levels of the factors that were significant (Figure 71). It is represented graphically using a bar graph. Individual factors or interactions can be analyzed if present.

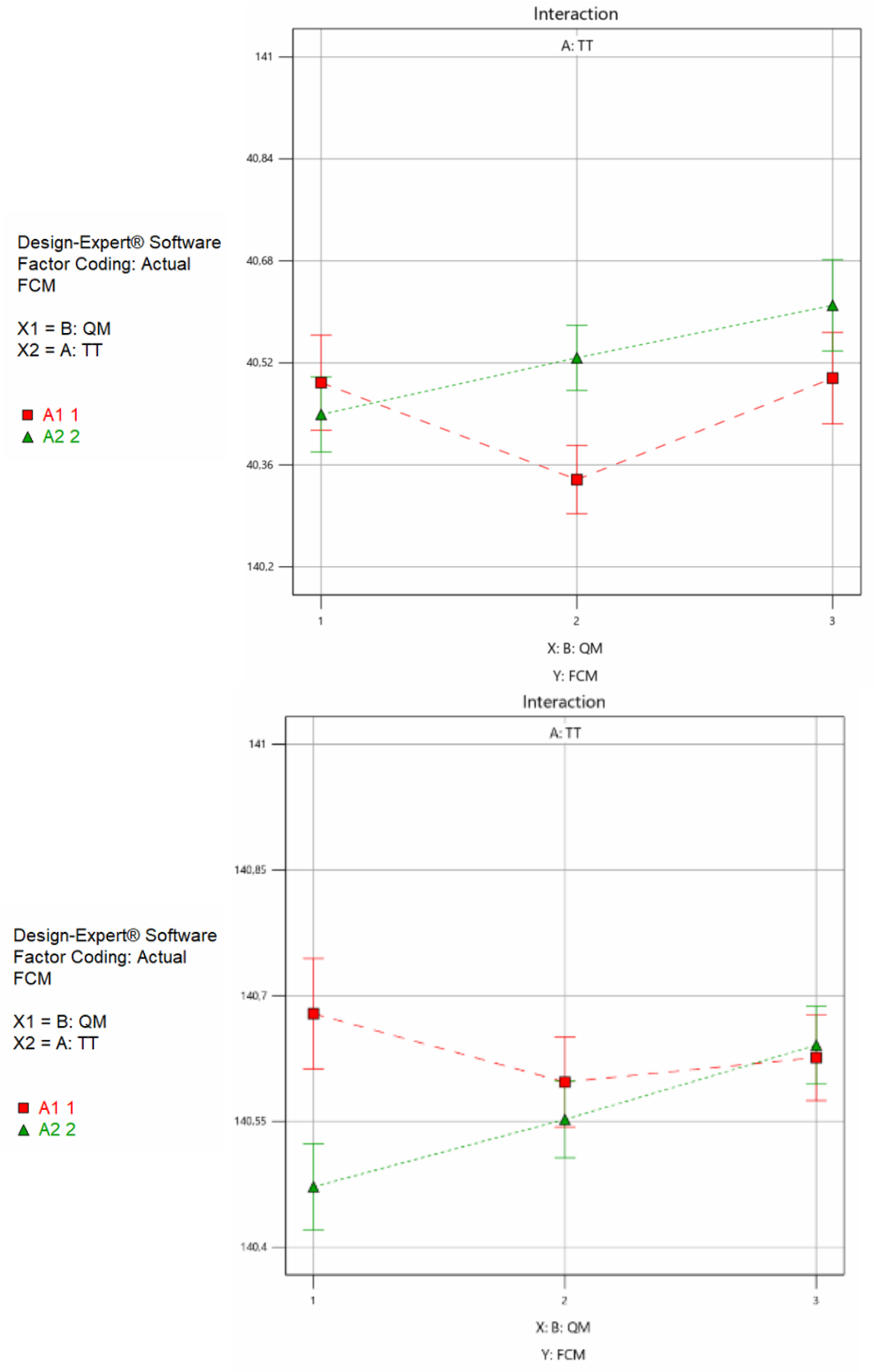

Figure 71: Comparison of cell voltage variation with respect to airflow rate (QM) and cooling temperature (TT) in the first (a) and second (b) 10 kW test.

In Figure 71 (*a* and *b*), the abscissa represents the airflow rate Levels (1, 2, and 3), while the color of the straight lines define the temperature Levels studied, with A1 (the red line) defining

the first Level with a lower temperature value, while A2 (the green line) the second Level (described in Table 24); the y-axis shows the experimental values of the stack voltage.

From the interaction graph related to Figure 71 (*a)*, it is possible to see that for a low and high Levels of *QM* there are no differences from a statistical point of view between a higher or lower *TT* value; in fact, the green and red LSD bands overlap. Instead, for a medium Level of *QM*, the LSD bands do not overlap and therefore there are differences from a statistical point of view.

Considering only the red line or the green line, it can be seen that for the red line (*TT* Level 1) the bars overlap in low and high Levels of *QM*, while it does not happen at the medium value. For the green line (*TT* Level 2), it can be seen that the bars overlap between the three Levels of *QM* and thus there are no statistical differences depending on the *QM* values.

From the interaction graph related to Figure 71 (*b)*, it is possible to see that for medium and high Levels of *QM* there are no differences from a statistical point of view between the two Levels of *TT*. On the other hand, for a low Level of *QM*, the LSD bands do not overlap and therefore there are differences from a statistical point of view.

Considering only the red line or the green line, it can be seen that the bars overlap between the three Levels of *QM* and thus there are no statistical differences depending on the *QM* values.

20 kW tests

In this case, as described above, the output values will be different, but other than that, the procedure always remains the same. Figure 72 shows the effect of input variables on FC stack voltage in the first and second tests, and the data are shown in Table 25.

From the interaction graph, Figure 72, it's possible to see that the LSD bands do not overlap and therefore there are differences from a statistical point of view regarding the effect of input variables.

In addition, a significant increase in the output variable – the FC stack voltage – can be appreciated in the transition from Level 1 to Level 3 relating to the airflow.

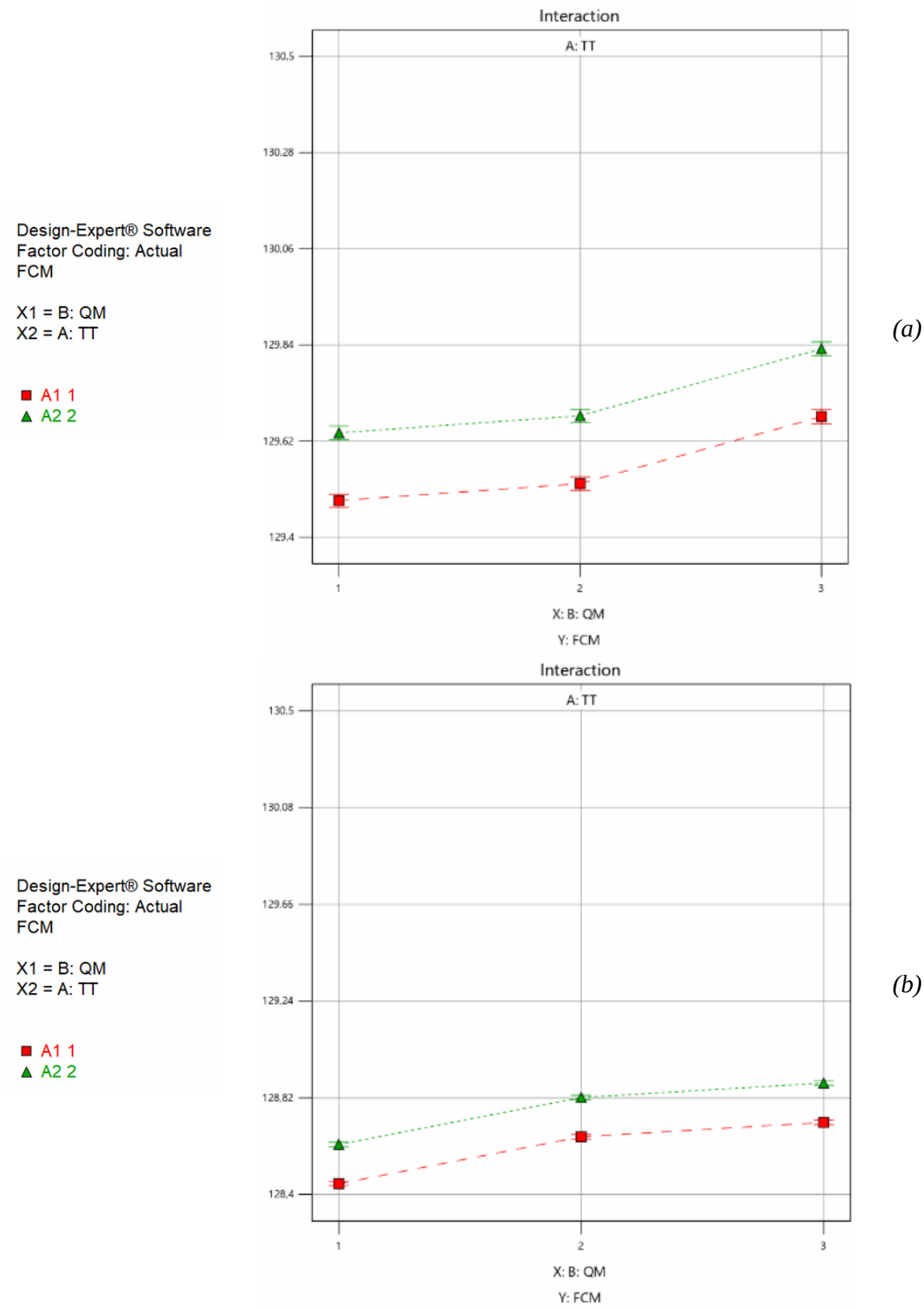

Figure 72: Comparison of cell voltage variation with respect to airflow rate (QM) and cooling temperature (TT) in the first (a) and second (b) 20 kW test.

30 kW tests

From the interaction graph in Figure 73 *(a)*, it is possible to see that for a medium and high

Levels of QM there are no differences from a statistical point of view between a more or less high TT value; in fact, the green and red LSD bands overlap. However, for a low Level of QM, the LSD bands do not overlap and therefore there are differences from a statistical point of view.

Considering only the red line or the green line, it can be seen that for the red line the bars do not overlap in low and high Levels of *QM*. For the green line, it can be seen that the bars overlap between the low and medium Levels of *QM* but not with the high Level.

In addition, a significant increase in the FC stack voltage – the output variable – can be appreciated in the transition from Level 1 to Level 3 relating to the airflow.

From the interaction graph in Figure 73 *(b)*, it is possible to see that for a low and medium Levels of *QM* there are no differences from a statistical point of view between the two Levels of *TT*, while for a high Level of *QM* the LSD bands do not overlap. Considering only the red line or the green line, it can be seen that the bars do not overlap between the three Levels of *QM*. Only for the green line, it is possible to appreciate an increase in the objective function, while for the red line there is an increase from the low to the medium value of *QM*, but at the high value of the *QM*, the objective function decreases.

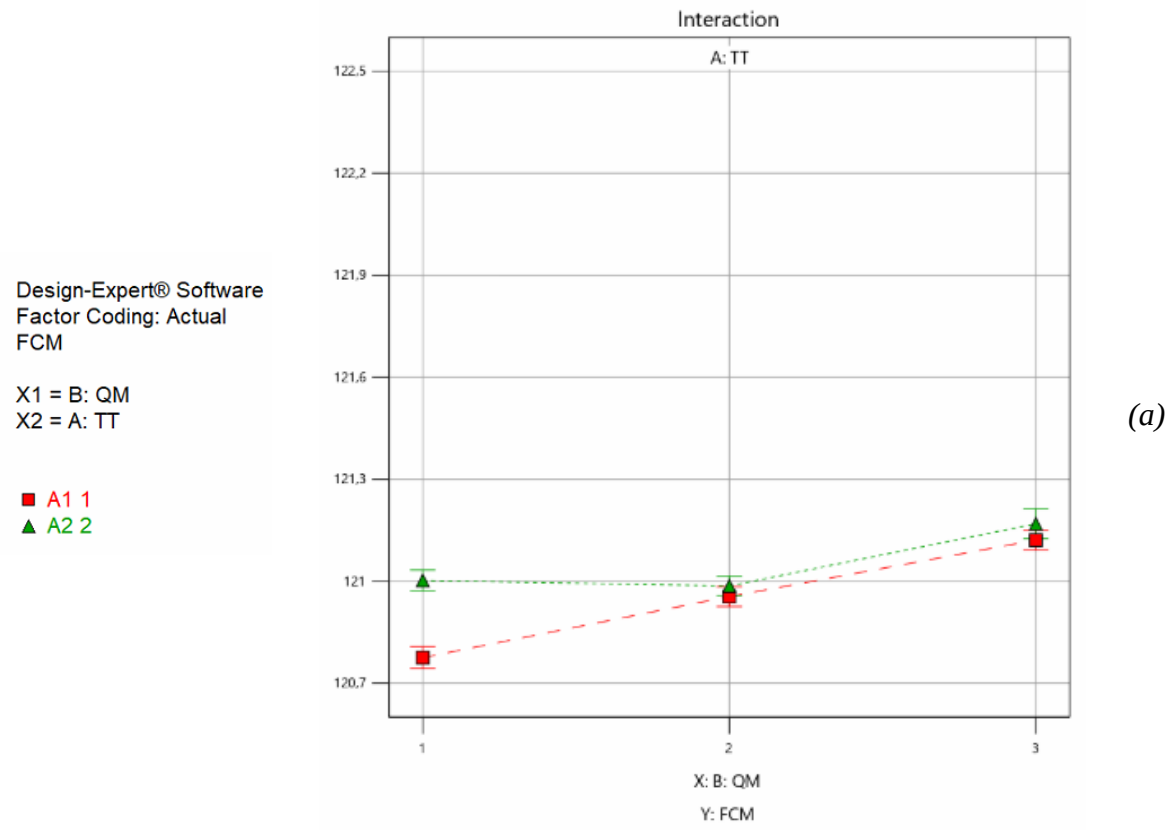

(a)

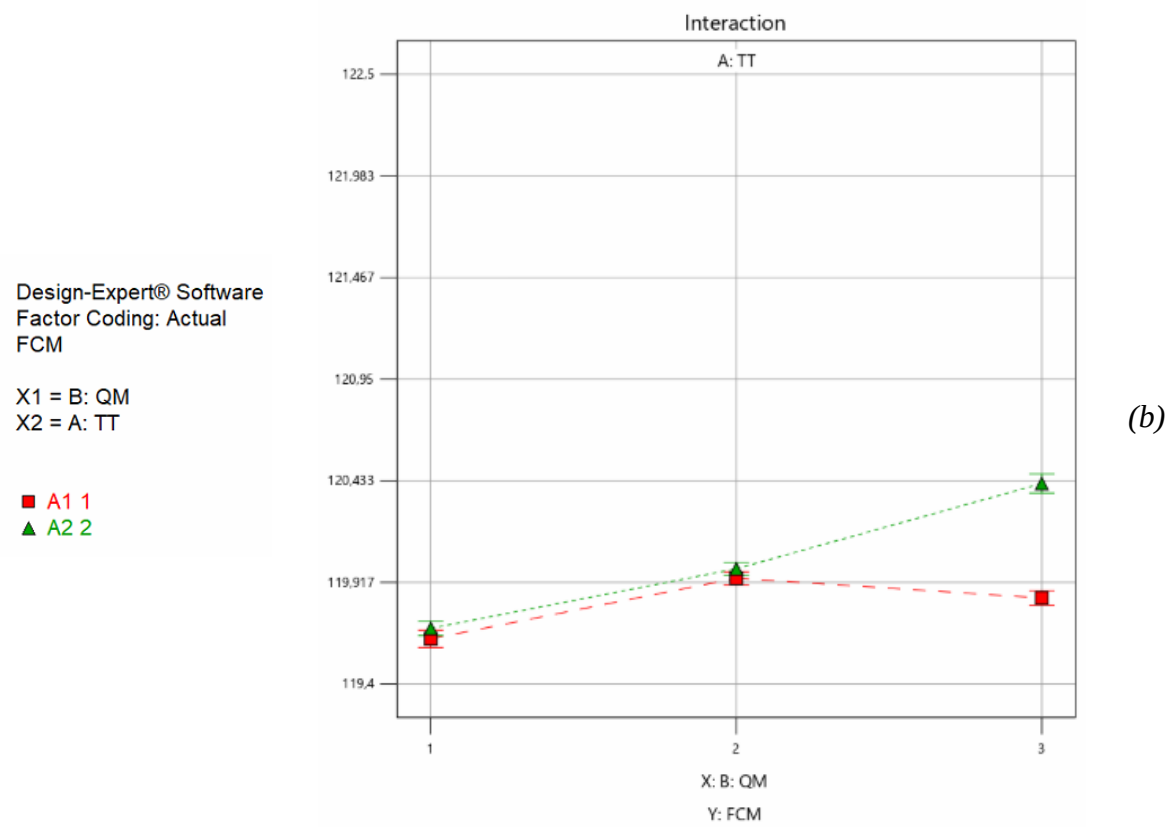

(b)

Figure 73: Comparison of cell voltage variation with respect to airflow rate (QM) and cooling temperature (TT) in the first (a) and second (b) 30 kW test.

Since the voltage variations passing between intervals is more appreciable based on the airflow rate correlation, which is the input data that varies the most, Table 28 shows the voltage increase measured in each test as a percentage. A total of 18 values are reported, two for each test, calculated via Equation 44:

$$\%V_{increased} = \frac{V_{fin} - V_{in}}{V_{in}} * 100 \qquad \textit{Equation 44}$$

V_{fin} and V_{in} are the voltage values, respectively on the final and initial interval. Therefore, for each test, there will be two values, one on the percentage increase between the first and second interval of the airflow, and the other between the second and third interval. The voltage value chosen is the average between the voltage over the first and second temperature range.

Table 28: Increase in the percentage value of cell voltage for each step in the airflow rate.

Stack power output	**Test number**	**$\%V_{increased}$ related to the first *QM* step**	**$\%V_{increased}$ related to the second QM step**
10kW	1	1,66%	0,80%
10kW	2	1,62%	0,75%
10kW	3	1,70%	0,53%
20kW	1	1,30%	0,42%

20kW	2	1,10%	0,57%
20kW	3	1,10%	0,62
30kW	1	0,58%	0,35%
30kW	2	0,44%	0,56%
30kW	3	0,39%	0,67%

Summarizing the results, among the parameters presented there is a very significant statistical variability in the airflow, while the temperature presents statistical equality; therefore, taking a single input factor, the term that causes the FC stack voltage to vary more is the airflow rate, with a proportional increase, with a variable slope based on the load and the number of tests. In fact, although at 10 kW and 20 kW the first *QM* variation from Level 1 to Level 2 always provides a greater voltage increase ($\%V_{increased}$) compared to the variation from Level 2 to Level 3, for the tests at 30 kW, especially in the last one, there is a greater voltage increase in the variation from *QM* Level 2 to Level 3 than from Level 1 to Level 2, underlining an opposite behavior. Thus, not only the airflow rate determines the variation of the stack voltage, but also the level of load and the time the system is active are other relevant factors. The temperature, on the other hand, considering only two Levels, does not significantly influence the voltage variation. This result must be deepened in future studies since the temperature range chosen is lower than the airflow rate variation range, and results could be affected by this assumption.

6. General conclusions and future developments

In the present Thesis, Polymer Electrolyte Membrane Fuel Cells have been thoroughly studied to understand the State of Art and assess their application fields, especially for maritime applications. The output of the analysis is comprehensive of several findings:

- Establishment of a PEM fuel cell degradation method that allows for the calculation of a so-called Reduction Effect based on different experimental results (from literature or own experiments).
- Development of a PEMFC stack recovery procedure with a focus on careful re-humidification of the membranes.
- Re-design of key subsystems (cooling, air supply) in a PEMFC-system consisting of 8 stacks (parallel operation of two branches) supplied with one single large air compressor (cathode side) and a common hydrogen gas feed (anode side).
- Testing and demonstration of PEMFC system performance under static, dynamic, and typical maritime load profiles.
- Proposal for a statistical method (Response Surface methodology) that can be used to determine the performance of PEMFC stacks concerning key operating parameters (e.g., temperature and humidity).

The next Sections will summarize these findings in a more detailed description.

6.1. PEMFC degradation

The interest in PEMFC technology is rising due to its characteristics such as high power density, zero noise and vibration during operation, good efficiency, and the potential to be completely zero-emission devices if the hydrogen employed is produced by an electrolysis process fed by RES. For this reason, PEM fuel cells are now being employed in different applications, ranging from stationary to transport applications, including the maritime field. However, cost and useful lifetime are still significant bottlenecks to the spread of the technology.

In this context, degradation processes should be fully understood, in order to prevent them by choosing the most suitable operative conditions and prolonging their lifetime. To this aim, in the present Thesis, the main degradation mechanisms and their effects have been investigated via a thorough literature review, and the results are shown in Chapter 3. The main degradation processes individuated are mechanical and chemical ones. They can be verified on all the components of a PEMFC stack; nevertheless, the most sensitive ones resulted to be the polymer membrane and the catalyst, which are as well among the largest cost components of the FC.

As regards the membrane, it can be chemically degraded by the presence of ionic components, that bond with the open sulphonic chains which should be instead responsible for the transport of hydrogen protons from the anode to the cathode. Ionic components can enter the cathodic circuit and reach the membrane, and for this reason, the reactant at the cathode should not contain them. Besides, some free radicals are produced during normal operation. However, their presence can be enhanced by wrong thermal-humidity management, which results to be frequent during variable load operation as well as responsible for further mechanical degradation. This underlines the importance of implementing a correct control strategy on the cooling circuit, to avoid the membrane's swelling and shrinking depending on the water content. In case the latter is not accomplished, flooding or drying issues can be verified as well on the membrane: therefore, proton exchange is not efficient in parts of the cell's electrochemically active area, causing an overload on the remaining part that has to compensate to maintain the required reaction rate. Here, a temperature increase can be reached, leading to membrane thinning, pinholes development, and finally membrane failure.

The Catalyst Layer consists of small platinum-based material particles spread on the membrane, where Triple-Phase Boundaries can be individuated. Here, both at the anode and cathode, reactants are ionized allowing the reactions that eventually make the current flow on an external circuit to produce power. Since platinum is highly reactive, its main degradation mode is by chemical attacks: contaminants may reach it through the reactants' flows, even though some restrictions are established especially for what concerns the hydrogen gas. When the reaction between the CL and the contaminants is verified, it can be partially reversible, however, losses are strongly increased, resulting in a voltage degradation that may lead to failure of the operation. From the mechanical degradation point of view, the presence of water can cause Pt particles migration, sintering, and aggregation. These phenomena cause an irreversible reduction of the electrochemically active area and, therefore, a voltage decrease. Since the amount of liquid water depends on the thermal-humidity management, it once again highlighted the cruciality of a good cooling control strategy, especially during the transient load operation. The latter results in any case the most detrimental working regime for PEMFC and thus highly investigated in the latest research works found in the literature. Several simulation models in fact try to predict the voltage decrease due to the requested load and its variations during the time.

A few research papers available in the literature deal with degradation due to contamination issues, reporting results of Accelerated and Long Lasting Stress Tests. In detail, the objective of the analyses is to quantify the consequent voltage degradation and build models to predict it.

In the present Thesis, the results of the stress test have been collected and evaluated considering contaminant type and concentration, exposure time, and current density during the experiments. Finally, it has been possible to determine the Reduction Effect based on experimental results: RE can help to predict the effect of exposure to contaminants on voltage decay and thus foresee the possible PEMFC lifetime if the environment where it is operating contains poisoning compounds (i.e., traffic urban areas, engine rooms, etc.), also considering their concentration.

6.2. Experimental activities

The University of Genova hosts the HI-SEA system, a joint Laboratory with Fincantieri. The system is made up of eight PEMFC stacks sized 30 kW each, for a total power installation of 240 kW, and it is provided with Balance of Plant components. This allows the Research group to carry on a challenging and deep investigation of a PEMFC system sized as real applications, with interacting auxiliaries and fully dedicated to the assessment of the technology for the maritime field. Since the system was earlier part of a previous project, a commissioning stage was necessary to understand its state of health. First, it was verified that a damage to some cells of FCM02 had no severe consequences on the global performance of the same stack as well as on the system. In fact, the damage that occurred during the previous project was due to an inappropriate control strategy, where parameters such as the inlet air mass flow rate were not acquired when the FC modules were shut down. Moreover, the cooling fluid conductivity was not measured, which led to additional issues. The problematics have been solved, and by removing the damaged cells and reassembling FCM02 it was possible to employ it again. Therefore, as the PEM fuel cells had remained inactive for some years before being installed in the HI-SEA laboratory, a dedicated recovery procedure was developed and tested on the stacks. In fact, inactivity leads to membrane hydration issues, that can eventually be solved by applying the dedicated procedure. The procedure is therefore focused on the re-establishment of the proper humidity on the membranes, by a variation of the cooling temperature setpoint ad partial load operation.

Once the PEMFC were recovered, a first test campaign has been developed. The latter aimed to understand the suitability of the chosen components and their interaction, and it led to some changes in the BoP. The cooling circuit has been improved by inserting three-way valves on each branch of the system, controlled by a dedicated PID; the cathodic circuit has instead been improved by inserting a pressure reductor before each FCM's mass flow controller, allowing it to operate in the correct pressure range thus reducing instabilities. A ball valve has been inserted

as well in the system, after each cathodic outlet, to create backpressure. The lessons learned from the test campaign can be summarized as follows:

- The cooling circuit must be automatically controlled, in order to keep its temperature close to setpoint values – determined by the current that crosses a stack – and as constant as possible during the constant load operation.
- It is possible to operate the system with just one industrial compressor, which is useful in the optic of installing an FC system onboard a ship. Pressure regulators, though, are necessary to stabilize the pressure before the air MFCs that must send a precise flow rate to the stacks to allow the operation.
- The presence of backpressure to increase pressure at the cathode outlet brings benefits in terms of voltage, which is enhanced and more stable.

Benefits from the BoP adjustments have been proven experimentally and through a stack voltage model developed on Matlab-Simulink. The model calculates the characteristic curves of the FCMs from experimental and theoretical data; its results can be compared with the V-I curves provided by Nuvera Fuel Cell and the results of the V-I curves obtained with the experimental campaign. This comparison – implemented before and after changing the BoP – has verified that the global performance of the FCMs has been improved. Thanks to the adjustments, it was finally possible to fully operate the whole system with a good performance, and thus a second experimental campaign started.

The campaign aimed to demonstrate that a modular, real scale FC system designed in mixed parallel-series configuration, with BoP components that simulate its installation on the ship environment, is able to operate under typical maritime load conditions: it must be considered that the system represents a real power module for maritime application, that can give useful information related to the system performance but that has lower flexibility compared to smaller experimental test rigs. The experimental test results obtained demonstrated that the FCS can positively respond to static, dynamic, and typical maritime operative load profiles. It was also assessed the ability of the system to work simultaneously with two parallel branches. Furthermore, important advice and criteria for the design, construction, and control of similar FC complete systems can be drawn from this analysis. This is particularly relevant considering that the interest in FC application for the maritime field is growing significantly, while experimental studies on complete PEMFC systems are very limited. Nevertheless, the BoP has a very strong influence on the FCM performance, as the tests demonstrated that a not correct design in electrical or fluid architecture can cause significant instabilities. There are many lesson-learned from the experimental campaign:

- The control and setting of the cooling circuit, crucial for the stability and life of an FCS to keep a correct humidity level in the polymer membranes, have been investigated via the Static load tests. It has been verified that, in the design of the control system, it must be considered that an increase in the airflow rate – necessary due to the aging of the cells – can also increase the water removal by drag forces; hence, it must be followed by a re-adaptation of the temperature in the system.
- In the Dynamic load tests, air flowrate variation is the limiting factor to the dynamic performance of the HI-SEA system, which employs a single industrial compressor to provide the air flowrate to the eight FCM. A single industrial compressor can therefore deal with the system's requirements for a static load operation, but it may be too slow in adapting to a new set point in dynamic load operation. Some extra BoP components can therefore be useful, such as the MFC devices installed for each FC stack and the pressure regulators that allow the MFCs to work in their optimal pressure range. Nevertheless, the dynamic operation must be adequate to the system's limitations, unless a dedicated control strategy (i.e., increasing the airflow rate with a small advance to the requirement of a load step) is implemented to avoid low cell voltage values.
- This type of test opened the path to the next one, the Operative profile test. Employing the maximum current ramps allowed by the system, the operative profile has been defined and implemented: the FC system is verified to be able of providing a correct load following, with successful control of the cooling circuit, of the anodic and cathodic delivery loops.
- The Electric Power Conversion is a key element for FCS control. Parallel operation of branches in the HI-SEA system is possible, both including and excluding DC/DC converters. To have a constant output voltage from the FCS, a DC/DC for each branch is needed. This operation mode has been successfully implemented in the HI-SEA system. An important conclusion is that when load-following voltage control is implemented, every converter must communicate with the others through a PMS to avoid problems of current conduction, which can otherwise lead to sudden load changes and damage to the FC stacks.
- The presented analysis demonstrates that different design and control strategies can be implemented in an FCS and that they are dependent on the FC specifications as well as on the BoP specifications.

6.3.FC voltage model via DoE

Since some instabilities in the HI-SEA system cannot be avoided and can cause excessive stress to the FC in the long term, it was chosen to investigate them more in detail. The HI-SEA FCS's BoP is in fact made up of components that represent the naval environment; however, they can create instabilities in the system which influence the FC performance and in particular the voltage. Design of Experiment has been applied to the experimental data acquired: the DoE is a statistical approach to the optimization of reactions and processes that allows varying several factors simultaneously to sift the reaction space to identify the optimal values. An important evolution of DoE is the so-called Response Surface Methodology, which aims to define the optimal design (the grid of candidate points in the experimental region) to build regression models for the objective function.

Constant load tests were developed on the FCS and analyzed via DoE, to verify the influence of current and cooling temperature oscillations, classified as the independent variables, on the objective function – the total stack voltage. The results, reported in the present Thesis for the representative case study of FCM07 for a power output of 20 kW, have been obtained through the software Design Expert (Version 12.0, Stat-Ease, USA). DE software provides test matrices for screening up to 50 factors at a time. The statistical significance of these factors is established with variance analysis and graphing tools that help identify the impact of each factor on desired outcomes, revealing anomalies in the data if any. The software allowed to draw the survey domain, the Response Surface, and the confidence intervals of the stack voltage for the case study. This means that for any operating condition, considering the instabilities in the cooling temperature value, the range of stack voltage is foreseen. If the range is not maintained, there may be anomalies in the FCS operation to be solved.

The second part of the DoE study was not only considering temperature but also air mass flowrate's instabilities and their interaction effect on the objective function – the total FCM voltage. Constant load tests were implemented on the FCS (10, 20, and 30kW per stack), and repeated three times each. Temperature values have been divided into two categories, while air flowrate values into three. Among the parameters presented, it was proven a very significant statistical variability of the airflow, while the temperature is close to or presents statistical equality; therefore, taking a single input factor, it was verified that the term that causes the cell voltage to vary more is the airflow rate, in a proportional increase, with a variable slope based on the load and the number of tests. In fact, although at 10kW and 20kW the first range jump provides a greater voltage increase compared to the second, for the test at 30kW there is a

greater voltage increase in the second range jump than in the first, therefore an opposite behavior. So it has been proven that not only the air flow rate determines the variation of voltage, but also the type of load and the time the system is active is other relevant factor. The temperature, on the other hand, considering only two intervals, does not greatly influence the cell voltage variation, probably also since the temperature range is sometimes tens of orders lower than the flow rate range. The results of the statistical analysis developed via DE can become the reference for the creation of a precise performance monitoring system for the PEMFC installation: if the stack voltage lays out of the confidence intervals, anomalies can be rapidly detected, significantly reducing the operation in stressing conditions that can affect the state of health of the PEMFCs. Besides, thanks to the second part of the analysis, the correct setpoint values of cooling temperature and airflow rate can be defined, to obtain the best performance by the HI-SEA system during operation.

6.4. Recommendations for future work

The present Thesis can be the starting point for different activities.

As regards the degradation topic, the research could be extended to include more contaminants and more experimental results available in the literature. This will allow to define more precise equations and to predict the average voltage decay as well as the FC useful life depending on the environmental conditions/the gas quality. Besides, the investigation could go further to include the effects of liquid water presence, which affects the state of health of both the membrane and the catalyst layer.

The experimental activities gave interesting results, positively assessing the potential of the PEMFC system for maritime applications. The research can be expanded towards the implementation and validation of simulation models that consider the FC system as a whole. New tests can investigate in detail the influence of the DC/DC converters as well as the hybridization of the system: in fact, an AC/DC is already installed in the Laboratory, and it could be exploited for the simulation of a battery pack. This can allow experiments concerning different energy and power management systems and control strategies. Finally, the installation of a dedicated system could lead to contamination tests, to directly prove the effectiveness of the equations defined in this Thesis regarding the prediction of voltage decay.

The statistical approach resulted useful from two points of view: the first one concerns the setup of a monitoring system dedicated to the FC system under investigation. In fact, thanks to the Design of Experiment it is possible to define confidence intervals and foresee the correct values for input parameters considering the actual state of health of the system. This monitoring system

is to be developed in future work. The second source of interest for the statistical approach lies in the opportunity to optimize the setpoints of input parameters. In fact, these variables should be updated depending on the aging of the FC system, and the Design of Experiment can give useful information based on the real data collected during the experimental activity. Thus, the performance of the system can be enhanced. The analysis should therefore be repeated to include more variables (i.e., anodic mass flow and pressure, cathodic pressure and temperature, purging synchronization).

7. Bibliography

[1] IEA. Technology Roadmap. SpringerReference 2015:81. https://doi.org/10.1007/SpringerReference_7300.

[2] Olabi AG, Wilberforce T, Abdelkareem MA. Fuel cell application in the automotive industry and future perspective. Energy 2021;214:118955. https://doi.org/10.1016/j.energy.2020.118955.

[3] Panwar NL, Kaushik SC, Kothari S. Role of renewable energy sources in environmental protection: A review. Renew Sustain Energy Rev 2011;15:1513–24. https://doi.org/10.1016/j.rser.2010.11.037.

[4] Evans A, Strezov V, Evans TJ. Assessment of utility energy storage options for increased renewable energy penetration. Renew Sustain Energy Rev 2012;16:4141–7. https://doi.org/10.1016/j.rser.2012.03.048.

[5] UNFCCC. Paris Agreement. 2015.

[6] International Maritime Organization (IMO) official website n.d. https://www.imo.org/en/MediaCentre/HotTopics/Pages/Reducing-greenhouse-gas-emissions-from-ships.aspx (accessed September 8, 2021).

[7] Rutherford D, Comer B. The International Maritime Organization'S Initial Greenhouse Gas Strategy 2018. https://www.theicct.org.

[8] ABS. Setting the course to Low Carbon Shipping - 2030 Outlook/2050 Vision 2019:72.

[9] Winnes H, Styhre L, Fridell E. Reducing GHG emissions from ships in port areas. Res Transp Bus Manag 2015;17:73–82. https://doi.org/10.1016/j.rtbm.2015.10.008.

[10] UNFCCC. The Paris Agreement 2015:26. www.unfccc.int.

[11] IMO. Third Greenhouse Gas Study. 2015.

[12] Tronstad T, Astrand H, Haugom G, Langfeldt L. Study on the use of fuel cells in shipping. Study commissioned by European Maritime Safety Agency (EMSA) 2017. www.emsa.europa.eu.

[13] Wang H, Zhou P, Wang Z. Reviews on current carbon emission reduction technologies and projects and their feasibilities on ships. J Mar Sci Appl 2017;16:129–36. https://doi.org/10.1007/s11804-017-1413-y.

[14] Brynolf S, Magnusson M, Fridell E, Andersson K. Compliance possibilities for the future ECA regulations through the use of abatement technologies or change of fuels. Transp Res Part D Transp Environ 2014;28:6–18. https://doi.org/10.1016/j.trd.2013.12.001.

[15] Brynolf S, Magnusson M, Fridell E, Andersson K. Compliance possibilities for the future ECA regulations through the use of abatement technologies or change of fuels. Transp Res Part D Transp Environ 2013;28. https://doi.org/10.1016/j.trd.2013.12.001.

[16] Elam CC, Padró CEG, Sandrock G, Luzzi A, Lindblad P, Hagen EF. Realizing the hydrogen future: The International Energy Agency's efforts to advance hydrogen energy technologies. Int J Hydrogen Energy 2003;28:601–7. https://doi.org/10.1016/S0360-3199(02)00147-7.

[17] Orecchini F. The era of energy vectors. Int J Hydrogen Energy 2006;31:1951–4. https://doi.org/10.1016/j.ijhydene.2006.01.015.

[18] Kołwzan K, Narewski M. Alternative Fuels for Marine Applications. Latv J Chem 2013;51:398–406. https://doi.org/10.2478/v10161-012-0024-9.

[19] Veldhuis IJS, Richardson RN, Stone HBJ. Hydrogen fuel in a marine environment. Int J Hydrogen Energy 2007;32:2553–66. https://doi.org/10.1016/j.ijhydene.2006.11.013.

[20] Carter D, Ryan M, Wing J. The Fuel Cell Industry Review 2012. 2012. https://doi.org/10.1595/147106712x657535.

[21] DOE, U.S. Department of Energy. 2011 Fuel Cell Technologies Market Report. 2012.

[22] Ahmadi P, Torabi SH, Afsaneh H, Sadegheih Y, Ganjehsarabi H, Ashjaee M. The effects of driving patterns and PEM fuel cell degradation on the lifecycle assessment of hydrogen fuel cell vehicles. Int J Hydrogen Energy 2020;45:3595–608. https://doi.org/10.1016/j.ijhydene.2019.01.165.
[23] Inal OB, Deniz C. Assessment of fuel cell types for ships: Based on multi-criteria decision analysis. J Clean Prod 2020;265:121734. https://doi.org/10.1016/j.jclepro.2020.121734.
[24] Bicer Y, Dincer I, Zam C, Vezina G, Raso F. Comparative life cycle assessment of various ammonia production methods 2016;135. https://doi.org/10.1016/j.jclepro.2016.07.023.
[25] Whiston MM, Azevedo IL, Litster S, Whitefoot KS, Samaras C, Whitacre JF. Expert assessments of the cost and expected future performance of proton exchange membrane fuel cells for vehicles. Proc Natl Acad Sci U S A 2019;116:4899–904. https://doi.org/10.1073/pnas.1804221116.
[26] Dincer I. Green methods for hydrogen production. Int J Hydrogen Energy 2012;37:1954–71. https://doi.org/10.1016/j.ijhydene.2011.03.173.
[27] Safari F, Dincer I. Assessment and optimization of an integrated wind power system for hydrogen and methane production. Energy Convers Manag 2018;177:693–703. https://doi.org/10.1016/j.enconman.2018.09.071.
[28] Ahmadi P, Dincer I, Rosen MA. Energy and exergy analyses of hydrogen production via solar-boosted ocean thermal energy conversion and PEM electrolysis. Int J Hydrogen Energy 2013;38:1795–805. https://doi.org/10.1016/j.ijhydene.2012.11.025.
[29] Safari F, Javani N, Yumurtaci Z. Hydrogen production via supercritical water gasification of almond shell over algal and agricultural hydrochars as catalysts. Int J Hydrogen Energy 2018;43:1071–80. https://doi.org/10.1016/j.ijhydene.2017.05.102.
[30] Bartolozzi I, Rizzi F, Frey M. Comparison between hydrogen and electric vehicles by life cycle assessment: A case study in Tuscany, Italy. Appl Energy 2013;101:103–11. https://doi.org/10.1016/j.apenergy.2012.03.021.
[31] Hwang JJ, Kuo JK, Wu W, Chang WR, Lin CH, Wang SE. Lifecycle performance assessment of fuel cell/battery electric vehicles. Int J Hydrogen Energy 2013;38:3433–46. https://doi.org/10.1016/j.ijhydene.2012.12.148.
[32] Ahmadi P, Kjeang E. Comparative life cycle assessment of hydrogen fuel cell passenger vehicles in different Canadian provinces. Int J Hydrogen Energy 2015;40:12905–17. https://doi.org/10.1016/j.ijhydene.2015.07.147.
[33] Hwang JJ, Chen YJ, Kuo JK. The study on the power management system in a fuel cell hybrid vehicle. Int J Hydrogen Energy 2012;37:4476–89. https://doi.org/10.1016/j.ijhydene.2011.11.127.
[34] Evangelisti S, Tagliaferri C, Brett DJL, Lettieri P. Life cycle assessment of a polymer electrolyte membrane fuel cell system for passenger vehicles. J Clean Prod 2017;142:4339–55. https://doi.org/10.1016/j.jclepro.2016.11.159.
[35] Granovskii M, Dincer I, Rosen MA. Life cycle assessment of hydrogen fuel cell and gasoline vehicles. Int J Hydrogen Energy 2006;31:337–52. https://doi.org/10.1016/j.ijhydene.2005.10.004.
[36] Idrogeno: accumulo e trasporto n.d. http://www.eniscuola.net/argomento/idrogeno/. (accessed January 18, 2022).
[37] Park YD, Olson DL, Landau A, Pinkas M. Assessment of hydrogen-induced precipitation in a nickel-copper alloy using thermoelectric power. Corrosion 2006;62:395–402. https://doi.org/10.5006/1.3278277.
[38] Cavo M, Gadducci E, Rattazzi D, Rivarolo M, Magistri L. Dynamic analysis of PEM fuel cells and metal hydrides on a zero-emission ship : A model-based approach Number

of Transfer Unit. Int J Hydrogen Energy 2021. https://doi.org/10.1016/j.ijhydene.2021.07.104.
[39] Cavo M, Gadducci E, Rivarolo M, Magistri L, Dellacasa A, Romanello M, et al. Thermal integration of PEM Fuel Cells and metal hydrides storage system for Zero Emission Ultimate Ship (ZEUS). E3S Web Conf 2022;334:04004. https://doi.org/10.1051/e3sconf/202233404004.
[40] Tronstad T, Langfeldt L. Study on the use of fuel cells in shipping. 2017.
[41] Choi CH, Yu S, Han IS, Kho BK, Kang DG, Lee HY, et al. Development and demonstration of PEM fuel-cell-battery hybrid system for propulsion of tourist boat. Int J Hydrogen Energy 2016;41:3591–9. https://doi.org/10.1016/j.ijhydene.2015.12.186.
[42] Bicer Y, Dincer I. Clean fuel options with hydrogen for sea transportation: A life cycle approach. Int J Hydrogen Energy 2018;43:1179–93. https://doi.org/10.1016/j.ijhydene.2017.10.157.
[43] Gadducci E, Lamberti T, Bellotti D, Magistri L, Massardo AF. BoP incidence on a 240 kW PEMFC system in a ship-like environment, employing a dedicated fuel cell stack model. Int J Hydrogen Energy 2021;46:24305–17. https://doi.org/10.1016/j.ijhydene.2021.04.192.
[44] Borgogna G, Speranza E, Lamberti T, Nicola Traverso A, Magistri L, Gadducci E, et al. Design and development of a laboratory for the study of PEMFC system for marine applications. E3S Web Conf 2019;113:1–8. https://doi.org/10.1051/e3sconf/201911302020.
[45] Gadducci E, Lamberti T, Magistri L, Massardo AF. Experimental assessment of FCS for marine application. In: Cigolotti V, editor. Proc. EFC2019, Naples: 2020, p. 235–6.
[46] Boudghene Stambouli A, Traversa E. Fuel cells, an alternative to standard sources of energy. Renew Sustain Energy Rev 2002;6:295–304. https://doi.org/10.1016/S1364-0321(01)00015-6.
[47] van Biert L, Godjevac M, Visser K, Aravind P V. A review of fuel cell systems for maritime applications. J Power Sources 2016;327:345–64. https://doi.org/10.1016/j.jpowsour.2016.07.007.
[48] Sharaf OZ, Orhan MF. An overview of fuel cell technology: Fundamentals and applications. Renew Sustain Energy Rev 2014;32:810–53. https://doi.org/10.1016/j.rser.2014.01.012.
[49] De-Troya JJ, Álvarez C, Fernández-Garrido C, Carral L. Analysing the possibilities of using fuel cells in ships. Int J Hydrogen Energy 2016;41:2853–66. https://doi.org/10.1016/J.IJHYDENE.2015.11.145.
[50] Proton Motor n.d. https://www.proton-motor.de/gb/zero-emission-solution/hyrange/.
[51] Ballard n.d. http://ballard.com/fuel-cell-solutions/fuel-cell-power-products/motive-modules.
[52] PowerCell n.d.
[53] Cummins n.d.
[54] Rivarolo M, Rattazzi D, Lamberti T, Magistri L. Clean energy production by PEM fuel cells on tourist ships: A time-dependent analysis. Int J Hydrogen Energy 2020;45:25747–57. https://doi.org/10.1016/j.ijhydene.2019.12.086.
[55] Rivarolo M, Rattazzi D, Magistri L. Best operative strategy for energy management of a cruise ship employing different distributed generation technologies. Int J Hydrogen Energy 2018;43:23500–10. https://doi.org/10.1016/j.ijhydene.2018.10.217.
[56] Madsen RT, Klebanoff LE, Caughlan SAM, Pratt JW, Leach TS, Appelgate TB, et al. Feasibility of the Zero-V: A zero-emissions hydrogen fuel-cell coastal research vessel. Int J Hydrogen Energy 2020;45:25328–43. https://doi.org/10.1016/J.IJHYDENE.2020.06.019.

[57] Nazir H, Muthuswamy N, Louis C, Jose S, Prakash J, Buan MEM, et al. Is the H2 economy realizable in the foreseeable future? Part III: H2 usage technologies, applications, and challenges and opportunities. Int J Hydrogen Energy 2020;45:28217–39. https://doi.org/10.1016/j.ijhydene.2020.07.256.
[58] Li X, Han K, Song Y. Dynamic behaviors of PEM fuel cells under load changes. Int J Hydrogen Energy 2020;45:20312–20. https://doi.org/10.1016/j.ijhydene.2019.12.034.
[59] Wu P, Bucknall R. Hybrid fuel cell and battery propulsion system modelling and multi-objective optimisation for a coastal ferry. Int J Hydrogen Energy 2020;45:3193–208. https://doi.org/10.1016/J.IJHYDENE.2019.11.152.
[60] Bassam AM, Phillips AB, Turnock SR, Wilson PA. Development of a multi-scheme energy management strategy for a hybrid fuel cell driven passenger ship. Int J Hydrogen Energy 2017;42:623–35. https://doi.org/10.1016/J.IJHYDENE.2016.08.209.
[61] Pesce M, Terzi S, Al-Jawasreh RIM, Bommarito C, Calgaro L, Fogarin S, et al. Selecting sustainable alternatives for cruise ships in Venice using multi-criteria decision analysis. Sci Total Environ 2018;642:668–78. https://doi.org/10.1016/J.SCITOTENV.2018.05.372.
[62] Rivarolo M, Rattazzi D, Magistri L, Massardo AF. Multi-criteria comparison of power generation and fuel storage solutions for maritime application. Energy Convers Manag 2021;244:114506. https://doi.org/10.1016/j.enconman.2021.114506.
[63] Shih NC, Weng BJ, Lee JY, Hsiao YC. Development of a 20 kW generic hybrid fuel cell power system for small ships and underwater vehicles. Int. J. Hydrogen Energy, vol. 39, Pergamon; 2014, p. 13894–901. https://doi.org/10.1016/j.ijhydene.2014.01.113.
[64] Psoma A, Sattler G. Fuel cell systems for submarines: From the first idea to serial production. J Power Sources 2002;106:381–3. https://doi.org/10.1016/S0378-7753(01)01044-8.
[65] Han J, Han J, Ji H, Yu S. "Model-based" design of thermal management system of a fuel cell "air-independent" propulsion system for underwater shipboard. Int J Hydrogen Energy 2020;45:32449–63. https://doi.org/10.1016/j.ijhydene.2020.08.233.
[66] Pfeifer A, Prebeg P, Duić N. Challenges and opportunities of zero emission shipping in smart islands: A study of zero emission ferry lines. ETransportation 2020;3:100048. https://doi.org/10.1016/j.etran.2020.100048.
[67] Fincantieri. Fincantieri: Dry dock works start for experimental vessel ZEUS 2020. www.fincantieri.com (accessed January 12, 2021).
[68] IEC 62282-3-200:2015 | IEC Webstore | battery, energy efficiency, energy storage 2015. https://webstore.iec.ch/publication/23736 (accessed January 21, 2022).
[69] Han J, Han J, Yu S. Experimental analysis of performance degradation of 3-cell PEMFC stack under dynamic load cycle. Int J Hydrogen Energy 2020;45:13045–54. https://doi.org/10.1016/j.ijhydene.2020.02.215.
[70] Chugh S, Chaudhari C, Sonkar K, Sharma A, Kapur GS, Ramakumar SSV. Experimental and modelling studies of low temperature PEMFC performance. Int J Hydrogen Energy 2020;45:8866–74. https://doi.org/10.1016/j.ijhydene.2020.01.019.
[71] Yin L, Li Q, Chen W, Wang T, Liu H. Experimental analysis of optimal performance for a 5 kW PEMFC system. Int J Hydrogen Energy 2019;44:5499–506. https://doi.org/10.1016/j.ijhydene.2018.08.157.
[72] Chen K, Hou Y, Jiang C, Pan X, Hao D. Experimental investigation on statistical characteristics of cell voltage distribution for a PEMFC stack under dynamic driving cycle. Int J Hydrogen Energy 2021. https://doi.org/10.1016/j.ijhydene.2021.09.092.
[73] Thermochemical Power Group - University of Genoa n.d. http://www.tpg.unige.it/TPG/.
[74] Scott K, Xing L. Direct Methanol Fuel Cells. Adv. Chem. Eng., vol. 41, 2012, p. 145–96. https://doi.org/10.1016/B978-0-12-386874-9.00005-1.

[75] P. Panayiotou G, A. Kalogirou S, A. Tassou S. PEM Fuel Cells for Energy Production in Solar Hydrogen Systems. Recent Patents Mech Eng 2012;3:226–35. https://doi.org/10.2174/2212797611003030226.
[76] Borah M, Dhakate S. Expanded Graphite Composite Based Bipolar Plate for PEM Fuel Cell: Development of Low Density and Low Cost Composite Bipolar Plate for Proton Exchange Membrane Fuel Cell. Lambert Acad Publ 2016.
[77] Baroutaji A, Carton JG, Sajjia M, Olabi AG. Materials in PEM Fuel Cells. Elsevier B.V.; 2015. https://doi.org/10.1016/b978-0-12-803581-8.04006-6.
[78] Ogungbemi E, Ijaodola O, Khatib FN, Wilberforce T, El Hassan Z, Thompson J, et al. Fuel cell membranes – Pros and cons. Energy 2019;172:155–72. https://doi.org/10.1016/j.energy.2019.01.034.
[79] Verma A, Pitchumani R. Influence of membrane properties on the transient behavior of polymer electrolyte fuel cells. J Power Sources 2014;268:733–43. https://doi.org/10.1016/j.jpowsour.2014.06.065.
[80] Schmittinger W, Vahidi A. A review of the main parameters influencing long-term performance and durability of PEM fuel cells. J Power Sources 2008;180:1–14. https://doi.org/10.1016/j.jpowsour.2008.01.070.
[81] Li H, Tang Y, Wang Z, Shi Z, Wu S, Song D, et al. A review of water flooding issues in the proton exchange membrane fuel cell. J Power Sources 2008;178:103–17. https://doi.org/10.1016/j.jpowsour.2007.12.068.
[82] Laribi S, Mammar K, Sahli Y, Koussa K. Analysis and diagnosis of PEM fuel cell failure modes (flooding & drying) across the physical parameters of electrochemical impedance model: Using neural networks method. Sustain Energy Technol Assessments 2019;34:35–42. https://doi.org/10.1016/j.seta.2019.04.004.
[83] Yousfi-Steiner N, Moçotéguy P, Candusso D, Hissel D, Hernandez A, Aslanides A. A review on PEM voltage degradation associated with water management: Impacts, influent factors and characterization. J Power Sources 2008;183:260–74. https://doi.org/10.1016/j.jpowsour.2008.04.037.
[84] Dafalla AM, Jiang F. Stresses and their impacts on proton exchange membrane fuel cells: A review. Int J Hydrogen Energy 2018;43:2327–48. https://doi.org/10.1016/j.ijhydene.2017.12.033.
[85] Baroutaji A, Carton JG, Sajjia M, Olabi AG. Materials in PEM Fuel Cells. Ref Modul Mater Sci Mater Eng 2016. https://doi.org/10.1016/B978-0-12-803581-8.04006-6.
[86] Shabani B, Andrews J, Watkins S. Energy and cost analysis of a solar-hydrogen combined heat and power system for remote power supply using a computer simulation. Sol Energy 2010;84:144–55. https://doi.org/10.1016/j.solener.2009.10.020.
[87] Faghri A, Guo Z. Challenges and opportunities of thermal management issues related to fuel cell technology and modeling. Int J Heat Mass Transf 2005;48:3891–920. https://doi.org/10.1016/j.ijheatmasstransfer.2005.04.014.
[88] Asghari S, Akhgar H, Imani BF. Design of thermal management subsystem for a 5 kW polymer electrolyte membrane fuel cell system. J Power Sources 2011;196:3141–8. https://doi.org/10.1016/j.jpowsour.2010.11.077.
[89] Kandlikar SG, Lu Z. Thermal management issues in a PEMFC stack - A brief review of current status. Appl Therm Eng 2009;29:1276–80. https://doi.org/10.1016/j.applthermaleng.2008.05.009.
[90] Ramousse J, Lottin O, Didierjean S, Maillet D. Heat sources in proton exchange membrane (PEM) fuel cells. J Power Sources 2009;192:435–41. https://doi.org/10.1016/j.jpowsour.2009.03.038.
[91] Lampinen MJ. Analysis of Free Energy and Entropy Changes for Half-Cell Reactions. J Electrochem Soc 1993;140:3537. https://doi.org/10.1149/1.2221123.

[92] Berning T. Three-Dimensional Computational Analysis of Transport Phenomena in a PEM Fuel Cell. University of Victoria, 2002.
[93] Ondrejička K, Ferencey V, Stromko M. Modeling of the air-cooled PEM fuel cell. IFAC-PapersOnLine 2019;52:98–105. https://doi.org/10.1016/j.ifacol.2019.12.740.
[94] Lee J, Gundu MH, Lee N, Lim K, Lee SW, Jang SS, et al. Innovative cathode flow-field design for passive air-cooled polymer electrolyte membrane (PEM) fuel cell stacks. Int J Hydrogen Energy 2020;45:11704–13. https://doi.org/10.1016/j.ijhydene.2019.07.128.
[95] Wu J, Galli S, Lagana I, Pozio A, Monteleone G, Yuan XZ, et al. An air-cooled proton exchange membrane fuel cell with combined oxidant and coolant flow. J Power Sources 2009;188:199–204. https://doi.org/10.1016/j.jpowsour.2008.11.078.
[96] Islam R, Shabani B. Prediction of electrical conductivity of TiO2 water and ethylene glycol-based nanofluids for cooling application in low temperature PEM fuel cells. Energy Procedia 2019;160:550–7. https://doi.org/10.1016/j.egypro.2019.02.205.
[97] Le Canut JM, Abouatallah RM, Harrington DA. Detection of Membrane Drying, Fuel Cell Flooding, and Anode Catalyst Poisoning on PEMFC Stacks by Electrochemical Impedance Spectroscopy. J Electrochem Soc 2006;153:A857–64. https://doi.org/10.1149/1.2179200.
[98] Saleh IMM, Ali R, Zhang H. Simplified mathematical model of proton exchange membrane fuel cell based on horizon fuel cell stack. J Mod Power Syst Clean Energy 2016;4:668–79. https://doi.org/10.1007/s40565-016-0196-5.
[99] F. Laurencelle et al. Characterization of a Ballard MK5-E Proton Exchange Membrane Fuel Cell Stack. Fuel Cells 2001;1.
[100] Mann RF, Amphlett JC, Hooper M a. I, Jensen HM, Peppley B a., Roberge PR. Development and application of a generalised steady-state electrochemical model for a PEM fuel cell. J Power Sources 2000;86:173–80. https://doi.org/10.1016/S0378-7753(99)00484-X.
[101] Kunusch C, Puleston P, Mayosky M. Sliding-Mode Control of PEM Fuel Cells. 1st ed. Springer-Verlag London; 2012. https://doi.org/10.1007/978-1-4471-2431-3.
[102] Amphlett JC. Performance Modeling of the Ballard Mark IV Solid Polymer Electrolyte Fuel Cell. J Electrochem Soc 1995;142:9. https://doi.org/10.1149/1.2043959.
[103] Ariza HE, Correcher A, Sánchez C, Pérez-Navarro Á, García E. Thermal and Electrical Parameter Identification of a Proton Exchange Membrane Fuel Cell Using Genetic Algorithm. Energies 2018, Vol 11, Page 2099 2018;11:2099. https://doi.org/10.3390/EN11082099.
[104] Benouioua D, Candusso D, Harel F, Picard P, François X. On the issue of the PEMFC operating fault identification: Generic analysis tool based on voltage pointwise singularity strengths. Int J Hydrogen Energy 2018;43:11606–13. https://doi.org/10.1016/j.ijhydene.2017.09.177.
[105] Sahlin SL, Araya SS, Andreasen SJ, Kær SK. Electrochemical Impedance Spectroscopy (EIS) Characterization of Reformate-operated High Temperature PEM Fuel Cell Stack. Int J Power Energy Res 2017;1. https://doi.org/10.22606/ijper.2017.11003.
[106] Wang H, Gaillard A, Hissel D. Online electrochemical impedance spectroscopy detection integrated with step-up converter for fuel cell electric vehicle. Int J Hydrogen Energy 2019;44:1110–21. https://doi.org/10.1016/j.ijhydene.2018.10.242.
[107] Chung CG, Kim L, Sung YW, Lee J, Chung JS. Degradation mechanism of electrocatalyst during long-term operation of PEMFC. Int J Hydrogen Energy 2009;34:8974–81. https://doi.org/10.1016/j.ijhydene.2009.08.094.
[108] Abaoud HA, Ghouse M, Lovell K V., Al-Motairy GN. A hybrid technique for fabricating PEMFC's low platinum loading electrodes. Int J Hydrogen Energy 2005;30:385–91. https://doi.org/10.1016/j.ijhydene.2004.07.003.

[109] Curtin DE, Lousenberg RD, Henry TJ, Tangeman PC, Tisack ME. Advanced materials for improved PEMFC performance and life. J Power Sources 2004;131:41–8. https://doi.org/10.1016/j.jpowsour.2004.01.023.
[110] Tailoka F, Fray DJ, Kumar R V. Application of Nafion electrolytes for the detection of humidity in a corrosive atmosphere. Solid State Ionics 2003;161:267–77. https://doi.org/10.1016/S0167-2738(03)00145-0.
[111] Smitha B, Sridhar S, Khan AA. Solid polymer electrolyte membranes for fuel cell applications - A review. J Memb Sci 2005;259:10–26. https://doi.org/10.1016/j.memsci.2005.01.035.
[112] Passalacqua E, Lufrano F, Squadrito G, Patti A, Giorgi L. Influence of the structure in low-Pt loading electrodes for polymer electrolyte fuel cells. Electrochim Acta 1998;43:3665–73. https://doi.org/10.1016/S0013-4686(98)00124-8.
[113] Chun YG, Kim CS, Peck DH, Shin DR. Performance of a polymer electrolyte membrane fuel cell with thin film catalyst electrodes. J Power Sources 1998;71:174–8. https://doi.org/10.1016/S0378-7753(97)02792-4.
[114] Wang M, Woo K Do, Lou T, Zhai Y, Kim DK. Defining catalyst layer ingredients in PEMFC by orthogonal test and C-V method. Int J Hydrogen Energy 2005;30:381–4. https://doi.org/10.1016/j.ijhydene.2004.09.018.
[115] Ambrosio EP, Francia C, Manzoli M, Penazzi N, Spinelli P. Platinum catalyst supported on mesoporous carbon for PEMFC. Int J Hydrogen Energy 2008;33:3142–5. https://doi.org/10.1016/j.ijhydene.2008.03.045.
[116] HC. Hydrogen scaling up : A sustainable pathway for the global energy transition. Hydrog Counc 2017:80.
[117] International Energy Agency. Technology Roadmap 2014. https://doi.org/10.1007/SpringerReference_7300.
[118] Zhou D, Gao F, Breaz E, Ravey A, Miraoui A. Degradation prediction of PEM fuel cell using a moving window based hybrid prognostic approach. Energy 2017;138:1175–86. https://doi.org/10.1016/j.energy.2017.07.096.
[119] Zhan Y, Guo Y, Zhu J, Li L. Natural degradation and stimulated recovery of a proton exchange membrane fuel cell. Int J Hydrogen Energy 2014;39:12849–58. https://doi.org/10.1016/j.ijhydene.2014.06.073.
[120] Wu J, Yuan XZ, Martin JJ, Wang H, Yang D, Qiao J, et al. Proton exchange membrane fuel cell degradation under close to open-circuit conditions. Part I: In situ diagnosis. J Power Sources 2010;195:1171–6. https://doi.org/10.1016/j.jpowsour.2009.08.095.
[121] Shabani B, Hafttananian M, Khamani S, Ramiar A, Ranjbar AA. Poisoning of proton exchange membrane fuel cells by contaminants and impurities: Review of mechanisms, effects, and mitigation strategies. J Power Sources 2019;427:21–48. https://doi.org/10.1016/j.jpowsour.2019.03.097.
[122] Yan WM, Chu H Sen, Liu YL, Chen F, Jang JH. Effects of chlorides on the performance of proton exchange membrane fuel cells. Int J Hydrogen Energy 2011;36:5435–41. https://doi.org/10.1016/j.ijhydene.2011.01.158.
[123] Mikkola MS, Rockward T, Uribe FA, Pivovar BS. The effect of NaCl in the cathode air stream on PEMFC performance. Fuel Cells 2007;7:153–8. https://doi.org/10.1002/fuce.200600206.
[124] Valdés-López VF, Mason T, Shearing PR, Brett DJL. Carbon monoxide poisoning and mitigation strategies for polymer electrolyte membrane fuel cells – A review. Prog Energy Combust Sci 2020;79. https://doi.org/10.1016/j.pecs.2020.100842.
[125] Wang C, Zhang J, Wang S, Hao S, Li J, Mao Z, et al. Degradation study of Membrane Electrode Assembly with PTFE/Nafion composite membrane utilizing accelerated stress technique. Int J Hydrogen Energy 2016;41:16212–9.

https://doi.org/10.1016/j.ijhydene.2016.04.215.
[126] Inaba M, Kinumoto T, Kiriake M, Umebayashi R, Tasaka A, Ogumi Z. Gas crossover and membrane degradation in polymer electrolyte fuel cells. Electrochim Acta 2006;51:5746–53. https://doi.org/10.1016/j.electacta.2006.03.008.
[127] Wong CY, Wong WY, Loh KS, Mohamad AB. Study of the plasticising effect on polymer and its development in fuel cell application. Renew Sustain Energy Rev 2017;79:794–805. https://doi.org/10.1016/j.rser.2017.05.154.
[128] Lim C, Ghassemzadeh L, Van Hove F, Lauritzen M, Kolodziej J, Wang GG, et al. Membrane degradation during combined chemical and mechanical accelerated stress testing of polymer electrolyte fuel cells. J Power Sources 2014;257:102–10. https://doi.org/10.1016/j.jpowsour.2014.01.106.
[129] Ghassemzadeh L, Holdcroft S. Quantifying the structural changes of perfluorosulfonated acid ionomer upon reaction with hydroxyl radicals. J Am Chem Soc 2013;135:8181–4. https://doi.org/10.1021/ja4037466.
[130] Ghassemzadeh L, Peckham TJ, Weissbach T, Luo X, Holdcroft S. Selective formation of hydrogen and hydroxyl radicals by electron beam irradiation and their reactivity with perfluorosulfonated acid ionomer. J Am Chem Soc 2013;135:15923–32. https://doi.org/10.1021/ja408032p.
[131] Fletcher T, Thring R, Watkinson M. An Energy Management Strategy to concurrently optimise fuel consumption & PEM fuel cell lifetime in a hybrid vehicle. Int J Hydrogen Energy 2016;41:21503–15. https://doi.org/10.1016/j.ijhydene.2016.08.157.
[132] Sajid Hossain M, Shabani B. Metal foams application to enhance cooling of open cathode polymer electrolyte membrane fuel cells. J Power Sources 2015;295:275–91. https://doi.org/10.1016/j.jpowsour.2015.07.022.
[133] Gadducci E, Lamberti T, Magistri L, Rivarolo M, Dellacasa A, Campora B, et al. Characterization and experimental comparison of commercial PEMFC stacks for marine applications. E3S Web Conf 2022;334:04003. https://doi.org/10.1051/e3sconf/202233404003.
[134] Jao TC, Ke ST, Chi PH, Jung G Bin, Chan SH. Degradation on a PTFE/Nafion membrane electrode assembly with accelerating degradation technique. Int J Hydrogen Energy 2010;35:6941–9. https://doi.org/10.1016/j.ijhydene.2010.03.118.
[135] Çalık A, Yıldırım S, Tosun E. Estimation of crack propagation in polymer electrolyte membrane fuel cell under vibration conditions. Int J Hydrogen Energy 2017;42:23347–51. https://doi.org/10.1016/j.ijhydene.2017.02.119.
[136] Ahmed HEU, Banan R, Zu JW, Bazylak A. Free vibration analysis of a polymer electrolyte membrane fuel cell. J Power Sources 2011;196:5520–5. https://doi.org/10.1016/j.jpowsour.2010.10.112.
[137] Zhou Z, Wu J. LOW TO MIDDLE VIBRO-ACOUSTIC NOISE PREDICTION IN SHIP CABIN BY USING PLATE-CAVITY 2018;25:149–57.
[138] Rajalakshmi N, Pandian S, Dhathathreyan KS. Vibration tests on a PEM fuel cell stack usable in transportation application. Int J Hydrogen Energy 2009;34:3833–7. https://doi.org/10.1016/j.ijhydene.2009.03.002.
[139] Hou Y, Hao D, Shen C, Shao Z. Experimental investigation of the steady-state efficiency of fuel cell stack under strengthened road vibrating condition. Int J Hydrogen Energy 2013;38:3767–72. https://doi.org/10.1016/j.ijhydene.2013.01.037.
[140] Hou Y, Zhou B, Zhou W, Shen C, He Y. An investigation of characteristic parameter variations of the polarization curve of a proton exchange membrane fuel cell stack under strengthened road vibrating conditions. Int J Hydrogen Energy 2012;37:11887–93. https://doi.org/10.1016/j.ijhydene.2012.05.030.
[141] Haji Hosseinloo A, Ehteshami MM. Shock and vibration effects on performance

reliability and mechanical integrity of proton exchange membrane fuel cells: A critical review and discussion. J Power Sources 2017;364:367–73. https://doi.org/10.1016/j.jpowsour.2017.08.037.
[142] Ahn S, Koh H, Lee J, Park J. Dependence between the vibration characteristics of the proton exchange membrane fuel cell and the stack structural feature. Environ Res 2019;173:48–53. https://doi.org/10.1016/j.envres.2019.03.022.
[143] Breziner L, Strahs P, Hutapea P. Effect of vibration on the liquid water transport of PEM fuel cells. Int. Mech. Eng. Congr. Expo., American Society of Mechanical Engineers; 2009, p. 17–22.
[144] Imen SJ, Shakeri M. Reliability Evaluation of an Open-Cathode PEMFC at Operating State and Longtime Vibration by Mechanical Loads. Fuel Cells 2016;16:126–34. https://doi.org/10.1002/fuce.201500144.
[145] Hou Y, Zhou W, Shen C. Experimental investigation of gas-tightness and electrical insulation of fuel cell stack under strengthened road vibrating conditions. Int J Hydrogen Energy 2011;36:13763–8. https://doi.org/10.1016/j.ijhydene.2011.07.092.
[146] Hou Y, Zhang X, Lu X, Hao D, Ma L, Li P. AC impedance characteristics of a vehicle PEM fuel cell stack under strengthened road vibrating conditions. Int J Hydrogen Energy 2014;39:18362–8. https://doi.org/10.1016/j.ijhydene.2014.09.054.
[147] Hou Y, Hao D, Shen J, Li P, Zhang T, Wang H. Effect of strengthened road vibration on performance degradation of PEM fuel cell stack. Int J Hydrogen Energy 2016;41:5123–34. https://doi.org/10.1016/j.ijhydene.2016.01.072.
[148] Wang X, Wang S, Chen S, Zhu T, Xie X, Mao Z. Dynamic response of proton exchange membrane fuel cell under mechanical vibration. Int J Hydrogen Energy 2016;41:16287–95. https://doi.org/10.1016/j.ijhydene.2016.06.082.
[149] Qiu D, Peng L, Lai X, Ni M, Lehnert W. Mechanical failure and mitigation strategies for the membrane in a proton exchange membrane fuel cell. Renew Sustain Energy Rev 2019;113:109289. https://doi.org/10.1016/j.rser.2019.109289.
[150] Liu D, Case S. Durability study of proton exchange membrane fuel cells under dynamic testing conditions with cyclic current profile. J Power Sources 2006;162:521–31. https://doi.org/10.1016/j.jpowsour.2006.07.007.
[151] Wu B, Zhao M, Shi W, Liu W, Liu J, Xing D, et al. The degradation study of Nafion/PTFE composite membrane in PEM fuel cell under accelerated stress tests. Int J Hydrogen Energy 2014;39:14381–90. https://doi.org/10.1016/j.ijhydene.2014.02.142.
[152] Grigoriev SA, Dzhus KA, Bessarabov DG, Millet P. Failure of PEM water electrolysis cells: Case study involving anode dissolution and membrane thinning. Int J Hydrogen Energy 2014;39:20440–6. https://doi.org/10.1016/j.ijhydene.2014.05.043.
[153] Moein-Jahromi M, Kermani MJ, Movahed S. Degradation forecast for PEMFC cathode-catalysts under cyclic loads. J Power Sources 2017;359:611–25. https://doi.org/10.1016/j.jpowsour.2017.05.102.
[154] Wilson MS. Surface Area Loss of Supported Platinum in Polymer Electrolyte Fuel Cells. J Electrochem Soc 1993;140:2872. https://doi.org/10.1149/1.2220925.
[155] Garche J, Dyer CK, Moseley PT, Ogumi Z, Rand DAJ, Scrosati B. Encyclopedia of Electrochemical Power Sources. 1st ed. Elsevier B.V.; 2009.
[156] Ferreira PJ, la O' GJ, Shao-Horn Y, Morgan D, Makharia R, Kocha S, et al. Instability of Pt/C Electrocatalysts in Proton Exchange Membrane Fuel Cells. J Electrochem Soc 2005;152:A2256. https://doi.org/10.1149/1.2050347.
[157] Selvaganesh SV, Selvarani G, Sridhar P, Pitchumani S, Shukla AK. Durable electrocatalytic-activity of Pt–Au/C cathode in PEMFCs 2011;13:12623–34. https://doi.org/10.1039/C1CP20243J.
[158] Zhang Y, Chen S, Wang Y, Ding W, Wu R, Li L, et al. Study of the degradation

mechanisms of carbon-supported platinum fuel cells catalyst via different accelerated stress test. J Power Sources 2015;273:62–9. https://doi.org/10.1016/j.jpowsour.2014.09.012.
[159] Debe MK, Schmoeckel AK, Vernstrom GD, Atanasoski R. High voltage stability of nanostructured thin film catalysts for PEM fuel cells. J Power Sources 2006;161:1002–11. https://doi.org/10.1016/j.jpowsour.2006.05.033.
[160] Hiraoka F, Matsuzawa K, Mitsushima S. Degradation of Pt/C Under Various Potential Cycling Patterns. Electrocatalysis 2013;4. https://doi.org/10.1007/s12678-012-0105-2.
[161] Merzougui B, Swathy S. Rotating Disk Electrode Investigations of Fuel Cell Catalyst Degradation Due to Potential Cycling in Acid Electrolyte. J Electrochem Soc 2006;153:A2220. https://doi.org/10.1149/1.2353752.
[162] Paik CH, Saloka G, Graham G. Influence of Cyclic Operation on PEM Fuel Cell Catalyst Stability. Electrochem Solid-State Lett 2007;10:B39. https://doi.org/10.1149/1.2400204.
[163] Riese A, Banham D, Ye S, Sun X. Accelerated Stress Testing by Rotating Disk Electrode for Carbon Corrosion in Fuel Cell Catalyst Supports. J Electrochem Soc 2015;162:F783–8. https://doi.org/10.1149/2.0911507jes.
[164] Selvaganesh SV, Selvarani G, Sridhar P, Pitchumani S, Shukla AK. A Durable RuO2-Carbon-Supported Pt Catalyst for PEFCs: A Cause and Effect Study. J Electrochem Soc 2012;159:B463–70. https://doi.org/10.1149/2.jes113440.
[165] Zhou ZM, Shao ZG, Qin XP, Chen XG, Wei ZD, Yi BL. Durability study of Pt-Pd/C as PEMFC cathode catalyst. Int J Hydrogen Energy 2010;35:1719–26. https://doi.org/10.1016/j.ijhydene.2009.12.056.
[166] Bi W, Sun Q, Deng Y, Fuller TF. The effect of humidity and oxygen partial pressure on degradation of Pt/C catalyst in PEM fuel cell. Electrochim Acta 2009;54:1826–33. https://doi.org/10.1016/j.electacta.2008.10.008.
[167] Bi W, Fuller TF. Temperature Effects on PEM Fuel Cells Pt/C Catalyst Degradation. J Electrochem Soc 2008;155:B215. https://doi.org/10.1149/1.2819680.
[168] Borup R, Davey J, Xu H, Ofstad A, Garzon F, Pivovar B. PEM Fuel Cell Durability. Fuel Cell 2008:1039–45.
[169] Paik C, Jarvi T, O'Grady W. Extent of PEMFC cathode surface oxidation by oxygen and water measured by CV. Electrochem Solid State Lett 2004;7:A82–4. https://doi.org/10.1149/1.1649698.
[170] Dubau L, Durst J, Castanheira L, Maillard F, Lamibrac A, Dillet J, et al. Various Scales of Aging Heterogeneities upon PEMFC Operation - A Link between Local MEA Materials Degradation and the Cell Performance. ECS Trans 2015;69:133–46. https://doi.org/10.1149/06917.0133ecst.
[171] Chen H, Pei P, Song M. Lifetime prediction and the economic lifetime of proton exchange membrane fuel cells. Appl Energy 2015;142:154–63. https://doi.org/10.1016/j.apenergy.2014.12.062.
[172] Moein-Jahromi M, Kermani MJ. Performance prediction of PEM fuel cell cathode catalyst layer using agglomerate model. Int J Hydrogen Energy 2012;37:17954–66. https://doi.org/10.1016/j.ijhydene.2012.09.120.
[173] Moein-Jahromi M, Movahed S, Kermani MJ. Numerical study of the cathode electrode in the Microfluidic Fuel Cell using agglomerate model. J Power Sources 2015;277:180–92. https://doi.org/10.1016/j.jpowsour.2014.12.019.
[174] Burlatsky SF, Gummalla M, Atrazhev V V., Dmitriev D V., Kuzminyh NY, Erikhman NS. The Dynamics of Platinum Precipitation in an Ion Exchange Membrane. J Electrochem Soc 2011;158:B322. https://doi.org/10.1149/1.3532956.
[175] Thangavelautham J. Degradation in PEM Fuel Cells and Mitigation Strategies Using System Design and Control. Prot Exch Membr Fuel Cell 2018.

https://doi.org/10.5772/intechopen.72208.
[176] Yue M, Jemei S, Gouriveau R, Zerhouni N. Review on health-conscious energy management strategies for fuel cell hybrid electric vehicles: Degradation models and strategies. Int J Hydrogen Energy 2019;44:6844–61. https://doi.org/10.1016/j.ijhydene.2019.01.190.
[177] Odeim F, Roes J, Wülbeck L, Heinzel A. Power management optimization of fuel cell/battery hybrid vehicles with experimental validation. J Power Sources 2014;252:333–43. https://doi.org/10.1016/j.jpowsour.2013.12.012.
[178] Zhang Q, Lin R, Cui X, Xia SX, Yang Z, Chang YT. Study of the two-phase dummy load shut-down strategy for proton exchange membrane fuel cells. J Power Sources 2017;341:230–9. https://doi.org/10.1016/j.jpowsour.2016.11.098.
[179] St-Pierre J. PEMFC contaminant tolerance limit - Foreign cations in ionomers. Int J Hydrogen Energy 2011;36:5527–35. https://doi.org/10.1016/j.ijhydene.2011.01.143.
[180] Zhao Y, Setzler BP, Wang J, Nash J, Wang T, Xu B, et al. An Efficient Direct Ammonia Fuel Cell for Affordable Carbon-Neutral Transportation. Joule 2019;3:2472–84. https://doi.org/10.1016/J.JOULE.2019.07.005.
[181] Moradi Bilondi A, Abdollahzadeh M, Kermani MJ, Heidary H, Havaej P. Numerical study of anode side CO contamination effects on PEM fuel cell performance; and mitigation methods. Energy Convers Manag 2018;177:519–34. https://doi.org/10.1016/j.enconman.2018.09.076.
[182] Zhai Y, Bender G, Bethune K, Rocheleau R. Influence of cell temperature on sulfur dioxide contamination in proton exchange membrane fuel cells. J Power Sources 2014;247:40–8. https://doi.org/10.1016/j.jpowsour.2013.08.054.
[183] Reshetenko T, Laue V, Krewer U, Artyushkova K. Poisoning effects of sulfur dioxide in an air stream on spatial proton exchange membrane fuel cell performance. J Power Sources 2019;438:226949. https://doi.org/10.1016/j.jpowsour.2019.226949.
[184] Reshetenko T, Laue V, Krewer U, Artyushkova K. Study of degradation and spatial performance of low Pt-loaded proton exchange membrane fuel cells under exposure to sulfur dioxide in an oxidant stream. J Power Sources 2020;458:228032. https://doi.org/10.1016/j.jpowsour.2020.228032.
[185] Lemaire O, Barthe B, Rouillon L, Franco A. Mechanistic Investigations of NO2 Impact on ORR in PEM Fuel Cells: a Coupled Experimental and Multi-scale Modeling Approach. ECS Trans 2019;25:1595–604. https://doi.org/10.1149/1.3210715.
[186] Angelo M, Bethune K, Rocheleau R. The Impact of sub ppm Carbon Monoxide and ppm Level {CO}/Toluene and Methylcyclohexane/{CO} Mixtures on {PEMFC} Performance and Durability. Electrochem Soc 2019;28:169–81. https://doi.org/10.1149/1.3502348.
[187] Anja Talke, Ulrich Misz, Gerhard Konrad, Angelika Heinzel. Impact of Air Contaminants on Subscale Single Fuel Cells and an Automotive Short Stack. J Electr Eng 2015;3:70–9. https://doi.org/10.17265/2328-2223/2015.02.003.
[188] Yuan XZ, Li H, Yu Y, Jiang M, Qian W, Zhang S, et al. Diagnosis of contamination introduced by ammonia at the cathode in a polymer electrolyte membrane fuel cell. Int J Hydrogen Energy 2012;37:12464–73. https://doi.org/10.1016/j.ijhydene.2012.05.125.
[189] Shi W, Yi B, Hou M, Shao Z. The effect of H2S and CO mixtures on PEMFC performance. Int J Hydrogen Energy 2007;32:4412–7. https://doi.org/10.1016/j.ijhydene.2007.06.029.
[190] Talke A, Misz U, Konrad G, Heinzel A, Klemp D, Wegener R. Influence of urban air on proton exchange membrane fuel cell vehicles – Long term effects of air contaminants in an authentic driving cycle. J Power Sources 2018;400:556–65. https://doi.org/10.1016/j.jpowsour.2018.08.063.

[191] Ruano P, Delgado LL, Picco S, Villegas L, Tonelli F, Merlo M, et al. Carbon Monoxide Urban Air Pollution Cardiac Effects. Intech 2016:13.
[192] Haiduc I, Beldean-Galea M. Variation of Greenhouse Gases in Urban Areas-Case Study: CO2, CO and CH4 in Three Romanian Cities. Intech 2016:13.
[193] Misz U, Talke A, Heinzel A, Beckhaus P. Effects, Damage Characteristics and Recovery Potential of Traffic-induced Nitric Oxide Emissions in PEM Fuel Cells under Variable Operating Conditions. Fuel Cells 2018;18:594–601. https://doi.org/10.1002/fuce.201700214.
[194] Shell. Marine Fuels: ULSFO 0.1%S Max. Shell Trading and Supply 2014:1–2.
[195] Zamel N, Li X. Effect of contaminants on polymer electrolyte membrane fuel cells. Prog Energy Combust Sci 2011;37:292–329. https://doi.org/10.1016/j.pecs.2010.06.003.
[196] Verdaguer-Casadevall A, Hernandez-Fernandez P, Stephens IEL, Chorkendorff I, Dahl S. The effect of ammonia upon the electrocatalysis of hydrogen oxidation and oxygen reduction on polycrystalline platinum. J Power Sources 2012;220:205–10. https://doi.org/10.1016/j.jpowsour.2012.07.141.
[197] Uribe F, Gottesfeld S, Zawodzinski TA. Effect of ammonia as potential fuel impurity on PEMFC performance. J Electrochem Soc 2002;149:A293.
[198] Banga S, Varshney PK. Effect of impurities on performance of biodiesel: A review. J Sci Ind Res (India) 2010;69:575–9.
[199] Zhang X, Mustafa F. Contamination of Membrane-Electrode Assemblies by Ammonia in Polymer Electrolyte Fuel Cells. ECS Trans 2019;25:1565–74. https://doi.org/10.1149/1.3210712.
[200] International Organization for Standardization. ISO 14687:2019. Hydrogen fuel quality—product specification. 2019.
[201] SAE International. SAE J2719:2020. Hydrogen fuel quality for fuel cell vehicles 2020.
[202] European Committee on Standardisation. EN 17124:2018. Hydrogen fuel product specification and quality assurance Proton Exchange Membrane (PEM) fuel cell applications for road vehicles 2018.
[203] Postole G, Auroux A. The poisoning level of Pt/C catalysts used in PEM fuel cells by the hydrogen feed gas impurities: The bonding strength. Int J Hydrogen Energy 2011;36:6817–25. https://doi.org/10.1016/j.ijhydene.2011.03.018.
[204] Kim JD, Park Y Il, Kobayashi K, Nagai M, Kunimatsu M. Characterization of CO tolerance of PEMFC by ac impedance spectroscopy. Solid State Ionics 2001;140:313–25. https://doi.org/10.1016/S0167-2738(01)00842-6.
[205] Wagner N, Gülzow E. Change of electrochemical impedance spectra (EIS) with time during CO-poisoning of the Pt-anode in a membrane fuel cell. J Power Sources 2004;127:341–7. https://doi.org/10.1016/j.jpowsour.2003.09.031.
[206] Rubio MA, Urquia A, Dormido S. Diagnosis of performance degradation phenomena in PEM fuel cells. Int J Hydrogen Energy 2010;35:2586–90. https://doi.org/10.1016/j.ijhydene.2009.03.054.
[207] Baschuk JJ, Li X. Carbon monoxide poisoning of proton exchange membrane fuel cells. Int J Energy Res 2001;25:695–713. https://doi.org/doi:10.1002/er.713.
[208] Bétournay MC, Bonnell G, Edwardson E, Paktunc D, Kaufman A, Lomma AT. The effects of mine conditions on the performance of a PEM fuel cell. J Power Sources 2004;134:80–7. https://doi.org/10.1016/j.jpowsour.2004.02.026.
[209] United States Environmental Protecion Agency (EPA). Air Trends 2020. https://www.epa.gov/air-trends/.
[210] Regione Liguria. Qualità dell'aria 2021. https://servizi.regione.liguria.it/page/welcome/QUALITA_ARIA.
[211] Chen CY, Chen CC, Hsu SW, Lai MP, Lai WH, Yang WM. Behavior of a proton

exchange membrane fuel cell in reformate gas. Energy Procedia 2012;29:64–71. https://doi.org/10.1016/j.egypro.2012.09.009.
[212] Profatilova I, Jacques P-A, Escribano S. Evaluation of Parameters Accelerating the Aging of PEMFCs Operating under Reformate Containing Carbon Monoxide. J Electrochem Soc 2018;165:F3251–60. https://doi.org/10.1149/2.0281806jes.
[213] Shi Z, Song D, Zhang J, Liu Z-S, Knights S, Vohra R, et al. Transient Analysis of Hydrogen Sulfide Contamination on the Performance of a PEM Fuel Cell. J Electrochem Soc 2007;154:B609. https://doi.org/10.1149/1.2731045.
[214] Urdampilleta I, Uribe F, Rockward T, Brosha EL, Pivovar B, Garzon FH. PEMFC Poisoning with H2S: Dependence on Operating Conditions. ECS Trans 2019;11:831–42. https://doi.org/10.1149/1.2780996.
[215] Shi W, Yi B, Hou M, Jing F, Ming P. Hydrogen sulfide poisoning and recovery of PEMFC Pt-anodes. J Power Sources 2007;165:814–8. https://doi.org/10.1016/j.jpowsour.2006.12.052.
[216] Gomez YA, Oyarce A, Lindbergh G, Lagergren C. Ammonia Contamination of a Proton Exchange Membrane Fuel Cell. J Electrochem Soc 2018;165:F189–97. https://doi.org/10.1149/2.0761803jes.
[217] Talke A, Misz U, Konrad G, Heinzel A. Influence of Nitrogen Compounds on PEMFC: A Comparative Study. J Electrochem Soc 2018;165:F3111–7. https://doi.org/10.1149/2.0181806jes.
[218] Jing F, Hou M, Shi W, Fu J, Yu H, Ming P, et al. The effect of ambient contamination on PEMFC performance. J Power Sources 2007;166:172–6. https://doi.org/10.1016/j.jpowsour.2006.12.103.
[219] Mohtadi R, Lee WK, Van Zee JW. Assessing durability of cathodes exposed to common air impurities. J Power Sources 2004;138:216–25. https://doi.org/10.1016/j.jpowsour.2004.06.036.
[220] Zhai J, Hou M, Liang D, Shao Z, Yi B. Investigation on the electrochemical removal of SO 2 in ambient air for proton exchange membrane fuel cells. Electrochem Commun 2012;18:131–4. https://doi.org/10.1016/j.elecom.2012.02.015.
[221] Gadducci E, Reboli T, Magistri L, Massardo AF. Catalyst degradation under different testing conditions – a review. In: Bucheli O, Geisser G, Moore F, Spirig M, editors. Proc. EFCF 2021 Low-Temperature Electrolysers, Fuel Cells H2 Process., 2021, p. 1–10.
[222] Home - Bluenergy Revolution n.d. https://bluenergyrevolution.com/ (accessed January 21, 2022).
[223] De Marco G, Malkow T, Tsotridis G, Pilenga A. EU Harmonised Test Protocols for PEMFC-MEA Testing in Single Cell Configuration for Automotive Applications 2015. https://ec.europa.eu/jrc/en/publications-list (accessed January 22, 2022).
[224] Lamberti T. TESEO Project, High Efficiency Technologies For On-Board Energy And Environmental Sustainability, PON02_00153_2939517, 2012-2015 n.d.
[225] Banerjee R, Ge N, Han C, Lee J, George MG, Liu H, et al. Identifying in operando changes in membrane hydration in polymer electrolyte membrane fuel cells using synchrotron X-ray radiography. Int J Hydrogen Energy 2018;43:9757–69. https://doi.org/10.1016/j.ijhydene.2018.03.224.
[226] Yap HT, Schofield N. Test characterisation of a H2 PEM fuel cell. VPPC 2007 - Proc 2007 IEEE Veh Power Propuls Conf 2007:551–8. https://doi.org/10.1109/VPPC.2007.4544185.
[227] Gadducci E, Lamberti T, Magistri L, Massardo AF. Recovery procedure for 30 kW PEM Fuel Cell stacks. In: Cigolotti V, editor. Proc. EFC2019, Naples: 2020, p. 231–2. https://doi.org/978-88-8286-386-9.
[228] Gadducci E, Magistri L, Lamberti T. Assessment of PEMFC system performance for

marine application. EFCF 2019 Low-Temp. Fuel Cells, Electrolysers H2 Process. Lucerne Switz., 2019, p. 29–41.
[229] Hoeflinger J, Hofmann P. Air mass flow and pressure optimisation of a PEM fuel cell range extender system. Int J Hydrogen Energy 2020;45:29246–58. https://doi.org/10.1016/j.ijhydene.2020.07.176.
[230] Halvorsen IJ, Pivac I, Bezmalinović D, Barbir F, Zenith F. Electrochemical low-frequency impedance spectroscopy algorithm for diagnostics of PEM fuel cell degradation. Int J Hydrogen Energy 2020;45:1325–34. https://doi.org/10.1016/j.ijhydene.2019.04.004.
[231] DNV-GL. Propulsion, power generation and auxiliary systems. 2015.
[232] Chiche A, Lindbergh G, Stenius I, Lagergren C. Design of experiment to predict the time between hydrogen purges for an air-breathing PEM fuel cell in dead-end mode in a closed environment. Int J Hydrogen Energy 2021;46:13806–17. https://doi.org/10.1016/j.ijhydene.2021.01.035.
[233] Wallnöfer-Ogris E, Pertl P, Trattner A. Quasi-stationary UI-characteristic model of a PEM fuel cell–Evaluating the option of self-humidifying operation. Int J Hydrogen Energy 2020;45:32464–77. https://doi.org/10.1016/j.ijhydene.2020.08.254.
[234] Ramschak E, Peinecke V, Prenninger P, Schaffer T, Baumgartner W, Hacker V. Online stack monitoring tool for dynamically and stationary operated fuel cell systems. Fuel Cells Bull 2006;2006:12–5. https://doi.org/10.1016/S1464-2859(06)71207-X.
[235] Pei P, Li Y, Xu H, Wu Z. A review on water fault diagnosis of PEMFC associated with the pressure drop. Appl Energy 2016;173:366–85. https://doi.org/10.1016/j.apenergy.2016.04.064.
[236] Büchi FN. Operating Proton Exchange Membrane Fuel Cells Without External Humidification of the Reactant Gases. J Electrochem Soc 1997;144:2767. https://doi.org/10.1149/1.1837893.
[237] Riascos LAM. Relative humidity control in polymer electrolyte membrane fuel cells without extra humidification. J Power Sources 2008;184:204–11. https://doi.org/10.1016/j.jpowsour.2008.06.032.
[238] Hao L, Yu H, Hou J, Song W, Shao Z, Yi B. Transient behavior of water generation in a proton exchange membrane fuel cell. J Power Sources 2008;177:404–11. https://doi.org/10.1016/j.jpowsour.2007.11.034.
[239] Huang X, Solasi R, Zou Y, Feshler M, Reifsnider M, Condit D, et al. Mechanical endurance of polymer electrolyte membrane and PEM fuel cell durability. J Polym Sci 2006:2346–57. https://doi.org/10.1002/polb.
[240] Suresh P V., Jayanti S. Effect of air flow on liquid water transport through a hydrophobic gas diffusion layer of a polymer electrolyte membrane fuel cell. Int J Hydrogen Energy 2010;35:6872–86. https://doi.org/10.1016/j.ijhydene.2010.04.052.
[241] Wang J. Barriers of scaling-up fuel cells: Cost, durability and reliability. Energy 2015;80:509–21. https://doi.org/10.1016/j.energy.2014.12.007.
[242] He W, Lin G, Van Nguyen T. Diagnostic Tool to Detect Electrode Flooding in Proton-Exchange Membrane Fuel Cells. AIChE J 2003;49:3221–8. https://doi.org/10.1002/aic.690491221.
[243] Zhang S, Yuan X, Wang H, Mérida W, Zhu H, Shen J, et al. A review of accelerated stress tests of MEA durability in PEM fuel cells. Int J Hydrogen Energy 2009;34:388–404. https://doi.org/10.1016/j.ijhydene.2008.10.012.
[244] Liu W, Cleghorn SJC. Effects of relative humidity on membrane durability in PEM fuel cells. ECS Trans 2006.
[245] Gadducci E, Magistri L, Lamberti T. Analysis of consequences of cells rupture on PEMFC module performance. EFCF 2019 Low-Temp. Fuel Cells, Electrolysers H2

Process. Lucerne Switz., Luzern: European Fuel Cell Forum 2019; 2019, p. 126–33.
[246] Ji M, Wei Z. A review of water management in polymer electrolyte membrane fuel cells. Energies 2009;2:1057–106. https://doi.org/10.3390/en20401057.
[247] NETL. Seventh Edition Fuel Cell Handbook. vol. 7 Edition. 2004.
[248] Gadducci E, Lamberti T, Magistri L, Massardo AF. Proceedings of EFC2019. In: Cigolotti V, editor. Proc. EFC2019, vol. 01, Naples: 2020, p. 231–2.
[249] Qi Z, Kaufman A. Improvement of water management by a microporous sublayer for PEM fuel cells. J Power Sources 2002;109:38–46. https://doi.org/10.1016/S0378-7753(02)00058-7.
[250] Chinannai MF, Lee J, Ju H. Study of the characteristics of temperature rise and coolant flow rate control during malfunction of PEM fuel cells. Int J Hydrogen Energy 2021;46:11160–75. https://doi.org/10.1016/j.ijhydene.2020.04.221.
[251] Van Nguyen T, White RE. A Water and Heat Management Model for Proton-Exchange-Membrane Fuel Cells. J Electrochem Soc 1993;140:2178–86. https://doi.org/10.1149/1.2220792.
[252] Park G, Gajic Z. Sliding mode control of a linearized polymer electrolyte membrane fuel cell model. J Power Sources 2012;212:226–32. https://doi.org/10.1016/j.jpowsour.2012.04.014.
[253] Matraji I, Laghrouche S, Wack M. Pressure control in a PEM fuel cell via second order sliding mode. Int J Hydrogen Energy 2012;37:16104–16. https://doi.org/10.1016/j.ijhydene.2012.08.007.
[254] De Campo M. Analysis and modeling of PEM Fuel Cell Systems. Univeristy of Genoa, 2019.
[255] Gadducci E, Saccaro S, Rivarolo M, Magistri L. Response Surface Methodology for 30 kW PEMFC stack characterization. E3S Web Conf 2022;334:04006. https://doi.org/10.1051/e3sconf/202233404006.
[256] Bendato I, Cassettari L, Mosca M, Mosca R. A design of experiments/response surface methodology approach to study the economic sustainability of a 1MWe photovoltaic plant. Renew Sustain Energy Rev 2015;51:1664–79. https://doi.org/10.1016/J.RSER.2015.07.074.
[257] Montgomery DC. Design and analysis of experiments n.d.
[258] Myers H Raymond MCD& A-CCC. Response Surface Methodology: Process and Product Optimization Using ... - 2016:894.
[259] Cheng SJ, Miao JM, Wu SJ. Use of metamodeling optimal approach promotes the performance of proton exchange membrane fuel cell (PEMFC). Appl Energy 2013;105:161–9. https://doi.org/10.1016/j.apenergy.2013.01.001.
[260] Ghasabehi M, Shams M, Kanani H. Multi-objective optimization of operating conditions of an enhanced parallel flow field proton exchange membrane fuel cell. Energy Convers Manag 2021;230:113798. https://doi.org/10.1016/j.enconman.2020.113798.
[261] Kanani H, Shams M, Hasheminasab M, Bozorgnezhad A. Model development and optimization of operating conditions to maximize PEMFC performance by response surface methodology. Energy Convers Manag 2015;93:9–22. https://doi.org/10.1016/J.ENCONMAN.2014.12.093.
[262] Correa G, Borello F, Santarelli M. Sensitivity analysis of stack power uncertainty in a PEMFC-based powertrain for aircraft application. Int J Hydrogen Energy 2015;40:10354–65. https://doi.org/10.1016/J.IJHYDENE.2015.05.133.
[263] Jin L, Wang XJ, Zhu JW, Wang CF, Zhou TT, Zhang XW. Sensitivity analysis of proton exchange membrane fuel cell performance to operating parameters and its applicability assessment under different conditions. Energy Convers Manag 2021;228:113727. https://doi.org/10.1016/J.ENCONMAN.2020.113727.

[264] Charoen K, Prapainainar C, Sureeyatanapas P, Suwannaphisit T, Wongamornpitak K, Kongkachuichay P, et al. Application of response surface methodology to optimize direct alcohol fuel cell power density for greener energy production. J Clean Prod 2017;142:1309–20. https://doi.org/10.1016/J.JCLEPRO.2016.09.059.
[265] Jahnke T, Futter G, Latz A, Malkow T, Papakonstantinou G, Tsotridis G, et al. Performance and degradation of Proton Exchange Membrane Fuel Cells: State of the art in modeling from atomistic to system scale. J Power Sources 2016;304:207–33. https://doi.org/10.1016/J.JPOWSOUR.2015.11.041.
[266] Mahmoodi F, Rahimi R. Experimental and numerical investigating a new configured thermal coupling between metal hydride tank and PEM fuel cell using heat pipes. Appl Therm Eng 2020;178:115490. https://doi.org/10.1016/J.APPLTHERMALENG.2020.115490.
[267] Jeon SW, Cha D, Kim HS, Kim Y. Analysis of the system efficiency of an intermediate temperature proton exchange membrane fuel cell at elevated temperature and relative humidity conditions. Appl Energy 2016;166:165–73. https://doi.org/10.1016/j.apenergy.2015.12.123.
[268] Moein-Jahromi M, Kermani MJ. Three-dimensional multiphase simulation and multi-objective optimization of PEM fuel cells degradation under automotive cyclic loads. Energy Convers Manag 2021;231:113837. https://doi.org/10.1016/j.enconman.2021.113837.
[269] Amphlett JC, Baumert RM, Mann RF, Peppley BA, Roberge PR, Harris TJ. Performance Modeling of the Ballard Mark IV Solid Polymer Electrolyte Fuel Cell I. Mechanistic Model Development Physical Properties, Assumptions, and Approximations. J Electrochem Soc 1995;142.